Karlsruher Institut für Technologie

Insights in New Physics through Di-Higgs Production and Precision Phenomenology

Zur Erlangung des akademischen Grades eines

DOKTORS DER NATURWISSENSCHAFTEN

von der KIT-Fakultät für Physik
des Karlsruher Instituts für Technologie (KIT)

genehmigte

DISSERTATION

von

M.Sc. Felix Egle

aus Ehingen (Donau)

Referentin: Prof. Dr. M. M. Mühlleitner (KIT, Karlsruhe)
Korreferent: Prof. Dr. R. Santos (ISEL & U. LISBOA, Lisbon)

Tag der mündlichen Prüfung: 25. Oktober 2024

Eidesstattliche Versicherung gemäß § 13 Absatz 2 Ziffer 3 der Promotionsordnung des Karlsruher Instituts für Technologie (KIT) für die KIT-Fakultät für Physik:

1. Bei der eingereichten Dissertation zu dem Thema

   Insights in New Physics through Di-Higgs Production and Precision Phenomenology

   handelt es sich um meine eigenständig erbrachte Leistung.

2. Ich habe nur die angegebenen Quellen und Hilfsmittel benutzt und mich keiner unzulässigen Hilfe Dritter bedient. Insbesondere habe ich wörtlich oder sinngemäß aus anderen Werken übernommene Inhalte als solche kenntlich gemacht.

3. Die Arbeit oder Teile davon habe ich bislang nicht an einer Hochschule des In- oder Auslands als Bestandteil einer Prüfungs- oder Qualifikationsleistung vorgelegt.

4. Die Richtigkeit der vorstehenden Erklärungen bestätige ich.

5. Die Bedeutung der eidesstattlichen Versicherung und die strafrechtlichen Folgen einer unrichtigen oder unvollständigen eidesstattlichen Versicherung sind mir bekannt.

Ich versichere an Eides statt, dass ich nach bestem Wissen die reine Wahrheit erklärt und nichts verschwiegen habe.

Karlsruhe, den 17. September 2024

. . . . . .
(Full name)

Dedicated to my loving grandmothers.

Abstract

In this thesis, we perform precision calculations and phenomenological studies in various new physics scenarios. First, we investigate the complex singlet extension of the Standard Model (CxSM), where we calculate electroweak higher-order corrections to Higgs decays. We work out several renormalization schemes and perform an extensive parameter scan, including theoretical and experimental constraints. We use the obtained parameter sample to analyze the typical sizes of the next-to-leading-order (NLO) corrections and their impact on the allowed parameter space. In the second project, we consider a composite 2-Higgs doublet model (2HDM), where we investigate di-Higgs production. We give a brief introduction to composite Higgs models as well as the composite 2HDM and describe the calculation of the leading-order (LO) di-Higgs cross section and the quantum chromodynamics (QCD) NLO corrections in the heavy top limit. We introduce the setup we used to obtain a set of viable parameter points, including theoretical and experimental constraints, in particular the constraints from *resonant* and *non-resonant* di-Higgs searches. We then investigate the impact of the composite 2HDM on Higgs pair production compared to the Standard Model (SM) and other 2HDM-like models, both on the inclusive cross section as well as the invariant mass and p_T distributions. Here, interesting interference effects appear in the composite 2HDM that can be used to distinguish the composite 2HDM from other 2HDM realizations. Finally, in the third project we consider the next-to-minimal supersymmetric extension of the SM (NMSSM), where we calculate the decays of supersymmetric particles and implement them into a new code that can be used for phenomenological studies. We give a brief introduction to supersymmetry and the NMSSM. We describe the calculation and implementation of the various two-body, three-body, and radiative loop decays, as well as the NLO QCD corrections to the two-body decays of the supersymmetric particles. Finally, we describe the setup we use to obtain viable parameter points and discuss example benchmark point scenarios.

Zusammenfassung

In dieser Dissertation führen wir präzise Berechnungen und phänomenologische Studien in verschiedenen Szenarien neuer Physik durch. Als Erstes untersuchen wir die komplexe Singulett-Erweiterung des Standardmodells (CxSM), in der wir elektroschwache Korrekturen höherer Ordnung für Higgs-Zerfälle berechnen. Wir erarbeiten verschiedene Renormierungsschemata und führen einen umfangreichen Parameterscan durch, in dem theoretische und experimentelle Einschränkungen berücksichtigt werden. Wir verwenden die erhaltenen Parameterpunkte, um die typischen Größen der Korrekturen nächstführender Ordnung (NLO) und deren Einfluss auf den erlaubten Parameterbereich zu untersuchen. In dem zweiten Projekt betrachten wir ein composite 2-Higgs-Dublett-Modell (2HDM), in welchem wir die Produktion von Higgs-Paaren untersuchen. Wir geben eine kurze Einführung in composite Higgs-Modelle, in welchen das Higgs-Teilchen nicht elementar, sondern ein zusammengesetztes Teilchen ist, und in das betrachtete composite 2HDM. Weiterhin beschreiben wir die Berechnung des Wirkungsquerschnitts für die Higgs-Paar-Produktion in führender Ordnung (LO) sowie die NLO-Korrekturen der Quantenchromodynamik (QCD) im schweren Quark-Limes. Wir beschreiben die Einrichtung des Parameterscans, um erlaubte Parameterpunkte zu erhalten, welche die relevanten theoretischen und experimentellen Einschränkungen erfüllen, insbesondere von *resonanten* und *nicht-resonanten* Untersuchungen von Higgs-Paar-Produktion. Anschließend untersuchen wir den Einfluss des composite 2HDM auf Higgs-Paar-Produktion im Vergleich zum Standardmodell (SM) und anderen 2HDM-Modellen, sowohl auf den inklusiven Wirkungsquerschnitt als auch auf invariante Massen- und p_T-Verteilungen. Hierbei treten

interessante Interferenzeffekte im composite 2HDM auf, welche verwendet werden können, um zwischen dem composite 2HDM und anderen 2HDM-Realisierungen zu unterscheiden. Schließlich betrachten wir im dritten Projekt die nächstminimale supersymmetrische Erweiterung des SM (NMSSM), berechnen die Zerfälle der supersymmetrischen Teilchen und implementieren die Resultate in einen neuen Code, welcher für phänomenologische Studien verwendet werden kann. Wir geben eine kurze Einführung in das Konzept der Supersymmetrie und in das NMSSM. Dann beschreiben wir die Berechnung der 2-Körper-, der 3-Körper- und der schleifeninduzierten Zerfälle, sowie die NLO QCD Korrekturen zu den 2-Körperzerfällen der supersymmetrischen Teilchen. Abschließend beschreiben wir den Programmaufbau, den wir verwenden, um gültige Parameterpunkte zu erhalten und disktuieren exemplarische Benchmark-Punkt-Szenarien.

Contents

List of Abbreviations

2HDM	2-Higgs doublet model
BR	branching ratio
BSM	beyond SM
CKM	Cabibbo-Kobayashi-Maskawa matrix
COM	centre-of-mass
CxSM	complex singlet extension of the SM
DM	dark matter
$\overline{\text{DR}}$	dimensional reduction
EDM	electric dipole moment
EW	electroweak
EWPO	electroweak precision observable
EWSB	electroweak symmetry breaking
FCNC	flavour-changing neutral current
IR	infrared
LHC	Large Hadron Collider
LO	leading order
LSP	lightest supersymmetric particle
MCMC	Markov Chain Montecarlo
MFV	minimal flavour violation
$\overline{\text{MS}}$	modified minimal subtraction
MSSM	minimal supersymmetric extension of the SM
NGB	Nambu Goldstone boson
NLO	next-to-leading order
NMSSM	next-to-minimal supersymmetric extension of the SM
NNLO	next-to-next-to-leading order
NP	new physics
OS	on-shell
pd	process-dependent
PDF	particle distribution function
QCD	quantum chromodynamics
RG	renormalization group
SFOEWPT	strong first-order EW phase transition
SILH	strongly interacting little Higgs
SM	Standard Model
SLHA	SUSY Les Houches Accord
SUSY	supersymmetry
UV	ultraviolett
VEV	vacuum expectation value
ZEM	zero external momentum

CHAPTER 1

Introduction

The currently well established theory in particle physics is the Standard Model of Particle Physics (SM) [1–3]. Its particle content was mostly discovered in the 20th century. The interplay between theory and experiment led to discoveries of new particles, that resulted in new developments and predictions on the theory side, which itself was then followed by new discoveries. The last particle to be discovered was the Higgs boson. It was predicted already in the 1960s [4–8], and was needed to complete the SM. The Higgs boson, however, was only discovered almost 50 years after its prediction, in 2012 at the Large Hadron Collider (LHC) [9, 10]. Therefore, new physics (NP) in this thesis entails theories beyond the SM (BSM).

With the SM we have a theoretically consistent and experimentally well tested theory, but we know that BSM theories should be realized in nature, as there are several unexplained phenomena. For example, we know that there exists a new form of matter in the universe, called Dark Matter (DM). Its relic density was measured e.g. by the Planck collaboration [11]. This new form of matter constitutes a sizeable amount of the total matter density in the universe. A possible explanation is a new kind of particle. There is, however, no suitable candidate in the SM, and we have to invoke BSM theories to accommodate new particles that can fill the role of DM. Another unexplained phenomena is the matter-antimatter asymmetry in the universe [12], i.e. why we observe more matter than anti-matter in the universe. This asymmetry can be explained dynamically by a mechanism called electroweak (EW) baryogenesis [13–21], provided the Sakharov conditions [22] are fulfilled. The SM could in principle fulfil all conditions, but it would need a Higgs mass of about 70-80 GeV [23, 24] for an EW phase transition to be of strong first order [25–27], which is in contrast to the discovered Higgs mass of 125 GeV. Additionally, the CP violation within the SM is not large enough [28–30]. Thus, we have to resort to BSM theories to incorporate the conditions for baryogenesis and explain the matter-antimatter asymmetry via this mechanism.

In addition to the mentioned unexplained phenomena, there are also theoretically motivated reasons for new physics beyond the SM. The SM is a phenomenologically motivated theory, that describes the experimental observations well but gives no deeper explanations. For example, it does not explain why there are 3 generations of fermions and what the origin of the Yukawa couplings and therefore the masses of the fermions is. Next, we have a description for the mass generation for fermions and gauge bosons via the Higgs mechanism, but there is no dynamical explanation of why the Higgs boson obtains a vacuum expectation value

(VEV). Another theoretical issue is the hierarchy problem, that raises the question of the naturalness of a light Higgs boson (light compared to e.g. the Planck scale [31]). We will give a more detailed description of the hierarchy problem in Sec. 2.2.

Although it seems evident that new physics beyond the SM exists, and we gathered some hints for it (e.g. DM), we have not yet found any clear deviation from the SM within our experiments. Therefore, one of the current approaches in particle physics is to precisely measure the SM masses, couplings and interactions. At the same time, from a theoretical point of view, the complementary goal is to give precise theoretical predictions, both for the SM and BSM theories, in order to compare them with experiments and provide benchmark scenarios. Moreover, interactions that have not been measured experimentally and therefore leave room for new physics are also investigated. One important, so far not measured interaction is the Higgs self-interaction, which can be determined in Higgs pair production. We will give an overview over di-Higgs production in Sec. 2.3. One of the main goals of this thesis is thus to contribute to the overall effort of precision phenomenology in particle physics.

An interesting point is that all of the above described issues of the SM are related to the Higgs sector in the SM or can be explained by theories that alter or extend the Higgs sector, compared to the SM. Thus, in this thesis we will consider theories that are motivated by these experimental phenomena and/or theoretical issues and are suited to explain one or more of them. There are several approaches one can take. One idea is to simply extend the SM Higgs sector with additional scalar singlets or doublets, with one possible model being the complex singlet extension of the SM (CxSM) [32–44], which is considered in the first project contained in this thesis. The CxSM is obtained from the SM by extending the scalar sector with an additional complex singlet, which already leads to an interesting phenomenology, as it can e.g. provide a DM candidate. These scalar extensions of the SM can be used to accommodate for the unexplained phenomena, e.g. DM or the matter-antimatter asymmetry, but they do not solve the theoretical issues of the SM described above. They can be seen as a phenomenological exploration of the possible NP landscape. Another approach to NP is to take one of the theoretical problems of the SM and use it as a motivation towards new theories. For example, the hierarchy problem can be used as a motivation for composite Higgs models [45–54] or supersymmetric models [55–64]. These models can be seen as a UV completion of the SM at higher energies and are used to try to explain both the theoretical issues of the SM as well as the unexplained experimental phenomena. In this thesis we consider a composite 2-Higgs-doublet model (2HDM) [65–69] and the next-to-minimal supersymmetric extension of the SM (NMSSM) [70, 71]. As a side remark, we thus consider theories with an additional complex singlet (the CxSM), 2 Higgs doublets (the composite 2HDM), and 2 Higgs doublets and one complex scalar singlet (the NMSSM), highlighting the available possibilities for new physics in the Higgs sector.

The overarching goal of this thesis is to explore these different avenues towards new phyiscs. We perform calculations to give precise predictions and do phenomenological studies to be able to compare with current and future experimental results. The work shown in this thesis is based on the research papers in Refs. [72–74] and ongoing work that will soon be published.

We now present the structure of the thesis. First, in Chapter 2 we introduce some concepts and notations. We present the SM Higgs sector in Sec. 2.1, which leads us to the discussion of the hierarchy problem (Sec. 2.2) and some possible explanations, i.e. compositeness and supersymmetry (SUSY). We then describe the theoretical and experimental status of di-Higgs production in Sec. 2.3 and highlight the importance of this measurement for the SM and BSM models.

After this introduction, we move on to the three projects contained in this thesis. In Part I, we discuss the CxSM, where we calculate the electroweak (EW) next-to-leading-order (NLO)

corrections to Higgs decays and investigate their impact. We first give an introduction to the model and the setup we use in Chapter 3. Then, we discuss the renormalization of the model and the calculations that we performed to obtain the NLO corrected decay widths in the Chapters 4 and 5. Next, we describe the implementation of our analytical results into the code `EWsHDECAY`, present our setup to obtain viable parameter points, including the discussion of theoretical and experimental constraints, and examine the typical sizes of the NLO corrections and their impact on the phenomenological landscape in Chapter 6. We give a conclusion of the project in Chapter 7.

In the next project (Part II), we consider a composite 2HDM, where we analyze di-Higgs production in this model. In Chapter 8 we give an introduction to composite Higgs models, and the specific realization that we use. Next, we present the calculation we performed to obtain the leading-order (LO) cross section for di-Higgs production, given the couplings of the composite 2HDM in an effective Lagrangian approach in Chapter 9. We also mention the NLO quantum chromodynamics (QCD) corrections in the heavy quark limit. Furthermore, in Chapter 10 we describe the implementation of our analytic results for the cross sections and the setup we used to obtain viable parameter points, which we then used for our phenomenological study. We analyze the impact of the composite 2HDM on di-Higgs production, compared to the SM and other 2HDM models, both on inclusive results as well as differential distributions. Finally, we give a conclusion to the project in Chapter 11.

In the third and final project (Part III) contained in this thesis, we discuss a supersymmetric model, the NMSSM. We calculate the supersymmetric particle decays in this model and implement them into an extended version of the program `SDECAY` [75, 76], which is then combined with the program `NMSSMCALC` [77–82] to perform phenomenological studies. We first give an introduction to supersymmetry (SUSY) and the NMSSM in Chapter 12, where we also renormalize the model for the NLO QCD corrections, which we included. Next, we describe the calculation of the supersymmetric decays in the NMSSM in Chapter 13, including two-body and three-body decays, radiative loop decays as well as NLO QCD corrections to the two-body decays. In Chapter 14 we present the implementation of our calculation and the setup we use to perform parameter scans. We then discuss some benchmark point scenarios. Finally, we give a conclusion in Chapter 15.

After we discussed the third and final project in this thesis, we give an overall summary and outlook in Chapter 16.

CHAPTER 2

Prerequisites

Before introducing the projects that are contained in this thesis, we review some important aspects relevant for upcoming parts. In Sec. 2.1, we first briefly summarize the Standard Model (SM) scalar sector. Next, we discuss the hierarchy problem (Sec. 2.2), which is one of the core motivations for composite Higgs models and supersymmetric models considered in the parts II and III. Finally, in Sec. 2.3 we elaborate on the importance of measuring the Higgs self-coupling via Higgs pair production, the current experimental and theoretical status and how we apply the experimental limits on di-Higgs production in our models.

2.1. The Scalar Sector of the Standard Model

In this section we will give a brief introduction to the SM, following [83]. With the discovery of the Higgs boson [9, 10] almost five decades after its proposal [4–8], the SM is complete, all predicted particles have been found. The SM is a gauge theory with an $SU(3)_c \times SU(2)_L \times U(1)_Y$ gauge group [1–3], where the $SU(3)_c$ describes the quantum chromodynamics (QCD) interactions with the gluon g and the $SU(2)_L \times U(1)_Y$ the electroweak (EW) interactions with the gauge bosons W, Z and the photon γ. The gluon, the W and Z bosons and the photon are the particles mediating the forces. Experimentally it was found that the W and Z bosons are massive, but mass terms for these fields in the Lagrangian are forbidden by the gauge symmetry. Similarly, mass terms for chiral fermions, where left- and right-handed fields transform differently under the $SU(2)_L$ symmetry, are also forbidden. Thus, the Higgs mechanism was introduced as an elegant solution to obtain massive gauge bosons and fermions via spontaneous symmetry breaking, i.e. without explicitly breaking the gauge symmetries.

In the following, we give a brief introduction into the Higgs sector of the SM (cf. e.g. [84]). We have a complex $SU(2)_L$ scalar doublet Φ, where the scalar Lagrangian $\mathcal{L}_{\text{Scalar}}$ is given by

$$\mathcal{L}_{\text{Scalar}} = (D_\mu \Phi)^\dagger (D^\mu \Phi) - V_{\text{SM}} \,. \tag{2.1}$$

Here D_μ is the covariant derivative [85],

$$D_\mu = \partial_\mu + ig\frac{\sigma^a}{2} W_\mu^a + ig'\frac{Y}{2} B_\mu \,, \tag{2.2}$$

with W_μ^a $(a = 1, 2, 3)$ and B_μ being the $SU(2)_\mathrm{L}$ and $U(1)_\mathrm{Y}$ gauge boson fields from the SM and g, g' the corresponding gauge couplings, the hypercharge Y and σ^a the Pauli matrices. The scalar potential V_SM can be written as

$$V_\mathrm{SM} = \frac{\mu^2}{2}\Phi^\dagger\Phi + \frac{\lambda}{4}\left(\Phi^\dagger\Phi\right)^2 , \tag{2.3}$$

with the mass parameter μ^2 and the quartic coupling λ. Since the Higgs doublet Φ transforms under the SM EW gauge groups, no other renormalizable terms are allowed in the potential.

Next, we expand Φ as

$$\Phi = \begin{pmatrix} G^+ \\ \frac{1}{\sqrt{2}}\left(v + H + iG^0\right) \end{pmatrix} , \tag{2.4}$$

where we introduced the scalar fields H, G^0, G^+ and the vacuum expectation value (VEV) v. The fields G^0 and G^+ are so-called would-be Goldstone bosons, as they will be absorbed by the W and Z bosons to obtain massive gauge fields. The VEV v is chosen in order to satisfy the minimization condition

$$\frac{\partial V_\mathrm{SM}}{\partial v} = 0 , \tag{2.5}$$

i.e. with Eq. (2.4) we expand the Lagrangian around the minimum of the potential. In this case we obtain the relation

$$0 = \frac{v}{2}\left(\mu^2 + \frac{v^2\lambda}{2}\right) . \tag{2.6}$$

The quartic coupling λ has to be positive for the potential to be bounded from below, and therefore we need $\mu^2 < 0$ to obtain a non-zero VEV v. We then can relate λ to the Higgs mass parameter μ^2 and the VEV v via

$$\lambda = \frac{-2\mu^2}{v^2} . \tag{2.7}$$

The interactions with fermions are given by the Yukawa Lagrangian $\mathcal{L}_\mathrm{Yuk}$,

$$\mathcal{L}_\mathrm{Yuk} = -\bar{L}_\mathrm{L} Y_l \Phi l_\mathrm{R} - \bar{Q}_\mathrm{L} Y_d \Phi d_\mathrm{R} - \bar{Q}_\mathrm{L} Y_u \tilde{\Phi} u_\mathrm{R} + \mathrm{h.c.} , \tag{2.8}$$

where we have in general complex matrices Y_l, Y_d, Y_u, for the leptons and the up- and down-quarks, respectively, and

$$\tilde{\Phi} \equiv i\sigma_2\Phi^* . \tag{2.9}$$

Here, L, Q depict the left-chiral doublets and l_R, d_R, u_R the right-chiral fields, and we have the Pauli matrix σ_2. Expanding the doublet Φ again with Eq. (2.4) results in mass terms for the fermions.

With this setup, we then obtain masses for the gauge bosons m_V and masses for the fermions m_f that are proportional to the Higgs VEV v, i.e.

$$m_f \sim y_f v , \qquad m_V \sim g v , \tag{2.10}$$

with the Yukawa couplings y_f for the fermions and the gauge couplings g of the gauge bosons. The mass of the Higgs is proportional to the Higgs mass parameter, i.e. $m_h^2 \sim |\mu^2|$. Thus,

the scalar sector of the SM is already determined by the Higgs mass and the VEV v since the quartic self-coupling λ can be derived with Eq. (2.7).

This already concludes the introduction to the SM Higgs sector. There are, however, some interesting remarks to be made. First of all, the setup with only one Higgs doublet is the minimal choice that can be made and is compatible with experimental data. One could, however, extend this setup with additional singlet or doublet fields (as we will do in part I) and obtain new theories with rich phenomenologies.

Another interesting point is the fact that the Higgs mass parameter μ^2 is the only dimensionful parameter in the SM.[1] If we now consider the SM as a low-energy effective theory that resolves to a UV complete theory at higher energies, we can use naive dimensional analysis to estimate the Higgs mass parameter. We would then expect that the dimensionful quantity is proportional to some mass scale Λ given by the UV complete theory, e.g. the cutoff scale where our effective theory of the SM is no longer valid. Since we have not yet found any physics beyond the SM, we expect this scale Λ to be rather large, with an ultimate upper limit at the Planck scale, M_{planck} [31],

$$M_{\text{planck}} \sim \frac{1}{\sqrt{G_{\text{N}}}} \sim 1 \times 10^{19}\,\text{GeV}\,, \tag{2.11}$$

with the gravitational constant G_{N}, where we expect a new theory to emerge that unites particle physics and general relativity.

Thus, we would expect the Higgs mass parameter and therefore the Higgs mass to be rather heavy, which is in strong contrast with the experimental value of a 125 GeV Higgs boson. This apparent discrepancy is called the hierarchy problem and will be discussed in the following section.

Another remark to be made is that in the SM the scalar sector is already determined by the VEV v and the Higgs mass m_h, i.e. all the Higgs self-couplings can be calculated and predicted. Thus, measuring the Higgs self-interactions gives key insights into the nature of the Higgs boson, and whether the SM correctly describes the Higgs boson and the Higgs mechanism, as we will discuss in more detail in Sec. 2.3.

2.2. The Hierarchy Problem

In this section, we describe the hierarchy problem in more detail and give some conceptual ideas to solve it. We follow here the reviews on the hierarchy problem given in [62, 86–90].

As already mentioned in Sec. 2.1, the hierarchy problem is essentially the tension between the naive prediction that a certain value has to be large, whereas the experiments measure a relatively small value without an apparent reason in the theory (where large and small have to be seen in the context). In the SM, this is the case, as already explained, for the Higgs mass. The mass parameter in the scalar potential (and therefore the Higgs mass) would naively be expected in an effective field theory approach to be of the order of the cut-off scale of the theory, as described in Sec. 2.1. Even if the coefficient is absent at leading order, it would be generated at loop level if the SM Higgs couples to the new heavy physics, and we again would have the scaling relation $\mu \sim \Lambda$.

Thus, we are in a paradox situation that we expect new physics to appear at higher energies that either would be in conflict with the measured SM-like Higgs or lead to massive fine

[1] if we consider the potential parameters μ^2 and λ as input and use Eq. (2.7) to then relate μ^2 and the VEV v. Furthermore, we can relate all the gauge boson and fermion masses to the VEV v and use the dimensionless Yukawa and gauge couplings as input.

tuning issues. A possible solution is to develop a mechanism that is incorporated into a UV complete theory at higher energies and leads to a relatively small Higgs mass. There are several approaches to this mechanism (see e.g. [88, 91] for a list of approaches). We will focus in the following on symmetry based solutions.

One possible idea to solve the hierarchy problem is the concept of technical naturalness [92]. Here, symmetries are used to explain how a parameter can be naturally small. In the SM, we have masses for fermions and gauge bosons, and we can ask the question if they also would obtain large corrections from new physics contributions at higher energies. This is, however, not the case, since they are protected by symmetries. In the case of fermions, it is the chiral symmetry (i.e. left- and right-handed parts of fermions transform differently in the SM, and a mass term would mix them), and in the gauge boson case it is the gauge symmetry. Mass terms for these fields are therefore forbidden in the SM, and we need the Higgs mechanism to spontaneously break the symmetries and obtain masses for fermions and gauge bosons. Thus, in the limit of vanishing fermion or gauge boson masses, we no longer break these symmetries. These vanishing masses are protected by the symmetries in the sense that we cannot break the symmetries with higher-order corrections, i.e. we cannot reintroduce the mass terms through loop effects. The masses are zero to all orders. Following this statement, we see that the loop corrections in the case of non-vanishing masses have to be proportional to the masses themselves since then the higher-order corrections vanish in the case of zero masses.

Thus, we conclude that the corrections to the masses have to be proportional to the masses themselves and cannot be proportional to some new physics scale Λ at higher energies (at least not quadratically, we can still have a logarithmic dependence that does not negate our arguments and is better behaved, i.e. would not lead to large corrections and no hierarchy problem). Therefore, if the masses are small, they remain small because of the protection of the symmetry that is broken by the mass parameter. This mechanism is called technical naturalness.

In the SM, the Higgs mass parameter respects all the symmetries of the SM, and therefore setting it to zero does not restore any symmetries, the parameter is not technically natural. Therefore, a possible solution to the hierarchy problem is to relate the Higgs mass parameter to some new symmetry in order to make it technically natural. Moreover, from the point of view of a UV complete theory, using symmetries at higher energies is an elegant way to obtain light particles (compared to e.g. the Planck scale) and in fact all elementary particles found thus far in the SM have mass parameters that are protected by symmetries and are therefore technically natural, except for the Higgs boson.

In the following, we will describe two possible theories with symmetry solutions to the hierarchy problem that will play a role later in this thesis. One possible symmetry extension is supersymmetry (SUSY). We will give a short introduction to SUSY in Sec. 12.1 and refer to the excellent reviews [62–64, 70, 71, 93, 94]. In SUSY, an additional symmetry is introduced, which relates fermions and bosons and also their masses and interactions. The scalar Higgs thus obtains a so-called superpartner, the Higgsino, a chiral fermion. As we already saw, the masses of chiral fermions are technically natural, and via SUSY this then also translates to the scalar Higgs mass. This protection manifests itself if one for example calculates the loop corrections to the Higgs mass. If SUSY is realized in nature, the contributions from fields in the loops would cancel out with the contributions from their superpartners (see e.g. [63] for an explicit calculation).

Another possible solution to the hierarchy problem is the usage of the Goldstone boson theorem. Here, we introduce an additional symmetry that is spontaneously (and later explicitly) broken, and the Higgs is one of the scalar Goldstone bosons. Due to the remaining Goldstone

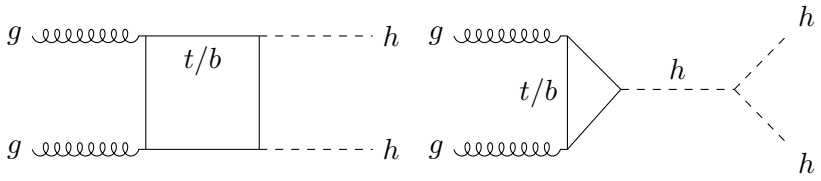

Figure 2.1.: The Feynman diagrams appearing in the SM, contributing to Higgs pair production with top and bottom quarks (t, b) in the loop. The diagrams here and in the following were created with [96].

boson shift-symmetry, i.e. we can shift the fields by a constant, only terms containing derivatives of the fields are allowed in the Lagrangian, whereas mass terms and terms in the scalar potential are forbidden. Thus, the Goldstone bosons are massless. By explicitly breaking the additional symmetry, we can generate a mass term that is then technically natural. This approach is used e.g. in composite Higgs models (see Sec. 8.1 and the reviews [54, 86, 88, 95]). Moreover, we know that this approach is already realized in nature, as it can be used to explain why the mass of the pion meson is light compared to the QCD scale (cf. [54]).

To conclude, we see that the hierarchy problem is one of the remaining unsolved theoretical issues of the SM and it can be used to incorporate solution mechanisms that can lead to interesting new theories beyond the SM.

2.3. Higgs Pair Production

After the discovery of the Higgs at the LHC, the next step has been to measure all the properties of the Higgs boson and its couplings [97, 98]. One important interaction, however, that has not been measured experimentally yet is the Higgs self-interaction. It is not only a predicted coupling from the SM that has not yet been verified, but it also gives further insight into the Higgs potential and a validation of the mechanism of electroweak symmetry breaking (EWSB).

Experimentally, the Higgs self-interaction can be measured via Higgs pair production. In the SM, the most important channel at the LHC is gluon fusion into di-Higgs production. The relevant Feynman diagrams are given in Fig. 2.1 where we have a box and a triangle diagram with quarks in the loop. The triangle diagram contains the dependence on the trilinear Higgs coupling. The box and triangle contributions, however, interfere destructively, leading to an overall small cross section. The calculation for di-Higgs production at LO was performed in [99–101]. The first higher-order corrections were performed in the heavy top limit [102]. Since then, many higher-order calculations have been performed [103–134] with the total di-Higgs cross section value given as 31.05 fb at next-to-next-to-leading order (NNLO) $\text{FT}_{\text{approx}}$ [117], i.e. in the heavy-top limit with full leading-order (LO) and next-to-leading-order (NLO) mass effects and full mass dependence in the one-loop double real corrections at NNLO QCD. Additionally, Higgs pair production has been discussed in theories beyond the SM, e.g. in [135–151], in composite Higgs models [152–156], and SUSY models [157–163].

Due to the destructive interference at LO, the cross section of di-Higgs production is small and therefore challenging to measure experimentally. The experimental searches can be divided into two categories, *non-resonant* and *resonant* searches. In *non-resonant* searches the current experimental limits are 2.4-times the SM prediction with the trilinear couplings to be constrained to $-1.4 < \kappa_\lambda < 6.1$ for the ATLAS experiment [164], and 3.4-times the SM

prediction and $-1.24 < \kappa_\lambda < 6.49$ for CMS [98]. Here, κ_λ is defined as the trilinear coupling normalized to the SM trilinear coupling,

$$\kappa_\lambda = \frac{\lambda_{hhh}}{\lambda_{hhh}^{\mathrm{SM}}}\,, \tag{2.12}$$

and thus describes the deviation from the SM prediction. It should be noted that the limits on κ_λ do not assume any beyond SM (BSM) contributions to the overall cross sections, and therefore the cross section limits are better suited to constrain models beyond the SM. In BSM theories, we can have additional particles, couplings, or diagrams that can contribute to the overall cross section and also lead to deviations in differential distributions. One important contribution may occur if additional heavy scalars are present in the theory that can be resonantly produced and then decay into a pair of SM-like Higgs bosons. This can increase the overall cross section significantly.

In *resonant* searches, an additional heavy scalar with mass m_H and a small width Γ_H is assumed, and the expected distribution of this setup is compared with the experimentally measured results. Thus, by varying m_H in the hypothesis, either a discovery for a certain mass can be made or upper limits on the cross sections depending on the heavy Higgs mass can be obtained. Thus far, no resonant Higgs has been found. We use the upper limits from [165–177] as *resonant* constraints on our models.

Finally, we describe how we applied the *resonant* and *non-resonant* limits on our models with extended scalar sectors where we potentially have a SM-like Higgs h and a heavy Higgs H. In our approach, we follow [150]. We start with the categorization of parameter points in a model. If for a given parameter point the heavy Higgs mass m_H is smaller than $2m_h$, with the SM-like mass m_h, i.e. no resonant enhancement of the triangle diagram is kinematically possible, the point will be labelled *non-resonant*. Moreover, if the heavy Higgs contribution is small compared to the full cross section, it would not be distinguishable from an experimental point of view, based on the total cross section measurement. Thus, we define a point to be *non-resonant* if the single heavy Higgs production and decay into SM-like Higgs pairs is less than 10 % of the total di-Higgs cross section. We then apply *non-resonant* limits on the full cross section.

The *resonant* limits, in principle, are applied to all parameter points. Here we calculate the single heavy Higgs production cross section times branching ratio into a pair of SM-like Higgs times the branching ratios of the SM-like Higgs into the final state considered in the various experimental analyses [165–177]. If the parameter point exceeds one of the experimental limits, it is rejected. The experimental searches, however, apply the narrow width approximation. Therefore, their limits can only be safely employed if the total width of the heavy Higgs is small. We thus only apply *resonant* limits to points with a total width that satisfies

$$\frac{\Gamma_H}{m_H} \leq 5\,\%\,. \tag{2.13}$$

Otherwise, the resonant limits will not be considered.

Part I.

Electroweak Corrections to Higgs Decays in the Complex Singlet Extension of the Standard Model

CHAPTER 3

Introduction to the CxSM

In this project, we studied the complex singlet extension of the Standard Model (CxSM). By adding only a complex scalar singlet to the theory, it is one of the simplest extensions of the Standard Model (SM). The scalar sector is, in our realization of the model, increased by an additional Higgs boson and a dark matter (DM) candidate. Thus, the model exhibits an interesting phenomenology and may answer (or at least give hints to) some of the open questions of the SM, as for example the nature of DM. Models obtained by adding singlets (or doublets) have a good theoretical motivation. Extended Higgs sectors naturally emerge in theories beyond the SM, e.g. in supersymmetric theories at least two Higgs doublets are needed for a consistent theory [62]. Moreover, the parameters of the potential in these theories are free parameters (in contrast to e.g. the composite or the supersymmetric case in part II and III, where the Higgs potential is more constrained), but they do not solve the hierarchy problem and can be seen as an agnostic approach to explore the phenomenological landscape beyond the SM.

Singlet extensions of the SM have been studied in the literature [32–44]. Our goals in this project were to analyze the allowed parameter ranges and the calculation of the next-to-leading-order (NLO) electroweak (EW) corrections of all Higgs decay channels in this model. We then analyzed the behaviour of these corrections, what sizes they typically have, if they can become sizeable and why, what the theoretical uncertainty estimate based on the choice of a specific renormalization scheme is and if the corrections have a significant impact on the parameter space.

In the following, we present our approach. We choose a suitable set of input parameters, work out the renormalization of the model, calculate the NLO corrections to all Higgs decay channels in the theory, generate a viable set of parameter points considering the most relevant theoretical and experimental constraints, and then perform an analysis to answer the above mentioned questions.

In this chapter, we give the theoretical description of the model, set our notation and the symmetries that we impose on our scalar potential, describe our chosen set of input parameters and list the theoretical and experimental constraints we applied.

This part follows our published results [72, 73] and takes over, where needed, some results from [178].

3.1. The CxSM Lagrangian

The CxSM is obtained from the SM by extending the scalar sector by a complex singlet field $\mathbb{S}$. The additional scalar field is uncharged under all SM gauge groups and only couples to the SM Higgs doublet. These types of models are also called Higgs portal models.

The general structure of the Lagrangian is

$$\mathcal{L}_{\text{CxSM}} = \mathcal{L}_{\text{SM}\setminus\{\text{Scalars}\}} + \mathcal{L}_{\text{S}}, \tag{3.1}$$

where $= \mathcal{L}_{\text{SM}\setminus\{\text{Scalars}\}}$ refers to the SM Lagrangian without the Higgs sector and $\mathcal{L}_{\text{S}}$ describes the extended scalar part,

$$\mathcal{L}_{\text{S}} = (D_\mu \Phi)^\dagger (D^\mu \Phi) + \partial_\mu \mathbb{S}^* \partial^\mu \mathbb{S} - V_{\text{Scalar}}\,, \tag{3.2}$$

with the SM Higgs doublet Φ, the covariant derivative D_μ (see Eq. (2.2)) and the scalar potential V_{Scalar}. We impose a global $U(1)$ symmetry on the scalar singlet that is softly broken. The scalar potential then reads (compare with [42, 43], where also other realizations are discussed),

$$V_{\text{Scalar}} = \frac{m^2}{2}\Phi^\dagger\Phi + \frac{\lambda}{4}\left(\Phi^\dagger\Phi\right)^2 + \frac{\delta_2}{2}\Phi^\dagger\Phi|\mathbb{S}|^2 + \frac{b_2}{2}|\mathbb{S}|^2 + \frac{d_2}{4}|\mathbb{S}|^4 + \left(\frac{b_1}{4}\mathbb{S}^2 + a_1\mathbb{S} + c.c.\right), \tag{3.3}$$

with the potential parameters m^2, λ, δ_2, b_2 and d_2 that are real and the soft breaking parameters b_1 and a_1 that can be complex in general. We split up the scalar fields into their real and imaginary components and also the vacuum expectation values (VEVs) v, v_S and v_A,

$$\Phi = \begin{pmatrix} G^+ \\ \frac{1}{\sqrt{2}}\left(v + H + iG^0\right) \end{pmatrix}, \; \mathbb{S} = \frac{1}{\sqrt{2}}(v_S + S + i(v_A + A))\,. \tag{3.4}$$

As is the case in the SM, the $G^\pm$ and G^0 will become the Goldstone bosons for the $W^\pm$ and Z bosons. The real scalar fields H, S, A will give the particle spectrum of the scalar sector.

We specify our realization of the CxSM further by imposing a $\mathbb{Z}_2$ symmetry separately on the real part S and the imaginary part A of the complex singlet field $\mathbb{S}$, i.e. the Lagrangian has to be invariant under both $S \to -S$ and $A \to -A$. Thus, $a_1 = 0$ and b_1 is real. We impose these $\mathbb{Z}_2$ symmetries in order to obtain a stable DM candidate. The $\mathbb{Z}_2$ symmetry for A needs to be conserved and not be spontaneously broken, i.e. $v_A = 0$, whereas we spontaneously break the symmetry of the field S with a nonzero value for the VEV v_S. We obtain for the potential

$$V_{\text{Scalar}} = \frac{m^2}{2}\Phi^\dagger\Phi + \frac{\lambda}{4}\left(\Phi^\dagger\Phi\right)^2 + \frac{\delta_2}{2}\Phi^\dagger\Phi|\mathbb{S}|^2 + \frac{b_2}{2}|\mathbb{S}|^2 + \frac{d_2}{4}|\mathbb{S}|^4 + \left(\frac{b_1}{4}\mathbb{S}^2 + c.c.\right). \tag{3.5}$$

Expanding the scalar fields in the potential according to Eq. (3.4), we see that the fields H and S mix. Rotating the fields via the relation

$$\begin{pmatrix} h_1 \\ h_2 \end{pmatrix} = R_\alpha \begin{pmatrix} H \\ S \end{pmatrix}, \tag{3.6}$$

with the rotation matrix

$$R_\alpha = \begin{pmatrix} \cos\alpha & \sin\alpha \\ -\sin\alpha & \cos\alpha \end{pmatrix} \equiv \begin{pmatrix} c_\alpha & s_\alpha \\ -s_\alpha & c_\alpha \end{pmatrix}, \tag{3.7}$$

we can rotate the gauge eigenstates H and S into the mass eigenstates h_1 and h_2 with masses $m_{h_1} \leq m_{h_2}$, i.e. we have

$$\text{diag}(m_{h_1}^2, m_{h_2}^2) \equiv D_{hh}^2 = R_\alpha \mathcal{M} R_\alpha^T \,, \tag{3.8}$$

for the mass matrix given D_{hh}^2 in the basis of the mass eigenstates. The matrix $\mathcal{M}$ in the gauge eigenstate basis (H, S) is given by

$$\mathcal{M} = \begin{pmatrix} \frac{v^2\lambda}{2} & \frac{\delta_2 v v_S}{2} \\ \frac{\delta_2 v v_S}{2} & \frac{d_2 v_S^2}{2} \end{pmatrix} + \begin{pmatrix} \frac{T_1}{v} & 0 \\ 0 & \frac{T_2}{v_S} \end{pmatrix}, \tag{3.9}$$

where the tadpole parameters T_1, T_2 are defined as

$$\frac{\partial V}{\partial v} \equiv T_1 \;\Rightarrow\; \frac{T_1}{v} = \frac{m^2}{2} + \frac{\delta_2 v_S^2}{4} + \frac{v^2\lambda}{4}, \tag{3.10a}$$

$$\frac{\partial V}{\partial v_S} \equiv T_2 \;\Rightarrow\; \frac{T_2}{v_S} = \frac{b_1 + b_2}{2} + \frac{\delta_2 v^2}{4} + \frac{v_S^2 d_2}{4} \,. \tag{3.10b}$$

The mass term of the field A reads

$$m_A^2 = \frac{-b_1 + b_2}{2} + \frac{\delta_2 v^2}{4} + \frac{v_S^2 d_2}{4} = -b_1 + \frac{T_2}{v_S}, \tag{3.11}$$

and it does not mix with the other scalar fields. At tree-level we have $T_1 = T_2 = 0$.

Since we rotate the SM Higgs field H and the singlet field S into the mass eigenstates h_1 and h_2, they will couple to the SM particles with a coupling modifier defined by the rotation angle, i.e. we obtain

$$g_{h_i SM\,SM} = g_{H_{\text{SM}} SM\,SM} k_i \,, \quad k_i \equiv \begin{cases} \cos\alpha \,, & i = 1 \\ -\sin\alpha \,, & i = 2 \end{cases} \,, \tag{3.12a}$$

$$g_{h_i h_j SM\,SM} = g_{H_{\text{SM}} H_{\text{SM}} SM\,SM} k_i k_j \tag{3.12b}$$

for any coupling $g_{h_i SM\,SM}$ (or $g_{h_i h_j SM\,SM}$) between h_i (and h_j) and two SM particles ($i, j = 1, 2$). The $g_{H_{\text{SM}} SM\,SM}$ symbolizes the SM Higgs couplings to two SM particles, the $g_{H_{\text{SM}} H_{\text{SM}} SM\,SM}$ the quartic couplings between two SM Higgs and two SM particles.

Finally, in the scalar potential we have 6 free parameters (m, λ, δ_2, b_2, d_2, b_1) that we can exchange with the help of the above mentioned relations to our chosen set of input parameters:

$$v \,,\; v_S \,,\; \alpha \,,\; m_{h_1} \,,\; m_{h_2} \,,\; m_A. \tag{3.13}$$

The potential parameters can be written in terms of the chosen input parameters as

$$\lambda = \frac{m_{h_1}^2 + m_{h_2}^2 + \cos 2\alpha (m_{h_1}^2 - m_{h_2}^2)}{v^2} \,, \tag{3.14a}$$

$$d_2 = \frac{m_{h_1}^2 + m_{h_2}^2 + \cos 2\alpha (m_{h_2}^2 - m_{h_1}^2)}{v_S^2} \,, \tag{3.14b}$$

$$\delta_2 = \frac{(m_{h_1}^2 - m_{h_2}^2)\sin 2\alpha}{v v_S} \,, \tag{3.14c}$$

$$m^2 = \frac{1}{2}\left(\cos 2\alpha (m_{h_2}^2 - m_{h_1}^2) - \frac{v(m_{h_1}^2 + m_{h_2}^2) + v_S (m_{h_1}^2 - m_{h_2}^2)\sin 2\alpha}{v} \right) \,, \tag{3.14d}$$

$$b_2 = \frac{1}{2}\left(2m_A^2 - m_{h_1}^2 - m_{h_2}^2 + \cos 2\alpha (m_{h_1}^2 - m_{h_2}^2) - \frac{v(m_{h_1}^2 - m_{h_2}^2)\sin 2\alpha}{v_S} \right) \,, \tag{3.14e}$$

$$b_1 = -m_A^2 \,. \tag{3.14f}$$

3.2. Theoretical and Experimental Constraints

In this section, we describe the various experimental and theoretical constraints we considered and applied to our parameter scans in order to obtain a valid parameter sample. We follow here mainly the works in [72, 178, 179] where more details can be found. All constraints described here are implemented in the code `ScannerS` [42, 179] or applied additionally to the parameter sample.

3.2.1. Theoretical Constraints

The following theoretical constraints were considered.

- **Boundedness from Below:**

  In order to do a perturbative expansion around the minimum of the scalar potential chosen by the input parameters, the potential has to be bounded from below. Otherwise, the ground state would not be stable. The constraints

  $$\lambda > 0 \wedge d_2 > 0 \wedge (\delta_2^2 < \lambda d_2 \,\text{if}\, \delta_2 < 0), \tag{3.15}$$

  have to be fulfilled for the potential parameters (compare with [178, 179]).

- **Vacuum Stability:**

  Apart from the condition that the potential is bounded from below, it has to be checked that the EW minimum of the potential with $v = 246\,\text{GeV}$ chosen by the input parameters is actually the global minimum. Otherwise, the ground state would be metastable and the system could move into a deeper global minimum, which does not have $v = 246\,\text{GeV}$ and is hence unphysical. It can be shown, however, that the chosen minimum $(v, v_S, v_A = 0)$ is the global minimum of the potential (at least at tree level), if

  $$\delta_2^2 < \lambda d_2, \tag{3.16}$$

  holds, which is automatically the case with our chosen set of input parameters (see [72, 178] for more details). Therefore, the minimum $(v, v_S, v_A = 0)$ is automatically the global minimum and stable at tree level.

- **Perturbative Unitarity:**

  Due to the freedom in the input parameters, the quartic scalar couplings can become sizeable, and the resulting interactions can violate unitarity, i.e. a perturbative approach is not possible. Unitarity constraints are obtained by constraining the eigenvalues λ_i of the $2 \to 2$ scattering matrix $\mathcal{M}_{2\to 2}$ via (c.f. [180])

  $$|\lambda_i| \leq 8\pi\,. \tag{3.17}$$

  This results in the relations (see also [178, 179])

  $$|\lambda| \leq 16\pi \wedge |d_2| \leq 16\pi \wedge |\delta_2| \leq 16\pi \wedge \left|\frac{3}{2}\lambda + d_2 \pm \sqrt{\left(\frac{3}{2}\lambda - d_2\right)^2 + 2\delta_2^2}\right| \leq 16\pi\,. \tag{3.18}$$

3.2.2. Experimental Constraints

The following experimental constraints were considered.

- **Electroweak Precision Parameters:**

  The beyond SM (BSM) deviations from the electroweak precision observables (EWPOs) can be parametrized by the S, T, U parameters [181, 182]. They are given in terms of the gauge boson self-energies, that obtain additional contributions in the CxSM. These deviations have to be within the experimental limits. `ScannerS` uses a fit result and compares the theoretical and experimental values for their compatibility.

- **Higgs Searches and Measurements:**

  Since the discovery of the Higgs boson, its properties and couplings to SM particles have been measured, and searches for additional scalar particles were conducted. In the CxSM the couplings of the SM-like Higgs are modified and we have additional scalars that can be detected. Thus, in turn the CxSM parameter space is constrained in order to avoid the experimental limits. `ScannerS` implements these limits via the tools `HiggsBounds` [183–187] and `HiggsSignals` [188, 189]. Moreover, we additionally checked for *resonant* di-Higgs constraints, where we followed the approach in [150], see also Secs. 2.3 and 6.2.

- **Dark Matter Searches and Cosmological Constraints:**

  The CxSM contains a viable dark matter candidate that can contribute to the DM abundance in the universe. Thus, we have to constrain the parameter space in order to not exceed the measured value of the DM relic density (we allow for smaller abundances and therefore additional contributions from other sources). `ScannerS` uses the tool `MicrOMEGAs` [190–192] to calculate the relic density and include this constraint.

  Additionally, the CxSM is constrained by direct detection searches for DM. Due to a cancellation at LO, the tree-level cross section is negligible in the CxSM [193, 194]. The one-loop corrected cross sections (cf. [195, 196]), however, have to be below the experimental limits, where we considered [197–199]. We will discuss these constraints in more detail in Sec. 6.2.

CHAPTER 4

Renormalization of the CxSM

In quantum field theories, UV and IR divergences can appear in higher-order calculations. In order to obtain meaningful results, they have to be treated properly. The UV divergences are cancelled through regularization and renormalization (cf. [85]). IR divergences have to be treated differently, see Sec. 5.3.1.

A common regularization prescription is (the so-called) dimensional regularization, in which the appearing loop integrals are not calculated in 4 but in $D = 4 - 2\epsilon$ dimensions. The divergences will then appear as ϵ^{-1} poles in the calculation. Constant terms that reappear throughout the calculation are often combined into

$$\Delta_\epsilon \equiv \frac{1}{\epsilon} - \gamma_\mathrm{E} + \ln(4\pi)\,, \tag{4.1}$$

with the Euler constant γ_E.

Next, a given input parameter is redefined via a renormalized parameter λ and the counterterm parameter $\delta\lambda$ as

$$\lambda_0 = \lambda + \delta\lambda\,, \tag{4.2}$$

where λ_0 is the bare parameter that appears in the unrenormalized Lagrangian. Similarly, the bare field Φ_0 appearing in the Lagrangian is shifted by the field wave function Z_Φ via

$$\Phi_0 = \sqrt{Z_\Phi}\Phi \approx (1 + \frac{\delta Z_\Phi}{2})\Phi\,. \tag{4.3}$$

We expanded the square root up to NLO. The counterterm $\delta\lambda$ and the wave function renormalization constant δZ_Φ are determined by renormalization conditions. In a renormalizable theory, as is the SM, the UV-divergent parts of the counterterms cancel the UV divergences, leading to UV finite physical observables. The renormalization conditions furthermore fix the finite parts of the counterterms. For more details on renormalization we refer to other works, e.g. [85, 200].

In this chapter, we discuss the renormalization of the CxSM. We will follow the prescriptions given in [72, 73] and [178]. Similar renormalization schemes have been worked out for other

models [201, 202]. We will start by discussing the renormalization of the scalar sector and describe the different renormalization schemes of the additional input parameters in the model that we worked out and applied in this project in Sec. 4.1. We will then mention the fermion and gauge boson sectors (Sec. 4.2), where we applied the prescriptions described in [200]. Finally, we also discuss how we change between renromalization schemes in Sec. 4.3, as this will be useful to discuss the theoretical uncertainty of our calculations.

4.1. Scalar Sector

In this section, we describe the renormalization of the scalar sector. We start with the renormalization of the fields and the mass parameters (Sec. 4.1.1) and also comment on how we renormalized the tadpoles. Then, we move on to the remaining input parameters, i.e. the schemes we applied to renormalize the mixing angle α (Sec. 4.1.2) and the singlet VEV v_S (Sec. 4.1.3).

4.1.1. Mass and Field Renormalization

We split up our fields and masses into renormalized fields and masses and corresponding counterterms. Thus, we write

$$A_0 = \sqrt{Z_A} A \approx \left(1 + \frac{\delta Z_A}{2}\right) A \,, \tag{4.4}$$

$$m^2_{A,0} = m^2_A + \delta m^2_A \,, \tag{4.5}$$

for the scalar field A and

$$\begin{pmatrix} h_{1,0} \\ h_{2,0} \end{pmatrix} = \sqrt{Z_{hh}} \begin{pmatrix} h_1 \\ h_2 \end{pmatrix} \approx \left(1 + \frac{\delta Z_{hh}}{2}\right) \begin{pmatrix} h_1 \\ h_2 \end{pmatrix} , \tag{4.6}$$

$$D^2_{hh,0} = D^2_{hh} + \delta D^2_{hh} \,, \tag{4.7}$$

for the mass eigenstates h_1 and h_2. At one-loop level the eigenstates can mix. Therefore, we have to account for these contributions in the counterterms via the matrices δZ_{hh} and δD_{hh},

$$\delta Z_{hh} = \begin{pmatrix} \delta Z_{h_1 h_1} & \delta Z_{h_1 h_2} \\ \delta Z_{h_2 h_1} & \delta Z_{h_2 h_2} \end{pmatrix} , \qquad \delta D^2_{hh} = \begin{pmatrix} \delta D^2_{h_1 h_1} & \delta D^2_{h_1 h_2} \\ \delta D^2_{h_1 h_2} & \delta D^2_{h_2 h_2} \end{pmatrix} . \tag{4.8}$$

We introduce tadpole counterterms δT_i for the tadpole contributions T_i, that are defined via

$$\hat{T}_i = T_i - \delta T_i = 0 \qquad (i = 1, 2) \,, \tag{4.9}$$

i.e. the renormalized tadpoles $\hat{T}_i$ vanish.

Moreover, we use a tadpole scheme that follows the approach in [203] (and was also applied in [201, 202]). In this scheme we introduce an additional shift in the VEVs that leads to the inclusion of the tadpoles in the self-energies and therefore the counterterms as well. Self-energy contributions with tadpoles included are labelled as Σ^{tad}. Moreover, tadpole corrections have to be included in the vertex corrections. For a detailed prescription of this procedure, see [178].

Here, we only state the results for the counterterms, and obtain

$$\delta m_A^2 = \mathrm{Re}\left(\Sigma_A^{\mathrm{tad}}(m_A^2)\right), \tag{4.10a}$$

$$\delta Z_A = -\mathrm{Re}\left(\left.\frac{\partial\Sigma_A^{\mathrm{tad}}(p^2)}{\partial p^2}\right|_{p^2=m_A^2}\right), \tag{4.10b}$$

$$\delta m_{h_i}^2 = \mathrm{Re}\left(\Sigma_{h_ih_i}^{\mathrm{tad}}(m_{h_i}^2)\right), \tag{4.10c}$$

$$\delta Z_{h_ih_i} = -\mathrm{Re}\left(\left.\frac{\partial\Sigma_{h_ih_i}^{\mathrm{tad}}(p^2)}{\partial p^2}\right|_{p^2=m_{h_i}^2}\right), \tag{4.10d}$$

$$\delta Z_{h_ih_j} = \frac{2}{m_{h_i}^2 - m_{h_j}^2}\mathrm{Re}\left(\Sigma_{h_ih_j}^{\mathrm{tad}}(m_{h_j}^2)\right)(i \neq j). \tag{4.10e}$$

4.1.2. Renormalization of the Mixing Angle α

The remaining input parameters in the scalar sector will be discussed next. We start with the renormalization of the mixing angle α. We write the bare parameter α_0 as a combination of the renormalized parameter and the corresponding counterterm $\delta\alpha$,

$$\alpha_0 = \alpha + \delta\alpha\,. \tag{4.11}$$

To obtain a relation for the counterterm, we follow the prescription introduced in [204]. In this scheme we relate the bare mass eigentates h_i^0 to the renormalized eigenstates h_i by rotating with the mixing matrix $\mathcal{R}$ given in Eq. (3.7) to the gauge eigenstates h and s and then introduce counterterms. We obtain the relation

$$\begin{pmatrix} h_{1,0} \\ h_{2,0} \end{pmatrix} = R_{\alpha,0}\begin{pmatrix} h_0 \\ s_0 \end{pmatrix} \approx R_{\delta\alpha}R_\alpha\sqrt{Z_{\mathrm{G}}}\begin{pmatrix} h \\ s \end{pmatrix} = \sqrt{Z_M}\begin{pmatrix} h_1 \\ h_2 \end{pmatrix}, \tag{4.12}$$

$$\sqrt{Z_M} \equiv R_{\delta\alpha}R_\alpha\sqrt{Z_{\mathrm{G}}}R_\alpha^T\,. \tag{4.13}$$

Here, Z_{G} is the field strength renormalization matrix used to renormalize the gauge eigenstates (for more details, see [178] and compare with [201, 202]). From this relation we obtain the result

$$\delta\alpha = \frac{\delta Z_{h_1h_2} - \delta Z_{h_2h_1}}{4}\,. \tag{4.14}$$

This prescription, however, leads to a gauge-dependent counterterm and moreover to gauge-dependent decay widths. To circumvent this problem and obtain gauge-independent results, we implemented a modified prescription (cf. [201, 202]). We used the so-called pinch technique [205–209] in order to obtain gauge-independent scalar self-energies and in turn a gauge-independent counterterm $\delta\alpha$. This scheme was also applied in [201, 202] for other theories, and the details for the CxSM can be found in [178]. The pinched self-energy is composed of Σ^{tad} and an additional contribution Σ^{add}, and given by $(i,j=1,2)$

$$\begin{aligned} i\Sigma_{h_ih_j}^{\mathrm{pinch}}(p^2) &= i\Sigma_{h_ih_j}^{\mathrm{tad}}(p^2) + i\Sigma_{h_ih_j}^{\mathrm{add}}(p^2) \\ &= \left. i\Sigma_{h_ih_j}^{\mathrm{tad}}(p^2)\right|_{\{\xi=1\}} \\ &+ \frac{-ig^2}{32\pi^2 c_{\mathrm{W}}^2}\left(p^2 - \frac{m_{h_i}^2 + m_{h_j}^2}{2}\right)k_ik_jB_0(p^2, m_Z^2, m_Z^2) \\ &+ \frac{-ig^2}{16\pi^2}\left(p^2 - \frac{m_{h_i}^2 + m_{h_j}^2}{2}\right)k_ik_jB_0(p^2, m_W^2, m_W^2)\,, \end{aligned} \tag{4.15}$$

with ξ denoting the gauge parameters ($\xi = \xi_W, \xi_Z$), k_i defined in Eq. (3.12), c_W the cosine of the weak mixing angle, m_W and m_Z the masses of the W and Z boson, p the momentum and B_0 a 1-loop integral [200, 210, 211].

There is an additional freedom in the choice of the mass scale used in the self-energies for the counterterm $\delta\alpha$. The two possibilities we implemented are,

- OS scheme: Set the momenta to the OS masses, $p^2 = m_{h_i}^2 (i = 1, 2)$.
- p^* scheme: Set the momenta to $p^2 = p^* \equiv \dfrac{m_{h_1}^2 + m_{h_2}^2}{2}$.

At the end, this results in the following two choices for the counterterm that we apply:

$$\delta\alpha_{p^*} = \frac{1}{(m_{h_1}^2 - m_{h_2}^2)} \mathrm{Re}\left(\Sigma_{h_1 h_2}^{\mathrm{tad}}(p_*^2)\Big|_{\{\xi=1\}} \right) , \tag{4.16a}$$

$$\delta\alpha_{\mathrm{OS}} = \frac{1}{2(m_{h_1}^2 - m_{h_2}^2)} \mathrm{Re}\left(\Sigma_{h_1 h_2}^{\mathrm{pinch}}(m_{h_1}^2) + \Sigma_{h_1 h_2}^{\mathrm{pinch}}(m_{h_2}^2) \right) . \tag{4.16b}$$

Here, Σ^{pinch} is the scalar self-energy with the pinched contributions added. In the case of the p^* scheme the additional contributions vanish. The notation $\xi = 1$ here means, that the gauge-independent result is equal to the result obtained if the gauge parameters ξ are set to 1.

4.1.3. Renormalization of the Singlet VEV v_S

The remaining input parameter in the scalar sector to be renormalized, is the singlet VEV v_S. We split the bare parameter into the renormalized parameter and its counterterm,

$$v_{S,0} = v_S + \delta v_S \, . \tag{4.17}$$

For the renormalization of v_S we used a process-dependent (pd) scheme (cf. [201, 202] and see [178] for more details). In this prescription we use a physical process and demand that the parameter that is renormalized is given by the LO relation of this process and all higher-order corrections are absorbed by the counterterm. In our case, we used a decay to obtain the process-dependent counterterm, by demanding

$$\Gamma_{X\to YZ}^{\mathrm{LO}} = \Gamma_{X\to YZ}^{\mathrm{NLO}}, \tag{4.18}$$

between the decay width at LO and NLO. The chosen process has to depend on v_S already at tree level. In our case, only scalar decays can thus be used. We chose the two processes $h_i \to AA$ ($i = 1, 2$). Since the LO amplitude is real, Eq. (4.18) simplifies to

$$0 = \mathrm{Re}\left(\mathcal{A}_{h_i\to AA}^{\mathrm{NLO}}\right) = \mathrm{Re}\left(\mathcal{A}_{h_i\to AA}^{\mathrm{VC}} + \mathcal{A}_{h_i\to AA}^{\mathrm{VCT}}\right) , \tag{4.19}$$

where $\mathcal{A}^{\mathrm{NLO}}$ is the amplitude at NLO consisting of vertex corrections $\mathcal{A}^{\mathrm{VC}}$ and the counterterm contribution $\mathcal{A}^{\mathrm{VCT}}$. This can be further written as

$$0 = \mathrm{Re}\left(\mathcal{A}_{h_i\to AA}^{\mathrm{VC}}\right) - \lambda_{h_i AA}\left(\frac{\delta\lambda_{h_i AA}}{\lambda_{h_i AA}} + \delta Z_A + \frac{\delta Z_{h_i h_i}}{2} + \frac{\lambda_{h_j AA}}{\lambda_{h_i AA}} \frac{\delta Z_{h_j h_i}}{2} \right), \tag{4.20}$$

with the virtual vertex correction $\mathcal{A}^{\text{VC}}$ and the counterms inserted. Moreover, the trilinear couplings λ_{h_iAA} and their counterterms can be written as

$$\lambda_{h_1AA} = \frac{s_\alpha m_{h_1}^2}{v_S} \;\Rightarrow\; \delta\lambda_{h_1AA} = \frac{\delta m_{h_1}^2}{m_{h_1}^2}\lambda_{h_1AA} - \frac{\delta v_S}{v_S}\lambda_{h_1AA} + \cot(\alpha)\delta\alpha\lambda_{h_1AA}\,, \tag{4.21a}$$

$$\lambda_{h_2AA} = \frac{c_\alpha m_{h_2}^2}{v_S} \;\Rightarrow\; \delta\lambda_{h_2AA} = \frac{\delta m_{h_2}^2}{m_{h_2}^2}\lambda_{h_2AA} - \frac{\delta v_S}{v_S}\lambda_{h_2AA} - \tan(\alpha)\delta\alpha\lambda_{h_2AA}\,, \tag{4.21b}$$

Solving relation Eq. (4.20) for δv_S^{pd} we obtain the gauge-independent counterterm for v_S in the pd scheme.

The counterterm obtained by this procedure, however, is only valid if the underlying process is kinematically allowed, i.e. in our case if $m_{h_i} > 2m_A$ ($i = 1$ or $i = 2$). Otherwise, the pd scheme cannot be used.

In order to improve on this insufficiency, we implemented the so-called zero momentum (ZEM) scheme, where instead of using the physical decay $h_i \to AA$ with all momenta set on-shell, we now set all external momenta to zero and then again demand

$$0 = \text{Re}\left(\mathcal{A}^{\text{NLO}}_{h_i\to AA}(\{p^2 = 0\})\right)\,, \tag{4.22}$$

as we did in Eq. (4.19), where $p^2 = 0$ stands for all external momenta set to zero. This approach was already applied in [212] for a different model. For more details on the approach in the CxSM, see [178].

One detail that we have to take into account in this case, is that the external leg corrections $\mathcal{A}^{\text{Leg}}_{h_i\to AA}(\{p^2 = 0\})$ are no longer exactly cancelled by the leg counterterms. Additionally, the resulting counterterm from this procedure would be gauge-dependent and also lead to gauge-dependent results. To circumvent this, we additionally used the pinched self-energies again in the definition of the δZ counterterms (thus labelled δZ^{pinch}) which turn up in the prescription δv_S^{ZEM}. Then, we obtain a gauge-independent counterterm and gauge-independent results. The relation to obtain δv_S^{ZEM} thus finally reads:

$$\begin{aligned} 0 = \text{Re}\left(\mathcal{A}^{\text{VC}}_{h_i\to AA}(\{p^2 = 0\}) + \mathcal{A}^{\text{Leg}}_{h_i\to AA}(\{p^2 = 0\})\right) \\ +\lambda_{h_iAA}\left(-\frac{\delta\lambda_{h_iAA}}{\lambda_{h_iAA}} + \delta Z_A + \frac{\delta Z^{\text{pinch}}_{h_ih_i}}{2} + \frac{\delta m_{h_i}^2}{m_{h_i}^2}\right. \\ \left. +\frac{2\delta m_A^2}{m_A^2} + \frac{\lambda_{h_jAA}}{\lambda_{h_iAA}}\frac{m_{h_i}^2}{m_{h_j}^2}\frac{\delta Z^{\text{pinch}}_{h_ih_j}}{2}\right). \end{aligned} \tag{4.23}$$

4.2. Fermion and Gauge Boson Sector

After the renormalization of the scalar sector, we now turn to the fermion and gauge boson part. We follow the prescription described in [200] and only briefly describe the schemes we used and give the relations for the counterterms. All self-energies appearing in the following will include the tadpole contributions. We will drop the suffix Σ^{tad} to simplify the notation.

4.2.1. Mass and Field Renormalization

We start with the fermions. In the following, we will split up the fermionic fields into left-handed and right-handed parts via $f_{\mathrm{L/R}} = P_{\mathrm{L/R}} f$, with the projection operators $P_{\mathrm{L/R}}$ given by

$$P_{\mathrm{L/R}} = \frac{1 \mp \gamma_5}{2} \,. \tag{4.24}$$

We introduce the wave function renormalization constants δZ for the left- and right-handed parts separately. Thus, we obtain

$$f_{0,\mathrm{L}} = \sqrt{Z^{f_\mathrm{L}}} f_\mathrm{L} \approx \left(1 + \frac{\delta Z^{f_\mathrm{L}}}{2}\right) f_\mathrm{L} \,, \tag{4.25a}$$

$$f_{0,\mathrm{R}} = \sqrt{Z^{f_\mathrm{R}}} f_\mathrm{R} \approx \left(1 + \frac{\delta Z^{f_\mathrm{R}}}{2}\right) f_\mathrm{R} \,, \tag{4.25b}$$

$$m_{f,0} = m_f + \delta m_f \,, \tag{4.25c}$$

where again the label 0 denotes the bare mass terms and fields. We also have introduced a mass counterterm δm_f for the fermion mass m_f. The δZ counterterms can, in general, be matrices if mixing between the fermions is considered.

Next, we divide the fermion self-energy Σ^f_{ij} in left- and right-handed parts,

$$\Sigma^f_{ij}(p^2) = \not{p} P_\mathrm{L} \Sigma^{f,\mathrm{L}}_{ij}(p^2) + \not{p} P_\mathrm{R} \Sigma^{f,\mathrm{R}}_{ij}(p^2) + m_{f,i} P_\mathrm{L} \Sigma^{f,\mathrm{Ls}}_{ij}(p^2) + m_{f,j} P_\mathrm{R} \Sigma^{f,\mathrm{Rs}}_{ij}(p^2) \,, \tag{4.26}$$

where we introduced indices i, j for the fermion generations and we also split up the part proportional to the mass into a left- and right handed part, compared to [200] (similar to our approach in Sec. 12.4. Applying OS conditions to the renormalized fermion self-energies leads to the following conditions for the fermionic counterterms:

$$\delta m_{f_i} = \frac{m_{f_i}}{2} \widetilde{\mathrm{Re}} \left(\Sigma^{f,\mathrm{L}}_{ii}(m^2_{f_i}) + \Sigma^{f,\mathrm{R}}_{ii}(m^2_{f_i}) + \Sigma^{f,\mathrm{Ls}}_{ii}(m^2_{f_i}) + \Sigma^{f,\mathrm{Rs}}_{ii}(m^2_{f_i}) \right) \,, \tag{4.27a}$$

$$\begin{aligned} \delta Z^{f_\mathrm{L}}_{ij} = \frac{2}{m^2_{f_i} - m^2_{f_j}} \widetilde{\mathrm{Re}} \Big(& m^2_{f_j} \Sigma^{f,\mathrm{L}}_{ij}(m^2_{f_j}) + m_{f_i} m_{f_j} \Sigma^{f,\mathrm{R}}_{ij}(m^2_{f_j}) \\ & + m^2_{f_i} \Sigma^{f,\mathrm{Ls}}_{ij}(m^2_{f_j}) + m^2_{f_j} \Sigma^{f,\mathrm{Rs}}_{ij}(m^2_{f_j}) \Big) \,, \end{aligned} \tag{4.27b}$$

$$\begin{aligned} \delta Z^{f_\mathrm{R}}_{ij} = \frac{2}{m^2_{f_i} - m^2_{f_j}} \widetilde{\mathrm{Re}} \Big(& m^2_{f_j} \Sigma^{f,\mathrm{R}}_{ij}(m^2_{f_j}) + m_{f_i} m_{f_j} \Sigma^{f,\mathrm{L}}_{ij}(m^2_{f_j}) \\ & + m_{f_i} m_{f_j} \Sigma^{f,\mathrm{Ls}}_{ij}(m^2_{f_j}) + m_{f_i} m_{f_j} \Sigma^{f,\mathrm{Rs}}_{ij}(m^2_{f_j}) \Big) \,, \end{aligned} \tag{4.27c}$$

$$\delta Z^{f_\mathrm{L}}_{ii} = -\widetilde{\mathrm{Re}} \Sigma^{f,\mathrm{L}}_{ii}(m^2_{f_i}) + K^f_i \,, \tag{4.27d}$$

$$\delta Z^{f_\mathrm{R}}_{ii} = -\widetilde{\mathrm{Re}} \Sigma^{f,\mathrm{R}}_{ii}(m^2_{f_i}) + K^f_i \,, \tag{4.27e}$$

$$\begin{aligned} K^f_i \equiv -m^2_{f_i} \frac{\partial}{\partial p^2} \widetilde{\mathrm{Re}} \Big(& \Sigma^{f,\mathrm{L}}_{ii}(p^2) + \Sigma^{f,\mathrm{R}}_{ii}(p^2) \\ & + \Sigma^{f,\mathrm{Ls}}_{ii}(p^2) + \Sigma^{f,\mathrm{Rs}}_{ii}(p^2) \Big) \Big|_{p^2 = m^2_{f_i}} \,, \end{aligned} \tag{4.27f}$$

where $\widetilde{\mathrm{Re}}$ indicates that the real part is only applied to the one-loop integrals, but not the potentially complex couplings.

Now, we move on to the gauge boson sector. Again, we write the bare fields and mass terms (labelled with a 0) in terms of renormalized fields, renormalized masses and their counterterms,

$$W_0^\pm \approx \left(1 + \frac{\delta Z_W}{2}\right) W^\pm \,, \tag{4.28a}$$

$$m_{W,0}^2 = m_W^2 + \delta m_W^2 \,, \tag{4.28b}$$

$$\begin{pmatrix} Z_0 \\ \gamma_0 \end{pmatrix} \approx \begin{pmatrix} 1 + \frac{\delta Z_{ZZ}}{2} & \frac{\delta Z_{Z\gamma}}{2} \\ \frac{\delta Z_{\gamma Z}}{2} & 1 + \frac{\delta Z_{\gamma\gamma}}{2} \end{pmatrix} \begin{pmatrix} Z \\ \gamma \end{pmatrix} \,, \tag{4.28c}$$

$$m_{Z,0}^2 = m_Z^2 + \delta m_Z^2 \,. \tag{4.28d}$$

Here we take into account that at one-loop level there can be mixing between the Z boson and the photon.

Moreover, we split the gauge boson self-energy $\Sigma_{\mu\nu}^{V_1V_2}$ $(V_1, V_2 = W, Z, \gamma)$ into a transverse (T) and longitudinal (L) part,

$$\Sigma_{\mu\nu}^{V_1V_2}(p^2) = -\left(g_{\mu\nu} - \frac{p_\mu p_\nu}{p^2}\right) \Sigma_{\mathrm{T}}^{V_1V_2}(p^2) - \frac{p_\mu p_\nu}{p^2} \Sigma_{\mathrm{L}}^{V_1V_2}(p^2) \,, \tag{4.29}$$

Applying OS conditions on the renormalized self-energies, we obtain the following conditions for the mass and field counterterms:

$$\delta m_V^2 = \widetilde{\mathrm{Re}} \Sigma_{\mathrm{T}}^{VV}(m_V^2) \, (V = W, Z) \,, \tag{4.30a}$$

$$\delta Z_W = -\widetilde{\mathrm{Re}} \left. \frac{\partial \Sigma_{\mathrm{T}}^{WW}(p^2)}{\partial p^2} \right|_{p^2 = m_W^2} \,, \tag{4.30b}$$

$$\begin{pmatrix} \delta Z_{ZZ} & \delta Z_{Z\gamma} \\ \delta Z_{\gamma Z} & \delta Z_{\gamma\gamma} \end{pmatrix} = \begin{pmatrix} -\widetilde{\mathrm{Re}} \left. \frac{\partial \Sigma_{\mathrm{T}}^{ZZ}(p^2)}{\partial p^2} \right|_{p^2 = m_Z^2} & 2\widetilde{\mathrm{Re}} \frac{\Sigma_{\mathrm{T}}^{\gamma Z}(0)}{m_Z^2} \\ -2\widetilde{\mathrm{Re}} \frac{\Sigma_{\mathrm{T}}^{\gamma Z}(m_Z^2)}{m_Z^2} & -\widetilde{\mathrm{Re}} \left. \frac{\partial \Sigma_{\mathrm{T}}^{\gamma\gamma}(p^2)}{\partial p^2} \right|_{p^2 = 0} \end{pmatrix} \,. \tag{4.30c}$$

4.2.2. Renormalization of the Electric Charge

The remaining parameter we have to renormalize in the fermion and gauge boson sectors is the electric charge e. Again, we introduce a counterterm δZ_e via

$$e_0 = (1 + \delta Z_e) e \,. \tag{4.31}$$

To obtain a prescription for the counterterm, the photon-electron-positron vertex is considered in the so-called Thomson limit, where the external particles are on shell with vanishing momentum transfer [85, 200]. This results in the relation

$$\delta Z_e^{\alpha(0)} = \frac{1}{2} \left. \frac{\delta \Sigma_{\gamma\gamma}^{\mathrm{T}}(p^2)}{\partial p^2} \right|_{p^2 = 0} + \frac{s_{\mathrm{W}}}{c_{\mathrm{W}}} \frac{\Sigma_{\gamma Z}^{\mathrm{T}}(0)}{m_Z^2} \,, \tag{4.32}$$

for the counterterm δZ_e, with $s_{\mathrm{W}}, c_{\mathrm{W}}$ being the sine and cosine of the weak mixing angle.

However, another issue arises, when light fermions are present in the model. The above relation then depends on large logarithimic corrections $(\log m_f^2)$ from small fermion masses

m_f. To resolve this, we follow the approach in [212, 213]. In order to improve the perturbative behaviour, the electromagnetic constant will be determined from the Fermi constant G_μ, via the relation

$$\alpha_{G\mu} = \frac{\sqrt{2}G_\mu m_W^2}{\pi}(1 - \frac{m_W^2}{m_Z^2}) \,, \tag{4.33}$$

which absorbs already parts of the radiative corrections. In order to avoid double counting, they have to be removed from the counterterm via the relation

$$\delta Z_e^{G_\mu} = \delta Z_e^{\alpha(0)} - \frac{\Delta r}{2} \,, \tag{4.34}$$

with Δr defined as [200, 214]

$$\begin{aligned}\Delta r = {} & \frac{\partial \Sigma_T^{\gamma\gamma}(p^2)}{\partial p^2}\bigg|_{p^2=0} - \frac{c_\mathrm{W}^2}{s_\mathrm{W}^2}\left(\frac{\Sigma_\mathrm{T}^{ZZ}(m_Z^2)}{m_Z^2} - \frac{\Sigma_\mathrm{T}^{WW}(m_W^2)}{m_W^2}\right) + \frac{\Sigma_\mathrm{T}^{WW}(0) - \Sigma_\mathrm{T}^{WW}(m_W^2)}{m_W^2} \\ & - 2\frac{c_\mathrm{W}}{s_\mathrm{W}}\frac{\Sigma_\mathrm{T}^{\gamma Z}(0)}{m_Z^2} + \frac{\alpha}{4\pi s_\mathrm{W}^2}\left(6 + \frac{7 - 4s_\mathrm{W}^2}{2s_\mathrm{W}^2}\log c_\mathrm{W}^2\right) .\end{aligned} \tag{4.35}$$

This removes the terms that contain logarithmic terms with small fermion masses and thus improves the perturbative behaviour of the counterterm.

4.3. Change of Renormalization Schemes

In this section, we briefly describe how to change from one renormalization scheme to another. The important issue is that input parameters always have to be defined in a given renormalization scheme. If another scheme is to be used, they also need to be converted to the new prescription (cf. e.g. [215]).

To obtain a relation between two schemes, the idea is that the bare parameter λ_0 is independent of the chosen renormalization scheme and can be used to relate the parameter in scheme R1 with the parameter expressed in scheme R2,

$$\lambda_{\mathrm{R2}} + \delta\lambda_{\mathrm{R2}} = \lambda_0 = \lambda_{\mathrm{R1}} + \delta\lambda_{\mathrm{R1}} \,. \tag{4.36}$$

We can solve for λ_{R2} to obtain a relation on how to convert a parameter from scheme R1 to R2,

$$\lambda_{\mathrm{R2}} = \lambda_{\mathrm{R1}} + \delta\lambda_{\mathrm{R1}} - \delta\lambda_{\mathrm{R2}} \,. \tag{4.37}$$

It is important to note here, that the counterterms $\delta\lambda_{\mathrm{R1}}, \delta\lambda_{\mathrm{R2}}$ themselves depend on the input parameters in the corresponding scheme. Thus, one can use this relation iteratively to converge to the desired renormalization scheme or use it linearly, i.e. use only the input parameters given in the input scheme and apply the relation once. This dependence on the scheme of the input parameters in the counterterms is a higher-order effect and should be small for a sufficient perturbative stability.

CHAPTER 5

Calculation of NLO Corrected Decay Widths in the CxSM

In this chapter, we describe the calculations of the LO and NLO Higgs decay widths for all possible channels in the CxSM. We briefly mention the kinematics and generic formula of two-body decays in Sec. 5.1, describe the LO Higgs decay widths that appear in the CxSM (Sec. 5.2) and then move on to the NLO-corrected widths (Sec. 5.3). Finally, we also discuss the inclusion of NLO^2 terms in the scalar Higgs-to-Higgs decay in Sec. 5.4.

It should be noted that we only discuss here on-shell (OS) decays and electroweak corrections. In the code implementation we also included off-shell decays into gauge bosons and the top quark and quantum chromodynamics (QCD) corrections, that we took over from `HDECAY` [216, 217] and `SHDECAY` [218]. For more details, see our description of the implementation in Sec. 6.1 and the manuals of `HDECAY` and `SHDECAY`.

5.1. Kinematics and General Formulas for Two-Body Decays

In the following, we present the generic formulas for two-body decays (for a proper derivation, see e.g. [85]). In order to calculate a decay width at a given order, the sum of all amplitudes (denoted as $\mathcal{A}$) has to be calculated. The following equations are then used to calculate the partial decay width of the considered process at LO and NLO:

$$\Gamma^{\text{LO}}_{f_1\to f_2 f_3} = S\frac{\lambda(m_1^2,m_2^2,m_3^2)}{16\pi m_1^3}\sum_{\text{d.o.f}}\left(|\mathcal{A}^{\text{LO}}_{f_1\to f_2 f_3}|^2\right)\,, \tag{5.1a}$$

$$\Gamma^{\text{NLO}}_{f_1\to f_2 f_3} = \Gamma^{\text{LO}}_{f_1\to f_2 f_3} + S\frac{\lambda(m_1^2,m_2^2,m_3^2)}{16\pi m_1^3}\sum_{\text{d.o.f}}\left(2\text{Re}\left[\left(\mathcal{A}^{\text{LO}}_{f_1\to f_2 f_3}\right)^* \mathcal{A}^{\text{NLO}}_{f_1\to f_2 f_3}\right]\right) \tag{5.1b}$$
$$\left(+\Gamma^{\text{real}}_{f_1\to f_2 f_3}\right)\,.$$

Here, the factor S is a symmetry factor, and in the case of identical final particle states ($f_2 = f_3$) we have $S = \frac{1}{2}$, otherwise $S = 1$. If the initial (f_1) or final state particles (f_2, f_3) are charged and there appear massless particles in the loops (e.g. photons) then real corrections have to be added as well (denoted as Γ^{real}). With $\sum_{\text{d.o.f}}$ we symbolize the sum over all degrees

of freedom (d.o.f.) in order to obtain the partial width, where we sum over polarization, spin and colour of outgoing particles and average over them for ingoing particles. In our case, we apply the loop expansion in the expression $|\mathcal{A}|^2$ to NLO and $|\mathcal{A}^{\text{NLO}}|^2$ is a higher-order effect and therefore neglected. It can become important, however, as will be discussed in Sec. 5.4. We also use the Källén function $\lambda(x, y, z)$,

$$\lambda(x, y, z) \equiv \sqrt{x^2 + y^2 + z^2 - 2xy - 2xz - 2yz}\,. \tag{5.2}$$

Furthermore, in two-body decays with one ingoing momentum p_1 and two outgoing momenta p_2 and p_3 with momentum conservation,

$$p_1 = p_2 + p_3\,, \tag{5.3}$$

we can express all scalar products in term of the masses m_i $(i = 1, 3)$ of the in- and outgoing particles,

$$p_i^2 = m_i^2\,, \qquad (i = 1, 2, 3)\,, \tag{5.4a}$$

$$p_1 \cdot p_2 = \frac{1}{2}(m_1^2 + m_2^2 - m_3^2)\,, \tag{5.4b}$$

$$p_1 \cdot p_3 = \frac{1}{2}(m_1^2 - m_2^2 + m_3^2)\,, \tag{5.4c}$$

$$p_2 \cdot p_3 = \frac{1}{2}(m_1^2 - m_2^2 - m_3^2)\,. \tag{5.4d}$$

We will use these relations and Eqs. (5.1) in the following to derive the formulas for the partial widths into the various decay channels.

5.2. Leading-Order Decay Widths in the CxSM

We now briefly describe the LO decay widths of the scalars h_1 and h_2 in the CxSM. First of all, the radiative loop decays $h_i \to gg$ and $h_i \to \gamma\gamma$ into gluons and photons are as in the SM, but multiplied by an additional factor $\cos^2\alpha$ or $\sin^2\alpha$ (compare to Eq. (3.12)). The other decay modes of the Higgs particles h_i are decays into fermions f, scalars Φ or massive vector bosons V. At LO, they can be written as (provided they are kinematically allowed)

$$\Gamma^{\text{LO}}_{h_i \to \Phi\Phi} = \frac{\lambda(m_{h_i}^2, m_\Phi^2, m_\Phi^2)}{32\pi m_{h_i}} \lambda_{h_i\Phi\Phi}^2\,, \tag{5.5a}$$

$$\Gamma^{\text{LO}}_{h_i \to VV} = \frac{S\lambda(m_{h_i}^2, m_V^2, m_V^2)}{64\pi m_{h_i} m_V^4} g_{h_iVV}^2 \left(m_{h_i}^2 - 4m_{h_i}^2 m_V^2 + 12 m_V^4\right)\,, \tag{5.5b}$$

$$\Gamma^{\text{LO}}_{h_i \to ff} = \frac{N_c\lambda(m_{h_i}^2, m_f^2, m_f^2)}{8\pi m_{h_i}} g_{h_iff}^2 \left(1 - 4\frac{m_f^2}{m_{h_i}^2}\right)\,. \tag{5.5c}$$

Here, N_c are the colour degrees of freedom ($N_c = 3$ for quarks and $N_c = 1$ for leptons), and $S = 1$ for $V = W$ and $S = \frac{1}{2}$ for $V = Z$. We additionally have $\Phi = h_1, A$ and f can be any lepton or quark, but we only considered third generations of fermions and the charm quark. The couplings g_{h_iff} and g_{h_iVV} are as in the SM with an additional factor, see Eq. (3.12). In

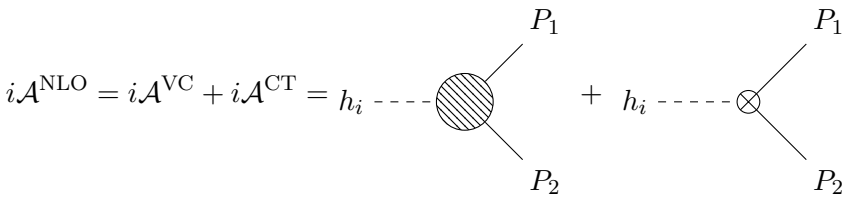

Figure 5.1.: Feynman diagram topologies appearing for a generic decay process $h_i \to P_1 P_2$ into two particles P_1 and P_2 with the vertex corrections $\mathcal{A}^{\text{VC}}$ and the counterterm contributions $\mathcal{A}^{\text{CT}}$.

order to calculate the h_i decays into scalars, we need the trilinear scalar couplings λ. They are given as

$$\lambda_{h_1h_1h_1} = 3m_{h_1}^2 \frac{v_S c_\alpha^3 + v s_\alpha^3}{v v_S}\,, \tag{5.6a}$$

$$\lambda_{h_1h_1h_2} = \frac{(2m_{h_1}^2 + m_{h_2}^2) s_\alpha c_\alpha (v s_\alpha - v_S c_\alpha)}{v v_S}\,, \tag{5.6b}$$

$$\lambda_{h_1h_2h_2} = \frac{(m_{h_1}^2 + 2m_{h_2}^2) s_\alpha c_\alpha (v c_\alpha + v_S s_\alpha)}{v v_S}\,, \tag{5.6c}$$

$$\lambda_{h_2h_2h_2} = 3m_{h_2}^2 \frac{v c_\alpha^3 - v_S s_\alpha^3}{v v_S}\,, \tag{5.6d}$$

$$\lambda_{h_iAA} = \begin{cases} \dfrac{m_{h_1}^2 s_\alpha}{v_s}\,, & i = 1 \\ \dfrac{m_{h_2}^2 c_\alpha}{v_s}\,, & i = 2 \end{cases}\,. \tag{5.6e}$$

if we set $\alpha = 0$ and decouple the h_2 and A fields from the rest of the SM, we see that $\lambda_{h_1h_1h_1}$ equals the SM trilinear couplings, given by $\lambda_{H_{\text{SM}}H_{\text{SM}}H_{\text{SM}}} = 3m_{H_{\text{SM}}}^2/v$, where H_{SM} is the SM Higgs and $m_{h_1} = m_{H_{\text{SM}}}$. Similarly, in the limit $\alpha = \pi/2$ we decouple h_1 and A and $\lambda_{h_2h_2h_2}$ equals the SM trilinear coupling and h_2 plays the role of the SM Higgs H_{SM}.

5.3. Next-to-Leading-Order Decay Widths in the CxSM

We now move on to the calculation of the NLO EW corrections to the h_1 and h_2 decays. The amplitude $\mathcal{A}^{\text{NLO}}$ of a given decay process at NLO can be split up into the sum of all virtual vertex corrections $\mathcal{A}^{\text{VC}}$ and the counterterm contributions $\mathcal{A}^{\text{CT}}$ (see also Fig. 5.1),

$$\mathcal{A}^{\text{NLO}} = \mathcal{A}^{\text{VC}} + \mathcal{A}^{\text{CT}}\,. \tag{5.7}$$

In principle, also leg corrections and leg counterterms contribute, but we use an on-shell prescription for the mass and field renormalization counterterms. Therefore, they cancel out exactly. If the final state particles are charged, and massless particles appear in the loops (e.g. photons) real corrections have to be considered. They will be discussed in Sec. 5.3.1.

The virtual corrections $\mathcal{A}^{\text{VC}}$ comprise all EW vertex corrections and potential tadpole contributions as explained in Sec. 4.1. The vertex contributions for all decay channels can be seen in Fig. 5.2. The counterterm amplitudes $\mathcal{A}^{\text{CT}}$ for the considered decays of h_1 and h_2 comprise of the counterterm for the coupling $\delta g/\delta\lambda$ and the field renormalization constants δZ for the involved fields, and is given by

$$\mathcal{A}^{\text{CT}}_{h_i \to ff} = \delta g_{h_i ff} + g_{h_n ff} \frac{\delta Z_{h_n h_i}}{2} + g_{h_i ff} \frac{\delta Z^{f_{\text{L}}} + \delta Z^{f_{\text{R}}}}{2}\,, \tag{5.8a}$$

$$\mathcal{A}^{\text{CT}}_{h_i \to VV} = \delta g_{h_i VV} + g_{h_n VV} \frac{\delta Z_{h_n h_i}}{2} + g_{h_i VV} \delta Z_{VV}\,, \tag{5.8b}$$

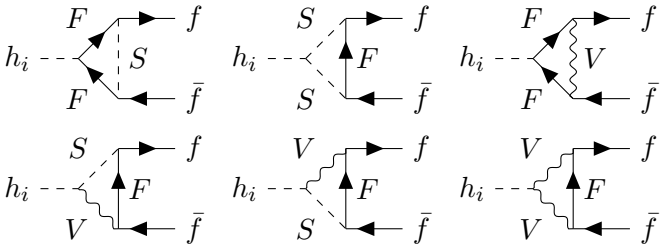

(a) Generic diagrams for the vertex corrections to the fermionic decay $h_i \to \bar{f}f$.

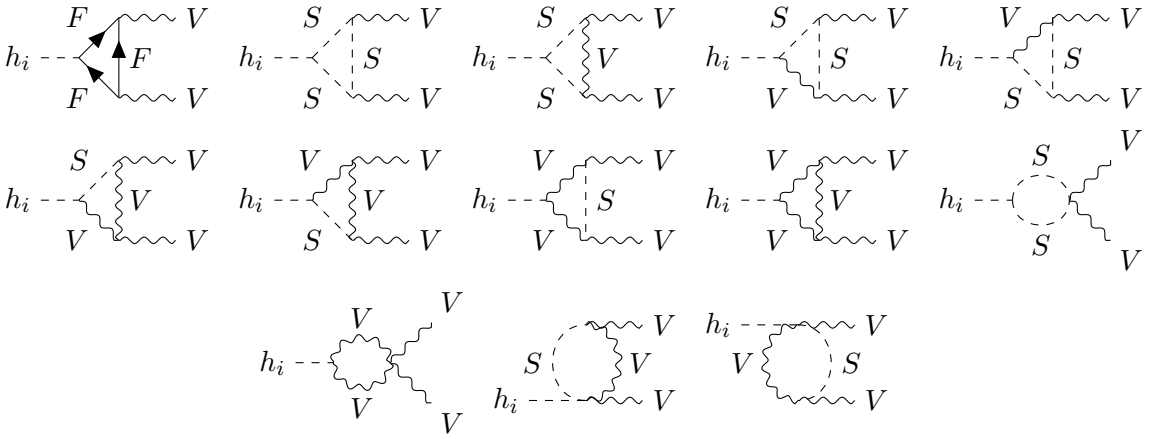

(b) Generic diagrams for the vertex corrections to the decay into gauge bosons, $h_i \to VV$.

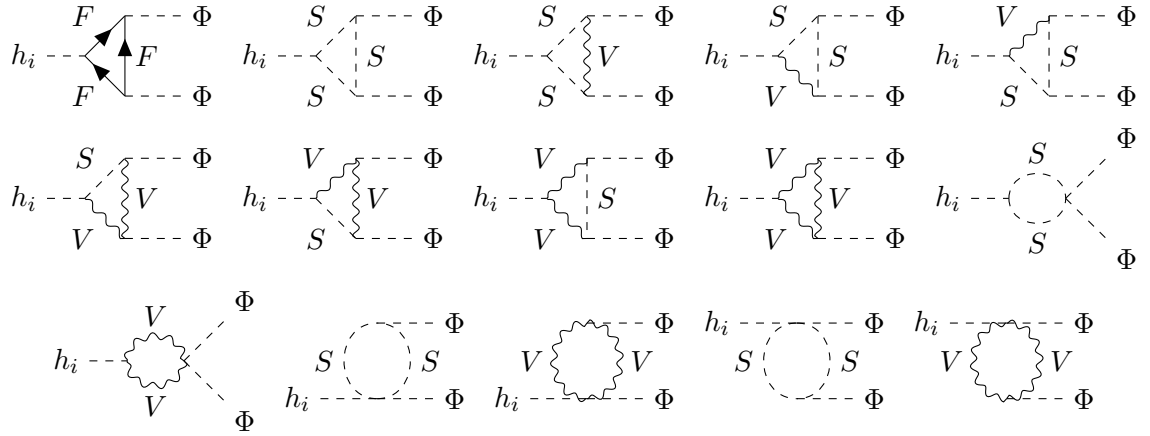

(c) Generic diagrams for the vertex corrections to the scalar decays, $h_i \to \Phi\Phi$.

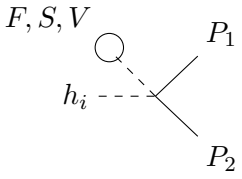

(d) Tadpole corrections to a generic decay $h_i \to P_1P_2$ that have to be considered (if the corresponding 4-point vertex exists) due to our choice in the tadpole renormalization (see Sec. 4.1.1). P_1, P_2 can be scalars or bosons.

Figure 5.2.: Generic diagrams for the vertex corrections to the different decay channels, where F denotes a generic fermion, $S = h_1, h_2, A$ a generic scalar and V a generic vector boson in the loop, and we ignored possible generation indices. Diagrams containing ghost particles are not shown but also have to be included in principle.

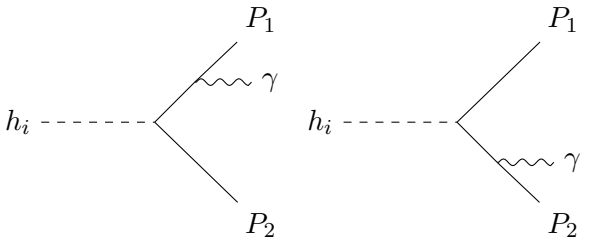

Figure 5.3.: Feynman diagram topologies contributing to the real corrections at NLO for a decay process $h_i \to P_1 P_2$ of two particles P_1 and P_2, where P_1, P_2 are either charged fermions or W bosons.

for the decays into fermions and bosons. The counterterm amplitudes for the $h_i \to AA$ decays ($i = 1, 2$) and the decay $h_2 \to h_1 h_1$ read

$$\mathcal{A}^{\text{CT}}_{h_i \to AA} = \delta\lambda_{h_i AA} + \lambda_{h_n AA}\frac{\delta Z_{h_n h_i}}{2} + \lambda_{h_i AA}\delta Z_{AA}\,, \tag{5.9a}$$

$$\mathcal{A}^{\text{CT}}_{h_2 \to h_1 h_1} = \delta\lambda_{h_2 h_1 h_1} + \lambda_{h_n h_1 h_1}\frac{\delta Z_{h_n h_i}}{2} + \lambda_{h_i h_m h_1}\delta Z_{h_m h_1}\,, \tag{5.9b}$$

Here, we implicitly sum over the indices $n, m = 1, 2$. The couplings themselves then have to be expressed in terms of input parameters and the corresponding counterterms inserted. Finally, the virtual corrections and the vertex counterterms are added, and Eq. (5.1b) is used to calculate the NLO corrected decay width. We checked analytically and numerically that our results are UV finite and gauge-independent. We applied all renormalization prescriptions described in Chapter 4.

5.3.1. Real Corrections

In the case of charged particles in the initial or final state, these particles can emit photons (see Fig. 5.3 for the Feynman diagrams contributing to these real corrections). Although this additional final state particle results in a different final state configuration, the decay width of this process at LO is at the same order in powers of the gauge couplings as the NLO decay width. Moreover, these so-called real corrections are needed to cancel remaining IR divergences in the NLO decay width arising from massless particles, i.e. the photon, appearing in the loops. Therefore, only the NLO decay width including these real corrections results in IR finite and therefore physically meaningful quantities (c.f. [200]).

Furthermore, we introduce an energy threshold ΔE and only account for soft photons with an energy smaller than this threshold. We assume that the soft photons are not detected in an experiment, and therefore these radiation processes cannot be distinguished from the decay without additional radiation and should be added to the decay width of the considered process. We refer to [200, 219] for more details and only give the result for the decay width obtained from the real corrections.

The real corrections to a generic decay process $h_i \to P_1 P_2$ with charged final state particles P_1, P_2 are given by,

$$\Gamma^{\text{real}}_{h_i \to P_1 P_2} = -\frac{Q^2 e^2}{2(2\pi)^3}\Gamma^{\text{LO}}(I_{22} + I_{33} - 2I_{23})\,, \tag{5.10}$$

with the LO decay width Γ^{LO}, the electric charge e and the fraction Q of the charge that the final state particles carry. The integrals I are defined as

$$I_{ii} = 2\pi \left(\log \frac{4\Delta E^2}{\lambda^2} + \frac{p_{i,0}}{|\mathbf{p}_i|} \log \frac{p_{i,0} - |\mathbf{p}_i|}{p_{i,0} + |\mathbf{p}_i|} \right) , \tag{5.11a}$$

$$I_{ij} = 4\pi \frac{p_i p_j}{(p_{i,0} + p_{j,0})|\mathbf{p}_i|} \tag{5.11b}$$
$$\left(\frac{1}{2} \log \frac{p_{i,0} + |\mathbf{p}_i|}{p_{i,0} - |\mathbf{p}_i|} \log \frac{4\Delta E^2}{\lambda^2} - \text{Li}_2 \left(\frac{2|\mathbf{p}_i|}{p_{i,0} + |\mathbf{p}_i|} \right) - \frac{1}{4} \log^2 \frac{p_{i,0} + |\mathbf{p}_i|}{p_{i,0} - |\mathbf{p}_i|} \right) .$$

Here, ΔE is the energy threshold as discussed, λ is the artificial photon mass introduced to regularize the expression, and Li_2 is the Spence function. We use the notation for our momenta given in Eqs. (5.3) and (5.4) and for I_{ij} we used the fact that $\mathbf{p}_i = -\mathbf{p}_j$ and $p_{i,0} = p_{j,0}$ (for $i, j = 2, 3$). The result for these integrals was taken from [200].

5.4. Decay Widths in the CxSM including NLO^2 Corrections

In the scalar decay $h_2 \to h_1 h_1$ it can occur that the coupling $\lambda_{h_1 h_1 h_2}$ vanishes, depending on the chosen input parameters. Comparing with Eq. (5.6b) this is the case if

$$\lambda_{h_1 h_1 h_2} = 0 \qquad \Rightarrow \qquad \tan\alpha = \frac{v_S}{v} . \tag{5.12}$$

As a result, the LO amplitude $\mathcal{A}^{\text{LO}}_{h_2 \to h_1 h_1}$ vanishes and therefore we have

$$\mathcal{A}^{\text{LO}}_{h_2 \to h_1 h_1} = 0 \qquad \Rightarrow \qquad \Gamma^{\text{LO}}_{h_2 \to h_1 h_1} = \Gamma^{\text{NLO}}_{h_2 \to h_1 h_1} = 0 . \tag{5.13}$$

The LO and NLO partial widths are zero (although in this case it would be more sensible to talk about tree-level and one-loop level for these partial widths, as LO should always denote the first non vanishing contribution). Thus, we have to consider the next term in the expansion, and we obtain

$$\Gamma^{\text{NNLOapprox}}_{h_2 \to h_1 h_1} = \Gamma^{\text{LO}}_{h_2 \to h_1 h_1} + \Gamma^{\text{NLO}}_{h_2 \to h_1 h_1} + \frac{\lambda(m_{h_1}^2, m_{h_2}^2, m_{h_2}^2)}{32\pi m_{h_1}^3} \left| \mathcal{A}^{\text{NLO}}_{h_1 \to h_2 h_2} \right|^2 , \tag{5.14}$$

where the label NNLOapprox stands for the inclusion of the $|\mathcal{A}^{\text{NLO}}|^2$ term but not the term

$$\left(2\text{Re} \left[\left(\mathcal{A}^{\text{LO}}_{h_1 \to h_2 h_2} \right)^* \mathcal{A}^{\text{NNLO}}_{h_1 \to h_2 h_2} \right] \right) , \tag{5.15}$$

that would be of the same order. If the tree-level amplitude vanishes exactly, this term is also zero, but it does contribute as soon as the coupling $\lambda_{h_1 h_1 h_2}$ deviates from zero. This would then entail, however, a full two-loop calculation, which we omitted and we only allowed for the inclusion of the NLO^2 contribution in the region of the parameter space where the trilinear coupling $\lambda_{h_1 h_1 h_2}$ vanishes.

Another detail we want to mention here is the following. When calculating the NLO^2 contribution with our setup of OS conditions, we only cancel the real part of the leg corrections, but the loop integrals appearing there can develop imaginary branch cuts and therefore corrections to the imaginary part of the NLO amplitude (that can also carry gauge dependencies that are needed for a gauge-independent NLO amplitude). Thus far, this was no issue as only the real part of the 1-loop amplitude was needed (as the tree-level amplitude is already real), but now they have to be explicitly included at the NLO^2 level.

We give a more detailed discussion of the behaviour close to the vanishing point of the trilinear coupling in Sec. 6.5.

CHAPTER 6

Numerical Evaluation

After introducing the model, describing the calculation and the methods we used to obtain our results, we can now move on to the implementation and the analysis of our findings.

In this chapter, we start with the description of the code that we developed to evaluate the NLO corrected Higgs decay widths we calculated (Sec. 6.1). In Sec. 6.2, we describe our setup and give some technical details on how we performed our calculations. Here, we also describe how we obtained our parameter sample and how we applied constraints. Furthermore, we analyze the EW corrections in Sec. 6.3, their typical sizes, the origins of large corrections and the theoretical renormalizaton scheme uncertainty. We also discuss the impact of NLO corrections on our parameter space in Sec. 6.4. At the end, we illustrate the NLO^2 contributions in the case of vanishing tree-level amplitudes for the $h_2 \to h_1 h_1$ decay (Sec. 6.5).

6.1. The Code `EWsHDECAY`

We implemented our calculations into a new code called `EWsHDECAY`. As its foundation we used the code `sHDECAY` [218], updated it with the newest version of `HDECAY 6.61` [216, 217] and then implemented our NLO corrections into it. The code `HDECAY` has already implemented all the Higgs decays, including QCD corrections (which are the same in our model) and off-shell decays into off-shell top quarks or off-shell gauge bosons for the SM. We could thus take over the QCD corrections and also the off-shell decays, which are used if the corresponding two-body decays are not kinematically allowed. They are then calculated without EW corrections. Otherwise, we use the on-shell decays and our EW corrections to the two-body decay processes.

The code is available at: `https://github.com/fegle/ewshdecay/`

In the following, we give a brief description of how to use `EWsHDECAY`, by giving a sample input file and discussing the input options. For more information, see [73] and the information given on the website of the code.

A sample input file may look like the following (only the parts relevant for our calculation are shown):

```
********************* real or complex singlet Model ********************
Singlet Extension: 1 - yes, 0 - no (based on SM w/o EW corrections)
Model: 1 - real broken phase, 2 - real dark matter phase
       3 - complex broken phase, 4 - complex dark matter phase
isinglet = 1
icxSM    = 4

...


*** complex singlet dark matter phase ***
alph1    = 0.2D0
m1       = 125.09D0
m2       = 270.D0
m3       = 60.D0
vs       = 300.D0
a1       = 0.0D0
******************* EW Corrections ********************
** Attention: This can only be used for the complex dark matter phase (icxSM
   =4) of the CxSM with a1=0 **
**** ielwcxsm = 0 LO, = 1 include NLO corrections
ielwcxsm = 1
**** ren. scheme: vsscheme = 1 pd, = 2 ZEM, pdprocess = 1 h1->AA, =2 h2->AA,
   alpha_mix =1 OS, =2 pstar
vsscheme = 2
pdprocess= 2
ralph_mix= 1
**** IR parameter - DeltaE is the detector resolution (in GeV);
DeltaE   = 10.0D0
**** NNLO approx: NNLOapprox=1, add NLO^2 term to h2h1h1 decay width if |tan(
   alpha)*(v/vs)-1|<=deltaNNLO
NNLOapp  = 0
deltaNNLO= 0.05D0
**** Parameter conversion, change input parameters vS and alpha accordingly,
   if given scheme above is not the specified input scheme
**** Paramcon = 0 no parameter conversion, =1 do parameter conversion
**** Standard scheme: stdvs = 1 pd, = 2 ZEM, stdproc = 1 h1->AA, =2 h2->AA,
   stdalpha =1 OS, =2 pstar
Paramcon = 0
stdvs    = 2
stdproc  = 2
stdalpha = 1
```

We will go through all options and their usage. First, with `isinglet=1` the mode to use the singlet extensions of the SM for the calculation of the Higgs decays is activated, and with `icxSM=4` our version of the model is chosen (in principle all the other singlet extensions from `sHDECAY` haven been taken over as well, but no NLO corrections are implemented for them). Next, the input parameters can be specified, where `alph1` is the mixing angle α, `m1` and `m2` are the Higgs masses m_{h_1} and m_{h_2}, `m3` is the DM mass m_A and `vs` is the singlet VEV v_S. One has to be aware that in the original `sHDECAY` version a slightly different CxSM model was implemented, where a_1 is in general non-zero, but in our model it has to be set to zero. Thus, if a_1 is not given as zero, then the code gives out a warning and does not calculate the NLO corrections.

The switch `ielwcxsm` turns on or off the NLO corrections, and with the variables `vsscheme`, `pdprocess` and `ralph_mix` the chosen renormalization schemes for v_S and α can be specified. By setting `vsscheme` to 1 or 2 the process-dependent scheme for v_S is used for on-shell decays or at zero external momentum (ZEM), respectively. With `pdprocess` the process to be used for this scheme is selected, 1 (2) for $h_1 \to AA$ ($h_2 \to AA$), see also Sec. 4.1.3. For α we can choose between the OS-pinched or the $p*$ scheme (see also Sec. 4.1.2).

Table 6.1.: The scan ranges for the input parameters of the CxSM, where m_s is the scalar mass that is not the 125 GeV Higgs. Taken from [73].

Parameter	Range	
	Lower	Upper
m_s	30 GeV	1000 GeV
m_A	10 GeV	1000 GeV
v_S	1 GeV	1000 GeV
α	-1.57	1.57

Table 6.2.: The SM input parameters used for the calculation. They were taken from the original `HDECAY` input file. The input parameters $\overline{m}_b$ and $\overline{m}_c$ denote the $\overline{\text{MS}}$ quark masses at the given scale. The other fermion masses not given are set to zero. We set the CKM matrix to unity. Table taken from [73].

SM parameter	Value
m_Z	91.153 48 GeV
m_W	80.3579 GeV
$m_{h_{125}}$	125.09 GeV
m_τ	1.776 82 GeV
$\overline{m}_b(m_b)$	4.18 GeV
$\overline{m}_c(3\text{ GeV})$	0.986 GeV
m_t	172.5 GeV
G_μ	$1.166\,378\,7 \times 10^{-5}\,\text{GeV}^{-2}$

The variable `DeltaE` sets the value for the energy cutoff ΔE in the real corrections (see also Sec. 5.3.1).

If `NNLOapp` is set to 1, then the NNLOapprox decay width is taken into account for the Higgs-to-Higgs decays (as discussed in Sec. 5.4), if the relation

$$|\tan(\alpha)\frac{v}{v_S} - 1| \leq \texttt{deltaNNLO}\,, \tag{6.1}$$

is fulfilled, for a chosen value of `deltaNNLO`, i.e. the NLO^2 contribution to the decay width is only considered in the vicinity of where the coupling $\lambda_{h_1h_1h_2}$ vanishes.

If `Paramcon` is set to one, then a parameter conversion is performed where `stdvs`, `stdproc` and `stdalpha` define the input scheme for the v_S and α renormalization (as described above), and the parameters are transformed into the schemes defined by `vsscheme`, `pdprocess` and `ralph_mix`. The transformation is performed as discussed in Sec. 4.3.

6.2. Setup and Parameter Scan

Here we give some technical details on how the calculation was performed, what values we used for our input parameters and how we obtained viable parameter points (cf. [178]).

For the computation of the LO and NLO decay widths, a model file was generated with the Mathematica package `SARAH 4.14.2` [220–223]. The tools `FeynArts 3.10` [224] and

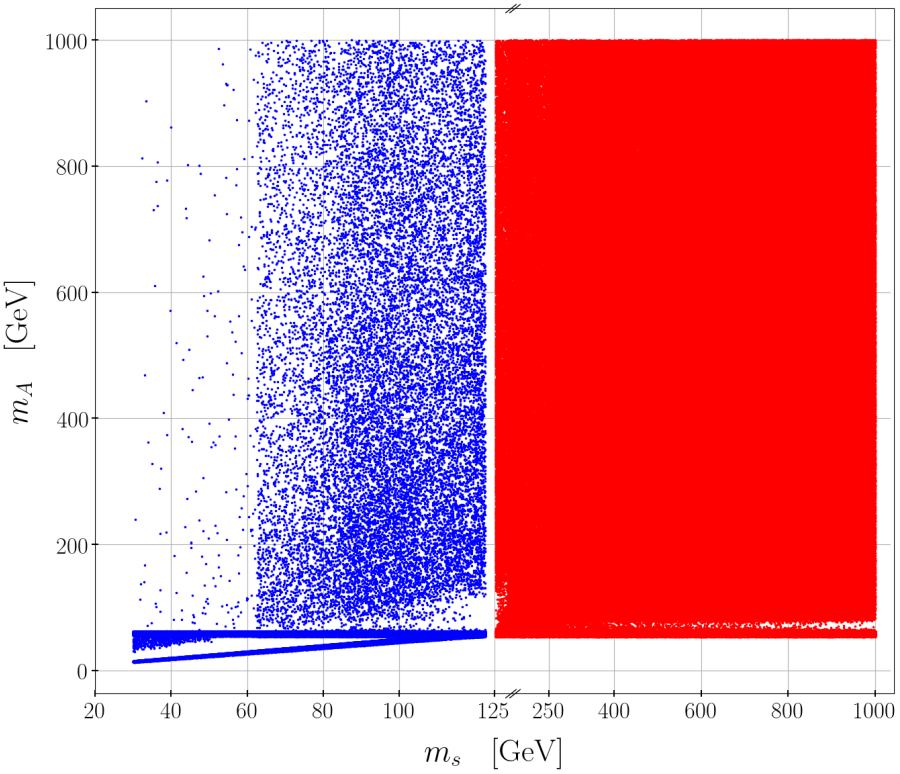

Figure 6.1.: The DM mass m_A plotted against the scalar mass m_s with scenario I ($h_1 = h_{125}$) highlighted in red and scenario II ($h_2 = h_{125}$) highlighted in blue. Figure taken from [73].

`FeynCalc 9.3.1` [225–228] were used to obtain Feynman diagrams and then mathematical expressions for the desired partial widths. The final results were implemented into the code `EWsHDECAY` (see Sec. 6.1). The loop integrals that appear in the calculation are evaluated using `LoopTools 2.15` [229, 230].

To obtain viable parameter points, we used the code `ScannerS` [42, 179]. This program package randomly scans the input parameters of a specified model in a certain range and checks generated parameter points against theoretical and experimental constraints (cf. Sec. 3.2). The constraints from Higgs searches and measurements were obtained from the tools `HiggsBounds` [183–187] and `HiggsSignals` [188, 189]. The DM relic density was calculated with the program `MicrOmegas` [190–192]. These programs were linked to `ScannerS`.

As mentioned in Sec. 3.2, the tree-level cross section for direct detection is negligible in the CxSM [193, 194]. Therefore, we took over results from [195, 196] for the loop-corrected DM-nucleon spin-independent cross section and compared them with experimental limits [197–199].

We used the code `BSMPT 2.6` [231–233] to check if our chosen minimum state is also stable at NLO, i.e. including higher-order corrections to the effective potential. No parameter point that we obtained in our sample was rejected by `BSMPT`. Additionally, we checked if we can have a strong first-order EW phase transition (SFOEWPT), which is needed for EW baryogenesis, as one of the Sakharov conditions [22]. No point in our sample had a SFOEWPT.

We also applied an additional cut on the Higgs masses, i.e. we demanded that the Higgs masses m_{h_1} and m_{h_2} differ by more than 2.5 GeV in order to suppress interfering Higgs signals, which would require a more special treatment in the analysis.

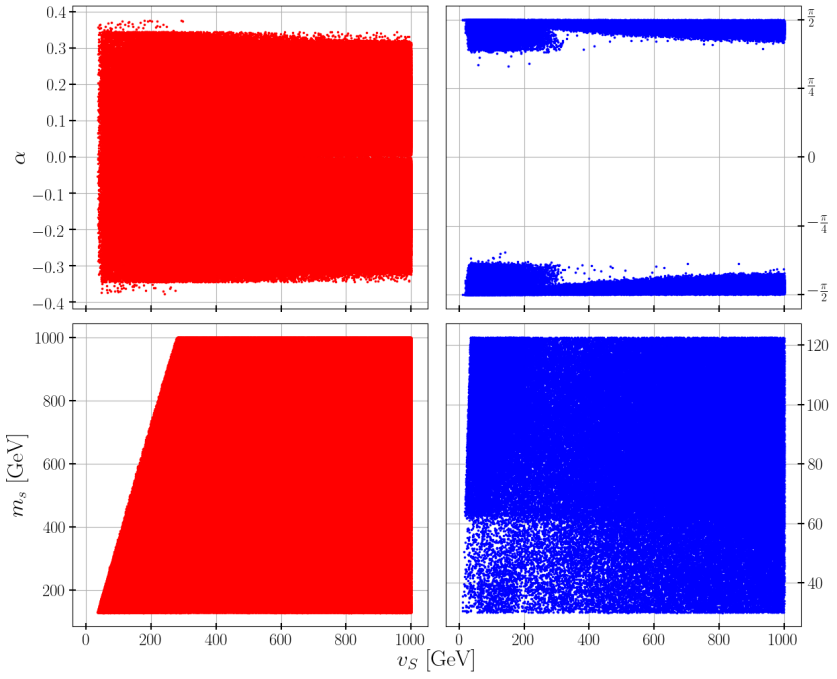

Figure 6.2.: The input parameters α and v_S plotted against each other in the upper row and m_S versus v_S in the lower row, divided into scenario I (left, red points) with $h_1 = h_{125}$ and scenario II (right, blue points) with $h_2 = h_{125}$. Figure taken from [73].

We applied *resonant* di-Higgs constraints, where we followed the prescription given in Sec. 2.3 (cf. [150]). We used NNLO single Higgs production cross sections for the heavy Higgs h_2 via gluon fusion by using the interpolation tables in `ScannerS` which were calculated with `SusHi` [234–236] and LO branching ratios, BR($h_2 \to h_1 h_1$), to calculate the resonant di-Higgs production cross sections (in Sec. 6.4 we will discuss the impact of NLO branching ratios when applying these limits). We compared our obtained values with experimental limits into various final states [165–177].

In total, we scanned for 2 million parameter points. The scan ranges for all input parameters are given in Tab. 6.1, the SM input parameters are given in Tab. 6.2. These points were checked against all constraints explained above.

In the following, we will split the parameter sample into two parts. The parts are classified by the 125 GeV Higgs mass, i.e. if the detected Higgs (denoted as h_{125}) with this mass is the lighter or the heavier Higgs in our model. We thus label points with $m_{h_1} = m_{h_{125}}$ scenario I, where we have a second Higgs m_{h_2} heavier than the 125 GeV Higgs. Points with $m_{h_2} = m_{h_{125}}$ we attribute to scenario II, where we have a second Higgs m_{h_1} lighter than the 125 GeV Higgs.

To give an overview over the allowed parameter space, we show some scatter plots where we display two input parameters against each other. These can be seen in Figs. 6.1 and 6.2. In Fig. 6.1 we show the correlation between the DM mass m_A and the scalar mass m_s, which is defined as the scalar Higgs mass m_{h_i} that is not the 125 GeV Higgs mass. We can see that for heavier masses there is no restriction, whereas for low masses the DM mass has to be close to either half the 125 GeV Higgs mass, or half the m_s mass. The reason is that for low masses the annihilation of DM into gauge bosons via the Higgs portal coupling is kinematically closed, and only the decay channel into bottom quark pairs (and lighter fermions) is available. Thus,

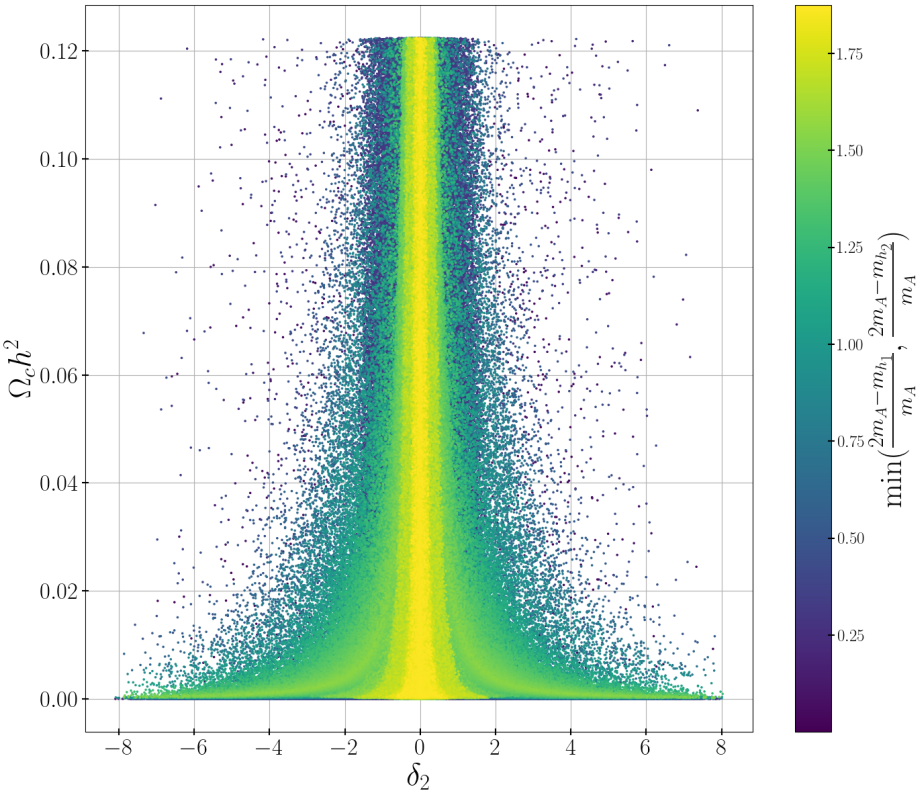

Figure 6.3.: The relic density $\Omega_c h^2$ plotted against the potential parameter δ_2 with the minimum of the quantities $(2m_A - m_{h_i})/m_A$, $i = 1, 2$ in colour code.

in order to reduce the obtained relic density below the observed value, the cross section needs to be enhanced, which can be achieved by choosing the DM mass close to half of one of the other scalar masses and thus resonantly enhancing the cross section and reducing the relic density.

In Fig. 6.2 (upper row), we display the input values α and v_S against each other. We see that the mixing angle is either restricted to values close to 0 in scenario I or close to $\pm\pi/2$. The reason is that the h_{125} couplings to the SM are well known, and as can be seen in Eq. (3.12), they scale with $\cos\alpha$ in scenario I and $\sin\alpha$ in scenario II, thus restricting α close to 0 or $\pm\pi/2$. For small values of v_S we have some outliers where the mixing angle can be larger (or further away from $\pm\pi/2$). For these points, the masses m_s and $m_{h_{125}}$ are close to each other, and `HiggsBounds` and `HiggsSignals` allow for larger mixing angles if the signals of the two Higgs particles overlap.

In Fig. 6.2 (lower row), we also see that m_s and v_S are correlated and large masses with small v_S are forbidden. This is due to the perturbative unitarity constraints that relate m_s and v_S (for more details, see [178]).

Next, in Fig. 6.3 we plot the relic density $\Omega_c h^2$ of all generated parameter points against the potential parameter δ_2 (see Eq. (3.14c)). We can see that we can find parameter points obtaining any value for the relic density, up to the observed value of $(\Omega_c h^2)^{\text{obs}}_{\text{DM}} = 0.120 \pm 0.001$ [11]. Furthermore, we see that for large δ_2 the relic density decreases, which is expected as it is the strength of the Higgs portal coupling, and thus all DM interactions with the Higgs bosons scale with δ_2 which results in a smaller relic density for larger couplings. An exception to this rule are the points with a small $(2m_A - m_{h_i})/m_A$ $(i = 1, 2)$ ratio. Here, as already mentioned, the DM annihilation cross section is resonantly enhanced, thus the parameter points are less dependent on δ_2.

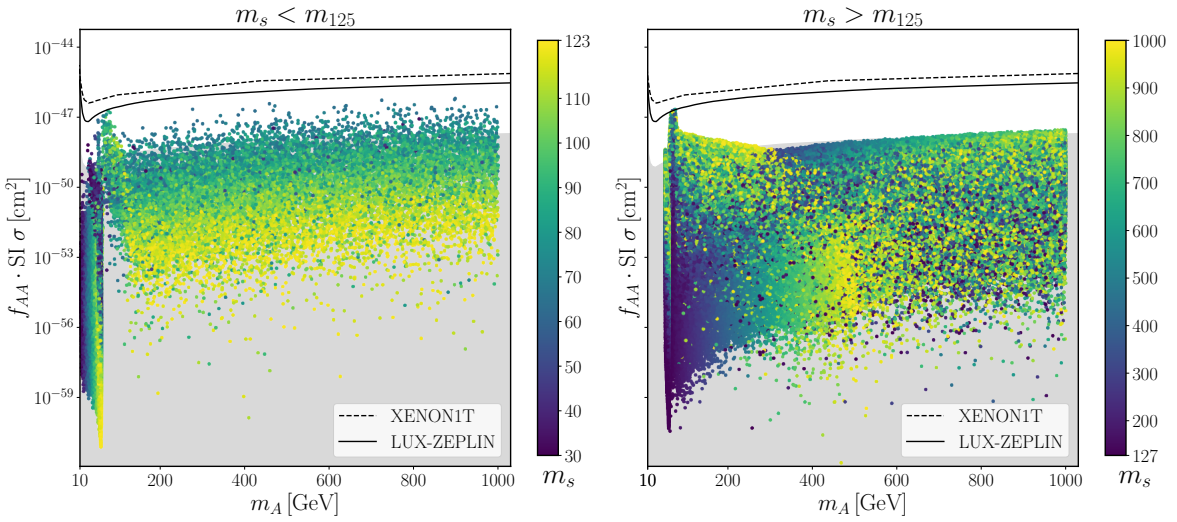

Figure 6.4.: The effective spin-independent DM nucleon scattering cross section ($f_{AA} \cdot \mathrm{SI}\,\sigma$) plotted against the DM mass for the two scenarios (scenario II: left, scenario I: right) with the scalar mass m_s in colour code. The limits from XENON1T [197] and LUX-ZEPLIN [199] are given by the dashed and full lines, respectively. The neutrino floor is indicated as the grey shaded area. Taken from [73].

Next, we discuss the direct detection constraints. First we define the quantity

$$f_{AA} = \frac{(\Omega_c h^2)_A}{(\Omega_c h^2)^{\mathrm{obs}}}\,, \tag{6.2}$$

i.e. the fraction of the relic density of a given parameter point calculated in our model and the observed relic density. In Fig. 6.4, the calculated effective spin-independent scattering cross section $f_{AA} \cdot \mathrm{SI}\,\sigma$ is plotted against the DM mass m_A. We see that most of our points lie well below the current experimental limits (only a few points were rejected by direct detection constraints), and the majority of points are even below the neutrino floor and will not be detectable by direct detection experiments. This emphasizes complementary search strategies, for example collider experiment searches, to explore regions of the parameter space that are difficult to detect or rule out with direct detection experiments. Therefore, precise theoretical predictions for observables at collider experiments, e.g. decay widths and branching ratios, are necessary to be able to compare with increasing experimental accuracy.

In Fig. 6.5 we depict the *resonant* di-Higgs constraints, which we applied on our parameter sample, where we only show the most stringent limits [174–177]. We see that the current experiments are already sensitive to our set of input parameters, and several points are excluded by applying the experimental limits. It is important to note, however, that multiple points are not rejected that lie above experimental limits. They are not rejected because their total heavy Higgs width exceeds 5 %, and we do not apply the *resonant* constraints as they use a narrow width approximation, which, in this case, is no longer valid (cf. Sec. 2.3 and [150]).

Considering *non-resonant* constraints, we can compare upper limits on the trilinear couplings, which are given in the κ_λ framework, i.e. the trilinear $\lambda_{h_{125}h_{125}h_{125}}$ coupling normalized to the SM value. The limits are $\kappa_\lambda \in [-1.4, 6.1]$ by ATLAS [164] and $\kappa_\lambda \in [-1.24, 6.49]$ by CMS [98]. In our sample we find the ranges $\kappa_\lambda \in [0.55, 1.10]$ for scenario I (i.e. $h_1 = h_{125}$) and $\kappa_\lambda \in [0.15, 1.21]$ for scenario II (i.e. $h_2 = h_{125}$). We are therefore still far away from experimental limits, and moreover, we cannot achieve negative trilinear couplings. We remark that for a more precise study one would have to calculate full di-Higgs cross section values,

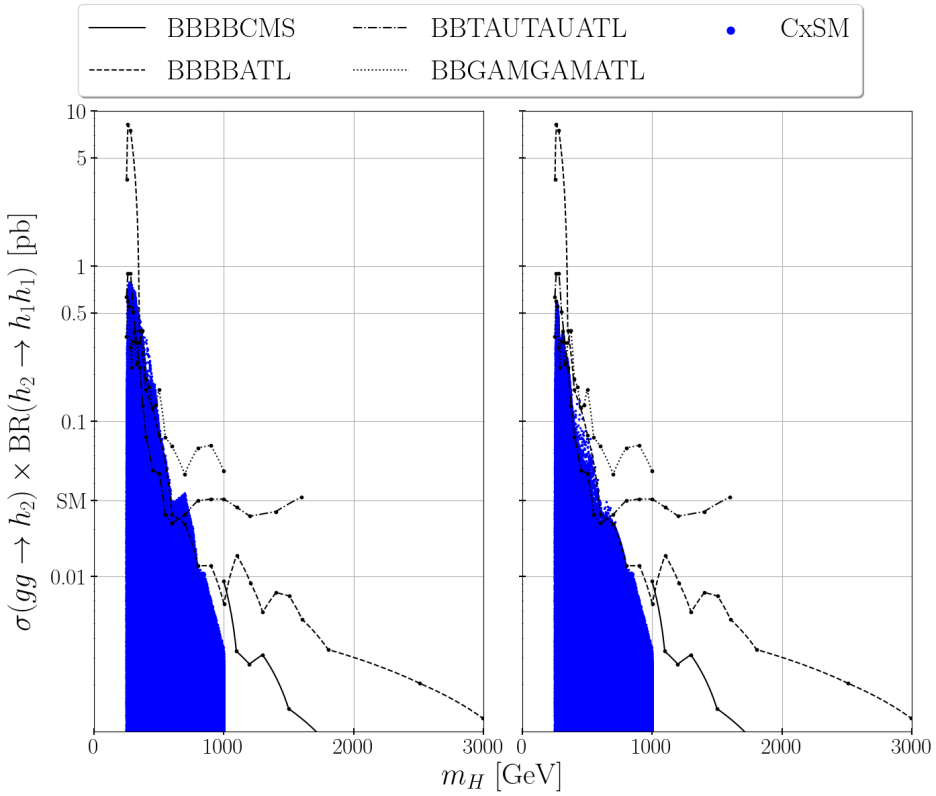

Figure 6.5.: The single heavy Higgs production cross section via gluon fusion ($\sigma(gg \to h_2)$) times branching ratio into two SM-like 125 GeV Higgs bosons ($\mathrm{BR}(h_2 \to h_1 h_1)$) for all parameter points (in blue). Additionally, the di-Higgs constraints into various final states [174–177] are indicated by the dashed lines. On the left we see all points before the constraints were applied, and on the right we see all remaining points after applying the constraints. The SM di-Higgs cross section value is also indicated on the y-axis. For the SM cross section, the NNLO $\mathrm{FT}_{\mathrm{approx}}$ value was taken from [117].

select *non-resonant* points and compare them with experimental limits on the cross section. Since our trilinear couplings (and the Yukawa couplings) are already quite constrained, we do not expect large deviations from our above analysis.

6.3. Size and Impact of the Electroweak NLO Corrections

We now turn to the discussion of the electroweak NLO corrections to Higgs decays in the CxSM. First, we define the relative corrections $\delta_{\mathrm{EW}}(h_i \to XX)$ as

$$\delta_{\mathrm{EW}}(h_i \to XX) = \frac{\Gamma^{\mathrm{NLO}}_{h_i \to XX} - \Gamma^{\mathrm{LO}}_{h_i \to XX}}{\Gamma^{\mathrm{LO}}_{h_i \to XX}}, \tag{6.3}$$

with a generic final state XX and the decay widths Γ of a given decay process $h_i \to XX$ ($i = 1, 2$) at LO and NLO, respectively. We use the following convention to label the combination of schemes which we used. ZEM is the ZEM scheme, and OS is the process-dependent scheme, used for the renormalization of v_S. With proc1, we label the process $h_1 \to AA$ and with proc2, the process $h_2 \to AA$ which is used in the ZEM or process-dependent scheme. We label the renormalization of α either with OS or with $p*$ for the OS-pinched or the p^*-pinched scheme, respectively. Thus, OSproc1-p^* would stand for the process-dependent scheme with $h_1 \to AA$ and OS states used for the renormalization of v_S and the p^*-pinched scheme used for the renormalization of α. The definitions of all schemes are given in Chapter 4.

Table 6.3.: Relative NLO corrections $\delta_{\mathrm{EW}}(h_i \to XX)$ for scenario I for all decay channels and renormalization schemes. Taken from [73].

	OSproc1-OS		OSproc1-p_*		OSproc2-OS		OSproc2-p_*	
	Min	Max	Min	Max	Min	Max	Min	Max
$h_1 \to cc$	−1.48 %	0.0 %	−1.43 %	0.0 %	−4.68 %	0.0 %	−4.82 %	0.0 %
$h_1 \to bb$	−1.44 %	0.0 %	−1.39 %	0.0 %	−4.64 %	0.0 %	−4.78 %	0.0 %
$h_1 \to \tau\tau$	−4.64 %	0.0 %	−4.59 %	0.0 %	−7.84 %	0.0 %	−7.98 %	0.0 %
$h_1 \to AA$	0.0 %	0.0 %	0.0 %	0.0 %	−2.1 %	6.76 %	−2.24 %	7.2 %
$h_2 \to cc$	−9.62 %	0.0 %	−10.0 %	0.0 %	−10.6 %	19.64 %	−10.95 %	24.99 %
$h_2 \to bb$	−9.18 %	4.85 %	−9.55 %	5.32 %	−10.16 %	19.71 %	−10.51 %	25.06 %
$h_2 \to \tau\tau$	−16.31 %	0.0 %	−16.76 %	0.0 %	−19.01 %	16.39 %	−19.47 %	21.74 %
$h_2 \to tt$	−6.15 %	5.46 %	−6.1 %	6.1 %	−6.15 %	11.04 %	−6.1 %	10.91 %
$h_2 \to WW$	−8.36 %	10.7 %	−8.36 %	10.92 %	−8.36 %	20.92 %	−8.36 %	22.95 %
$h_2 \to ZZ$	−2.27 %	5.69 %	−2.18 %	6.54 %	−2.27 %	13.41 %	−2.18 %	14.64 %
$h_2 \to h_1 h_1$	−14.15 %	10.64 %	−14.04 %	10.55 %	−99.39 %	>100 %	−98.24 %	>100 %
$h_2 \to AA$	−6.76 %	2.1 %	−7.2 %	2.24 %	0.0 %	0.0 %	0.0 %	0.0 %
	ZEMproc1-OS		ZEMproc1-p_*		ZEMproc2-OS		ZEMproc2-p_*	
	Min	Max	Min	Max	Min	Max	Min	Max
$h_1 \to cc$	−4.68 %	−0.93 %	−4.82 %	−0.66 %	−4.68 %	−0.93 %	−4.82 %	−0.66 %
$h_1 \to bb$	−4.64 %	−0.89 %	−4.78 %	−0.62 %	−4.64 %	−0.89 %	−4.78 %	−0.62 %
$h_1 \to \tau\tau$	−7.84 %	−4.08 %	−7.98 %	−3.82 %	−7.84 %	−4.08 %	−7.98 %	−3.82 %
$h_1 \to AA$	−3.51 %	5.73 %	−3.51 %	5.73 %	−4.62 %	9.49 %	−5.0 %	9.94 %
$h_2 \to cc$	−99.7 %	19.64 %	−99.77 %	24.99 %	−99.7 %	19.64 %	−99.77 %	24.99 %
$h_2 \to bb$	−99.94 %	19.71 %	−99.57 %	25.06 %	−99.94 %	19.71 %	−99.57 %	25.06 %
$h_2 \to \tau\tau$	−99.31 %	16.39 %	−98.96 %	21.74 %	−99.31 %	16.39 %	−98.96 %	21.74 %
$h_2 \to tt$	−99.28 %	11.04 %	−99.11 %	10.91 %	−99.28 %	11.04 %	−99.11 %	10.91 %
$h_2 \to WW$	−99.6 %	20.92 %	−99.59 %	22.95 %	−99.6 %	20.92 %	−99.59 %	22.95 %
$h_2 \to ZZ$	−99.89 %	13.41 %	−99.76 %	14.64 %	−99.89 %	13.41 %	−99.76 %	14.64 %
$h_2 \to h_1 h_1$	−99.95 %	>100 %	−100.0 %	>100 %	−99.92 %	>100 %	−99.88 %	>100 %
$h_2 \to AA$	−100.0 %	5.64 %	−100.0 %	5.82 %	−15.22 %	9.08 %	−15.22 %	9.08 %

In Tabs. 6.3 and 6.4 we summarize the minimal and maximal sizes of the EW corrections that we obtained for each decay channel and each renormalization scheme. Here, we did not convert the input parameters from one scheme to another but assumed that the input parameters were given in the chosen scheme. Thus, the values for each renormalization scheme should not be compared but considered individually. We also rejected relative EW corrections that were smaller than −100 %.

We see that many decay channels have relatively small to medium size corrections (up to 25 %) which is expected, as EW corrections should not be too large compared to the LO result. There are, however, several decay channels in various renormalization schemes that have very large EW corrections, and these need to be explained. Moreover, only the scalar decays depend on v_S as input at LO (since the couplings to SM particles only scale with $\cos\alpha$ or $\sin\alpha$, see Eqs. (3.12)). Thus, the other decay channels give the same result for both the process-dependent or ZEM scheme. The ZEM scheme, however, can be used for all parameter

Table 6.4.: Relative NLO corrections $\delta_{\mathrm{EW}}(h_i \to XX)$ for scenario II for all decay channels and renormalization schemes. Taken from [73].

	OSproc1-OS		OSproc1-p_*		OSproc2-OS		OSproc2-p_*	
	Min	Max	Min	Max	Min	Max	Min	Max
$h_1 \to cc$	−1.31 %	6.81 %	−1.47 %	2.14 %	−49.12 %	27.99 %	−48.25 %	38.5 %
$h_1 \to bb$	−1.29 %	6.02 %	−1.67 %	0.82 %	−49.17 %	27.17 %	−48.3 %	37.37 %
$h_1 \to \tau\tau$	−4.4 %	5.31 %	−4.47 %	1.61 %	−52.03 %	26.53 %	−51.15 %	37.54 %
$h_1 \to AA$	0.0 %	0.0 %	0.0 %	0.0 %	−5.57 %	3.63 %	−1.24 %	5.2 %
$h_2 \to cc$	−1.42 %	0.0 %	−1.42 %	0.0 %	−1.44 %	0.0 %	−1.43 %	0.0 %
$h_2 \to bb$	−1.38 %	0.0 %	−1.38 %	0.0 %	−1.4 %	0.0 %	−1.4 %	0.0 %
$h_2 \to \tau\tau$	−4.58 %	0.0 %	−4.57 %	0.0 %	−4.59 %	0.0 %	−4.59 %	0.0 %
$h_2 \to h_1h_1$	−10.61 %	46.48 %	−10.76 %	46.52 %	−11.64 %	>100 %	−11.71 %	>100 %
$h_2 \to AA$	−3.63 %	5.57 %	−5.2 %	1.24 %	0.0 %	0.0 %	0.0 %	0.0 %
	ZEMproc1-OS		ZEMproc1-p_*		ZEMproc2-OS		ZEMproc2-p_*	
	Min	Max	Min	Max	Min	Max	Min	Max
$h_1 \to cc$	−49.12 %	29.13 %	−48.25 %	38.5 %	−49.12 %	29.13 %	−48.25 %	38.5 %
$h_1 \to bb$	−49.17 %	28.29 %	−48.3 %	37.37 %	−49.17 %	28.29 %	−48.3 %	37.37 %
$h_1 \to \tau\tau$	−52.03 %	27.73 %	−51.15 %	37.54 %	−52.03 %	27.73 %	−51.15 %	37.54 %
$h_1 \to AA$	0.0 %	7.08 %	0.0 %	7.08 %	−3.03 %	8.13 %	−0.54 %	9.7 %
$h_2 \to cc$	−10.96 %	−1.35 %	−10.57 %	−1.35 %	−10.96 %	−1.36 %	−10.57 %	−1.35 %
$h_2 \to bb$	−10.92 %	−1.32 %	−10.53 %	−1.31 %	−10.92 %	−1.32 %	−10.53 %	−1.31 %
$h_2 \to \tau\tau$	−14.11 %	−4.51 %	−13.73 %	−4.5 %	−14.11 %	−4.51 %	−13.73 %	−4.5 %
$h_2 \to h_1h_1$	−72.49 %	>100 %	−58.37 %	>100 %	−30.3 %	>100 %	−30.29 %	>100 %
$h_2 \to AA$	−52.57 %	8.79 %	−47.71 %	4.94 %	−40.94 %	5.82 %	−40.94 %	5.82 %

points, whereas the OS process-dependent scheme can only be used if the decay chosen for the renormalization is kinematically allowed. Therefore, the sample used for the results with an OS renormalization is smaller, and the minimum and maximum value can be different compared to the ZEM scheme, even if the scheme change itself does not have an impact on specific decays. Furthermore, in scenario II, the decay channels into WW, ZZ and tt are kinematically not allowed, since we only consider on-shell decays.

The large corrections have several origins that will be explained in the following. First, we see that in the process-dependent scheme the EW corrections are in general smaller than in the ZEM scheme. The reason for this is because in the ZEM scheme we do not have kinematic restrictions on the scalar masses and we can have threshold effects that can increase the size of the counterterms and thus of the NLO corrections significantly. More precisely, if the difference $2m_A - m_{h_i}$ is small but positive (thus the process-dependent scheme cannot be applied), the integral $\mathrm{DB0}(m_{h_i}^2, m_A^2, m_A^2)$ (which shows up in the $\delta Z_{h_ih_i}$ counterterms) has a discontinuity, which can lead to large corrections.

Another reason for large corrections is that the scalar couplings can become large. Although we apply the perturbative unitarity constraints on the quartic couplings of the Higgs potential (cf. Sef. 3.2) the quartic couplings can still be larger than 4π (and therefore also the trilinear couplings appearing in the decay widths), which is often used as an upper limit for perturbativity. Thus, these large couplings can lead to large corrections. As can be seen in

Table 6.5.: Relative NLO corrections $\delta_{\mathrm{EW}}(h_i \to XX)$ for scenario I for all decay channels and renormalization schemes, after additional cuts were applied on the parameter space. Taken from [73].

	OSproc1-OS		OSproc1-p_*		OSproc2-OS		OSproc2-p_*	
	Min	Max	Min	Max	Min	Max	Min	Max
$h_1 \to cc$	−1.48 %	0.0 %	−1.43 %	0.0 %	−1.58 %	0.0 %	−1.49 %	0.0 %
$h_1 \to bb$	−1.44 %	0.0 %	−1.39 %	0.0 %	−1.54 %	0.0 %	−1.45 %	0.0 %
$h_1 \to \tau\tau$	−4.64 %	0.0 %	−4.59 %	0.0 %	−4.74 %	0.0 %	−4.64 %	0.0 %
$h_1 \to AA$	0.0 %	0.0 %	0.0 %	0.0 %	−2.1 %	6.27 %	−2.24 %	5.89 %
$h_2 \to cc$	−9.62 %	0.0 %	−10.0 %	0.0 %	−10.6 %	5.95 %	−10.95 %	8.45 %
$h_2 \to bb$	−9.18 %	3.96 %	−9.55 %	4.03 %	−10.16 %	6.58 %	−10.51 %	8.56 %
$h_2 \to \tau\tau$	−16.31 %	0.0 %	−16.76 %	0.0 %	−17.1 %	2.5 %	−17.69 %	5.0 %
$h_2 \to tt$	−6.05 %	5.32 %	−6.1 %	5.2 %	−6.05 %	7.28 %	−6.1 %	6.9 %
$h_2 \to WW$	−8.3 %	10.7 %	−8.36 %	10.92 %	−8.3 %	11.75 %	−8.36 %	12.24 %
$h_2 \to ZZ$	−2.16 %	5.65 %	−2.18 %	5.59 %	−2.16 %	8.67 %	−2.18 %	8.97 %
$h_2 \to h_1h_1$	−6.35 %	6.13 %	−6.7 %	5.41 %	−54.96 %	10.88 %	−54.18 %	10.53 %
$h_2 \to AA$	−6.27 %	2.1 %	−5.89 %	2.24 %	0.0 %	0.0 %	0.0 %	0.0 %
	ZEMproc1-OS		ZEMproc1-p_*		ZEMproc2-OS		ZEMproc2-p_*	
	Min	Max	Min	Max	Min	Max	Min	Max
$h_1 \to cc$	−1.58 %	−1.15 %	−1.49 %	−1.06 %	−1.58 %	−1.15 %	−1.49 %	−1.06 %
$h_1 \to bb$	−1.54 %	−1.11 %	−1.45 %	−1.02 %	−1.54 %	−1.11 %	−1.45 %	−1.02 %
$h_1 \to \tau\tau$	−4.74 %	−4.31 %	−4.64 %	−4.21 %	−4.74 %	−4.31 %	−4.64 %	−4.21 %
$h_1 \to AA$	−2.45 %	4.47 %	−2.45 %	4.47 %	−4.62 %	4.72 %	−5.0 %	4.57 %
$h_2 \to cc$	−17.65 %	5.95 %	−18.0 %	8.45 %	−17.65 %	5.95 %	−18.0 %	8.45 %
$h_2 \to bb$	−12.93 %	6.58 %	−13.33 %	8.56 %	−12.93 %	6.58 %	−13.33 %	8.56 %
$h_2 \to \tau\tau$	−28.84 %	2.5 %	−29.19 %	5.0 %	−28.84 %	2.5 %	−29.19 %	5.0 %
$h_2 \to tt$	−18.96 %	7.28 %	−18.95 %	6.9 %	−18.96 %	7.28 %	−18.95 %	6.9 %
$h_2 \to WW$	−21.15 %	11.75 %	−21.14 %	12.24 %	−21.15 %	11.75 %	−21.14 %	12.24 %
$h_2 \to ZZ$	−15.01 %	8.67 %	−15.0 %	8.97 %	−15.01 %	8.67 %	−15.0 %	8.97 %
$h_2 \to h_1h_1$	−49.8 %	89.17 %	−49.98 %	88.84 %	−55.45 %	11.58 %	−54.67 %	11.58 %
$h_2 \to AA$	−99.98 %	5.64 %	−99.99 %	5.82 %	−15.22 %	6.17 %	−15.22 %	6.17 %

the Eqs. (5.6), the couplings become large if v_S is chosen small compared to the scalar masses m_{h_i} $(i = 1, 2)$.

Another fact to consider is the interplay between the various applied constraints. They can already reject points that would otherwise lead to large corrections (coming from the above described origins), and thus only for certain scenarios and renormalization schemes do we observe large corrections in the Tabs. 6.3 and 6.4.

The decay channel $h_2 \to h_1h_1$ is more intricate. We already mentioned that the LO decay width of this process can vanish (see Sec. 5.4). Thus, in the region of parameter space where the coupling vanishes, the NLO corrections can become as large or even larger than the LO contribution. Moreover, as in the previous cases, large couplings and threshold effects can lead to large NLO corrections.

Table 6.6.: Relative NLO corrections $\delta_{\mathrm{EW}}(h_i \to XX)$ for scenario II for all decay channels and renormalization schemes, after additional cuts were applied on the parameter space. Taken from [73].

	OSproc1-OS		OSproc1-p_*		OSproc2-OS		OSproc2-p_*	
	Min	Max	Min	Max	Min	Max	Min	Max
$h_1 \to cc$	−1.31 %	5.31 %	−1.34 %	2.14 %	−1.31 %	12.78 %	−1.34 %	19.76 %
$h_1 \to bb$	−1.29 %	4.45 %	−1.32 %	0.82 %	−2.77 %	11.92 %	−1.32 %	18.51 %
$h_1 \to \tau\tau$	−4.4 %	3.93 %	−4.43 %	1.61 %	−4.4 %	11.39 %	−4.43 %	18.97 %
$h_1 \to AA$	0.0 %	0.0 %	0.0 %	0.0 %	−4.67 %	1.01 %	−1.24 %	1.52 %
$h_2 \to cc$	−1.42 %	0.0 %	−1.42 %	0.0 %	−1.44 %	0.0 %	−1.43 %	0.0 %
$h_2 \to bb$	−1.38 %	0.0 %	−1.38 %	0.0 %	−1.4 %	0.0 %	−1.4 %	0.0 %
$h_2 \to \tau\tau$	−4.58 %	0.0 %	−4.57 %	0.0 %	−4.59 %	0.0 %	−4.59 %	0.0 %
$h_2 \to h_1h_1$	−10.61 %	46.48 %	−10.76 %	46.52 %	−11.64 %	>100 %	−11.71 %	>100 %
$h_2 \to AA$	−1.01 %	4.67 %	−1.52 %	1.24 %	0.0 %	0.0 %	0.0 %	0.0 %
	ZEMproc1-OS		ZEMproc1-p_*		ZEMproc2-OS		ZEMproc2-p_*	
	Min	Max	Min	Max	Min	Max	Min	Max
$h_1 \to cc$	−1.31 %	12.78 %	−1.34 %	19.76 %	−1.31 %	12.78 %	−1.34 %	19.76 %
$h_1 \to bb$	−2.77 %	11.92 %	−1.32 %	18.51 %	−2.77 %	11.92 %	−1.32 %	18.51 %
$h_1 \to \tau\tau$	−4.4 %	11.39 %	−4.43 %	18.97 %	−4.4 %	11.39 %	−4.43 %	18.97 %
$h_1 \to AA$	0.0 %	2.56 %	0.0 %	2.56 %	−3.03 %	2.63 %	−0.54 %	3.19 %
$h_2 \to cc$	−5.64 %	−1.35 %	−5.54 %	−1.35 %	−5.64 %	−1.36 %	−5.54 %	−1.35 %
$h_2 \to bb$	−5.6 %	−1.32 %	−5.5 %	−1.31 %	−5.6 %	−1.32 %	−5.5 %	−1.31 %
$h_2 \to \tau\tau$	−8.8 %	−4.51 %	−8.69 %	−4.5 %	−8.8 %	−4.51 %	−8.69 %	−4.5 %
$h_2 \to h_1h_1$	−72.49 %	>100 %	−58.37 %	>100 %	−30.3 %	>100 %	−30.29 %	>100 %
$h_2 \to AA$	−17.37 %	5.76 %	−12.06 %	4.02 %	−13.53 %	2.84 %	−13.53 %	2.84 %

Another feature that appears in the ZEM scheme is that the counterterm δv_S in this scheme increases if the difference between the dark matter mass m_A and the scalar mass m_{h_i} increases ($i = 1$ if ZEMproc1 is chosen and $i = 2$ if ZEMproc2 is chosen, i.e. the difference between m_A and the mass of the initial state particle of the decay considered for the ZEM scheme). This leads to large corrections if we choose to renormalize with the ZEM1 scheme (i.e. the lighter Higgs mass) and go to large DM masses. Thus, the mass difference becomes large, and in turn the NLO corrections to the decays $h_i \to AA$ ($i = 1, 2$) and $h_2 \to h_1h_1$ can become sizable (recall that only they depend on the v_S renormalization).

To showcase our findings, we applied additional cuts to our parameter space to remove points with large scalar couplings and threshold effects. Therefore, we applied the constraints

- $|2m_A - m_{h_i}| > 9\,\mathrm{GeV}$,
- $|\lambda| < 4\pi$,

where λ here stands for all the quartic couplings $\lambda_{h_ih_jh_kh_l}, \lambda_{h_ih_jAA}, \lambda_{AAAA}$ $(i, j, k, l = 1, 2)$. We then obtain the sizes for the NLO corrections given in the Tabs. 6.5 and 6.6. We see that now only the decay channels $h_2 \to h_1h_1$ in several renormalization schemes and $h_i \to AA$ $(i = 1, 2)$ in the ZEMproc1 scheme still have large relative corrections. They originate, as explained, from the fact that the LO width can vanish for the decay $h_2 \to h_1h_1$ and the ZEMproc1 scheme can lead to large corrections for large mass differences $m_A - m_{h_1}$.

Table 6.7.: Relative corrections δ_{EW} and relative renormalization scheme uncertainties δ_{ren} for all decay channels and renormalization schemes for benchmark point `BP1`. The input parameters α and v_S are given in the corresponding renormalization scheme. Taken from [73].

	OSproc1-OS		OSproc1-p_*		OSproc2-OS		OSproc2-p_*	
α	0.1654		0.1655		0.1654		0.1655	
v_S	439.21 GeV		439.37 GeV		444.64 GeV		444.64 GeV	
	δ_{EW}	δ_{ren}	δ_{EW}	δ_{ren}	δ_{EW}	δ_{ren}	δ_{EW}	δ_{ren}
$h_1 \to cc$	−1.4 %	0.0 %	−1.4 %	0.0 %	−1.4 %	0.0 %	−1.4 %	0.0 %
$h_1 \to bb$	−1.36 %	0.0 %	−1.36 %	0.0 %	−1.36 %	0.0 %	−1.36 %	0.0 %
$h_1 \to \tau\tau$	−4.56 %	0.0 %	−4.56 %	0.0 %	−4.56 %	0.0 %	−4.56 %	0.0 %
$h_1 \to AA$	0.0 %	−3.01 %	0.0 %	−3.01 %	2.44 %	−0.64 %	2.37 %	−0.71 %
$h_2 \to cc$	−5.26 %	0.0 %	−5.33 %	−0.08 %	−5.26 %	0.0 %	−5.32 %	−0.07 %
$h_2 \to bb$	−1.23 %	0.0 %	−1.3 %	−0.07 %	−1.23 %	0.0 %	−1.3 %	−0.07 %
$h_2 \to \tau\tau$	−14.16 %	0.0 %	−14.22 %	−0.08 %	−14.15 %	0.0 %	−14.22 %	−0.08 %
$h_2 \to tt$	−2.23 %	0.01 %	−2.3 %	−0.05 %	−2.24 %	0.0 %	−2.31 %	−0.07 %
$h_2 \to WW$	−0.27 %	0.01 %	−0.34 %	−0.06 %	−0.28 %	0.0 %	−0.35 %	−0.07 %
$h_2 \to ZZ$	2.73 %	0.01 %	2.67 %	−0.06 %	2.73 %	0.0 %	2.66 %	−0.07 %
$h_2 \to h_1 h_1$	0.72 %	0.25 %	0.66 %	0.19 %	0.52 %	0.05 %	0.46 %	−0.01 %
$h_2 \to AA$	−2.46 %	−3.11 %	−2.39 %	−3.04 %	0.0 %	−0.67 %	0.0 %	−0.67 %
	ZEMproc1-OS		ZEMproc1-p_*		ZEMproc2-OS		ZEMproc2-p_*	
α	0.1654		0.1655		0.1654		0.1655	
v_S	447.05 GeV		447.21 GeV		446.14 GeV		446.14 GeV	
	δ_{EW}	δ_{ren}	δ_{EW}	δ_{ren}	δ_{EW}	δ_{ren}	δ_{EW}	δ_{ren}
$h_1 \to cc$	−1.4 %	0.0 %	−1.4 %	0.0 %	−1.4 %	0.0 %	−1.4 %	0.0 %
$h_1 \to bb$	−1.36 %	0.0 %	−1.36 %	0.0 %	−1.36 %	0.0 %	−1.36 %	0.0 %
$h_1 \to \tau\tau$	−4.56 %	0.0 %	−4.56 %	0.0 %	−4.56 %	0.0 %	−4.56 %	0.0 %
$h_1 \to AA$	3.51 %	0.4 %	3.51 %	0.4 %	3.11 %	0.0 %	3.03 %	−0.07 %
$h_2 \to cc$	−5.25 %	0.0 %	−5.32 %	−0.07 %	−5.25 %	0.0 %	−5.32 %	−0.07 %
$h_2 \to bb$	−1.23 %	0.0 %	−1.3 %	−0.07 %	−1.23 %	0.0 %	−1.3 %	−0.07 %
$h_2 \to \tau\tau$	−14.15 %	0.0 %	−14.22 %	−0.08 %	−14.15 %	0.0 %	−14.22 %	−0.08 %
$h_2 \to tt$	−2.25 %	0.0 %	−2.32 %	−0.07 %	−2.25 %	0.0 %	−2.32 %	−0.07 %
$h_2 \to WW$	−0.28 %	0.0 %	−0.35 %	−0.07 %	−0.28 %	0.0 %	−0.35 %	−0.07 %
$h_2 \to ZZ$	2.72 %	0.0 %	2.65 %	−0.07 %	2.73 %	0.0 %	2.66 %	−0.07 %
$h_2 \to h_1 h_1$	0.44 %	−0.03 %	0.37 %	−0.1 %	0.47 %	0.0 %	0.41 %	−0.06 %
$h_2 \to AA$	1.08 %	0.41 %	1.16 %	0.48 %	0.67 %	0.0 %	0.67 %	0.0 %

Next, we consider the theoretical renormalization scheme uncertainty. We use as an estimate the relative difference between two renormalization schemes δ_{ren}, which is defined as

$$\delta_{\text{ren}} = \frac{\Gamma^b - \Gamma^{\text{ZEMproc2-OS}}}{\Gamma^{\text{ZEMproc2-OS}}}\,, \tag{6.4}$$

Table 6.8.: Relative corrections δ_{EW} and relative renormalization scheme uncertainties δ_{ren} for all decay channels and renormalization schemes for benchmark point BP2. The input parameters α and v_S are given in the corresponding renormalization scheme. Taken from [73].

	OSproc2-OS		OSproc2-p_*	
α	-1.5669		-1.5668	
v_S	23.74 GeV		24.49 GeV	
	δ_{EW}	δ_{ren}	δ_{EW}	δ_{ren}
$h_1 \to cc$	14.45 %	-4.09 %	8.4 %	-9.16 %
$h_1 \to bb$	13.71 %	-4.11 %	7.66 %	-9.21 %
$h_1 \to \tau\tau$	12.86 %	-4.14 %	6.81 %	-9.28 %
$h_2 \to cc$	-1.38 %	0.0 %	-1.38 %	0.0 %
$h_2 \to bb$	-1.34 %	0.0 %	-1.34 %	0.0 %
$h_2 \to \tau\tau$	-4.54 %	0.0 %	-4.54 %	0.0 %
$h_2 \to AA$	0.0 %	47.22 %	0.0 %	47.22 %

	ZEMproc1-OS		ZEMproc1-p_*		ZEMproc2-OS		ZEMproc2-p_*	
α	-1.5669		-1.5668		-1.5669		-1.5668	
v_S	21.58 GeV		21.58 GeV		20.46 GeV		21.21 GeV	
	δ_{EW}	δ_{ren}	δ_{EW}	δ_{ren}	δ_{EW}	δ_{ren}	δ_{EW}	δ_{ren}
$h_1 \to cc$	17.4 %	-1.61 %	10.74 %	-7.19 %	19.33 %	0.0 %	11.11 %	-6.88 %
$h_1 \to bb$	16.66 %	-1.62 %	10.01 %	-7.24 %	18.59 %	0.0 %	10.38 %	-6.93 %
$h_1 \to \tau\tau$	15.81 %	-1.64 %	9.15 %	-7.29 %	17.74 %	0.0 %	9.52 %	-6.98 %
$h_2 \to cc$	-1.38 %	0.0 %	-1.38 %	0.0 %	-1.38 %	0.0 %	-1.38 %	0.0 %
$h_2 \to bb$	-1.34 %	0.0 %	-1.34 %	0.0 %	-1.34 %	0.0 %	-1.34 %	0.0 %
$h_2 \to \tau\tau$	-4.54 %	0.0 %	-4.54 %	0.0 %	-4.54 %	0.0 %	-4.54 %	0.0 %
$h_2 \to AA$	-18.93 %	19.35 %	-25.59 %	9.55 %	-32.07 %	0.0 %	-29.83 %	3.3 %

where b is the label for the chosen new renormalization scheme and we always use the ZEMproc2-OS scheme as the standard input scheme. We also have to convert the input parameters from the initial to the new scheme (see Sec. 4.3).

We selected two benchmark points to show examples for the sizes of the theoretical uncertainties which can occur. The first benchmark point, BP1, has the input parameters:

BP1: $m_{h_1} = 125.09\,\text{GeV}$, $m_{h_2} = 590.48\,\text{GeV}$, $m_A = 61.93\,\text{GeV}$, $v_S = 446.13\,\text{GeV}$, $\alpha = 0.1654$.

We summarized the changes in the input parameters dependent on the renormalization scheme, the EW corrections δ_{EW} and the theoretical uncertainty δ_{ren} for all decay channels in Tab. 6.7. First of all, we see that the theoretical uncertainty is zero for the ZEMproc2-OS scheme, which is our input scheme. Furthermore, the input parameters α and v_S change only slightly, which is also expected as the theoretical uncertainty for this benchmark point also only amounts up to about 3 %. Moreover, the relative EW corrections are small and do not exceed 15 %.

Additionally, we selected another benchmark point BP2 with the input parameters:

BP2: $m_{h_1} = 67.96\,\text{GeV}$, $m_{h_2} = 125.09\,\text{GeV}$, $m_A = 58.29\,\text{GeV}$, $v_S = 20.46\,\text{GeV}$, $\alpha = -1.5669$.

We see that here v_S is small compared to the scalar masses m_{h_1} and m_{h_2} and thus expect large couplings and potentially large EW corrections. In Tab. 6.8 we summarize again the relative EW corrections and the theoretical uncertainties for all decay channels. Since the decay $h_1 \to AA$ is kinematically not available for this benchmark point, we cannot use the OSproc1 schemes.

We see that the relative EW corrections are relatively large, especially for the decay $h_2 \to AA$, and also the theoretical uncertainty is large. We have to note, however, that in the OSproc2 decays we use the process $h_2 \to AA$ for renormalization and thus the NLO width equals the LO width. We then compare this LO result with the NLO width in the other scheme when we compute δ_{ren} for this change of renormalization schemes. Since the NLO corrections for this decay are large, the theoretical uncertainty is also substantial. If we change to other ZEM schemes, we see that the theoretical uncertainty can be large for the $h_2 \to AA$ decay, but if we only change the renormalization scheme for α (i.e. OS to p^*), we see that the theoretical uncertainty is only around 3 %. Similarly, if we consider the h_1 decays into SM fermions, we see that the theoretical uncertainty is larger if we change the renormalization scheme for α. Since these decays do not depend on the v_S counterterm, this is to be expected.

To summarize, we can observe, that the theoretical uncertainties are of small or moderate size, if the EW corrections are also small or moderate, but if the EW corrections turn large, the theoretical scheme uncertainties tend to increase as well.

6.4. Impact of NLO Corrections on the Parameter Space

We investigated the impact of NLO corrections on the allowed parameter space. In order to achieve this, we linked our code `EWsHDECAY` with `ScannerS` to use the NLO decay widths instead of the LO widths when checking for the implemented constraints described in Sec. 6.2. Moreover, we also applied the *resonant* di-Higgs constraints with NLO branching ratios. We used our generated parameter sample and rechecked for each point if it would be allowed with this setup. For the choice of renormalization scheme, we used the ZEMproc2-OS scheme, as it is one of the more stable schemes while also being applicable for the full parameter space (in contrast to the OSproc schemes).

As a result, a small fraction of parameter points that were allowed using LO widths, are now rejected at NLO. However, the overall shape of the parameter space did not change. We again rejected large negative NLO corrections which would lead to negative decay widths, and used then only the LO widths.

Next, we investigated the impact of NLO branching ratios on the di-Higgs constraints. If we consider LO branching ratios, the benchmark point `BP3`, given by

`BP3`: $m_{h_1} = 125.09\,\text{GeV}$, $m_{h_2} = 260.96\,\text{GeV}$, $m_A = 257.36\,\text{GeV}$, $v_S = 87.61\,\text{GeV}$, $\alpha = -0.312$,

has the highest allowed resonant di-Higgs production cross section. The trilinear (κ_{hhh}) and top-Yukawa (y_{t,h_i}) couplings normalized to the SM couplings for this benchmark point are given by

- $\kappa_{h_1h_1h_1} = 0.781\,, y_{t,h_1} = 0.952\,,$
- $\kappa_{h_2h_1h_1} = 1.122\,, y_{t,h_2} = 0.307\,.$

The cross sections using the LO branching ratio or the NLO branching ratio in all schemes that can be applied here are given by

- LO: $\sigma(gg \to h_2 \to h_1h_1) = 584.6\,\text{fb}\,,$

- ZEMproc1-OS: $\sigma(gg \to h_2 \to h_1 h_1) = 559.8\,\text{fb}\,(75.28\,\text{GeV}\,, -0.312)\,,$
- ZEMproc1-p^*: $\sigma(gg \to h_2 \to h_1 h_1) = 559.9\,\text{fb}\,(75.39\,\text{GeV}\,, -0.312)\,,$
- ZEMproc2-OS: $\sigma(gg \to h_2 \to h_1 h_1) = 600.2\,\text{fb}\,(87.61\,\text{GeV}\,, -0.312)\,,$
- ZEMproc2-p^*: $\sigma(gg \to h_2 \to h_1 h_1) = 600.1\,\text{fb}\,(87.60\,\text{GeV}\,, -0.312)\,,$

where we also give the values for v_S and α in the respective scheme in brackets.

If we now consider NLO branching ratios to constrain our parameter space, a different benchmark point `BP4`, given by

`BP4`: $m_{h_1} = 125.09\,\text{GeV}$, $m_{h_2} = 262.25\,\text{GeV}$, $m_A = 337.43\,\text{GeV}$, $v_S = 101\,\text{GeV}$, $\alpha = -0.317$,

has the highest cross section value. The trilinear and top-Yukawa couplings for this benchmark point are given by

- $\kappa_{h_1 h_1 h_1} = 0.783\,, y_{t,h_1} = 0.950\,,$
- $\kappa_{h_2 h_1 h_1} = 1.081\,, y_{t,h_2} = 0.312\,.$

The cross sections in all schemes are given by

- LO: $\sigma(gg \to h_2 \to h_1 h_1) = 577.61\,\text{fb}\,,$
- ZEMproc1-OS: $\sigma(gg \to h_2 \to h_1 h_1) = 524\,\text{fb}\,(85.59\,\text{GeV}\,, -0.317)\,,$
- ZEMproc1-p^*: $\sigma(gg \to h_2 \to h_1 h_1) = 524.2\,\text{fb}\,(85.72\,\text{GeV}\,, -0.318)\,,$
- ZEMproc2-OS: $\sigma(gg \to h_2 \to h_1 h_1) = 579\,\text{fb}\,(101.03\,\text{GeV}\,, -0.317)\,,$
- ZEMproc2-p^*: $\sigma(gg \to h_2 \to h_1 h_1) = 578.8\,\text{fb}\,(101.02\,\text{GeV}\,, -0.318)\,.$

We see that `BP3` has a higher cross section value in the ZEMproc2-OS scheme than `BP4` (recall that we use this scheme when we apply the constraints with NLO results), and therefore `BP3` is excluded if we apply the constraints with NLO results.

Overall, we see that points can be allowed at LO but are above the experimental limits with NLO branching ratios, and points can be rejected with LO branching ratios but be allowed with NLO values. Moreover, we do not apply the constraints if the total width is too large (as described in Sec. 2.3), but with the inclusion of the NLO corrections, a parameter point can cross from one categorization to the other, meaning that the total width can decrease or increase to be below or above our defined threshold, where we apply *resonant* constraints or not.

To summarize, points with a resonant di-Higgs cross section close to experimental bounds should be viewed with caution, as the inclusion of NLO corrections, a different choice of renormalization schemes or how the experimental limits are applied, i.e. what we define as a narrow width, might change the categorization of this parameter point, i.e. if it is still allowed or rejected by experimental constraints.

Another scenario, which we investigated, was the large NLO corrections to the scalar Higgs decay $h_2 \to h_1 h_1$ in the case of a small LO amplitude due to a vanishing coupling $\lambda_{h_2 h_1 h_1}$. We considered the benchmark point `BP5` from our sample of valid parameter points, given by

`BP5`: $m_{h_1} = 46.11\,\text{GeV}$, $m_{h_2} = 125.09\,\text{GeV}$, $m_A = 60.88\,\text{GeV}$, $v_S = 818.10\,\text{GeV}$, $\alpha = 1.390$.

Looking at the input parameters, we see that v_S is large compared to the scalar masses. Therefore, the scalar trilinear and quartic couplings are small. We thus do not expect large EW corrections, except for the decay $h_2 \to h_1 h_1$, since the quantities v_S/v and $\tan\alpha$ are of

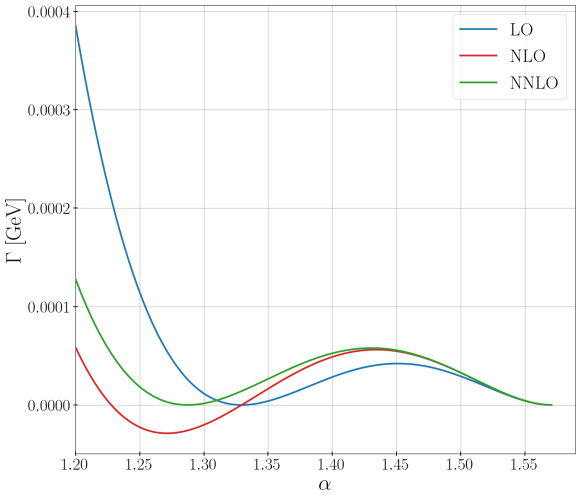

Figure 6.6.: The partial decay width Γ for the process $h_2 \to h_1 h_1$ for benchmark point `BP6` with varying α, at LO (blue), NLO (red), and approximate NNLO (green). Taken from [73].

the same order ($v_S/v = 3.32264\,, \tan\alpha = 5.47069$) and therefore the coupling $\lambda_{h_2 h_1 h_1}$ is close to its vanishing point. For this point we have $\delta_{\text{EW}} = 0.55$ (in the ZEMproc2-OS scheme) for the decay $h_2 \to h_1 h_1$, whereas the EW corrections for the other decay channels are only up to a few percent.

This point is valid when we use the LO decay widths, but when we use the NLO widths for our constraints, it is rejected by `HiggsSignals`. Thus, we see that the NLO corrections can indeed have a profound impact on certain areas of the parameter space, e.g. where the scalar trilinear Higgs coupling vanishes.

6.5. Analysis of NLO^2 Corrections

In this section we want to illustrate the NLO^2 contribution to the decay $h_2 \to h_1 h_1$. We use as a benchmark point:

`BP6`: $m_{h_1} = 60\,\text{GeV}$, $m_{h_2} = 125\,\text{GeV}$, $m_A = 40\,\text{GeV}$, $v_S = 1\,\text{TeV}$.

We do not specify α but vary it to see the different effects of the contribution to the approximate NNLO decay width. We show the dependence of the decay width on α in Fig. 6.6 for the LO, NLO and approximate NNLO result. For $\alpha = \arctan\dfrac{v_S}{v} \approx 1.33$ the tree-level amplitude and therefore the LO and NLO decay width vanish. Since we have a non-zero contribution from the NLO amplitude, the NLO^2 contribution is non-zero, and the approximate NNLO width does not vanish at this point and is the exact leading result in the sense that also the genuine two-loop contributions here vanish since they are multiplied with the LO amplitude (cf. Sec. 5.4). If we, however, move away from this point by varying α, we have to include genuine 2-loop contributions for a precise prediction.

We also see that for smaller angles the NLO width becomes negative and therefore unphysical, and the LO and NNLO approximate results always remain non-negative as expected. If we take the limit $\alpha \to \pi/2$ all contributions vanish since we then decouple the additional particles in the theory from the SM.

CHAPTER 7

Conclusion

In this part, we discussed our project, which is a continuation of [178], of calculating and analyzing electroweak corrections to Higgs decays in the CxSM. We first introduced the model and set up our notation. In our realization of the model with two separate $\mathbb{Z}_2$ symmetries, we have an additional Higgs boson and a stable DM candidate, leading to an interesting phenomenology. We described the theoretical and experimental constraints that we applied in order to obtain valid parameter points, which we then used as input.

We summarized the steps we took to renormalize the model in order to calculate higher-order corrections. We used an OS prescription for our fields and masses and applied the alternative tadpole scheme to obtain gauge-independent counterterms and results. We also specified different schemes for our input parameters, the process-dependent and the ZEM scheme for v_S and the OS- and p^*-pinched scheme for α, and we illustrated how to change from one renormalization scheme to another. Next, we described our calculation and the different contributions to our decay widths, including counterterms and real corrections to obtain UV and IR finite as well as gauge-independent results. Furthermore, we discussed the possibility of vanishing tree level amplitudes and the subsequent inclusion of NLO^2 contributions in the decay channel $h_2 \to h_1 h_1$.

We then moved on to the implementation of our calculation. We first described our code `EWsHDECAY` which contains all of our NLO corrections, and we gave an example on how to use it. In the code, it is possible to switch on or off the NLO corrections, to change from one renormalization scheme to another, including the conversion of parameters and to include the NLO^2 contributions for the $h_2 \to h_1 h_1$ decay. We then described our setup on how we performed our calculation and how we obtained viable parameter points with `ScannerS` and the additional constraints (i.e. direct detection and di-Higgs constraints), that we applied. We then illustrated the parameter space and gave some insights on the constraints and their impact on our sample. We found that our sample is sensitive to both direct detection and collider constraints, but many parameter points are below the neutrino floor and therefore difficult (if not impossible) to measure via direct detection. Thus, complementary search strategies at colliders are important. Moreover, the SM-like trilinear coupling is already constrained to be close to the SM value in our parameter sample, and we can also saturate the DM relic density.

We then discussed the typical sizes of the EW corrections to all Higgs decay channels in all possible renormalization schemes we worked out. We found that they are usually of small to moderate size (up to 25 %) but can become large if the scalar couplings are large and/or the scalar masses are chosen in a way that we have threshold effects, or our counterterms in one of the schemes become sizeable (in the ZEM scheme when the DM mass is large compared to the other scalar masses). We also considered the theoretical renormalization scheme uncertainty, i.e. the difference between two renormalization schemes, and concluded that it is well behaved if also the EW corrections are small.

We furthermore examined the impact of the NLO corrections on our parameter space, i.e. we rechecked our sample with constraints applied with NLO corrected widths and branching ratios. We concluded that, although some points are excluded or no longer excluded with the inclusion of NLO corrections, the overall shape of the allowed parameter regions does not change significantly. There are, however, some subtle impacts which the higher-order corrections can have on the constraints from di-Higgs searches and in the case of vanishing $\lambda_{h_2 h_1 h_1}$ trilinear coupling, since this coupling can be enhanced at NLO. It is also important to note that with increasing experimental accuracy, the higher-order corrections from theory become more important to map out the allowed parameter space. Finally, we discussed the impact of the NLO^2 contribution, which becomes important near the point where the tree level amplitude vanishes.

Part II.

Higgs Pair Production in a Realization of a Composite 2HDM

CHAPTER 8

Introduction

In this project, we investigated Higgs pair (or di-Higgs) production in a composite two-Higgs doublet model (2HDM). Our goal was to analyze and quantify the impact of the new particles and couplings from the composite sector of the theory on the overall cross section, as well as on differential distributions and compare these results to other models.

As we already mentioned in Chapter 1 and in Sec. 2.2, composite Higgs models are theoretically well motivated as they give a dynamical explanation of the Higgs mechanism and can solve the hierarchy problem. Moreover, in order not to run into fine-tuning issues, the scale of new physics of the composite sector cannot be too high, i.e. around a few TeV and therefore, these models are sensitive to current and future experiments. In these models, the Higgs potential is already determined by the composite sector, and we have a top-to-bottom approach where we have a UV complete theory, which produces effects at lower energies that can be observed. This is another approach compared to e.g. part I, where we expanded the scalar sector without a specific UV complete realization and an undetermined scalar potential.

Composite models, or more broadly spoken, theories with additional strong sectors have been discussed extensively in the literature (cf. e.g. [237–239], or for reviews, see [54, 86, 88, 95]) as an alternative approach to electroweak symmetry breaking. They came into conflict, however, with the electroweak precision measurements at the Large Electron-Positron Collider (LEP) (cf. [54]). Thus, a new class of models emerged, namely composite Higgs models [45–53], where a naturally lighter Higgs compared to a heavier composite sector can emerge with the help of the Goldstone boson theorem (compare e.g. to pions, that can be seen as pseudo-Nambu Goldstone bosons in chiral perturbation theory[2] and have lighter masses compared to the scale of Quantum Chromodynamics (QCD) or e.g. the proton mass, cf. [54]).

In this project, we furthermore focused on Higgs pair production. As already mentioned in Sec. 2.3, di-Higgs production is an interesting process to consider, as it has not been measured yet but can give key insights to the Higgs potential and is therefore very sensitive to physics beyond the SM that extends the scalar sector. Thus, di-Higgs production is an excellent tool to probe composite Higgs models and has been already discussed in the literature [152–156], but mainly for models with a minimal SM-like scalar sector, i.e. one Higgs doublet. In our project, we considered a composite Higgs model with a 2HDM-like extended scalar

[2] See e.g. [240] for an extensive review.

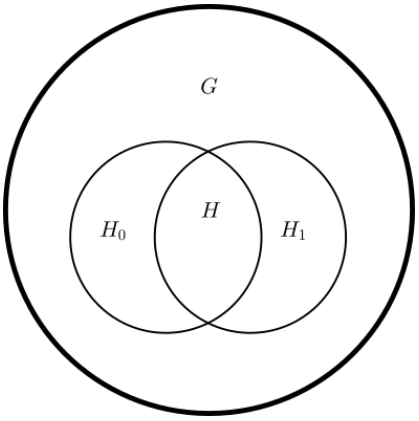

Figure 8.1.: Simplified sketch of the group structure for a generic composite Higgs model with a global symmetry G spontaneously broken to a subgroup H_1 and a gauged subgroup H_0 with the intersection $H = H_1 \cap H_0$ (cf. [54]).

sector where we have additional heavy Higgs particles, heavy top partners and new effective couplings that contribute to di-Higgs production.

We now present the content of this part. We will first give an introduction to composite Higgs models and then the realization of a composite 2HDM that we used. We then summarize the effective Lagrangian and the Feynman rules we used for our computation and describe the calculation of the di-Higgs cross section, where we also mention NLO corrections. Next, we highlight the implementation of our calculation and our setup to obtain viable parameter points satisfying theoretical and experimental constraints, especially di-Higgs constraints. Finally, we analyze the effects of our model for inclusive cross sections and differential distributions and compare the composite 2HDM to the SM and other 2HDM realizations.

In this chapter, we briefly summarize composite Higgs models in Sec. 8.1 and our composite 2HDM (Sec. 8.2). We will only mention the important details. For more information on composite Higgs models, we refer to [54, 86, 88] and for more information on the composite 2HDM see [69]. Furthermore, we introduce some notation for elementary 2HDMs in Sec. 8.3 and describe the theoretical and experimental constraints we applied on the composite 2HDM (Sec. 8.4).

The described setup and evaluation parts follow our published results [74].

8.1. Introduction to Composite Higgs Models

For this introduction, we follow mainly the reviews [54, 86, 88] where more information can be found.

In composite Higgs models, the Higgs boson is not an elementary field but emerges as a bound state of a strongly interacting sector (usually called composite sector). Therefore, the hierarchy problem is avoided, as the inner structure of the Higgs is resolved at a cutoff scale if one goes to higher energies. Thus, naively we would expect the Higgs mass to be of the order of this cutoff scale, where also the new physics from the composite sector emerges. In order to have a separation between the Higgs and the composite sector (to remedy the fact that we have not seen any other particles from the composite sector), the Higgs emerges as a pseudo Nambu-Goldstone boson (pNGB) of an enlarged global symmetry. This mechanism then leads to a naturally light Higgs, comparable to how pions in chiral pertubation theory can be naturally lighter than the QCD scale (cf. [54]).

In general terms, we have a global symmetry G that will be spontaneously broken to a symmetry H_1 at a scale f. Moreover, we have a symmetry group $H_0 \subset G$ that is gauged by external vector bosons (see Fig. 8.1 for a sketch of the group structure). The spontaneous symmetry breaking $G \to H_1$ then implies that we generate $n = \dim(G) - \dim(H_1)$ Goldstone bosons. If H is the intersection of H_1 and H_0, $H = H_1 \cap H_0$, then $n_0 = \dim(H_0) - \dim(H)$ Goldstone bosons are absorbed by as many vector bosons to obtain masses. The remaining $n - n_0$ Goldstone bosons are the (so far massless) scalars that will become the Higgs fields in our composite model.

The SM fields are in this setup defined as external to the new composite sector, and for simplicity, one identifies H_0 with the SM EW gauge group, i.e. $H_0 = G_{\text{SM}} \equiv SU(2)_{\text{L}} \times U(1)_{\text{Y}}$ (the colour group $SU(3)_{\text{c}}$ plays no role here as it is unbroken and can be omitted).

Moreover, two more conditions need to hold. The SM gauge group G_{SM} must be embeddable in the unbroken subgroup H_1, $G_{\text{SM}} \subset H_1$ as then G_{SM} is unbroken at tree level. Furthermore, the coset G/H_1 must contain at least one $SU(2)$ doublet that can then be identified as the Higgs doublet.

In the setup we have thus far, the overall symmetry G is spontaneously broken but not explicitly broken. Therefore, all the Goldstone bosons retain their shift symmetry (i.e. we can shift the fields by a constant, which means that we only have derivative interactions). We do not generate a scalar potential and our scalars are massless. Therefore, we want to explicitly break the symmetry G in order to generate a scalar potential and masses dynamically. We achieve this by coupling our strong sector to SM fields that do not transform under the global symmetry G, by introducing mixing terms in the Lagrangian and thus explicitly breaking the symmetry. This mechanism is called partial compositeness (first introduced in [241], see the reviews [86, 88] for more details). Another attractive feature of this approach is that it can generate the hierarchical flavour structure of the SM.

Another important mechanism is collective symmetry breaking [242–245]. It means that often in composite models the global symmetry (in our case G) is copied, with a gauged subgroup in only one of the copies. These symmetry copies are then collectively broken, i.e. only with the inclusion of several interaction terms in the Lagrangian. Thus, the loop corrections generated by these interactions that break this symmetry have to entail all of the symmetry-breaking parts and therefore the generated corrections are less cutoff sensitive, i.e. instead of a quadratic dependence on a UV cutoff scale, we only have a logarithmic dependence or even a UV finite result (see [86, 88] for more details).

With the described setup, we now generate a Higgs potential at loop level with SM fields, which in turn can break the electroweak symmetry and dynamically generate a VEV v. An important quantity then is the ratio

$$\xi = \frac{v^2}{f^2}\,, \tag{8.1}$$

i.e. the ratio of the dynamically generated quantity v and the scale of the new composite sector f. With naive dimensional analysis we then expect

$$m_h \sim g_{\text{SM}} v\,, \qquad m_\rho \sim g_\rho f\,, \tag{8.2}$$

where g_{SM} are typical SM couplings and ρ are fields in the composite sector with gauge couplings g_ρ. In the limit $f \to \infty$ ($\xi \to 0$) we can now see that the composite sector decouples, whereas the Higgs can remain light, and we recover the SM. The other limit ($\xi \to 1$) would lead us to Higgs masses of the order of the composite sector and to the regime of technicolour models.

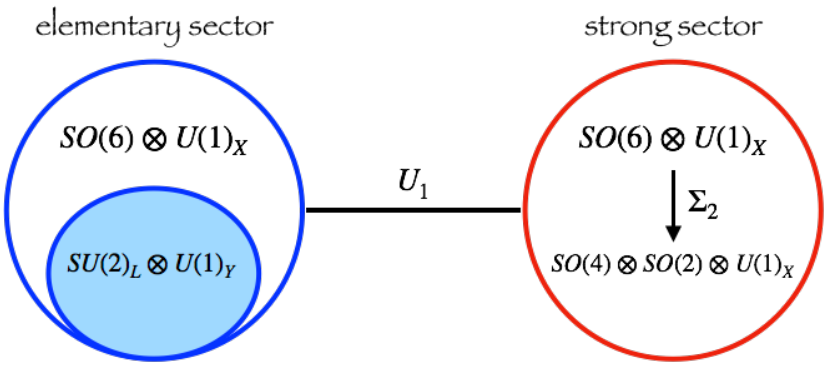

Figure 8.2.: Pictorial representation of the symmetry group of the Composite 2HDM. Taken from [69].

8.2. A Specific Realization of a Composite 2HDM

After a more general introduction to composite Higgs models, we will now discuss a specific realization [65–69]. In our setup we will furthermore have an extended Higgs sector, resembling a 2-Higgs Doublet model (2HDM).

We start by establishing the symmetry of the new composite sector. In our case we have $\mathcal{G} = SO(6)$, which is spontaneously (and then later explicitly) broken to $\mathcal{H} = SO(4) \times SO(2)$. Using the dimension of an $SO(N)$ theory given by $(N(N-1))/2$, we obtain $n = 15-(6+1) = 8$ broken symmetries and therefore the number of Goldstone bosons. In a 2HDM we also have 8 real scalar fields (3 of them will give masses to the W and Z boson). Thus, in the composite 2HDM, the scalar fields that constitute the 2HDM structure are (pseudo) Nambu Goldstone bosons.

To be more precise, the full coset structure is

$$\frac{\mathcal{G}}{\mathcal{H}} = \frac{SU(3)_c \times SO(6) \times U(1)_X}{SU(3)_c \times SO(4) \times SO(2) \times U(1)_X}\,, \tag{8.3}$$

where we added the unbroken $SU(3)_c$ colour group and an additional $U(1)_X$ gauge group that will contribute to the hypercharge (for more details on this additional gauge group, see e.g. [86]). The next step is that we double this construction, i.e. we have a two-sided approach (see also Fig. 8.2). We have two symmetry groups, $G_1, G_2 = SO(6) \times U(1)_X$, where G_2 is a gauged symmetry and describes spin-1 resonances through ρ_μ^X and ρ_μ^A ($A \in \mathrm{Adj}(SO(6))$), and G_1 is a global symmetry with only $SU(2)_\mathrm{L} \times U(1)_\mathrm{Y}$ gauged, i.e. only the SM gauge fields embedded. The Lagrangian of the gauge sector then reads

$$\begin{aligned}\mathcal{L}^{\text{gauge}}_{\text{C2HDM}} = {} & \frac{f_1^2}{4}\mathrm{Tr}\,|D_\mu U_1|^2 + \frac{f_2^2}{4}\mathrm{Tr}\,|D_\mu \Sigma_2|^2 - \frac{1}{4g_\rho^2}(\rho^A)_{\mu\nu}(\rho^A)^{\mu\nu} \\ & - \frac{1}{4g_{\rho_X}^2}(\rho^X)_{\mu\nu}(\rho^X)^{\mu\nu} - \frac{1}{4g_A^2}(A^A)_{\mu\nu}(A^A)^{\mu\nu} - \frac{1}{4g_X^2}X_{\mu\nu}X^{\mu\nu}\,,\end{aligned} \tag{8.4}$$

where we introduced the fields U_1 and Σ_2 and the composite gauge coupling g_ρ. U_1 is the link field that transforms under both symmetries G_1 and G_2. It realizes spontaneous symmetry breaking from $G_1 \times G_2$ to a diagonal symmetry group G. The field Σ_2 accounts for the breaking to $SO(4) \times SO(2) \times U(1)_X$. The SM EW gauge fields are embedded into the spurion fields $(A^A)_\mu$ and X_μ with the gauge couplings g_A and g_X. The terms $X_{\mu\nu}$, $(A^A)_{\mu\nu}$, $(\rho^A)_{\mu\nu}$ and $(\rho^X)_{\mu\nu}$ are the field strength tensors for the corresponding gauge fields X_μ, $(A^A)_\mu$, $(\rho^A)_\mu$ and $(\rho^X)_\mu$. The constants f_1 and f_2 are combined to the composite scale f, via

$$f^{-2} = f_1^{-2} + f_2^{-2}\,. \tag{8.5}$$

For a complete description of the covariant derivatives and the transformation properties of these fields, see [69]. The Nambu Goldstone boson (NGB) fluctuations are described by U, which is constructed via

$$U = e^{i\frac{\Pi}{f}}, \quad \Pi \equiv \sqrt{2}\phi_i^{\hat{a}} T_i^{\hat{a}} = -i \begin{pmatrix} 0_{4\times4} & \mathbf{\Phi} \\ -\mathbf{\Phi}^T & 0_{2\times2} \end{pmatrix}, \tag{8.6}$$

with the 8 broken $SO(6)$ generators $T_i^{\hat{a}}$ ($i = 1, 2$, $\hat{a} = 1, .., 4$), the real scalar fields $\phi_i^{\hat{a}}$ and $\mathbf{\Phi} \equiv (\phi_1^{\hat{a}}, \phi_2^{\hat{a}})$. These scalar fields can then be arranged into the doublets Φ_i,

$$\Phi_i = \frac{1}{\sqrt{2}} \begin{pmatrix} \phi_i^{\hat{2}} + i\phi_i^{\hat{1}} \\ \phi_i^{\hat{4}} - i\phi_i^{\hat{3}} \end{pmatrix}. \tag{8.7}$$

We furthermore have $\Sigma_2 = U_2 \Sigma_0 U_2^{\mathrm{T}}$, with $\Sigma_0 = \mathrm{diag}(0_{4\times4}, i\sigma_2)$ and σ_2 being one of the Pauli matrices. The U_i ($i = 1, 2$) are given by $U_i = \exp(i(f\Pi/f_i^2))$ with the NGB matrix Π given in Eq. (8.6). The VEVs of the scalar fields are given as $\langle \phi_i^{\hat{4}} \rangle = v_i$ ($i = 1, 2$), and we define $v^2 = v_1^2 + v_2^2$ and $\tan\beta \equiv v_2/v_1$ similar to an elementary 2HDM. The quantity v can be related to the SM VEV v_{SM} via

$$v_{\mathrm{SM}}^2 = f^2 \sin^2 \frac{v}{f}, \tag{8.8}$$

and in the $f \to \infty$ limit they coincide.

Now, we turn to the description of the fermionic sector. In contrast to the Lagrangian in the gauge sector, which is determined already by the imposed symmetries, the fermionic part is not uniquely determined. In this realization of the model, the SM fermions are embedded into the fundamental representation of $SO(6)$ and two resonances Ψ^I ($I = 1, 2$) are introduced. The fermionic Lagrangian is given by

$$\begin{aligned} \mathcal{L}_{\mathrm{C2HDM}}^{\mathrm{fermion}} = {} & (\bar{q}_L^{\mathbf{6}}) i \not{D} (q_L^{\mathbf{6}}) + (\bar{t}_R^{\mathbf{6}}) i \not{D} (t_R^{\mathbf{6}}) + \bar{\Psi}^I i \not{D} \Psi^I \\ & - \bar{\Psi}_{\mathrm{L}}^I (M_\Psi)^{IJ} \Psi_{\mathrm{R}}^J - \bar{\Psi}_{\mathrm{L}}^I \left[(Y_1)^{IJ} \Sigma_2 + (Y_2)^{IJ} \Sigma_2^2 \right] \Psi_{\mathrm{R}}^J \\ & + (\Delta_L)^I (\bar{q}_L^{\mathbf{6}}) U_1 \Psi_{\mathrm{R}}^I + (\Delta_R)^I (\bar{t}_R^{\mathbf{6}}) U_1 \Psi_{\mathrm{L}}^I + \mathrm{h.c.}\,. \end{aligned} \tag{8.9}$$

The fields q_L and t_R are embeddings of the top quark (other fermions can be embedded similarly) and Ψ^I are additional spin-1/2 resonances. The other input parameters appearing are the fermion couplings to resonances, Y_1, Y_2, the parameters determining partial compositeness Δ_L, Δ_R, and the composite fermion mass matrix M_Ψ. These parameters together with the parameters in the gauge sector Lagrangian will determine the Higgs potential of the model. With this formulation of the fermionic sector, we introduce several new fermionic resonances. We have 8 additional top-like heavy fermions (that will be referred to as top partners) and other more exotic resonances that do not play a role in di-Higgs production and are therefore not discussed here (cf. [69, 74] for more details).

In this configuration, we have the parameters in the fermionic sector, which are Y_1, Y_2, Δ_L, Δ_R and M_Ψ. Moreover, we enforce the UV finiteness of the Higgs potential at one-loop order by requiring the coefficients of the quadratic and logarithmic divergences to cancel. These conditions can be used to eliminate e.g. the M_Ψ matrix as an input parameter in terms of the other input parameters (cf. [69, 74]).

More details on the model can be found in [69], e.g. the flavour alignment in the Yukawa sector similar to the flavour-aligned 2HDM, how the Higgs potential is obtained via the Coleman-Weinberg formalism, how much tuning is required to obtain the correct values for electroweak symmetry breaking, and many other aspects.

To summarize the model, we have an additional strong sector with an $SO(6)$ symmetry and spontaneous breaking $SO(6) \to SO(4) \times SO(2)$, that generates a 2HDM-like structure. We then use partial compositeness of SM fields to explicitly break the symmetry, and generate masses for the scalar sector. With this setup, the scalar potential is determined by composite parameters. The top quark (and the other fermions) are incorporated into sextuplets, where at the end, we have 8 additional top partners. The input parameters that characterize our model are

$$Y_1^{IJ},\, Y_2^{IJ},\, \Delta_L^I,\, \Delta_R^I,\, g_\rho,\, f \quad (I,J=1,2)\,. \tag{8.10}$$

Our model thus resembles an elementary flavour-aligned 2HDM [246, 247], where we have a SM-like Higgs h, the CP-even heavy Higgs H, a pseudoscalar A and a charged Higgs $H^\pm$, with additional top partners and effective couplings, where the couplings and the Higgs potential are determined by the composite nature of the theory. In this setup, the mass of the lighter Higgs h scales like $m_h \sim v$, whereas the other Higgs states are proportional to the compositness scale f, i.e. $m_H \sim m_A \sim m_{H^\pm} \sim f$, up to corrections induced by mixing [69].

Finally, as we already mentioned in Sec. 8.1, if we take the limit $f \to \infty$ we decouple the composite sector, i.e. the H, A, and $H^\pm$ Higgs scalars and top partners become heavy and their couplings to SM particles go to zero. Furthermore, all the effective quartic scalar-scalar-fermion-fermion couplings $G_{hhT_iT_i}$ (for their description see Sec. 9.1) vanish. Thus, in this decoupling limit we retain the SM.

8.3. The Elementary 2HDM Lagrangian

In the last section, we mentioned that the described composite model resembles a 2HDM. Since we compare the composite 2HDM with other 2HDM realizations in Sec. 10.3.4 and in order to setup some more notation, we give a brief introduction into elementary 2HDMs [248–253] (see also [84] for a review), where the SM is extended by an additional Higgs doublet without any additional composite sector or other UV completion. We therefore have two complex $SU(2)_\mathrm{L}$ Higgs doublets Φ_1, Φ_2 and the scalar Lagrangian $\mathcal{L}_\mathrm{Scalar}$ is given by

$$\mathcal{L}_\mathrm{Scalar} = (D_\mu \Phi_1)^\dagger (D^\mu \Phi_1) + (D_\mu \Phi_2)^\dagger (D^\mu \Phi_2) - V_\mathrm{2HDM}\,, \tag{8.11}$$

with the covariant derivative D_μ (see Eq. (2.2)) and the scalar potential in the 2HDM,

$$\begin{aligned} V_\mathrm{2HDM} = {} & m_{11}^2|\Phi_1|^2 + m_{22}^2|\Phi_2|^2 - (m_{12}^2 \Phi_1^\dagger \Phi_2 + \mathrm{h.c.}) + \frac{\lambda_1}{2}(\Phi_1^\dagger\Phi_1)^2 + \frac{\lambda_2}{2}(\Phi_2^\dagger\Phi_2)^2 \\ & + \lambda_3(\Phi_1^\dagger\Phi_1)(\Phi_2^\dagger\Phi_2) + \lambda_4(\Phi_1^\dagger\Phi_2)(\Phi_2^\dagger\Phi_1) \\ & + \left(\frac{\lambda_5}{2}(\Phi_1^\dagger\Phi_2)^2 + \left[\lambda_6(\Phi_1^\dagger\Phi_1) + \lambda_7(\Phi_2^\dagger\Phi_2)\right](\Phi_1^\dagger\Phi_2) + \mathrm{h.c.}\right)\,, \end{aligned} \tag{8.12}$$

with the mass parameters m_{11}^2, m_{12}^2 and m_{22}^2 and the scalar couplings λ_i $(i = 1,..,7)$. In general, the parameters m_{12}^2, λ_5, λ_6 and λ_7 can be complex, the other parameters are real. The two Higgs doublets can be expanded as

$$\Phi_a = \begin{pmatrix} \phi_a^+ \\ \dfrac{v_a + \rho_a + i\eta_a}{\sqrt{2}} \end{pmatrix}\,, \qquad a = 1,2\,, \tag{8.13}$$

with the real scalar fields ρ_a, η_a, the charged scalars ϕ_a^+ and the VEVs v_a. If we have CP conservation, the two neutral CP-even fields ρ_a mix with a mixing angle α and we obtain the CP-even mass eigenstates h, H,

$$\begin{pmatrix} H \\ h \end{pmatrix} = \begin{pmatrix} \cos\alpha & \sin\alpha \\ -\sin\alpha & \cos\alpha \end{pmatrix} \begin{pmatrix} \rho_1 \\ \rho_2 \end{pmatrix} . \tag{8.14}$$

Similarly, the fields η_a and ϕ_a^+ are rotated with a mixing angle β into the CP-odd mass eigenstates G^0, A and into $G^\pm, H^\pm$, respectively, via

$$\begin{pmatrix} G^0 \\ A \end{pmatrix} = \begin{pmatrix} \cos\beta & \sin\beta \\ -\sin\beta & \cos\beta \end{pmatrix} \begin{pmatrix} \eta_1 \\ \eta_2 \end{pmatrix} , \tag{8.15a}$$

$$\begin{pmatrix} G^+ \\ H^+ \end{pmatrix} = \begin{pmatrix} \cos\beta & \sin\beta \\ -\sin\beta & \cos\beta \end{pmatrix} \begin{pmatrix} \phi_1^+ \\ \phi_2^+ \end{pmatrix} , \tag{8.15b}$$

where the G^0, G^+ are the neutral and charged Goldstone bosons, respectively, that are absorbed by the $W^\pm$ and Z bosons to obtain mass, and we have as physical mass eigenstates the pseudoscalar Higgs A and the charged Higgs $H^\pm$. In total, we obtain 5 physical Higgs fields. We have the following relation between the mixing angle β and the VEVs v_1, v_2,

$$\tan\beta = \frac{v_2}{v_1} , \tag{8.16}$$

and the VEVs have to reproduce the SM VEV v, i.e.

$$v^2 = v_1^2 + v_2^2 . \tag{8.17}$$

Next, we consider the Yukawa Lagrangian. In analogy to the SM in Eq. (2.8) we now have Yukawa matrices for the leptons and up- and down-quarks for both doublets, respectively, that can in general be arbitrary 3×3 complex matrices in flavour space. We can use the above defined mass eigenstates of the Higgs scalars and write the Yukawa Lagrangian in the general form [251]

$$\begin{aligned} -\mathcal{L}_{\text{Yukawa}} = & \\ & \sum_{F=U,D,L} \frac{1}{\sqrt{2}} \overline{F} \left(\kappa^F s_{\beta-\alpha} + \rho^F c_{\beta-\alpha}\right) F h + \frac{1}{\sqrt{2}} \overline{F} \left(\kappa^F c_{\beta-\alpha} - \rho^F s_{\beta-\alpha}\right) F H + \frac{\mathrm{i}}{\sqrt{2}} \overline{F} \gamma_5 \rho^F F A \\ & + \left[\overline{U} \left(V^{\text{CKM}} \rho^D P_{\text{R}} - \rho^U V^{\text{CKM}} P_{\text{L}}\right) D H^+ + \overline{\nu} \rho^L P_{\text{R}} L H^+ + \text{h.c.}\right] . \end{aligned} \tag{8.18}$$

Here we sum over all fermion types $F = U, D, L$ with F being a vector in flavour space of the specified fermion species, U the up-type, D the down-type quark, L the lepton and ν the neutrino fields. We introduced the abbreviations $s_{\beta-\alpha} = \sin(\beta-\alpha)$, $c_{\beta-\alpha} = \cos(\beta-\alpha)$. The matrices κ^F are given by

$$\kappa^F \equiv \frac{\sqrt{2} M^F}{v} , \tag{8.19}$$

with the fermion mass matrices M^F. The projection operators are given by $P_{\text{R/L}} = (1 \pm \gamma_5)/2$ and V^{CKM} is the quark CKM mixing matrix. The generality of the Yukawa couplings is now encoded in the, in principle, arbitrary complex matrices ρ^F. To avoid flavour-changing neutral currents (FCNC) at tree-level, we can require the alignment of the Yukawa couplings of the two scalar doublets, i.e. we demand that the matrices ρ^F are proportional to κ^F,

$$\rho^F = \zeta_F \kappa^F , \tag{8.20}$$

with a proportionality constant ζ_F. These are free parameters that can be different for each fermion generation and type. With this construction, we obtain the flavour-aligned 2HDM (A2HDM) [246, 247]. Another way of avoiding FCNCs is by imposing a discrete $\mathbb{Z}_2$ symmetry [254], which gives rise to four 2HDM types. These types can also be understood as concrete realizations of the A2HDM by specific choices for the ζ_F, e.g. setting $\zeta_F = \cot\beta$ for all fermion species results in the type-I 2HDM and $\zeta_U = \cot\beta$, $\zeta_D = \zeta_L = \tan\beta$ in the type-II 2HDM. The discrete $\mathbb{Z}_2$ symmetry also implies $\lambda_6 = \lambda_7 = 0$ and $m_{12}^2 = 0$, where a non-zero value for m_{12}^2 softly breaks the $\mathbb{Z}_2$ symmetry.

This concludes the brief overview of elementary 2HDMs. The major difference compared to the Composite 2HDM here is that (apart from the additional particles from the composite sector and the new effective couplings, e.g. the quartic scalar-scalar-fermion-fermion coupling) in the elementary 2HDM the parameters λ_i $(i = 1, .., 7)$, m_{11}, m_{12}, m_{22} and the ζ_F $(F = U, D, L)$ are input parameters that can be chosen freely (the ζ_F only in the A2HDM), whereas in the composite case they are derived from the composite input parameters.

8.4. Theoretical and Experimental Constraints

We now return to the composite 2HDM and we list in this section the theoretical and experimental constraints that we applied to our parameter scans in order to obtain a valid parameter sample for the composite 2HDM. We only give a brief summary and refer to [69, 74] for more details.

The parameter points were checked against the following constraints:

- **Reconstruction of SM Parameters**:

  The SM parameters, i.e. the SM VEV, the Higgs mass and the top quark mass, have to be properly reconstructed. Thus, it was demanded to obtain the SM-like Higgs mass within the interval $[120\,\text{GeV}, 130\,\text{GeV}]$ and the top mass within $[165\,\text{GeV}, 175\,\text{GeV}]$ [69].

- **Perturbativity Constraints**:

  As already mentioned, the scalar potential and the scalar couplings are determined by the composite parameters. We required that the quartic couplings λ_i from the scalar potential (see Eq. (8.12)) have to obey the relation $\lambda_i \leq \sqrt{4\pi}$.

- **Higgs Searches and Measurements**:

  The parameter points were checked against direct and indirect searches in the scalar sector via the tools `HiggsBounds` [183–187] and `HiggsSignals` [188, 189]. The latter checks for compatibility with current Higgs measurements and the former for compatibility with the searches for new Higgs resonances that have not been found (yet) but are present in our model. Moreover, these constraints indirectly lead to constraints on, for e.g. the composite scale f since the masses of the heavier scalars (in our case, the 125 GeV Higgs is always the lighter scalar h) scale with f. Additionally, we applied limits from di-Higgs searches that we will discuss in Sec. 10.2.

- **Flavour Constraints**:

  Similarly to elementary 2HDM models (cf. [179]), the additional scalars in our theory can contribute to flavour observables, e.g. the decays $b \to s\gamma$ and $B_s \to \mu\mu$. Since in our theory we have a flavour-aligned structure, the constraints come from a rescaling of the SM couplings. To safely evade these constraints, we apply the requirement $\zeta_b \lesssim 0.1\zeta_t$, where the ζ_t and ζ_b are the coupling modifiers (see Eq. (8.20)) of the top and bottom quarks to the heavy Higgs states H, A and $H^\pm$ (see [69] for more details).

- **Constraints on New Heavy Particles**:

  In the composite 2HDM, we have new heavy resonances in the composite sectors. The new spin-1 gauge fields can naturally have masses in the multi-TeV range and have been integrated out in our approach. The top partners, however, play an important role in our di-Higgs calculation. Their masses are constrained by searches at the LHC [255, 256]. One could in principle try to evade these constraints by taking into account exotic decays, e.g. heavy top partner decays into Ht, At, H^+b with the heavy scalar H, the pseudoscalar A, the charged scalar H^+ and the top and bottom quarks t and b. We, however, still only considered benchmark points with $m_{T_i} \geq 1.3\,\text{TeV}$ $(i = 1, .., 8)$ for the masses m_{T_i} of the heavy top partners.

CHAPTER 9

Calculation of Di-Higgs Production in the Composite 2HDM

In this chapter, we describe the steps we used to obtain from an effective Lagrangian approach the cross section formulas that we used for the calculation of Higgs pair production in our realization of a composite 2HDM. We present the effective Lagrangian in Sec. 9.1 together with the Feynman rules we obtained from it. Then we set our notation and briefly summarize how we obtained the LO cross section (Sec. 9.2.1) and also mention the NLO corrections in the heavy top limit in Sec. 9.2.2.

The calculation presented here follows similar works in other composite models [152–154] and our published results [74].

9.1. Effective Lagrangian and Feynman Rules for Higgs Pair Production

After integrating out the heavy spin-1 composite states, we are left with an effective Lagrangian $\mathcal{L}^{\text{eff}}$, which we will use in our calculations (for more information on how to obtain the effective Lagrangian and how the couplings depend on the input parameters, see [69]). In the following, we only write out the part that is relevant for di-Higgs production. The effective scalar Lagrangian can be written as

$$\begin{aligned}\mathcal{L}^{\text{eff}}_{\text{Scalar}} = &-\frac{1}{3!}\lambda_{hhh}h^3 - \frac{1}{2}\lambda_{hhH}h^2H - \frac{1}{2}\lambda_{hHH}hH^2 - \frac{1}{3!}\lambda_{HHH}H^3 \\ &- \frac{1}{2}\lambda_{hAA}hA^2 - \frac{1}{2}\lambda_{HAA}HA^2 \\ &- \lambda_{\phi^0 hA}\phi^0 hA - \lambda_{\phi^0 HA}\phi^0 HA \\ &+ \frac{v}{3f^2}\left(h_2\partial_\mu h_1 - h_1\partial_\mu h_2\right)\partial^\mu h_2 \\ &+ \frac{v}{3f^2}\left(2A\partial_\mu\phi^0\partial^\mu h_2 - \phi^0\partial_\mu A\partial^\mu h_2 - h_2\partial_\mu A\partial^\mu\phi^0\right) ,\end{aligned} \tag{9.1}$$

where h is the lighter and H the heavier Higgs boson, A the pseudoscalar Higgs, ϕ^0 the neutral Goldstone boson and $\lambda_{\varphi_1\varphi_2\varphi_3}$ the trilinear couplings ($\varphi_i = h, H, A, \phi^0 (i = 1, 3)$) that are derived from the fundamental composite parameters. The fields h_1 and h_2 are defined by

$$\begin{pmatrix} h_1 \\ h_2 \end{pmatrix} = \begin{pmatrix} c_\theta & -s_\theta \\ s_\theta & c_\theta \end{pmatrix} \begin{pmatrix} h \\ H \end{pmatrix} , \tag{9.2}$$

with $c_\theta = \cos\theta$, $s_\theta = \sin\theta$ and a mixing angle θ. Thus, we obtain

$$\frac{v}{3f^2}(h_2\partial_\mu h_1 - h_1\partial_\mu h_2)\partial^\mu h_2 = \frac{v}{3f^2}(s_\theta\,\partial_\mu h + c_\theta\,\partial_\mu H)(H\partial^\mu h - h\partial^\mu H)\,. \tag{9.3}$$

The first parts of Eq. (9.1) resemble an elementary 2HDM Lagrangian (compare with Sec. 8.3). In the composite 2HDM we have derivative scalar couplings, coming from the Goldstone boson nature of the Higgs (compare to the strongly interacting light Higgs (SILH) Lagrangian, e.g. in [153, 257]), that are not present in an elementary 2HDM. We can read off the Feynman rules relevant for di-Higgs production as

$$[h(p_1)h(p_2)h(p_3)] = -\,i\lambda_{hhh}\,, \tag{9.4a}$$

$$[h(p_1)h(p_2)H(p_3)] = -\,i\lambda_{hhH} - i\lambda^{(2)}_{hhH}(p_1^2 + p_2^2 - 2p_3^2)\,, \tag{9.4b}$$

with $\lambda^{(2)}_{hhH}$ defined as

$$\lambda^{(2)}_{hhH} = -\frac{v}{3f^2}s_\theta\,. \tag{9.5}$$

Similarly, we have the effective Yukawa Lagrangian

$$\begin{aligned}\mathcal{L}^{\text{eff}}_{\text{Yuk}} = &\big(-G_{hT_iT_j}\bar{T}_{L,i}T_{R,j}h - G_{HT_iT_j}\bar{T}_{L,i}T_{R,j}H + iG_{AT_iT_j}\bar{T}_{L,i}T_{R,j}A + \text{h.c.}\big)\\ &- G_{hhT_iT_j}\bar{T}_iT_jh^2 - G_{HHT_iT_j}\bar{T}_iT_jH^2 - G_{AAT_iT_j}\bar{T}_iT_jA^2\\ &- G_{hHT_iT_j}\bar{T}_iT_jhH + iG_{hAT_iT_j}\bar{T}_i\gamma_5T_jhA\\ &+ iG_{HAT_iT_j}\bar{T}_i\gamma_5T_jHA + iG_{\phi^0T_iT_j}\bar{T}_i\gamma_5T_j\phi^0\,,\end{aligned} \tag{9.6}$$

with the Yukawa couplings $G_{\varphi T_iT_j}$ with T_i being the top quark and its partners $(i,j = 1,..,9)$ and $\varphi = h, H, A, \phi^0$. We also have effective quartic couplings between two fermions and two scalars, $G_{\varphi_1\varphi_2T_iT_j}$, with a mass dimension of -1. Our convention for the notation here is that the T_i quarks are mass ordered, with T_1 being the heaviest and $T_9 = t$ the lightest particle, i.e. the SM top quark.

We note here that we assumed negligible partial compositeness of the bottom quark (and other light quarks), and therefore the bottom partners do not couple to the scalars h and H and play no role in di-Higgs production.

The Feynman rule for the quartic coupling is given by

$$[\bar{T}_iT_jhh] = -\,2iG_{hhT_iT_j}\,. \tag{9.7}$$

For the coupling with two fermions and one scalar we have

$$\begin{aligned}\mathcal{L}^{\text{eff}}_{\text{Yuk}} \subset &-G_{hT_iT_j}\bar{T}_{L,i}T_{R,j}h + \text{h.c.} = -G_{hT_iT_j}\bar{T}_{L,i}T_{R,j}h - G_{hT_iT_j}\bar{T}_{R,j}T_{L,i}h\\ &= -G_{hT_iT_j}\bar{T}_{L,i}T_{R,j}h - G_{hT_jT_i}\bar{T}_{R,i}T_{L,j}h\\ &= -G_{hT_iT_j}\bar{T}_iP_{\text{R}}T_jh - G_{hT_jT_i}\bar{T}_iP_{\text{L}}T_jh\\ &= -\bar{T}_i\left[G_{hT_iT_j}P_{\text{R}} + G_{hT_jT_i}P_{\text{L}}\right]T_jh\\ &= -\bar{T}_i\left[\frac{1}{2}\left(G_{hT_iT_j} + G_{hT_jT_i}\right) + \frac{\gamma_5}{2}\left(G_{hT_iT_j} - G_{hT_jT_i}\right)\right]T_jh\,,\end{aligned} \tag{9.8}$$

We can introduce abbreviations for the couplings,

$$g_{h\bar{T}_iT_j} = \frac{1}{2}\left(G_{h\bar{T}_iT_j} + G_{h\bar{T}_jT_i}\right)\,, \tag{9.9a}$$

$$g_{h\bar{T}_iT_j,5} = \frac{1}{2}\left(G_{h\bar{T}_iT_j} - G_{h\bar{T}_jT_i}\right)\,, \tag{9.9b}$$

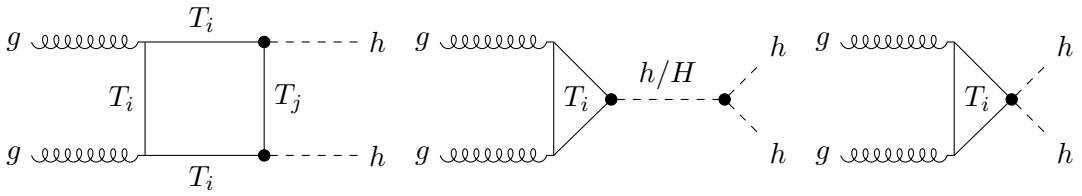

Figure 9.1.: Generic Feynman diagrams contributing to di-Higgs production via gluon fusion that appear in the composite 2HDM. The black dots indicate potentially new or deviating couplings compared to the SM. The indices i, j run from 1 to 9. Taken from [74].

and then obtain as the Feynman rule (and analogously also for the heavy Higgs H)

$$[\bar{T}_i T_j h] = -i(g_{h\bar{T}_i T_j} + \gamma_5 g_{h\bar{T}_i T_j,5})\,. \tag{9.10}$$

We also note that the top partners are coloured particles and thus couple to gluons in the same way as the top quark.

To summarize, we have the Feynman rules

$$[h(p_1)h(p_2)h(p_3)] = -i\lambda_{hhh}\,, \tag{9.11a}$$
$$[h(p_1)h(p_2)H(p_3)] = -i\lambda^{(1)}_{hhH} - i\lambda^{(2)}_{hhH}(p_1^2 + p_2^2 - 2p_3^2)\,, \tag{9.11b}$$
$$[\bar{T}_i T_j hh] = -2iG_{hhT_iT_j}\,, \tag{9.11c}$$
$$[\bar{T}_i T_j h] = -i(g_{h\bar{T}_i T_j} + \gamma_5 g_{h\bar{T}_i T_j,5})\,, \tag{9.11d}$$
$$[\bar{T}_i T_j H] = -i(g_{H\bar{T}_i T_j} + \gamma_5 g_{H\bar{T}_i T_j,5})\,. \tag{9.11e}$$

These are all the interactions that occur in our calculation of di-Higgs production. The derivation of these couplings with respect to the composite input parameters can be seen in [69].

9.2. Cross Section Calculation

In this section, we describe the calculation of the di-Higgs cross section. First, we introduce our notation and discuss the LO contribution, and then we also present the NLO corrections in the heavy top-limit. This calculation has been performed for the SM [99–102] and adapted for composite models in [152–154], which we will follow here.

9.2.1. Leading-Order Cross Section

Before we describe the calculation of the LO cross section, we set our notation. We introduce the Mandelstam variables,

$$\hat{s} = (p_1 + p_2)^2, \quad \hat{t} = (p_1 + p_3)^2, \quad \hat{u} = (p_2 + p_3)^2, \tag{9.12}$$

where p_1 and p_2 are the gluon momenta and p_3 and p_4 are the Higgs momenta, and all momenta are considered ingoing.

We define a set of projection operators $A_i^{\mu\nu}$ $(i = 1, 2)$,

$$A_1^{\mu\nu} = g^{\mu\nu} - \frac{p_1^\nu p_2^\mu}{(p_1 \cdot p_2)}\,, \tag{9.13a}$$

$$A_2^{\mu\nu} = g^{\mu\nu} + \frac{p_3^2 p_1^\nu p_2^\mu}{p_T^2 (p_1 \cdot p_2)} - \frac{2(p_3 \cdot p_2) p_1^\nu p_3^\mu}{p_T^2 (p_1 \cdot p_2)} - \frac{2(p_3 \cdot p_1) p_3^\nu p_2^\mu}{p_T^2 (p_1 \cdot p_2)} + \frac{2 p_3^\mu p_3^\nu}{p_T^2}\,, \tag{9.13b}$$

$$p_T^2 = 2\frac{(p_1 \cdot p_3)(p_2 \cdot p_3)}{(p_1 \cdot p_2)} - p_3^2\,, \tag{9.13c}$$

where we also defined the transverse momentum p_T. These projection operators satisfy

$$A_1 \cdot A_2 = 0, \quad A_1 \cdot A_1 = A_2 \cdot A_2 = 2\,. \tag{9.14}$$

Thus, we can express our amplitude for gluon fusion into Higgs pairs in terms of these orthogonal operators and their coefficients.

We now describe the contribution to the LO di-Higgs cross section. The generic diagrams that appear at LO in our composite 2HDM are depicted in Fig. 9.1. We see that compared to the SM case described in Sec. 2.3 (compare with Fig. 2.1) we have additional diagrams. In the quark loop we now also have the top partners, and in the case of the box diagram we can have different top partners due to the non-diagonal couplings $G_{h\bar{T}_i T_j}$ in Eq. (9.6). In the triangle diagram with a scalar propagator, we can additionally have a heavy Higgs H in the propagator, which will potentially lead to *resonant* enhancement. Finally, we have an additional triangle diagram without a scalar propagator due to the effective quartic scalar-scalar-fermion-fermion couplings $G_{hhT_iT_j}$.

We obtain for the LO amplitude

$$\mathcal{A}(gg \to hh) = \mathcal{A}_\triangle + \mathcal{A}_\square\,, \tag{9.15}$$

where $\mathcal{A}_\square$ is the sum of all box diagrams and $\mathcal{A}_\triangle$ the sum of all triangle diagrams from Fig. 9.1. These contributions can be written as

$$\mathcal{A}_\triangle = \frac{\alpha_s}{4\pi}\hat{s} A_1^{\mu\nu} \epsilon_\mu^a \epsilon_\nu^b \delta_{ab} \sum_{i=1}^{9} C_{i,\triangle}^{hh} F_\triangle(m_i)\,, \tag{9.16a}$$

$$\begin{aligned}\mathcal{A}_\square = \frac{\alpha_s}{4\pi}\hat{s} \epsilon_\mu^a \epsilon_\nu^b \delta_{ab} \sum_{i=1}^{9}\sum_{j=1}^{9} \Big[& A_1^{\mu\nu} \left(C_{i,j,\square}^{hh} F_\square(m_i, m_j) + C_{i,j,\square,5}^{hh} F_{\square,5}(m_i, m_j) \right) \\ & + A_2^{\mu\nu} \left(C_{i,j,\square}^{hh} G_\square(m_i, m_j) + C_{i,j,\square,5}^{hh} G_{\square,5}(m_i, m_j) \right) \Big]\,,\end{aligned} \tag{9.16b}$$

with the polarization vectors ϵ_μ^a of the ingoing gluons. We introduced the coefficients

$$C_{i,\triangle}^{hh} = \frac{g_{h\bar{T}_i T_i} \lambda_{hhh}}{\hat{s} - m_h^2} + \frac{g_{H\bar{T}_i T_i} \lambda_{Hhh}^{(1)}}{\hat{s} - m_H^2} + \frac{g_{H\bar{T}_i T_i} \lambda_{hhH}^{(2)} (2m_h^2 - 2\hat{s})}{\hat{s} - m_H^2} + 2 G_{hh\bar{T}_i T_i}\,, \tag{9.17a}$$

$$C_{ij,\square}^{hh} = g_{h\bar{T}_i T_j}\, g_{h\bar{T}_i T_j}\,, \tag{9.17b}$$

$$C_{ij,\square,5}^{hh} = g_{h\bar{T}_i T_j,5}\, g_{h\bar{T}_j T_i,5} = -g_{h\bar{T}_i T_j,5}\, g_{h\bar{T}_i T_j,5}\,. \tag{9.17c}$$

The form factors $F_\triangle, F_\square, F_{\square,5}, G_\square, G_{\square,5}$ can be found in App. A. Next, we calculate the differential cross section. The general formula for $2 \to 2$ scattering with massless ingoing particles and identical outgoing particles is given by

$$\frac{\mathrm{d}\sigma}{\mathrm{d}\hat{t}} = \frac{1}{16\pi\hat{s}^2} \sum_{\text{d.o.f.}} |\mathcal{A}|^2\,. \tag{9.18}$$

Combining this with our amplitudes we have for the differential cross section at LO

$$\begin{aligned}\frac{\mathrm{d}\hat{\sigma}(gg\to hh)}{\mathrm{d}\hat{t}} =& \frac{\alpha_s^2}{512(2\pi)^3}\times\Bigg[\left|\sum_{i=1}^{9} C_{i,\triangle}^{hh} F_{\triangle}(m_i)\right. \\ &\left.+\sum_{i=1}^{9}\sum_{j=1}^{9}\left(C_{ij,\square}^{hh}F_{\square}^{hh}(m_i,m_j)+C_{ij,\square,5}^{hh}F_{\square,5}^{hh}(m_i,m_j)\right)\right|^2 \\ &+\left|\sum_{i=1}^{9}\sum_{j=1}^{9}\left(C_{ij,\square}^{hh}G_{\square}^{hh}(m_i,m_j)+C_{ij,\square,5}^{hh}G_{\square,5}^{hh}(m_i,m_j)\right)\right|^2\Bigg]\,.\end{aligned} \tag{9.19}$$

Here we averaged over the ingoing degrees of freedom (indicated by $\sum_{\text{d.o.f.}}$ in Eq. (9.18)), i.e. the colour and the polarization of the incoming gluons.

In order to obtain the full partonic cross section we integrate over $\hat{t}$,

$$\hat{\sigma}(gg\to hh)=\int_{\hat{t}_-}^{\hat{t}_+}\mathrm{d}\hat{t}\,\frac{\mathrm{d}\hat{\sigma}(gg\to hh)}{\mathrm{d}\hat{t}},\quad \hat{t}_\pm=-\frac{\hat{s}}{2}\left(1-2\frac{m_h^2}{\hat{s}}\mp\sqrt{1-\frac{4m_h^2}{\hat{s}}}\right)\,, \tag{9.20}$$

with the integration boundaries $\hat{t}_\pm$. For the full hadronic cross section, i.e. the cross section for proton-proton collision into Higgs pairs, we have to take into account the particle distribution function (pdf) f_g of the gluon in the proton, i.e. we multiply with the gluon luminosity $\frac{\mathrm{d}\mathcal{L}^{gg}}{\mathrm{d}\tau}$,

$$\frac{\mathrm{d}\mathcal{L}^{gg}}{\mathrm{d}\tau}=\int_\tau^1\frac{\mathrm{d}x}{x}f_g(x,\mu_F)f_g(\tau/x,\mu_F)\,, \tag{9.21}$$

with the factorization scale μ_F, and integrate over the partonic centre-of-mass energy $\hat{s}$. The final result is given by

$$\sigma_{gg}(pp\to hh)=\int_{\tau_0}^1\mathrm{d}\tau\frac{\mathrm{d}\mathcal{L}^{gg}}{\mathrm{d}\tau}\hat{\sigma}(\hat{s}=\tau s)\,,\quad \tau_0=\frac{4m_h^2}{s}\,, \tag{9.22}$$

where the subscript gg indicates that we only considered gluon fusion as a production mechanism for the cross section, as there are also other production channels and s denotes the hadron collider centre-of-mass energy squared. In the following, we will often write $\sigma(gg\to hh)$ (without a hat) meaning also the full hadronic cross section with gluon fusion as the production mechanism to simplify the notation.

9.2.2. Next-to-Leading-Order Cross Section in the Heavy Top Limit

After the description of the LO cross section, we will briefly mention the NLO QCD corrections. They have been calculated in the heavy top limit [102] and then adapted for composite models in [154]. We can follow the same approach here and thus only mention the important details. More information can then be found in these works.

The NLO corrections are calculated in the heavy top limit, i.e. the quarks in the loops are integrated out, and an effective coupling is used. The strong coupling is renormalized in the modified minimal subtraction scheme ($\overline{\text{MS}}$) with 5 light-quark flavours. The cross section can be written as

$$\sigma_{\text{NLO}}(pp\to hh+X)=\sigma_{\text{LO}}+\Delta\sigma_{\text{virt}}+\underbrace{\Delta\sigma_{gg}+\Delta\sigma_{gq}+\Delta\sigma_{q\bar{q}}}_{\sigma_{\text{LO}}\text{ factorizes out}}\,, \tag{9.23}$$

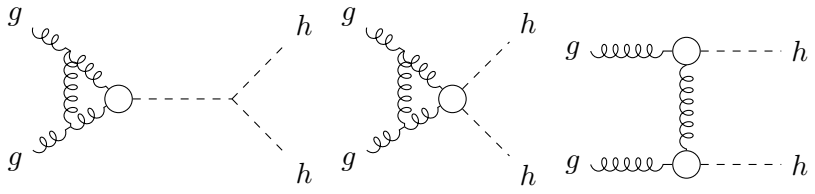

Figure 9.2.: Generic NLO Feynman diagrams contributing to the virtual corrections $\Delta\sigma_{\text{virt}}$ in di-Higgs production in the heavy top limit (compare with [102, 154]). The circles indicate the effective couplings.

where $\Delta\sigma_{gg}$, $\Delta\sigma_{gq}$ and $\Delta\sigma_{q\bar{q}}$ are the gg, gq and the qq induced real corrections where the LO cross section σ_{LO} (given by Eq. (9.22)) can be factorized. These corrections can be found in [102, 154].

The virtual corrections $\Delta\sigma_{\text{virt}}$ need closer inspection. They are given by the generic diagrams in Fig. 9.2 and can be written as

$$\Delta\sigma_{\text{virt}} = \frac{\alpha_s(\mu_R)}{\pi}\int_{\tau_0}^{1} \mathrm{d}\tau \frac{\mathrm{d}\mathcal{L}^{gg}}{\mathrm{d}\tau}\hat{\sigma}_{\text{LO}}(\hat{s}=\tau s)C\,, \tag{9.24a}$$

$$C = \pi^2 + \frac{11}{2} + \frac{33-2N_F}{6}\log\frac{\mu_R^2}{\hat{s}} + \text{Re}\frac{\int_{\hat{t}_-}^{\hat{t}_+}\mathrm{d}\hat{t}\frac{4}{9}(g_{hgg}^{\text{eff}})^2\left[(F_{\triangle}^{\text{LO}}+F_{\square}^{\text{LO}}) - \frac{p_T^2}{2\hat{t}\hat{u}}(\hat{s}-2m_h^2)G_{\square}^{\text{LO}}\right]}{\int_{\hat{t}_-}^{\hat{t}_+}\mathrm{d}\hat{t}\left[|F_{\triangle}^{\text{LO}}+F_{\square}^{\text{LO}}|^2 + |G_{\square}^{\text{LO}}|^2\right]}\,, \tag{9.24b}$$

$$p_T^2 = \frac{(\hat{t}-m_h^2)(\hat{u}-m_h^2)}{\hat{s}} - m_h^2\,, \tag{9.24c}$$

with the renormalization scale μ_R and the number of active flavours $N_F = 5$. We used the LO form factors $F_{\triangle}^{\text{LO}}$, $F_{\square}^{\text{LO}}$ and $G_{\square}^{\text{LO}}$ defined as

$$F_{\triangle}^{\text{LO}} = \sum_{i=1}^{9} C_{i,\triangle}^{hh} F_{\triangle}(m_i)\,, \tag{9.25a}$$

$$F_{\square}^{\text{LO}} = \sum_{i=1}^{9}\sum_{j=1}^{9} C_{i,j,\square}^{hh} F_{\square}(m_i,m_j) + C_{i,j,\square,5}^{hh} F_{\square,5}(m_i,m_j)\,, \tag{9.25b}$$

$$G_{\square}^{\text{LO}} = \sum_{i=1}^{9}\sum_{j=1}^{9} C_{i,j,\square}^{hh} G_{\square}(m_i,m_j) + C_{i,j,\square,5}^{hh} G_{\square,5}(m_i,m_j)\,. \tag{9.25c}$$

As already mentioned, the heavy quarks, including the top, are integrated out and we have the effective couplings

$$g_{hgg}^{\text{eff}} = \sum_{i=1}^{9}\frac{g_{h\bar{T}_iT_i}v}{m_{T_i}}\,, \tag{9.26}$$

that appear in Eq. (9.24). Here, it is also important to note that the full LO form factors are included after the heavy top limit was applied, i.e. we obtain the Born-improved NLO cross section.

CHAPTER 10

Numerical Evaluation

After the description of the model and the calculation, we can move on to the implementation and the illustration of our setup and analyze the obtained results. In this chapter, we first describe the setup we used to calculate di-Higgs production in Sec. 10.1, where we used the code `HPAIR` [258] and modified it to use it for the composite 2HDM. We also mention the other codes and program packages we used in order to obtain our results. Next, we discuss the parameter scan we performed to obtain viable parameter points, including the theoretical and experimental constraints we applied (Sec. 10.2), particularly the di-Higgs constraints and their impact on our parameter sample. Finally, we turn to the analysis of the obtained results in Sec. 10.3, where we first show the results on the full inclusive cross section (Sec. 10.3.1) and the interplay of different contributions from our model. Then, we discuss differential distributions (Sec. 10.3.2) and the impact of the new interactions and particles compared to the SM. At the end, we compare our model with other 2HDM-like models and how they can be distinguished in Sec. 10.3.4.

10.1. Implementation

We begin with the description of the implementation of our results. We used the code `HPAIR 2.0` [258] and implemented our form factors and NLO corrections from Secs. 9.2.1 and 9.2.2 (similar approaches were already performed in [152–154]). The code `HPAIR` calculates the di-Higgs cross section in the SM and the minimal supersymmetric extension of the

Table 10.1.: Additional input parameters used for the computation in `HIGLU` and `HPAIR`. See text for details. Taken from [74].

variable	value
$\alpha_s(m_Z)$	0.135
$\sqrt{s}$	13/14 TeV
PDF	MMHT2014lo68cl [259]
ren. and fac. scale	$m_{hh}/2$

SM (MSSM) [62, 93, 94] and can also calculate the invariant mass distribution. Furthermore, the NLO QCD corrections in the heavy top limit are included [102]. We modified the code by inserting our expressions for the LO cross section and the NLO QCD corrections as described in Secs. 9.2.1 and 9.2.2. We also implemented the possibility to calculate the p_T distribution (for details on the derivation see App. C). In order to evaluate the loop integrals that appear in the form factors, we furthermore linked the code with the package `LoopTools 2.15` [229, 230]. Since the top partners can be very heavy in some cases, we had to use quadruple precision in order to obtain numerically stable results. Additionally, the results were checked by an independent calculation with `QCDLoop` [260].

For the calculation of the di-Higgs cross section, the total widths of the h and H Higgs bosons are needed. Therefore, we implemented our model into the code `HDECAY 6.6.1.` [216, 217] to obtain the relevant total widths. `HDECAY` already includes QCD corrections and off-shell decays. Both can be taken over for our model. Furthermore, the heavy Higgs can decay into a top quark and a top partner or into a pair of top quark partners, which we additionally implemented at LO. Moreover, we needed the cross section for single Higgs production via gluon fusion to calculate the *resonant* di-Higgs cross sections and compare with experimental limits. For this purpose, we used the code `HIGLU` [261, 262], which calculates the single Higgs production via gluon fusion, and we extended it to our model at LO.

The implementation in `HPAIR` allows us to calculate the di-Higgs cross section at NLO in the heavy top limit. Due to the large computing time when calculating the NLO corrections for all points in our parameter sample, we only calculated the cross section at LO and applied a K-factor of

$$K \equiv \frac{\sigma_{\text{NLO}}}{\sigma_{\text{LO}}} \approx 2\,, \tag{10.1}$$

which approximates the size of the NLO corrections for inclusive SM-like Higgs pair production very well. We used some benchmark points to validate this assumption. Similar K-factors are obtained for other models [150]. For differential distributions, however, the calculation of NLO corrections would be required as they can alter the shape of the distributions. This computation is again computation time-intensive, and we thus only used the LO result. Moreover, finite top mass effects at NLO QCD, which are not available for this model, can further distort the shape of the LO distributions [110, 111, 116, 126]. Since we only want to show what kind of significant effects can arise in our model, this is reasonable as a first approximation. We used the same K-factor also for the single Higgs production.

For the cross section calculation in `HIGLU` and `HPAIR` we use the additional input specified in Tab. 10.1. Since we calculate the cross sections only at LO, we also only use a LO parton distribution function (PDF) for our calculation, with the renormalization and factorization scale μ_R, μ_F set to half of the invariant Higgs pair mass m_{hh}. Furthermore, we calculated all cross sections and the differential distributions at a centre-of-mass energy of 14 TeV. Since the *resonant* constraints that we applied, however, are extracted from data with a centre-of-mass energy of 13 TeV we calculated also the cross sections needed for the application of these constraints at this energy.

10.2. Parameter Scan and Constraints

We now describe the generation of our parameter set. First of all, the parameters were generated through a Markov Chain Montecarlo (MCMC) scan (cf. [69] for more details). Thus, the following investigation can be seen as an exploration of the parameter space that may not fully exhaust it. The fundamental parameters of the composite 2HDM are given by the composite scale f, the gauge couplings g_ρ of the strong composite interaction, the Yukawa

Table 10.2.: Scan ranges for the input parameters (cf. [74]).

Parameter	Range	
	Lower	Upper
f	700 GeV	3000 GeV
g_ρ	2	10
$\Delta^f_{\mathrm{L,R}}$	$-10f$	$10f$
$Y^{IJ}_{1,2}$	$-10f$	$10f$

Table 10.3.: A selection of parameters and their ranges in our dataset for the composite 2HDM (with a cut on the m_H mass at 3 TeV and the di-Higgs resonant constraints applied).

Parameter	Min	Max
m_H	181 GeV	3000 GeV
m_{T_8}	1300 GeV	23 206 GeV
m_{T_7}	1306 GeV	23 921 GeV
m_{T_6}	1329 GeV	25 269 GeV
m_{T_1}	2979 GeV	80 000 GeV
$\lambda_{hhh}/\lambda_{hhh,\mathrm{SM}}$	0.759	1.07
$\lambda_{Hhh}/\lambda_{hhh,\mathrm{SM}}$	-5.967	0.13
$g_{htt}/g_{htt,\mathrm{SM}}$	0.724	1.329
$g_{Htt}/g_{htt,\mathrm{SM}}$	-2.68	1.61
G_{hhtt}	$-0.000\,65\,\mathrm{GeV}^{-1}$	$0.001\,49\,\mathrm{GeV}^{-1}$
$\sigma(gg \to hh)/\sigma_{\mathrm{SM}}(gg \to hh)$	0.46	10.23

coupling matrices $Y_{1,2}$ and the partial compositeness matrices $\Delta_{\mathrm{L,R}}$ (see also Eq. (8.10)). Their scan ranges are shown in Tab. 10.2, where we see that the upper and lower bounds for $Y_{1,2}$ and $\Delta_{\mathrm{L,R}}$ depend on the chosen composite scale f.

We applied all the theoretical and experimental constraints described in Sec. 8.4. Additionally, we applied a cut on the heavy Higgs mass and excluded points with a mass larger than 3 TeV.

Next, we describe the application of di-Higgs constraints on our parameter space. Experimentally, the limits are divided into *resonant* and *non-resonant* limits that operate on different underlying assumptions. Thus, we need to define how we apply these limits on our parameter sample. We will follow the procedure outlined in Sec. 2.3 (cf. also with [150]). If for a given parameter point the heavy Higgs mass m_H is smaller than $2m_h$, there is no resonant enhancement of the triangle diagram, and the point will be labelled *non-resonant*. Moreover, if the heavy Higgs contribution is small compared to the full cross section (based on the inclusive cross section), it would not be distinguishable from an experimental point of view. Thus we define a point to be *non-resonant* if the single heavy Higgs production and decay into SM-like Higgs pairs in the narrow width approximation is less than 10 % of the total di-Higgs cross section, i.e.

$$\frac{\sigma(gg \to H) \times \mathrm{BR}(H \to hh)}{\sigma(gg \to hh)} \leq 10\,\%\,. \tag{10.2}$$

We then apply *non-resonant* limits on the full cross section.

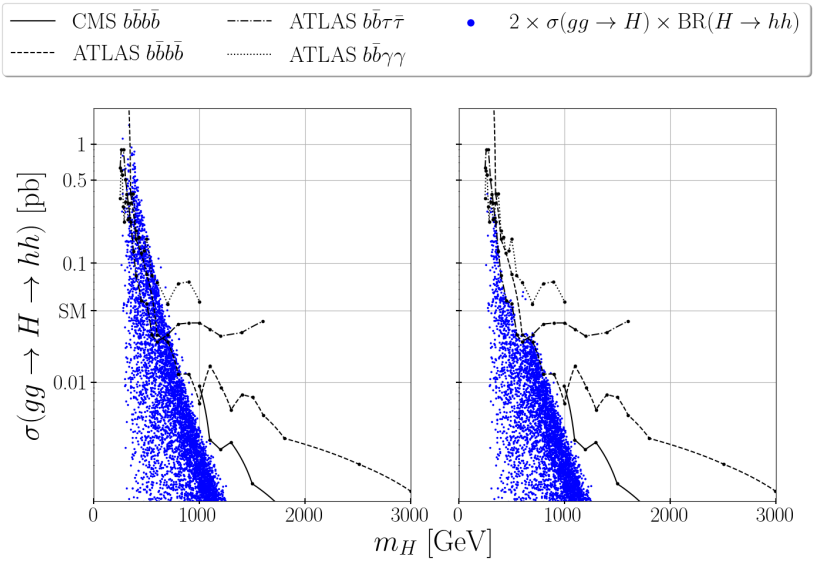

Figure 10.1.: The resonant di-Higgs cross section (single Higgs production with a K-factor approximating the NLO corrections from Eq. (10.1) times branching ratio) of all parameter points plotted against the heavy Higgs mass m_H. The black lines show the various experimental limits [174–177], where we divided the limits by the respective final state SM Higgs branching ratios. The plot left shows all parameter points before applying the limits, and the plot right after the limits were applied. The indicated SM cross section is $\sigma_{hh} = 2 \times 19.96\,\mathrm{fb}$, which was obtained from `HPAIR` for the SM at LO with our setup times the K-factor, $K = 2$. Taken from [74].

The *resonant* limits are applied to all parameter points. Here we calculate the single heavy Higgs (H) production cross section (obtained via our implementation in `HIGLU`) times branching ratios into a pair of SM-like Higgs times the branching ratios into the final state considered in the various experimental analyses [165–177]. If the parameter point exceeds one of the experimental limits, it is rejected. The experimental searches, however, apply the narrow width approximation. Their limits can only be safely employed if the total width of the heavy Higgs is small. We therefore only apply the *resonant* limits to points with a total width that satisfies

$$\frac{\Gamma_H}{m_H} \leq 5\,\% \,. \tag{10.3}$$

Otherwise, resonant bounds will not be considered for this parameter point.

In Fig. 10.1 we see the various experimental limits from *resonant* searches and how they impact our parameter sample. We only show the most stringent experimental limits [174–177] in the plot. We see that the experiments are already sensitive to our parameter sample. Moreover, there are still points above the experimental limits that are not rejected, because they do not satisfy the condition in Eq. (10.3).

We also considered *non-resonant* constraints on our parameter points, which we labelled as *non-resonant* according to our definition above. We found that the maximal cross section obtained in our sample is about 2.3 times the SM value. A recent ATLAS analysis combining several final states [164] obtains an upper bound on the *non-resonant* cross section of 2.4 times the SM. We thus see that by comparing these values, we cannot exclude any points yet with *non-resonant* limits, but the experiments start to become sensitive to our model in this regard. For a more sophisticated application of experimental *non-resonant* searches, a thorough analysis including differential distributions would be required, which is beyond the scope of this project.

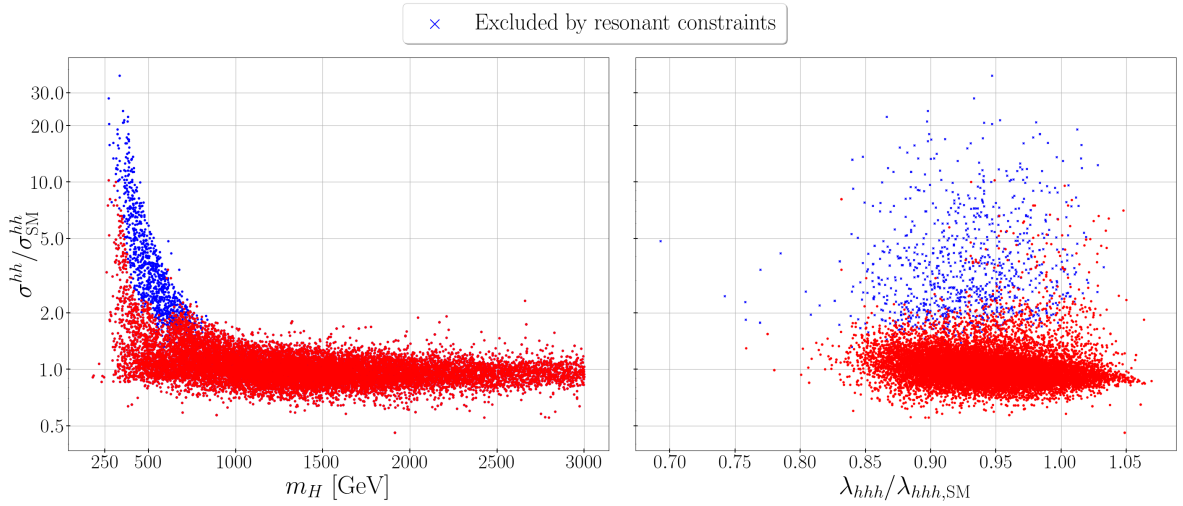

Figure 10.2.: The di-Higgs cross section normalized to the SM cross section of all parameter points plotted against the heavy Higgs mass m_H (left) and against the trilinear SM-like Higgs coupling λ_{hhh} normalized to the SM value (right) with points that are rejected by resonant constraints in blue crosses (left plot taken from [74]). All cross-section values are given at LO.

After applying all constraints, our parameter sample contained around 17 000 still allowed parameter points. In Tab. 10.3 we show the lower and upper limits of some of the masses and couplings in our model as well as the total cross section for di-Higgs production. First of all, we see our cuts made in the parameter space, i.e. that $m_H \leq 3\,\mathrm{TeV}$ and $m_{T_i} \geq 1.3\,\mathrm{TeV}$ $(i = 1, .., 8)$ for the heavy Higgs mass m_H and the heavy top partner masses m_{T_i}. Next, the SM-like trilinear Higgs coupling λ_{hhh} can differ from the SM value by up to $-24\,\%$. The SM-like top Yukawa coupling g_{htt}, however, can still deviate from $-25\,\%$ to $33\,\%$ of the SM value. Recent experimental limits [263] constrain the top Yukawa coupling to be closer to the SM, but they derive their limits from Higgs boson production measurements and assume no other contributions. Since the heavy top partners in our model also contribute to these processes, the experimental bounds can be relaxed, whereas more model independent limits on the top Yukawa coupling are currently less sensitive [264].

Next, the couplings λ_{Hhh}, g_{Htt} and G_{hhtt} can be positive or negative and therefore lead to different interference patterns in differential distributions depending on their signs, as we will see in the following sections. Finally, we see that the di-Higgs cross section can range from about 0.5 up to 10 times the SM value, i.e. we can have sizeable deviations from the SM, as we will discuss in more detail in the following.

10.3. Analysis

We will now move on to evaluate the results we obtained for our parameter sample and discuss the full inclusive cross section results as well as the differential distributions, and we compare the composite 2HDM with other models, namely an elementary type II 2HDM and a flavour-aligned 2HDM (which has a similar scalar sector as the composite 2HDM, without the additional top partners and effective quartic couplings).

10.3.1. Inclusive Results

We start with the results for the full inclusive cross section. In the left figure of Fig. 10.2 we show the prediction of the total cross section values normalized to the SM cross section, for

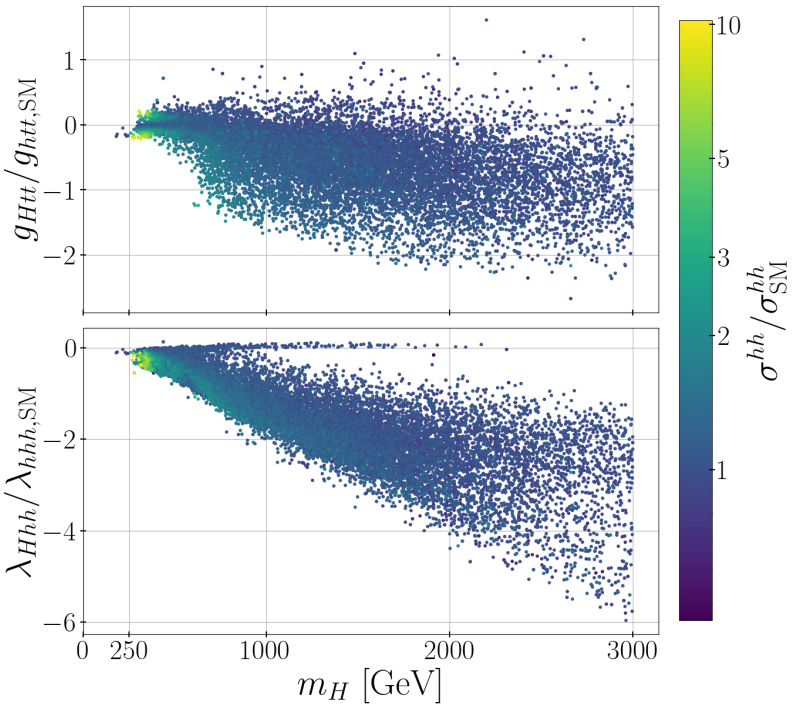

Figure 10.3.: The heavy Higgs top Yukawa coupling g_{Htt} normalized to the SM top Yukawa coupling (upper) and the λ_{Hhh} trilinear Higgs coupling normalized to the SM trilinear Higgs coupling (lower) plotted against the heavy Higgs mass m_H with the full di-Higgs cross section normalized to the SM value in colour code. All cross sections are given at LO.

our obtained parameter set plotted against the heavy Higgs mass m_H. We obtain a maximum cross section value of around 30 times the SM value. In the figure we also included the impact of the di-Higgs *resonant* constraints, as all points depicted as blue crosses are excluded by experimental limits, and the maximal value of the inclusive cross section after including these constraints is around 10 times the SM value (see also Tab. 10.3). This underlines the importance of including these resonant constraints.

Another important feature of the plot is the fact that with increasing mass m_H we move closer to the SM cross section value. This is to be expected since the heavy Higgs mass m_H scales with the composite scale f and in the limit of large f we decouple the composite sector and retain the SM. Additionally, the resonance contribution decreases with increasing m_H.

On the right side in Fig. 10.2 we show the di-Higgs cross section normalized to the SM value, plotted against the trilinear coupling λ_{hhh} of the SM-like Higgs boson. The interesting point here is that even in the case where the cross section is close to the SM value, we can still deviate in the trilinear coupling by up to more than $-20\,\%$ compared to the SM trilinear coupling. Thus, even if the SM di-Higgs cross section is measured, we can still deviate in the trilinear coupling in the composite 2HDM compared to the SM.

In Fig. 10.3 (upper), we show the heavy Higgs top Yukawa coupling g_{Htt} normalized to the SM Yukawa coupling, $g_{htt,\mathrm{SM}}$, and in Fig. 10.3 (lower) the heavy Higgs trilinear coupling λ_{Hhh} normalized to the SM trilinear coupling, $\lambda_{hhh,\mathrm{SM}}$, plotted against the heavy Higgs mass m_H, respectively. The total di-Higgs cross section at LO normalized to the SM cross section is shown additionally in the colour code. We see in both plots that the total cross section decreases with increasing Higgs mass (as is also visible in Fig. 10.2) since the resonance contribution decreases with increasing Higgs mass and the SM limit is approached. Furthermore, we can see a clear correlation between the total cross section and the Yukawa coupling as

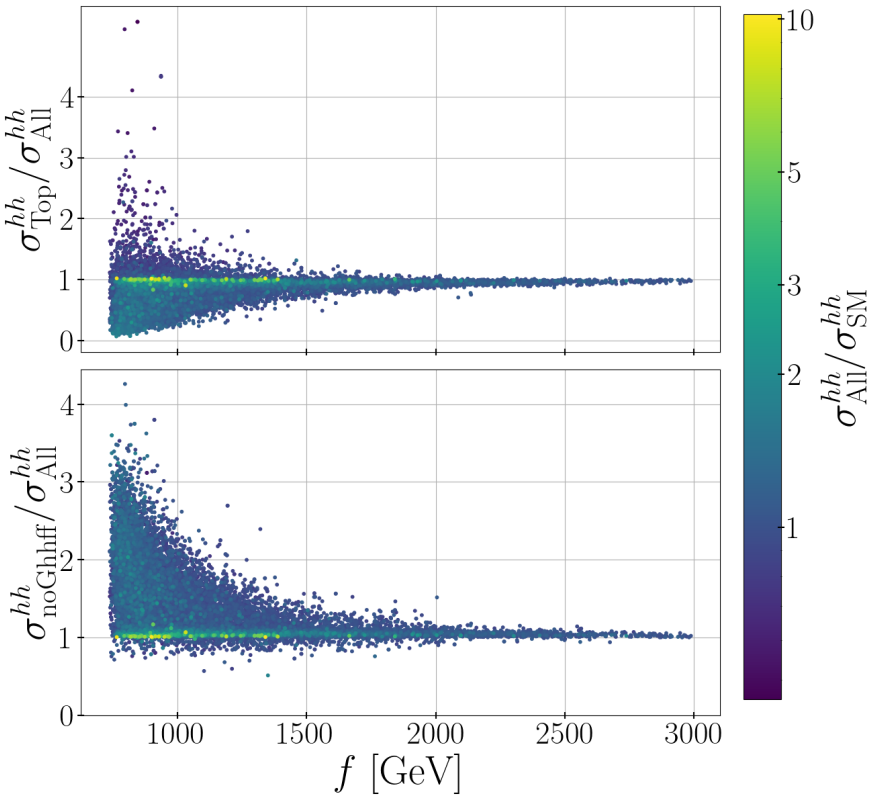

Figure 10.4.: The cross section including only the top quark contributions, divided by the full di-Higgs cross section (upper) and the cross section where the quartic couplings $G_{hhT_iT_i}$ ($i = 1, .., 9$) contributions are excluded normalized to the full cross section (lower) plotted against the composite scale f with the full di-Higgs cross section normalized to the SM cross section in colour code. All cross section values are given at LO.

expected, i.e. if we increase the (absolute) value of the coupling (for lighter m_H masses where the resonance contribution is more relevant), we increase the overall cross section. For the trilinear coupling λ_{Hhh}, we see a similar behaviour. Moreover, with increasing heavy Higgs mass m_H and therefore increasing composite scale f, we see that also the possible range of the couplings g_{Htt} and λ_{Hhh} becomes larger.

Next, we turn to the other contributions to the di-Higgs cross section, from the additional couplings and the particles from the composite sector. In the upper part in Fig. 10.4 we see the impact of the additional heavy top partners. We show here the ratio of the cross section obtained including only the top quark contributions, σ^{hh}_{Top}, i.e. all the Feynman diagrams in Fig. 9.1 where only the top quark is considered in the loops, normalized to the full cross section. Thus, if this ratio is close to 1, the top quark contributions already well approximate the full result, and the heavy quarks do not play a large role for the total cross section. If we deviate from 1 the heavy quark contributions become more significant, and we have important interference effects. We notice that the corrections of the top partners can be both positive or negative and significantly interfere constructively or destructively with the other contributions for values of the composite scale f below about 2 TeV. We see that the cross section with only top contributions can be more than 4 times larger than the total cross section, implying a strong destructive interference, if the heavy top partners are included. On the other hand, we see that the cross section with only top quarks can be significantly smaller than the full result as well, i.e. we have a constructive interference of the heavy quarks. Here, it is again important to note that the cross section σ^{hh}_{Top} includes diagrams involving

the quartic coupling G_{hhtt} and the heavy Higgs H resonance contribution. The σ^{hh}_{Top} cross section can therefore already significantly deviate from the SM-like contribution to the box and triangle diagrams.

Moreover, we see that points with very large cross sections have a ratio of 1 in this plot, i.e. the heavy tops do not play a major role for these parameter points. The large cross sections here originate from resonant contributions with the heavy Higgs H in the propagator. Since the heavy top partners are vector fermions, their Yukawa couplings do not scale with their mass, and thus their resonant contributions are suppressed by their heavy masses. To be more specific, in the SM, if we consider the heavy-top limit, the LO form factors approach a constant value [101] for the triangle diagram. Here, however, the top Yukawa coupling that scales with the top mass is included. Thus, if this limit is considered with Yukawa couplings that do not scale with the mass, the contribution vanishes. Moreover, the top partners are constrained to be heavier than 1.3 TeV. Therefore, the triangle diagrams with a heavy Higgs propagator and heavy top partners in the loop only have a relatively small impact.

Finally, for large composite scale values f, the contribution of the heavy quarks decreases again, as we approach the decoupling limit and the cross sections are already well approximated by only considering the top quark, i.e. the SM-like contributions (where also the quartic coupling contribution G_{hhtt} vanishes in this limit).

A similar situation can be seen in the lower part in Fig. 10.4, where we show the ratio of the cross section obtained without any quartic coupling $G_{hhT_iT_i}$ $(i = 1..9)$, denoted as $\sigma^{hh}_{\text{noGhhff}}$, normalized to the full cross section. Here, we include all diagrams in Fig. 9.1, including the top partner contributions, except the diagrams with a quartic coupling $G_{hhT_iT_i}$. Similarly to the upper plot, if the ratio deviates from 1, the impact of these quartic couplings increases, and we have more and more significant interference effects, in particular for scales $f \lesssim 2\,\text{TeV}$. Additionally, we notice a preference towards ratio values above 1, i.e. the inclusion of the quartic couplings decreases the overall cross section, and we have destructive interference. This preference is due to the fact that we have more points in our sample with a positive sign in the quartic couplings, which then leads to a destructive interference.

Moreover, similar to the upper plot in Fig. 10.4 we see that for large overall cross section values the ratio shown in the lower plot is close to 1, i.e. the quartic couplings do not play a significant role for these (resonantly enhanced) points.

Finally, we see again the decoupling limit for large values of f, i.e. the size of the contributions from the quartic couplings decreases.

10.3.2. Effects on Differential Distributions

After the discussion of the effects on the full cross section, we will now move to differential distributions and discuss the effects of the additional couplings and particles in the composite 2HDM. For this purpose, we chose four benchmark points, whose input parameters are summarized in App. B in Tab. B.1. We then calculated the invariant mass distribution (with the invariant mass denoted by Q in the following) and also the p_T distribution for these benchmark points. We analyzed the impact of the new composite interactions, i.e. we calculated the differential distributions with different subsets of diagrams included, to see their influence, namely the effects of the top partners and the effective quartic scalar-scalar-fermion-fermion couplings. We will also always show the SM prediction we obtained from `HPAIR` at LO (in blue). We then show the contributions obtained if we exclude the heavy quark contributions and the quartic coupling contributions (denoted by only top, no $G_{hhT_iT_i}$, in red), i.e. only diagrams with a top quark in the loop and no effective quartic couplings. This resembles an elementary 2HDM, and can thus be used for a comparison accordingly. We also display the

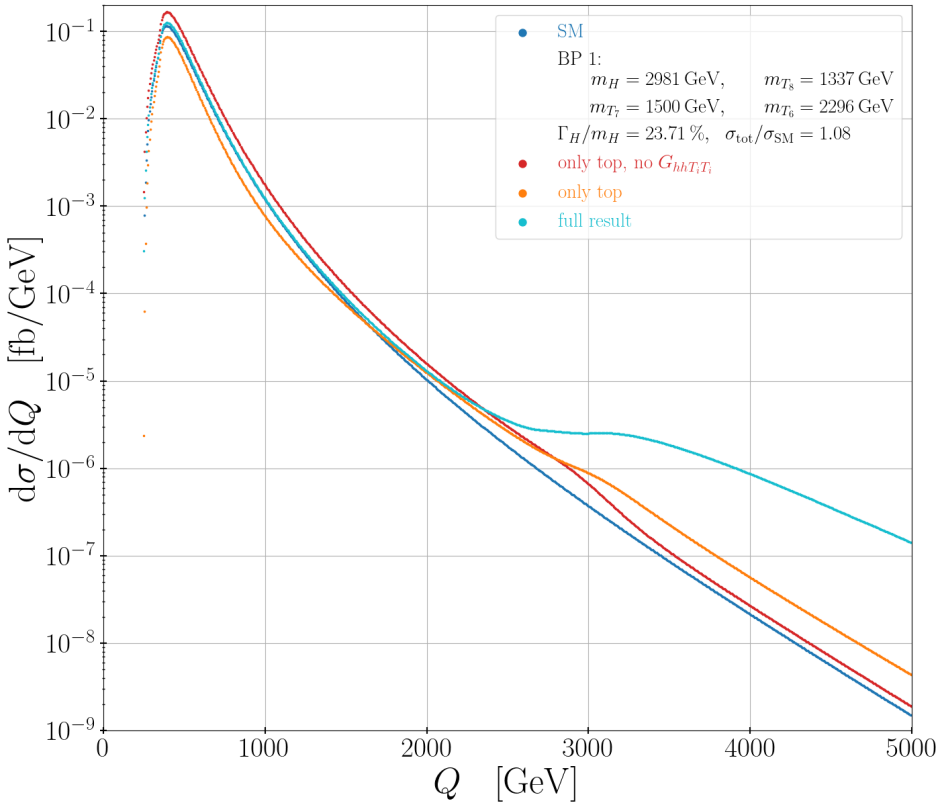

Figure 10.5.: The invariant mass distribution at LO for benchmark point `BP1` (see Tab. B.1 in App. B for the input values). Shown are the full result (in cyan), the result with only the top quark contribution and no quartic coupling contributions (red line), the result with only the top quark contribution and the G_{hhtt} coupling contribution (orange line) and the SM result (blue line) for comparison. Additional information about the heavy Higgs mass m_H, the top partner masses m_{T_i}, the heavy Higgs width Γ_H and the total cross section σ_{tot} (at LO) can be found in the legend. Taken from [74].

distribution if the quartic coupling G_{hhtt} of the SM-like Higgs and the top quark is included (in orange), and finally the full result including all contributions (in cyan).

We begin with `BP1`. In Fig. 10.5 we see the invariant mass distribution for this parameter point, where we also showcase some of the relevant parameters of the benchmark point in the legend of the plot. Here, we have a large heavy Higgs mass m_H, and thus, the resonant contribution is small.

Next, we see that for lower invariant mass values of Q the full result follows closely the SM result, and also the full cross section is close to the SM result. At two times the m_{T_8} mass (i.e. the lightest top partner), we see the heavy top partner threshold, and the distribution of the parameter point deviates from the SM result. Since the heavy top partners have to be heavy due to the experimental constraints and the differential distribution rapidly decreases with increasing Q, this threshold does not contribute significantly to the full cross section and will be very hard to measure experimentally.

Another interesting feature of this benchmark point is the following. If we exclude the heavy quark contributions and the quartic coupling contribution, we obtain the red line in the plot, which resembles an elementary 2HDM, where we can have modified couplings and the resonant triangle diagram with the heavy Higgs H. Here, this differential distribution is enhanced compared to the SM and we can also see the Higgs resonance, which is very broad here due to the large total width Γ_H. If we then include the quartic coupling, the distribution

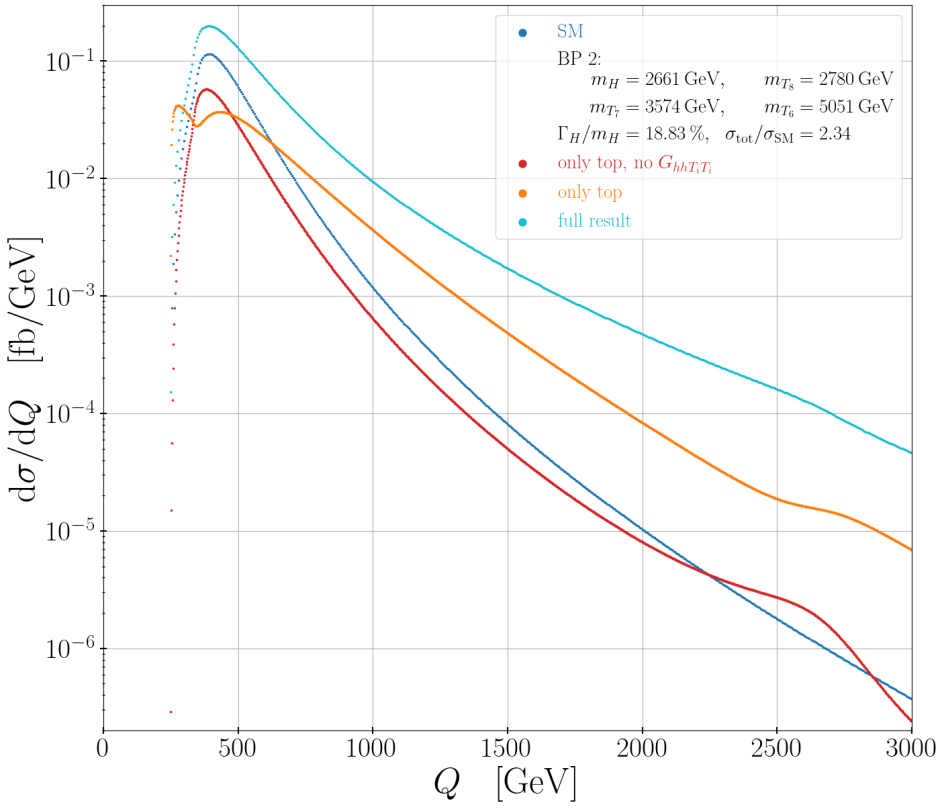

Figure 10.6.: The invariant mass distribution at LO for benchmark point BP2 (see Tab. B.1 in App. B for the input values). The colour code is the same as in Fig. 10.5. Figure taken from [74]

.

decreases and lies below the SM distribution. Finally, if we turn on all contributions, we increase our result again. Thus, for this benchmark point, the deviation of SM couplings increases the di-Higgs cross section (the resonant contribution plays no role here because m_H is quite heavy), whereas the quartic coupling contribution interferes destructively and the heavy quarks interfere constructively. We see here the behaviour already mentioned in the discussion of Fig. 10.4. All these contributions at the end lead to a SM-like result with an overall cross section of 1.08 times the SM value. Thus, even if the prediction of the SM is measured, we can have deviations from the SM couplings that will be compensated by additional contributions and will be indistinguishable experimentally in this case by di-Higgs production alone.

Another benchmark point with no clear resonance signal is BP2, which can be seen in Fig. 10.6. In this case we see a clear distinction between the benchmark point and the SM result, and the overall cross section is 2.34 times larger than the SM result. If we exclude the heavy quark contribution and the quartic coupling contribution (red line), we see that this time we are below the SM distribution until we come close to the Higgs resonance at the heavy Higgs mass m_H, which is very broad here due to the large total width Γ_H. If we include the quartic couplings (orange line), we see that they strongly interfere with the other contributions, resulting in a peak-dip-peak structure at energies below 500 GeV. Furthermore, the distributions fall off less rapidly with increasing Q. The reason here is that the quartic coupling contribution is significant in this case (as can be seen in the interference structure), and the quartic coupling contributions decrease more slowly with increasing Q, since the corresponding diagrams do not have an additional propagator (which scales with Q^{-2}) compared to the other triangle

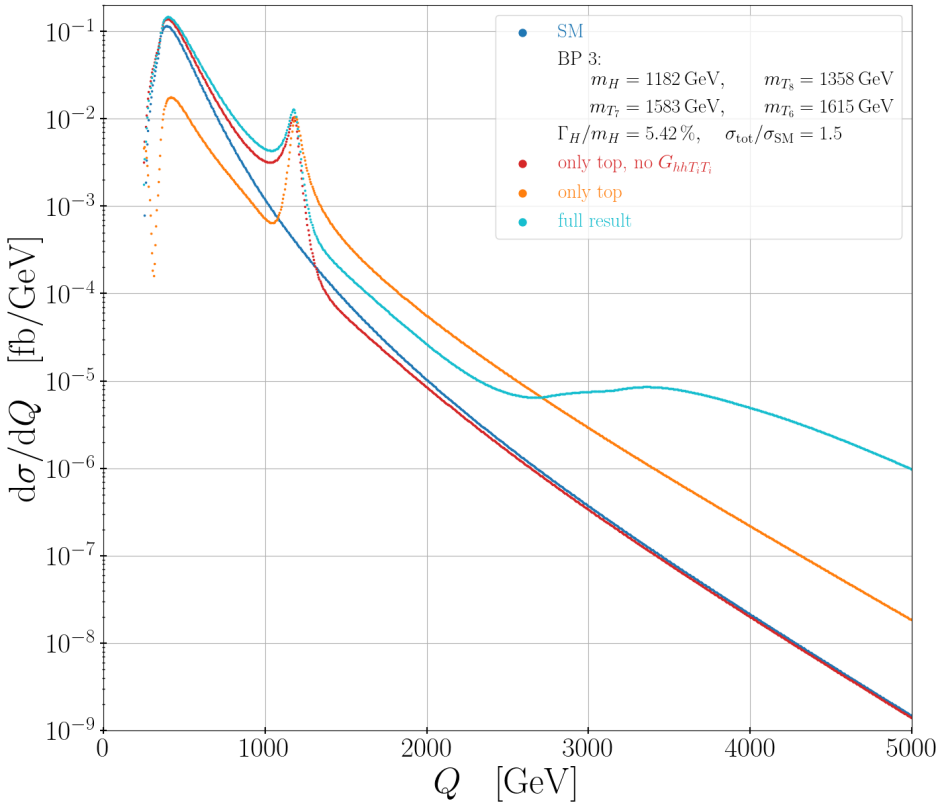

Figure 10.7.: The invariant mass distribution at LO for benchmark point `BP3` (see Tab. B.1 in App. B for the input values). The colour code is the same as in Fig. 10.5. Figure taken from [74].

contributions. Finally, if we include all contributions, we have an overall enhancement of the cross section, compared to the SM result.

Thus, due to the contributions of the heavy quarks and the quartic couplings that can enhance the overall cross section or interfere destructively, we can obtain different results in the *non-resonant* case. We can have a clear deviation from the SM di-Higgs cross section value, or a result close to the SM expectation even with deviations from the SM couplings,

Next, we turn to two benchmark points with a more visible resonant peak from the heavy Higgs. In Fig. 10.7 we see the invariant mass distribution for `BP3`. If we look only at small values for Q (less than 1 TeV), we see that the deviations from the couplings compared to the SM values (i.e. if we only consider the red line with only top quark contribution and no quartic couplings) result in an enhancement of the cross section, whereas the quartic coupling here interferes destructively (orange line) and the heavy quark contributions again interfere constructively (full result).

In the full result, we again see the heavy quark threshold limit starting at around 2.6 TeV. Additionally, we now have a clear resonance peak from the heavy Higgs at $Q = m_H = 1182\,\text{GeV}$. If we include or exclude certain contributions, the shape of the resonance peak changes, as the different contributions can interfere with each other. In this case, if we first consider only the top quark contributions without heavy quarks and quartic couplings (red line), we see that we first have constructive interference before the resonance and then destructive interference after the resonance (since the resonance contribution changes sign before and after the peak). Including the quartic coupling contributions inverts this behaviour, and finally, if the full result is considered, the interference structure becomes even more involved.

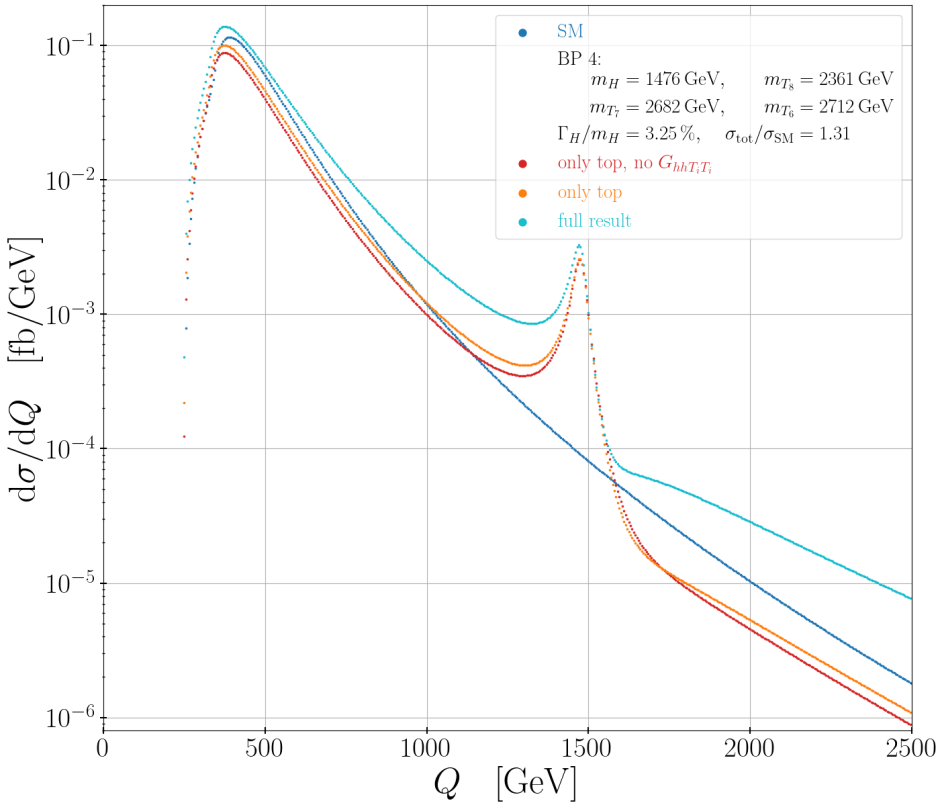

Figure 10.8.: The invariant mass distribution at LO for benchmark point `BP4` (see Tab. B.1 in App. B for the input values). The colour code is the same as in Fig. 10.5. Figure taken from [74].

Therefore, precisely measuring the shape of a resonance would also give insights into additional contributions and can be helpful to distinguish between an elementary 2HDM or the composite 2HDM realization. Another remark here is that although we have a visible resonance peak in the distribution, the total cross section is only 1.5-times the SM result, and we have a heavy Higgs width Γ_H slightly above 5 % (normalized to the heavy Higgs mass m_H), i.e. we do not apply resonant constraints on this point due to its relatively large width.

A similar behaviour can also be seen for `BP4` in Fig. 10.8. The difference here is that with only the top quark contribution and no quartic couplings (red line), we are below the SM expectation for small values of Q, and with the inclusion of the quartic coupling, the cross section is enhanced (compare orange to red line). Moreover, we also then have an enhancement before the resonance peak (which is here at $Q = m_H = 1476\,\text{GeV}$) and a suppression after the peak. If all contributions are considered, we have an overall enhancement of the cross section of about 30 % compared to the SM expectation.

For this benchmark point, we also show the p_T distribution in Fig. 10.9. Here also a peak is visible (which is not at the value of the heavy Higgs mass here), and a similar interference structure emerges compared to the invariant mass distribution. Thus, the aforementioned conclusions are also applicable to p_T distributions and they can in principle be used as well to disentangle various interference patterns.

10.3.3. Effects on Binned Distributions

Furthermore, we analyzed the expected number of events for a binned distribution. Here, we used our differential distributions and calculated the number of events, given the bin size,

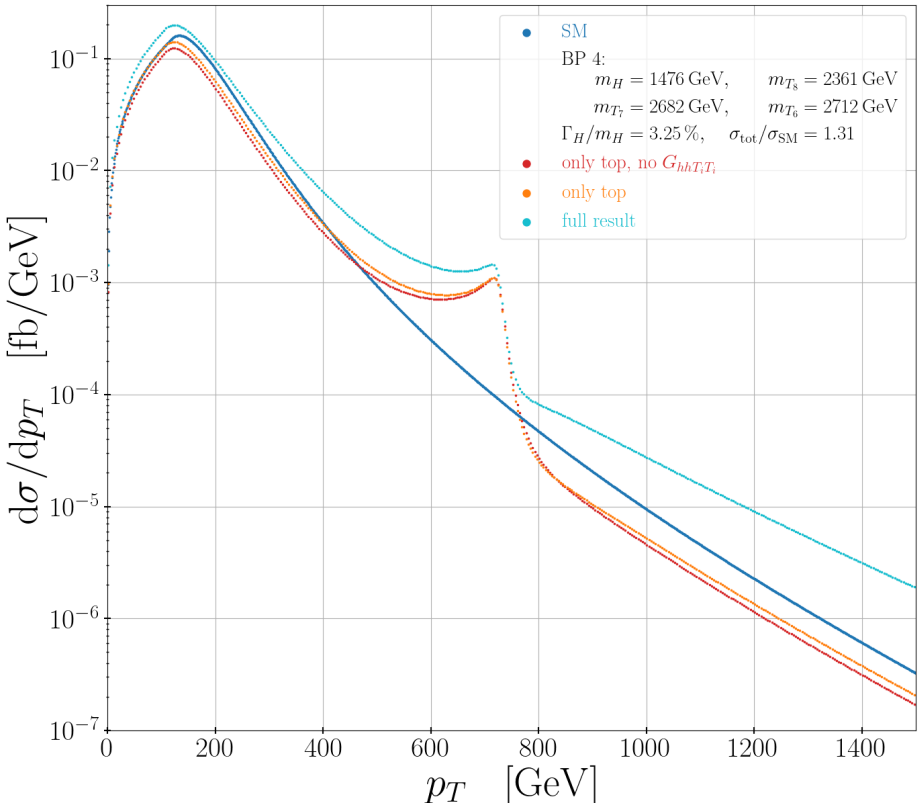

Figure 10.9.: The p_T distribution at LO for benchmark point `BP4` (see Tab. B.1 in App. B for the input values). The colour code is the same as in Fig. 10.5. Figure taken from [74].

luminosity and final state considered. We then constructed a simplified signal ratio S, given by

$$S = \frac{N_{\text{BP}}}{N_{\text{SM}}}\,, \tag{10.4}$$

where N_{BP} and N_{SM} are the events for a given bin for a selected benchmark point and the SM as comparison. In our case we used an integrated luminosity of $3000\,\text{fb}^{-1}$, a bin size of 40 GeV and the $bb\tau\tau$ final state (thus we multiplied the SM with the SM branching ratios, and our benchmark point with our calculated branching ratios). This approach clearly is a naive simplification, since we do not consider both theoretical (e.g. higher-order corrections) and experimental effects (e.g. acceptance and background, etc.), but it can be seen as a rough first estimate.

In Fig. 10.10 (upper), we see the binned distribution obtained for `BP3` and we also show the ratio S for this benchmark point for each bin, in Fig. 10.10 (lower). We see that the signal ratio S can become significant around the resonance peak region and at the threshold of the heavy quarks (i.e. at $2m_{T_8}$), but the latter will be difficult to measure due to the low event rate. These results depend on the chosen benchmark point, but similar effects can be expected for other benchmark scenarios.

10.3.4. Comparison with other 2HDM-like Models

In this section, we compare our realization of a composite 2HDM with other elementary 2HDMs. Since we have flavour-aligned Yukawa couplings in our composite 2HDM [69] it is evident to compare our model with a flavour-aligned 2HDM (A2HDM) [246]. As another model, we used a Type-II 2HDM, which resembles a supersymmetric model with potential

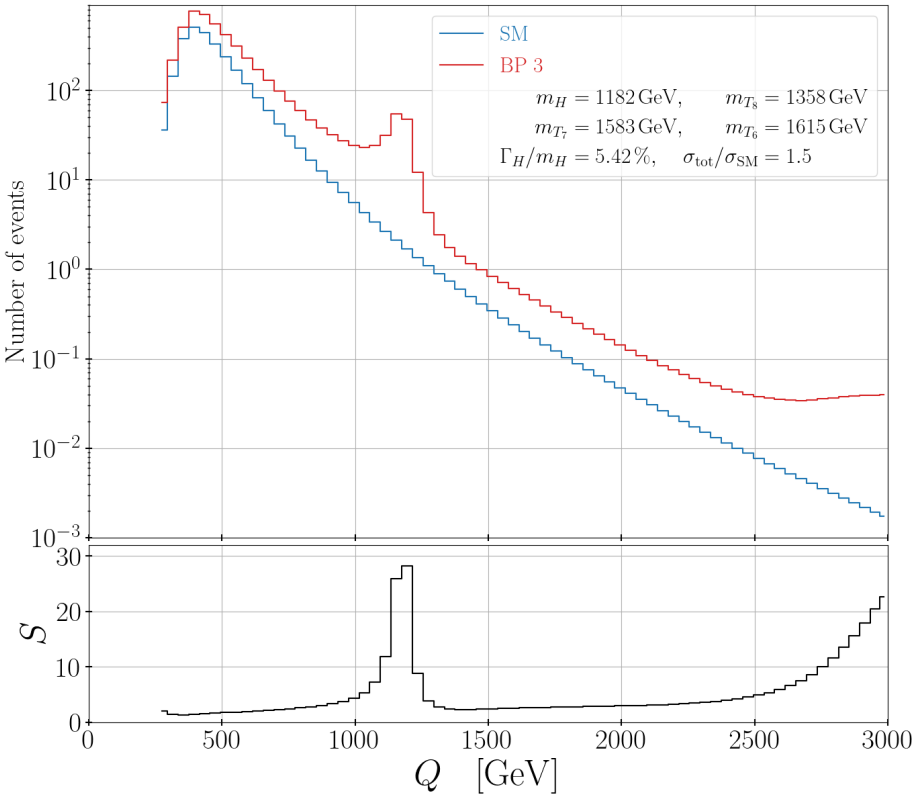

Figure 10.10.: Binned distribution of events for an integrated luminosity of $\mathcal{L} = 3000\,\text{fb}^{-1}$ and considering the $bb\tau\tau$ final state, plotted against the invariant mass Q for benchmark point `BP3` (red) and the SM as comparison (blue). The lower plot shows the signal to SM background ratio S defined as in Eq. (10.4). All cross sections are calculated at LO. The input values for `BP3` are given in Tab. B.1 in App. B. Taken from [74].

parameters not constrainted by supersymmetric relations and without the additional supersymmetric particles.

For the Type-II 2HDM we used the same dataset that was already used in [150] and therefore refer to this publication for more details on the constraints that were applied on the dataset.

For the generation of parameter points for the A2HDM, we used the code `2HDMC` [265]. We applied the following constraints (compare to the constraints we used in Sec. 3.2 and in Sec. 8.4). The code `2HDMC` checks for positivity of the potential, i.e. boundedness from below, and tree-level perturbative unitarity (cf. Sec. 3.2 and see also the manual of `2HDMC` [265]). Additionally, we used `HiggsBounds` and `HiggsSignals` again to check for compatibility with current Higgs searches and measurements.

In order to comply with flavour constraints, we used the same approach as in the composite 2HDM (see Sec. 8.4), i.e. we enforced the relation $\zeta_b \lesssim 0.1\zeta_t$, where the ζ_b and ζ_t are the coupling modifiers (see also Eq. (8.20)) of the top and bottom quark to the heavy Higgs states H, A and $H^\pm$.

To check the S, T, U parameters, which parametrize the deviations from the SM electroweak precision observables [181, 182], we used the code `ScannerS` [42, 179] again. Although the A2HDM is not implemented, we can still use `ScannerS` to check if the parameter points satisfy

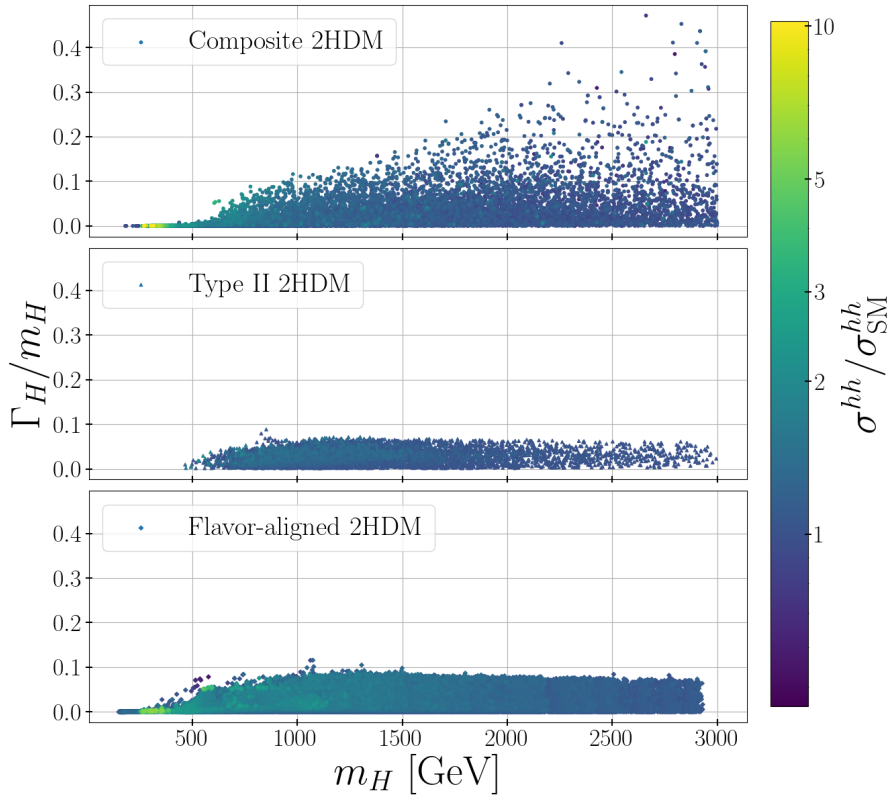

Figure 10.11.: The total heavy Higgs width divided by the heavy Higgs mass plotted against the heavy Higgs mass with the di-Higgs cross section normalized to the SM value in colour code. Shown are 3 plots for different models, the Composite 2HDM (upper), the Type-II 2HDM (middle) and the A2HDM (lower). The cross section values are given at LO. Taken from [74].

these constraints, as the S, T, U parameters are calculated from gauge boson self-energies, which are independent of the Yukawa-type of a given 2HDM model.[3]

Finally, we also included perturbativity constraints. We used the code `SARAH` [220–223] to calculate via the renormalization group (RG) the running of the Yukawa couplings y_k^F ($F = U, D, L$, $k = 1, 2$) given in the interaction basis (Φ_1, Φ_2) of the Higgs doublets and we required

$$|y_k^F(\Lambda)|^2 \leq \sqrt{4\pi}\,, \tag{10.5}$$

at a certain energy scale Λ. Here F denotes the fermion type, and k the index of the corresponding doublet. We also neglected the Yukawa couplings for the first and second generations of fermions and focused on the 3rd generation only. The 1-loop β functions are used for the running of the couplings, and we used as a cutoff $\Lambda \simeq 5\,\text{TeV}$.

The reason why we apply slightly different constraints for the A2HDM and the composite 2HDM is that we have different setups in mind. In the A2HDM we assume a weakly coupled theory and thus apply perturbative unitarity constraints and make sure that the couplings remain in the perturbative regime, whereas in the composite 2HDM we have a strongly coupled UV complete theory at higher energies.

With the generation of the parameter sample discussed, we can now move on to the comparison of the models. In Fig. 10.11 we show the total width of the heavy Higgs Γ_H normalized

[3] One may think that tadpole contributions to the self-energies have to be considered, which would be Yukawa-type dependent. They, however, cancel out exactly in the determination of the S, T, U parameters [266].

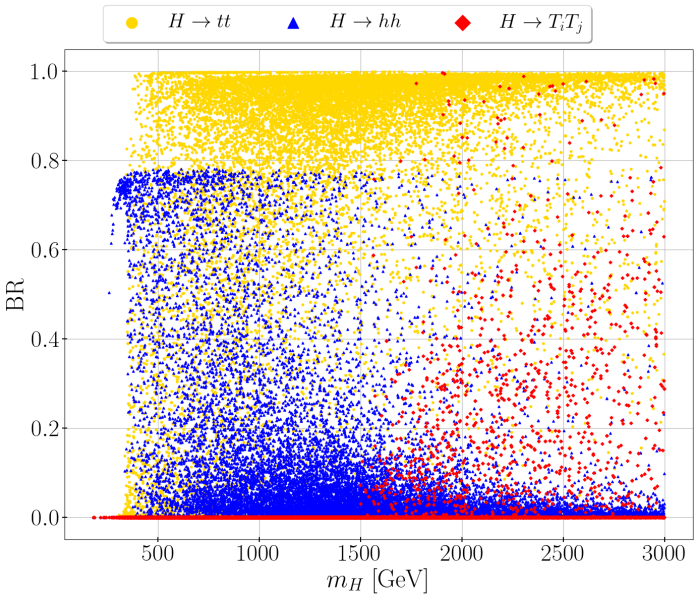

Figure 10.12.: The branching ratios (BRs) plotted against the heavy Higgs mass m_H for the various final states, $H \to tt$, $H \to hh$, $H \to T_iT_j$ $(i, j = 1, .., 9)$, with the top quark t and at least one of the T_i, T_j being one of the heavy top partners. The branching ratios of all T_iT_j final states are summed over. Taken from [74].

to the heavy Higgs mass m_H and in colour code the total di-Higgs cross section for all three models considered. The maximum cross sections, we then have in our sample, are around 2 times the SM value for the Type-II 2HDM, and around 6 times the SM value for the A2HDM. The reason why we cannot have large cross sections in the Type-II 2HDM is that we do not have heavy Higgs masses m_H below around 500 GeV anymore. This is because, first, the constraints on the S, T, U precision parameters force the mass differences between the scalars m_H, m_A and $m_{H^\pm}$ to be small, and, second, the flavour constraints force the charged Higgs mass to be heavy [267–270] i.e. lighter m_H masses are not allowed in the Type-II 2HDM. Therefore, points with a large resonant contribution are not present in this type of 2HDM, and we do not have large cross sections. In the A2HDM and the composite 2HDM, we have more freedom in our Yukawa structures to then evade the flavour constraints. Thus, we find points with lighter m_H masses and therefore resonant enhancements.

The other interesting feature in Fig. 10.11 are the total widths that can be obtained. In the Type-II 2HDM we have a maximum total width of 8.8 % (normalized to m_H), in the A2HDM we have 11.6 %, whereas in the composite 2HDM we can have up to 47 %. This large difference has a twofold origin. First, we use an effective low scale description of the composite 2HDM, a strongly coupled theory where the Yukawa couplings in this effective approach can be larger than in the other models. We also see that the total width in the composite 2HDM increases with larger Higgs masses m_H. This is due to the fact that the Yukawa coupling g_{Htt} increases with m_H (see also Fig. 10.3). Furthermore, in the composite 2HDM we have heavy top partners into which the heavy Higgs H can additionally decay, if it is heavy enough. In Fig. 10.12 we show the branching ratios of the heavy Higgs H into $t\bar{t}$, hh and T_iT_j, where t is the top quark and where in the decay channel T_iT_j at least one of the final state fermions is a top partner and not the top quark. In the plot, we add all branching ratios from all possible heavy top partner final states. We see that at around 1.5 TeV the $H \to T_iT_j$ becomes active. This is to be expected, since the heavy top partners have to be heavier than 1.3 TeV and then the decay channel to the lightest heavy top partner and a top

quark opens. We also see that this decay channel can become dominant. Thus, for Higgs masses heavier than 1.5 TeV we can enhance the total width further.

To summarize, in our composite 2HDM we can have significantly larger total widths Γ_H, which can interplay with the additional couplings and new particles that contribute to di-Higgs production and lead to more intricate interference effects in the differential distributions, compared to elementary 2HDM models.

CHAPTER 11

Conclusion

In this part, we discussed the calculation and evaluation of di-Higgs production in a composite 2HDM realization. We first gave a short introduction to composite Higgs models and to the composite 2HDM that we investigated. We described the symmetries of the composite sector, mentioned the gauge and fermion sector and summarized the important details needed for the later calculation. Furthermore, we introduced the notation for the scalar sector of elementary 2HDMs. We then described the various experimental and theoretical constraints that we applied on the composite 2HDM.

We summarized the Feynman rules obtained from the effective Lagrangian and described the various contributions to di-Higgs production in this model, where we have additional heavy top partners, a heavy Higgs boson H and effective quartic scalar-scalar-fermion-fermion couplings that can contribute. We then calculated the LO di-Higgs cross section and briefly mentioned the NLO corrections in the heavy top limit. We, however, used in the following a multiplicative K-factor to account for NLO corrections.

We described our implementation of our analytical results into the code `HPAIR`, the setup of our parameter scan and how we applied the theoretical and experimental constraints. We implemented the composite 2HDM into the codes `HDECAY` and `HIGLU` to also obtain the total widths, the branching ratios and the production cross sections via gluon fusion for the scalars in our model. We then analyzed the impact of the various constraints that we applied, in particular the *resonant* di-Higgs constraints that already constrain our parameter space. The *non-resonant* constraints did not yet exclude any parameter points but will be sensitive to our model as well in the near future.

We discussed the impact of the features of the model on di-Higgs production, on the inclusive results as well as the differential distributions. We analyzed points with different features. First, we discussed benchmark points with a SM-like cross section, where the resonant enhancement from the triangle diagram with a heavy Higgs propagator does not significantly enhance the cross section. The additional contributions from heavy top partners and/or effective quartic couplings then play a significant role, and interference effects between all contributions become important. Similar effects can be seen in the differential distributions, where, depending on the signs and sizes of the various contributions, intricate interference patterns can emerge both with or without a heavy Higgs resonance in the spectrum. We can

have points with a cross section close to the SM value, or we can have an enhancement of the overall cross section. Moreover, we can have resonant enhancement, similar to elementary 2HDMs. These distributions can then also be used to differentiate between an elementary 2HDM or a composite 2HDM. We also discussed binned distributions with a signal ratio in a simplified approach.

Finally, we compared the composite 2HDM with the type-II 2HDM and the flavour-aligned A2HDM. We showed that the type-II 2HDM is more constrained due to a combination of electroweak and flavour constraints, which can be more easily evaded in the A2HDM or composite 2HDM because of their more general Yukawa structure. Thus, we do not have lighter heavy Higgs masses m_H in the type-II 2HDM and therefore no large resonantly enhanced cross sections. Moreover, we see that in the composite 2HDM we can have significantly larger total widths Γ_H for the heavy Higgs H because of larger Yukawa couplings and additional possible decay channels into heavy top partners (or top and top partner).

Thus, the interplay between large total widths Γ_H and the additional contributions from heavy top partners and additional effective couplings can lead to intricate interference patterns in the differential distributions and can be used to distinguish between the composite 2HDM and other models.

Part III.

Supersymmetric Particle Decays in the Complex Next-to-Minimal Supersymmetric Extension of the Standard Model and Phenomenology

CHAPTER 12

Introduction

In this project, we investigated supersymmetric particle decays in the complex, i.e. CP-violating, next-to-minimal supersymmetric extension of the Standard Model (NMSSM) [70, 71]. Our goal was to extend the code `SDECAY` [75, 76], which calculates the supersymmetric particle decays in the minimal supersymmetric extension of the Standard Model (MSSM) [62, 93, 94], to calculate the decays for the NMSSM. Furthermore, we linked this code with the spectrum generator `NMSSMCALC` [77–82], which calculates the Higgs masses including loop corrections and already has a version of `HDECAY` [216, 217] implemented to calculate the Higgs decays in the NMSSM. Thus, we can use this program chain together with the program `BSMArt` [271], including experimental and theoretical constraints, to obtain valid benchmark parameter points.

Supersymmetry (SUSY), as previously mentioned in the introduction Chapter 1 and in Sec. 2.2, is a theoretically well motivated theory that can solve the hierarchy problem. Similar to the case of composite Higgs models (see part II), in order for SUSY to solve the hierarchy problem, the scale of supersymmetry cannot be too high, i.e. these models can be tested at current and future experiments. Furthermore, with the addition of the superpartners of the SM particles, and a stable lightest supersymmetric particle (LSP) due to R-parity, supersymmetric models have a very interesting phenomenology and can give well motivated explanations to unexplained phenomena, e.g. dark matter (DM). Moreover, SUSY may play a role in the unification of the fundamental forces and is a necessary ingredient for string theories, i.e. SUSY is also well motivated theoretically from a top-to-bottom (UV complete theory to low energy) perspective (see e.g. [62, 64] for an extensive review on SUSY). As we already mentioned in the introduction to the CxSM project in Chapter 3, supersymmetric models naturally have extended scalar sectors and can also be seen as special cases to generic multi-Higgs models, where in the supersymmetric case the scalar potential parameters are constrained (and we have additional particles in the theory, compare e.g. to the composite case in part II). Moreover, in supersymmetric extensions of the SM, we need at least an additional Higgs doublet to guarantee an anomaly-free theory and to obtain the correct Yukawa structure for the quarks [62]. Thus, extended scalar sectors appear naturally in supersymmetric theories. We will omit a detailed explanation of supersymmetry and instead refer to the excellent reviews [62–64, 70, 71, 93, 94], where further information can be found.

We now describe the content of this part of the thesis. We will first give a short introduction to SUSY, the NMSSM and its particle content. We then describe the renormalization that is needed for the QCD corrections to two-body decays. Moreover, we describe all the two- and three-body as well as the radiative loop decays. Furthermore, we present the QCD corrections for two-body decays to obtain precise results for the decay widths of the supersymmetric particles. Finally, we discuss our setup to obtain viable parameter points in the NMSSM parameter space to check our results and perform a first analysis.

In this chapter, we briefly summarize the features of SUSY in Sec. 12.1 and give an overview over the NMSSM (Sec. 12.2). We describe the particle content, set our notation and list the constraints we applied on our model to obtain viable parameter points, in Sec. 12.3. Furthermore, we describe the renormalization necessary for the QCD corrections (Sec. 12.4), where we define the field and mass renormalization in Sec. 12.4.2, the renormalization of the strong coupling constant (Sec. 12.4.3), the SUSY restoring counterterms that we need in our calculation, since we used dimensional regularization (Sec. 12.4.4) as well as the conversion from $\overline{\text{DR}}$ to OS parameters in Sec. 12.4.5.

The described setup and preliminary results are part of an ongoing project and will soon be published.

12.1. Introduction to Supersymmetry

In the following we give a brief introduction to SUSY, where we follow [272] and the reviews [62, 64, 70, 71, 93, 94], where more information can be found.

In supersymmetry, we extend the group of spacetime symmetries, the Poincaré group, by an additional symmetry with generator Q that relates fermions and bosons. The generator Q must be an anti-commuting spinor and obey the following relations with the generators $P^\mu, M^{\mu\nu}$ of the Poincaré group,

$$\{Q, Q^\dagger\} = 2\gamma^\mu P_\mu \,, \tag{12.1a}$$

$$\{Q, Q\} = \{Q^\dagger, Q^\dagger\} = 0 \,, \tag{12.1b}$$

$$[P^\mu, Q] = [P^\mu, Q^\dagger] = 0 \,, \tag{12.1c}$$

$$[M^{\mu\nu}, Q] = -\sigma^{\mu\nu} Q \,, \quad [M^{\mu\nu}, Q^\dagger] = -\sigma^{\mu\nu} Q^\dagger \,, \tag{12.1d}$$

to uphold the Coleman-Mandula theorem [273] with the Haag-Łopuszański-Sohnius extension [274]. Here, we have $\sigma^{\mu\nu} = i/4[\gamma^\mu, \gamma^\nu]$ with the gamma matrices γ^μ, and we suppressed spinor indices.

We have the symbolic relations

$$Q\,|\text{fermion}\rangle = |\text{boson}\rangle \,, \qquad Q\,|\text{boson}\rangle = |\text{fermion}\rangle \,, \tag{12.2}$$

i.e. Q can transform fermionic states into bosonic states and vice versa. It then quickly follows that a consistent theory with this extended symmetry requires the same number of bosonic and fermionic degrees of freedom, $n_B = n_F$, and identical masses for the related bosons and fermions, $m_B = m_F$. Therefore, each particle in the theory (e.g. in the SM) has a so-called superpartner with identical quantum numbers (e.g. mass, electrical charge, etc.), except for the spin.

Now, if a supersymmetric theory is constructed, one can categorize the fermionic and bosonic fields by constructing so-called superfields where fermionic and bosonic fields, which are related by the supersymmetry transformation, are combined. When we consider e.g. gauge

bosons, A^a_μ, and their respective superpartners, the gauginos, $\tilde{\lambda}^a$, they can be combined to vector superfields $\hat{A}^a = (A^a_\mu, \tilde{\lambda}^a)$. Similarly, we obtain chiral superfields $\hat{\Phi}_i = (\tilde{\Phi}_i, \Psi_i)$ for a Weyl spinor Ψ_i and their superpartners consisting of a complex scalar field $\tilde{\Phi}_i$. The Weyl spinors then result in the left- and right-handed parts of the Dirac fermions of the SM, and the complex scalars result in their superpartners, the so-called sfermions. Here, we already indicated with the tilde the supersymmetric partners to the already established SM particles.

Furthermore, another fundamental object in a supersymmetric theory is the superpotential $\mathcal{W}$, which is a holomorphic function of the superfields. The Lagrangian of the theory is thus determined by the gauge group and the superpotential $\mathcal{W}$.

Since we do not observe superpartners of the SM with identical masses, we know that in a supersymmetric extension of the SM supersymmetry has to be broken. Therefore, we introduce additional soft-breaking terms summarized in the Lagrangian $\mathcal{L}^{\text{soft}}$ that break SUSY softly, i.e. supersymmetry is only broken by dimensionful parameters. By only introducing these softly breaking terms into the theory, we break solely the requirement of equal masses for particles and their superpartners, while retaining the other attractive features of supersymmetric theories, as e.g. solving the hierarchy problem, the unification of the gauge couplings, etc.. A supersymmetric theory is therefore given by the field content, the gauge group, the superpotential $\mathcal{W}$ and the soft-breaking Lagrangian $\mathcal{L}^{\text{soft}}$.

We can write the general scalar potential of the theory as

$$V_\Phi = \mathcal{W}_i^* \mathcal{W}^i + \frac{1}{2} g_a^2 \left(\Phi_i^* T^a_{ij} \Phi_j\right)^2 + \text{soft-breaking terms}\,, \tag{12.3}$$

where we summed up all F-terms from the chiral superfields and the D-terms from the gauge multiplets contributing to the potential (for more details see e.g. [62]). Here, $\mathcal{W}_i = \partial\mathcal{W}/\partial\Phi_i$, with Φ_i being the scalars in the model, g_a the gauge couplings and T^a_{ij} being the generators of the gauge group.

We see that the scalar potential is already determined by the superpotential (i.e. the Yukawa couplings), the D-terms, that are obtained from the gauge interactions and the soft-breaking terms.

12.2. The Next-to-Minimal Supersymmetric Standard Model

We now give a short overview over the NMSSM, where we will mainly follow the reviews [70, 71] and [272].

The NMSSM is obtained from the MSSM [62, 93, 94] by introducing an additional superfield $\hat{S}$, which is a singlet under the SM gauge groups. The superpotential $\mathcal{W}_{\text{NMSSM}}$ of the NMSSM is given by

$$\mathcal{W}_{\text{NMSSM}} = \mathbf{Y}_u \hat{u}(\hat{Q}^{\mathrm{T}} \epsilon \hat{H}_u) - \mathbf{Y}_e \hat{e}(\hat{L}^{\mathrm{T}} \epsilon \hat{H}_d) - \mathbf{Y}_d \hat{d}(\hat{Q}^{\mathrm{T}} \epsilon \hat{H}_d) + \lambda \hat{S}(\hat{H}_u^{\mathrm{T}} \epsilon \hat{H}_d) + \frac{1}{3}\kappa \hat{S}^3\,, \tag{12.4}$$

where $\mathbf{Y}_u$, $\mathbf{Y}_e$, $\mathbf{Y}_d$ are the 3×3 Yukawa matrices, and λ and κ are dimensionless couplings between the Higgs ($\hat{H}_u, \hat{H}_d$) and the Singlet ($\hat{S}$) superfields. The definition of the superfields can be seen in Tab. 12.1. The main difference to the MSSM due to the inclusion of the singlet superfield $\hat{S}$ are the additional terms proportional to λ and κ. Moreover, ϵ is defined as

$$\epsilon = \begin{pmatrix} 0 & 1 \\ -1 & 0 \end{pmatrix}\,, \tag{12.5}$$

Table 12.1.: Field content of the NMSSM together with their quantum numbers [70]. The indices L, R denote the left- and right-chiral parts of the fermions, while for the scalar fields they indicate the chiral fermion they are related to. Here, Q denotes the quark doublet and not the SUSY generator.

Superfield		scalar	fermion	generations	$(U(1)_\mathrm{Y}, SU(2)_\mathrm{L}, SU(3)_\mathrm{C})$
quark-squark	$\hat{Q}$	$\tilde{Q} = (\tilde{u}_\mathrm{L}, \tilde{d}_\mathrm{L})^\mathrm{T}$	$Q = (u_\mathrm{L}, d_\mathrm{L})^\mathrm{T}$	3	$(\frac{1}{6}, \mathbf{2}, \mathbf{3})$
	$\hat{u}$	$\tilde{u}^*_\mathrm{R}$	$u^\dagger_\mathrm{R}$	3	$(-\frac{2}{3}, \mathbf{1}, \overline{\mathbf{3}})$
	$\hat{d}$	$\tilde{d}^*_\mathrm{R}$	$d^\dagger_\mathrm{R}$	3	$(\frac{1}{3}, \mathbf{1}, \overline{\mathbf{3}})$
lepton-slepton	$\hat{L}$	$\tilde{L} = (\tilde{v}, \tilde{l}_\mathrm{L})^\mathrm{T}$	$L = (v, l_\mathrm{L})^\mathrm{T}$	3	$(-\frac{1}{2}, \mathbf{2}, \mathbf{1})$
	$\hat{l}$	$\tilde{l}^*_\mathrm{R}$	$l^\dagger_\mathrm{R}$	3	$(1, \mathbf{1}, \mathbf{1})$
Higgs-Higgsino	$\hat{H}_u$	$H_u = (H_u^+, H_u^0)^\mathrm{T}$	$\tilde{H}_u = (\tilde{H}_u^+, \tilde{H}_u^0)^\mathrm{T}$	1	$(\frac{1}{2}, \mathbf{2}, \mathbf{1})$
	$\hat{H}_d$	$H_d = (H_d^0, H_d^-)^\mathrm{T}$	$\tilde{H}_d = (\tilde{H}_d^0, \tilde{H}_d^-)^\mathrm{T}$	1	$(-\frac{1}{2}, \mathbf{2}, \mathbf{1})$
	$\hat{S}$	S	$\tilde{S}$	1	$(0, \mathbf{1}, \mathbf{1})$
		Vector boson	fermion		
B-Bino	$\hat{B}$	B	$\tilde{B}$	1	$(0, \mathbf{1}, \mathbf{1})$
W-Wino	$\hat{W}$	W	$\tilde{W}$	1	$(0, \mathbf{3}, \mathbf{1})$
gluon-gluino	$\hat{G}$	g	$\tilde{g}$	1	$(0, \mathbf{1}, \mathbf{8})$

and determines the contraction of the Higgs doublet fields. Furthermore, a $\mathbb{Z}_3$ symmetry is imposed to forbid other dimensionful terms (see e.g. [70] for more details).

The superpotential in Eq. (12.4) solves the so-called μ-problem of the MSSM, where the supersymmetry respecting parameter μ has to be of the same order as the SUSY breaking parameters in the soft-breaking Lagrangian $\mathcal{L}^\mathrm{soft}$ in order to obtain EW symmetry breaking with a VEV v around the SM EW scale. The μ parameter and the soft breaking parameters, however, have different origins in the MSSM, and thus a new hierarchy problem is introduced. In the NMSSM, no dimensionful parameters remain in the superpotential, and the μ parameter is generated dynamically (then called μ_eff) by introducing a VEV for the scalar in the singlet superfield. Thus, μ_eff and the SUSY breaking parameters can naturally be of the same order.

After specifying the superpotential and the field content of the model, we also describe the soft-breaking terms. The Lagrangian $\mathcal{L}^\mathrm{soft}_\mathrm{NMSSM}$ is given by

$$\begin{aligned}
\mathcal{L}^\mathrm{soft}_\mathrm{NMSSM} = &- m^2_{H_d} H_d^\dagger H_d - m^2_{H_u} H_u^\dagger H_u - \mathbf{m}^2_{\tilde{Q}} \tilde{Q}^\dagger \tilde{Q} - \mathbf{m}^2_{\tilde{L}} \tilde{L}^\dagger \tilde{L} \\
&- \mathbf{m}^2_{\tilde{u}_\mathrm{R}} \tilde{u}^*_\mathrm{R} \tilde{u}_\mathrm{R} - \mathbf{m}^2_{\tilde{d}_\mathrm{R}} \tilde{d}^*_\mathrm{R} \tilde{d}_\mathrm{R} - \mathbf{m}^2_{\tilde{l}_\mathrm{R}} \tilde{l}^*_\mathrm{R} \tilde{l}_\mathrm{R} \\
&- \Big(-\mathbf{T}_l H_d^\mathrm{T} \epsilon \tilde{L} \tilde{l}^*_\mathrm{R} - \mathbf{T}_d H_d^\mathrm{T} \epsilon \tilde{Q} \tilde{d}^*_\mathrm{R} + \mathbf{T}_u H_u^\mathrm{T} \epsilon \tilde{Q} \tilde{u}^*_\mathrm{R} \\
&+ \frac{M_1}{2} \tilde{B}\tilde{B} + \frac{M_2}{2} \tilde{W}_i \tilde{W}_i + \frac{M_3}{2} \tilde{G}\tilde{G} + \mathrm{h.c.} \Big) \\
&- m^2_S |S|^2 + \left(T_\lambda S H_d^\mathrm{T} \epsilon H_u - \frac{1}{3} T_\kappa S^3 + \mathrm{h.c.} \right) ,
\end{aligned} \tag{12.6}$$

where M_1, M_2 and M_3 are the gaugino, m_{H_d} and m_{H_u} the doublet Higgs, $\mathbf{m}_{\tilde{Q}}$, $\mathbf{m}_{\tilde{L}}$,$\mathbf{m}_{\tilde{u}_\mathrm{R}}$, $\mathbf{m}_{\tilde{d}_\mathrm{R}}$ and $\mathbf{m}_{\tilde{l}_\mathrm{R}}$ the sfermion and m_S the singlet field mass parameters. Then, we have the trilinear couplings $\mathbf{T}_e$, $\mathbf{T}_d$, $\mathbf{T}_u$, T_λ and T_κ, which in general can be complex, as well as the gaugino masses. All parameters here are soft susy-breaking. We parametrize the soft susy-breaking trilinear couplings as

$$T_\kappa \equiv \kappa A_\kappa \,,\; T_\lambda \equiv \lambda A_\lambda \,, \tag{12.7a}$$

$$\mathbf{T}_i \equiv \mathbf{Y}_i \mathbf{A}_i \;(i = u, d, l) \,, \tag{12.7b}$$

with A_κ, A_λ and the $\mathbf{A}_i$ as complex parameters. The soft sfermion masses $\mathbf{m}_{\tilde{Q}}$, $\mathbf{m}_{\tilde{L}}$, $\mathbf{m}_{\tilde{u}_\mathrm{R}}$, $\mathbf{m}_{\tilde{d}_\mathrm{R}}$, $\mathbf{m}_{\tilde{l}_\mathrm{R}}$ and the $\mathbf{A}_i$ can in general be matrices, but we assume them to be diagonal in flavour space in order to avoid large flavour changing effects at tree-level [62]. Thus, we have minimal flavour violation (MFV), where the only flavour violation occurs in the CKM matrix. We can have, however, left-right mixing between the sfermions $\tilde{f}_{\mathrm{L/R}}$.

The scalar Higgs potential in the NMSSM is given by [70],

$$\begin{aligned} V_\mathrm{NMSSM} =& V_F + V_D + V_\mathrm{soft} \\ =& |\lambda|^2 |S|^2 \left(H_u^\dagger H_u + H_d^\dagger H_d \right) + \left| \lambda (H_u^\mathrm{T} \epsilon H_d) + \kappa S^2 \right|^2 \\ &+ \frac{1}{2} g_2^2 |H_u^\dagger H_d|^2 + \frac{1}{8} (g_1^2 + g_2^2) \left(H_u^\dagger H_u - H_d^\dagger H_d \right)^2 \\ &+ m_{H_u}^2 H_u^\dagger H_u + m_{H_d}^2 H_d^\dagger H_d + m_S^2 |S|^2 + \left(\lambda A_\lambda (H_u^\mathrm{T} \epsilon H_d) S + \frac{1}{3} \kappa A_\kappa S^3 + \mathrm{c.c.} \right) . \end{aligned} \tag{12.8}$$

It consists of the F-terms, D-terms and the soft-breaking contributions as described in Sec. 12.1. We can express the scalar doublets H_d, H_u and the singlet field S as

$$H_d = \begin{pmatrix} \frac{1}{\sqrt{2}}(v_d + h_d + i a_d) \\ H_d^- \end{pmatrix} , \qquad H_u = e^{i\varphi_u} \begin{pmatrix} H_u^+ \\ \frac{1}{\sqrt{2}}(v_u + h_u + i a_u) \end{pmatrix} , \tag{12.9}$$

$$S = \frac{1}{\sqrt{2}} e^{i\varphi_s} (v_s + h_s + i a_s) \,,$$

with the phases φ_u and φ_s, the VEVs v_u, v_d, and v_s, the real scalar fields h_u, h_d, h_s, a_u, a_d and a_s and the charged fields H_u^+ and H_d^-. We define $\tan\beta$ as the fraction

$$\tan\beta \equiv \frac{v_u}{v_d} \,, \tag{12.10}$$

and obtain the SM VEV via the relation

$$v^2 = v_u^2 + v_d^2 \,. \tag{12.11}$$

The effective parameter μ_eff, which plays the same role as the μ-parameter in the MSSM, is now generated by the VEV v_s and given by,

$$\mu_\mathrm{eff} \equiv \frac{\lambda v_s e^{i\varphi_s}}{\sqrt{2}} \,. \tag{12.12}$$

The MSSM can be obtained from the NMSSM in the limit $\lambda, \kappa \to 0$ with λ/κ, the product λv_s (i.e. μ_eff) and the parameters A_λ and A_κ fixed. This limit corresponds to $v_s \to \infty$ and therefore a decoupling of the singlet S, and we retain the MSSM particle content.

We now formulate the tadpole (or minimization) conditions,

$$\frac{\partial}{\partial\phi} V_{\text{NMSSM}}\Big|_{\{\phi\}=0} = 0\,, \tag{12.13}$$

where we derivate the potential with respect to the scalar fields $\phi = h_u,\, h_d,\, h_s,\, a_u,\, a_d,\, a_s$. We obtain a set of equations that we can use to eliminate potential parameters for a chosen set of input parameters. We choose the set of input parameters as:

$$\begin{aligned}&\tan\beta,\, \lambda,\, v_s,\, \varphi_s,\, \kappa,\, A_\kappa,\, M_{H^\pm}(A_\lambda),\, \varphi_u,\, \mathbf{A}_u,\, \mathbf{A}_d\,, \mathbf{A}_l\,, M_1,\, M_2,\, M_3,\\ &\mathbf{m}_{\tilde{Q}},\, \mathbf{m}_{\tilde{L}},\, \mathbf{m}_{\tilde{u}_\text{R}},\, \mathbf{m}_{\tilde{d}_\text{R}},\, \mathbf{m}_{\tilde{l}_\text{R}}\,.\end{aligned} \tag{12.14}$$

Here, we have the freedom to either use $M_{H^\pm}$ or A_λ as input. Additional parameters are the SM parameters, i.e. the gauge boson masses M_W, M_Z, the electric charge e, the strong coupling constant α_s, the quark and lepton masses and the CKM matrix elements.

In order to have real up-quark Yukawa couplings and therefore real quark masses in the Lagrangian, we rotate the left- and right-handed up-quark fields $q_{\text{L/R}}$ [81],

$$q_\text{L} \to e^{-i\frac{\varphi_u}{2}} q_\text{L}\,, \quad q_\text{R} \to e^{+i\frac{\varphi_u}{2}} q_\text{R}\,. \tag{12.15}$$

Similarly, the gluino mass term M_3 can have a complex phase φ_{M_3}, i.e.

$$M_3 = e^{i\varphi_{M_3}} |M_3|\,. \tag{12.16}$$

Thus, we rotate the gluino field

$$\tilde{g}_\text{L} \to e^{i\frac{\varphi_{M_3}}{2}} \tilde{g}_\text{L}\,, \quad \tilde{g}_\text{R} \to e^{-i\frac{\varphi_{M_3}}{2}} \tilde{g}_\text{R}\,, \tag{12.17}$$

to obtain a real mass term [275]. The Feynman rules involving up-type quarks or gluinos have to be adjusted accordingly.

Next, we briefly discuss the particle content in the NMSSM. All particles with identical quantum numbers can in general mix, and we have to diagonalize the mass matrices to obtain the physical mass eigenstates and the mixing angles. All the masses of the mass eigenstates are sorted in ascending order. First of all, we have the neutral Higgs scalars, where in the complex NMSSM we have CP-mixed states, i.e. the h_u, h_d, h_s, a_u, a_d and a_s can in general all mix (one of the mixed states will be the neutral would-be Goldstone boson that is absorbed by the Z boson). The Higgs mass matrix will be denoted by $\mathcal{M}_H$ and the Higgs rotation matrix $\mathcal{R}^H$ and we have the relation

$$\text{diag}(m^2_{h_1}, m^2_{h_2}, m^2_{h_3}, m^2_{h_4}, m^2_{h_5}) = \mathcal{R}^H \mathcal{M}_H (\mathcal{R}^H)^\text{T}\,. \tag{12.18}$$

Similarly, we have for the neutral higgsinos $\tilde{H}^0_u$, $\tilde{H}^0_d$, $\tilde{S}$ and gauginos $\tilde{B}$, $\tilde{W}$ the mass matrix $\mathcal{M}_{\tilde{\chi}^0}$ and the rotation matrix Z. We denote the mass eigenstates, the neutralinos, with $\tilde{\chi}^0_i$ $(i = 1, .., 5)$, and we obtain

$$\text{diag}(m_{\tilde{\chi}^0_1}, m_{\tilde{\chi}^0_2}, m_{\tilde{\chi}^0_3}, m_{\tilde{\chi}^0_4}, m_{\tilde{\chi}^0_5}) = Z^* \mathcal{M}_{\tilde{\chi}^0} Z^\dagger\,. \tag{12.19}$$

We note that the neutralinos are Majorana fermions.

The charged higgsinos $\tilde{H}^+_u$, $\tilde{H}^-_d$ mix with the charged gauginos $\tilde{W}$ and we have the mass matrix $\mathcal{M}_{\tilde{\chi}^\pm}$ and the rotation matrices $\mathcal{V}$ and $\mathcal{U}$. We label the mass eigenstates, the charginos, as $\tilde{\chi}^\pm_i$ $(i = 1, 2)$, and we have

$$\text{diag}(m_{\tilde{\chi}^0_1}, m_{\tilde{\chi}^0_2}) = \mathcal{U}^* \mathcal{M}_{\tilde{\chi}^\pm} \mathcal{V}^\dagger\,. \tag{12.20}$$

Finally, the scalar superpartners of the fermions also mix in general, and we have the mass matrices $\mathcal{M}_{\tilde{f}}$ and the rotation matrix $W^{\tilde{f}}$ that diagonalizes the mass matrix,

$$\text{diag}(m^2_{\tilde{f}_1}, m^2_{\tilde{f}_2}) = W^{\tilde{f}} \mathcal{M}_{\tilde{f}} W^{\tilde{f}\dagger}\,, \tag{12.21}$$

leading to the mass eigenstates $\tilde{f}_1$, $\tilde{f}_2$ for each type of fermion f (lepton, up- and down quark, the sneutrinos do not mix in our case). We here only considered left-right mixing and no flavour mixing. In general, we can also denote the mixing matrix $W^{\tilde{f}}$ as a 6×6 matrix rotating the fields $(\tilde{f}_{1,\text{L}}, \tilde{f}_{1,\text{R}}, \tilde{f}_{2,\text{L}}, \tilde{f}_{2,\text{R}}, \tilde{f}_{3,\text{L}}, \tilde{f}_{3,\text{R}})^{\text{T}}$ into the corresponding mass eigenstates (with $1, 2, 3$ here being the generation index).

The gluinos do not mix with other fields, and their mass is already determined by the soft breaking mass parameter M_3. Gluinos are also Majorana fermions.

We will omit the presentation of the mass matrices of the Higgs scalars, the charginos/neutralinos and sfermions. They can be found in the literature [62, 70, 71]. We will, however, give the squark mass matrices in more detail in Sec. 12.4.1, as they will become important in the context of the QCD corrections to the two-body decays. This concludes the brief introduction to the NMSSM.

12.3. Theoretical and Experimental Constraints

In the following we list the theoretical and experimental constraints that we applied to obtain valid parameter points. We followed the approach in [276]. The following constraints were used to check the parameter points:

- **Higgs Searches and Measurements:**

  The parameter points where checked against current Higgs measurements and searches via the tool `HiggsTools` [277], which is the combination of the codes `HiggsSignals` [188, 189] and `HiggsBounds` [183–187] . Thus, `HiggsTools` checks for both compatibility with current Higgs measurements and compatibility with searches for new Higgs resonances. We furthermore required in our setup that the SM-like Higgs boson in our spectrum has a mass in the range $[122\,\text{GeV}, 128\,\text{GeV}]$.

- **SUSY searches:**

  The NMSSM is constrained by searches for supersymmetric particles that give limits on the allowed mass ranges for the SUSY particles. We use the code `SModels` [278–282] to check for compatibility with current SUSY searches.

- **EDM Constraints:**

  In the NMSSM, we can have potentially complex couplings and masses that can lead to CP-violation already at tree level. They can contribute to electric dipole moments (EDMs), and therefore the constraints from experimental limits have to be considered. The code `NMSSMCALC` calculates the EDMs [283, 284] and normalizes them to the experimental upper limits from [285–289]. The obtained ratio can then be used to check if the considered parameter input is still allowed. In our scans, however, we did not apply the EDM constraints for illustrative purposes as we wanted to see the impact of the complex phases on the decay channels.

- **Perturbative Unitarity:**

  We require the inequality

$$\lambda^2 + \kappa^2 \leq 1\,, \tag{12.22}$$

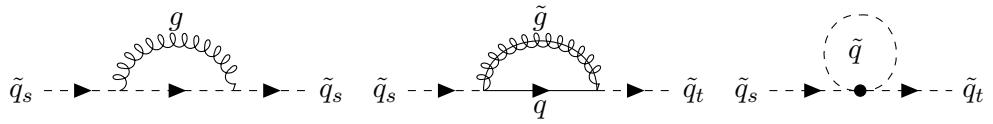

(a) One-loop contributions to the squark self-energy ($s, t = 1, .., 6$).

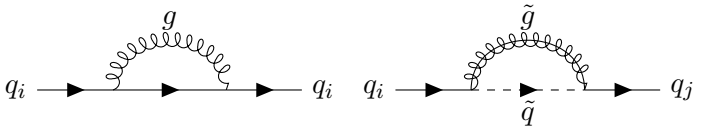

(b) One-loop contributions to the quark self-energy ($i, j = 1, .., 3$).

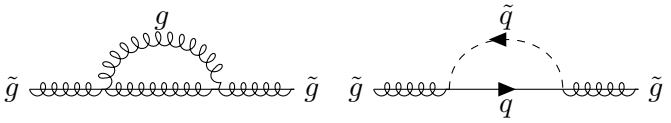

(c) One-loop contributions to the gluino self-energy.

Figure 12.1.: One-loop QCD corrections to the squark, quark and gluino self-energies.

to be satisfied in order to relax the requirement for perturbative unitarity below the scale of grand unification [276, 290].

12.4. Renormalization of the NMSSM for the QCD Corrections

In this section, we describe the renormalization of the squark, quark and gluino fields, their masses and the strong coupling constant in order to calculate the QCD corrections to the decays of supersymmetric particles, where we followed [200, 291, 292]. We performed our calculation in the dimensional regularization scheme, i.e. we performed the integration of the loop integrals in $D = 4 - 2\epsilon$ dimensions and also treated the gamma matrices in D dimensions. This prescription breaks SUSY, and we have to introduce additional SUSY restoring counterterms that we describe in Sec. 12.4.4. We also describe the conversion of the input parameters that are given in the dimensional reduction ($\overline{\text{DR}}$) scheme to the on-shell (OS) scheme that we applied in Sec. 12.4.5.

12.4.1. Quark and Squark Mass and Rotation Matrices

We present in the following the squark mass and rotation matrices, as well as the quark rotation matrices and the resulting CKM matrix, as they have to be renormalized for the QCD corrections.

The squark mass matrix (in the following $q = u, d$ for up- and down-type squarks and quarks) can be written as

$$\mathcal{M}_{\tilde{u}} = \begin{pmatrix} m_{\tilde{Q}}^2 + m_u^2 + \dfrac{-g_1^2 + 3g_2^2}{24} v^2 \cos(2\beta) & m_u \left(A_u^* e^{-i\varphi_u} - \mu_{\text{eff}} \cot\beta \right) \\ m_u \left(A_u e^{i\varphi_u} - \mu_{\text{eff}}^* \cot\beta \right) & m_{\tilde{u}_R}^2 + m_u^2 + \dfrac{g_1^2}{6} v^2 \cos(2\beta) \end{pmatrix}, \tag{12.23a}$$

$$\mathcal{M}_{\tilde{d}} = \begin{pmatrix} m_{\tilde{Q}}^2 + m_d^2 + \dfrac{-g_1^2 - 3g_2^2}{24} v^2 \cos(2\beta) & m_d \left(A_d^* - \mu_{\text{eff}} e^{i\varphi_u} \tan\beta \right) \\ m_d \left(A_d - \mu_{\text{eff}}^* e^{-i\varphi_u} \tan\beta \right) & m_{\tilde{d}_R}^2 + m_d^2 - \dfrac{g_1^2}{12} v^2 \cos(2\beta) \end{pmatrix}, \tag{12.23b}$$

where g_1 and g_2 are the $U(1)_Y$ and $SU(2)_Y$ gauge couplings, respectively, and the matrix is given in the $(\tilde{q}_\mathrm{L}, \tilde{q}_\mathrm{R})$ basis. The squarks $\tilde{q} = (\tilde{q}_\mathrm{L}, \tilde{q}_\mathrm{R})^\mathrm{T}$ are then rotated into mass eigenstates $\tilde{q}^m = (\tilde{q}_1, \tilde{q}_2)^\mathrm{T}$ via

$$\tilde{q}^m = W^{\tilde{q}} \tilde{q}\,, \tag{12.24}$$

with the squark rotation matrix $W^{\tilde{q}}$, which then diagonalizes the squark mass matrix,

$$\begin{pmatrix} m_{\tilde{q}_1^2} & 0 \\ 0 & m_{\tilde{q}_2^2} \end{pmatrix} = W^{\tilde{q}} \mathcal{M}_{\tilde{q}} W^{\tilde{q}\dagger}\,. \tag{12.25}$$

We also introduce the quark rotation matrices $U^{q_\mathrm{L/R}}$. The left- and right-chiral quarks $q_\mathrm{L/R}$ are rotated into the mass eigenstates $q^m_\mathrm{L/R}$ via

$$q^m_\mathrm{L/R} = U^{q_\mathrm{L/R}} q_\mathrm{L/R}\,, \tag{12.26}$$

The CKM matrix V^CKM in our notation is then defined as

$$V^\mathrm{CKM} = U^{u_\mathrm{L}} U^{d_\mathrm{L}\dagger}\,. \tag{12.27}$$

These conventions will come up again in the following section, where we renormalize the quark and squark fields and mixing matrices to obtain QCD-corrected results at NLO.

12.4.2. Field and Mass Renormalization

Similar to the CxSM renormalization in Chapter 4, we write the bare squark, quark and gluino fields and their masses as

$$\tilde{q}_0 = \left(1 + \frac{1}{2}\delta Z^{\tilde{q}}\right)\tilde{q}\,, \qquad m^2_{\tilde{q},0} = m^2_{\tilde{q}} + \delta m^2_{\tilde{q}}\,, \tag{12.28a}$$

$$q_\mathrm{L/R,0} = \left(1 + \frac{1}{2}\delta Z^{q_\mathrm{L/R}}\right) q_\mathrm{L/R}\,, \qquad m_{q,0} = m_q + \delta m_q\,, \tag{12.28b}$$

$$\tilde{g}_\mathrm{L/R,0} = (1 + \frac{1}{2}\delta Z^{\tilde{g}_\mathrm{L/R}})\tilde{g}_\mathrm{L/R}\,, \qquad m_{\tilde{g},0} = m_{\tilde{g}} + \delta m_{\tilde{g}}\,, \tag{12.28c}$$

where the label 0 indicates the bare fields and the δZ are the field renormalization constants. Since the gluinos are Majorana, fermions we have $\delta Z^{\tilde{g}_\mathrm{L}} = \delta Z^{\tilde{g}_\mathrm{R}}$.

In principle, the complex phase of the gluino mass term, φ_{M_3} needs to be renormalized as well. We can, however, choose $\delta\varphi_{M_3} = 0$ [275].

We will again use the OS scheme as we did in Sec. 4.1.1. The fermion self-energy can be split into several parts,

$$\Sigma^q_{ij}(p^2) = \not{p}\Sigma^{q,\mathrm{L}}_{ij}(p^2)P_\mathrm{L} + \not{p}\Sigma^{q,\mathrm{R}}_{ij}(p^2)P_\mathrm{R} + \Sigma^{q,\mathrm{Ls}}_{ij}(p^2)P_\mathrm{L} + \Sigma^{q,\mathrm{Rs}}_{ij}(p^2)P_\mathrm{R}\,, \tag{12.29}$$

where we used a slightly different setup than in Eq. (4.26), to comply with the notation in [291]. The contribution to the self-energies at one-loop order can be seen in Fig. 12.1. We skip the derivation of the renormalization conditions (cf. Sec. 4.1.1 and [200, 291]) and only list the results. For the field renormalization constants and the mass counterterm of the squarks we obtain $(s, t = 1, .., 6)$

$$\delta m^2_{\tilde{q}_s} = \widetilde{\mathrm{Re}}\Sigma^{\tilde{q}}_{ss}(m^2_{\tilde{q}_s})\,, \tag{12.30a}$$

$$\delta Z^{\tilde{q}}_{st} = \begin{cases} -\widetilde{\mathrm{Re}}\dfrac{\partial \Sigma^{\tilde{q}}_{ss}(p^2)}{\partial p^2}\Big|_{p^2=m^2_{\tilde{q}_s}} & s = t \\ \dfrac{2}{m^2_{\tilde{q}_s} - m^2_{\tilde{q}_t}}\widetilde{\mathrm{Re}}\Sigma^{\tilde{q}}_{st}(p^2 = m^2_{\tilde{q}_t}) & s \neq t \end{cases}. \tag{12.30b}$$

The field and mass counterterms for the fermions, i.e. the quarks and gluinos are given by $(i, j = 1, 2, 3)$

$$\delta m_{q_i} = \frac{1}{2}\widetilde{\mathrm{Re}}\left(m_{q_i}(\Sigma^{q,\mathrm{L}}_{ii}(m^2_{q_i}) + \Sigma^{q,\mathrm{R}}_{ii}(m^2_{q_i})) + \Sigma^{q,\mathrm{Ls}}_{ii}(m^2_{q_i}) + \Sigma^{q,\mathrm{Rs}}_{ii}(m^2_{q_i})\right), \tag{12.31a}$$

$$\begin{aligned}\delta Z^{q_\mathrm{L}}_{ij} = {} & \frac{2}{m^2_{q_i} - m^2_{q_j}}\Big(m_{q_i}\widetilde{\mathrm{Re}}\Sigma^{q,\mathrm{Ls}}_{ij}(m^2_{q_j}) + m_{q_j}\widetilde{\mathrm{Re}}\Sigma^{q,\mathrm{Rs}}_{ij}(m^2_{q_j}) \\ & + m^2_{q_j}\widetilde{\mathrm{Re}}\Sigma^{q,\mathrm{L}}_{ij}(m^2_{q_j}) + m_{q_i}m_{q_j}\widetilde{\mathrm{Re}}\Sigma^{q,\mathrm{R}}_{ij}(m^2_{q_j})\Big)\ (i \neq j)\,,\end{aligned} \tag{12.31b}$$

$$\begin{aligned}\delta Z^{q_\mathrm{R}}_{ij} = {} & \frac{2}{m^2_{q_i} - m^2_{q_j}}\Big(m_{q_j}\widetilde{\mathrm{Re}}\Sigma^{q,\mathrm{Ls}}_{ij}(m^2_{q_j}) + m_{q_i}\widetilde{\mathrm{Re}}\Sigma^{q,\mathrm{Rs}}_{ij}(m^2_{q_j}) \\ & + m_{q_i}m_{q_j}\widetilde{\mathrm{Re}}\Sigma^{q,\mathrm{L}}_{ij}(m^2_{q_j}) + m^2_{q_j}\widetilde{\mathrm{Re}}\Sigma^{q,\mathrm{R}}_{ij}(m^2_{q_j})\Big)\ (i \neq j)\,,\end{aligned} \tag{12.31c}$$

$$\begin{aligned}\delta Z^{q_{\mathrm{L/R}}}_{ii} = {} & -\widetilde{\mathrm{Re}}\Sigma^{q,\mathrm{L/R}}_{ii}(m^2_{q_i}) \\ & - m_{q_i}\frac{\partial}{\partial p^2}\widetilde{\mathrm{Re}}\left(m_{q_i}(\Sigma^{q,\mathrm{L}}_{ii}(p^2) + \Sigma^{q,\mathrm{R}}_{ii}(p^2)) + \Sigma^{q,\mathrm{Ls}}_{ii}(p^2) + \Sigma^{q,\mathrm{Rs}}_{ii}(p^2)\right)\Big|_{p^2=m^2_{q_i}}\,,\end{aligned} \tag{12.31d}$$

$$\begin{aligned}\delta Z^{\tilde{g}_{\mathrm{L/R}}} = {} & -\widetilde{\mathrm{Re}}\Sigma^{\tilde{g},\mathrm{L/R}}(m^2_{\tilde{g}}) \\ & - m_{\tilde{g}}\frac{\partial}{\partial p^2}\widetilde{\mathrm{Re}}\left(m_{\tilde{g}}(\Sigma^{\tilde{g},\mathrm{L}}(p^2) + \Sigma^{\tilde{g},\mathrm{R}}(p^2)) + \Sigma^{\tilde{g},\mathrm{Ls}}(p^2) + \Sigma^{\tilde{g},\mathrm{Rs}}(p^2)\right)\Big|_{p^2=m^2_{\tilde{g}}}\,.\end{aligned} \tag{12.31e}$$

Since we consider squark and quark mixing, we also renormalize the mixing matrices. We introduce counterterms via

$$U^{q_{\mathrm{L/R}}}_0 = (\mathbb{1} + \delta u^{q_{\mathrm{L/R}}})U^{q_{\mathrm{L/R}}}\,, \tag{12.32a}$$

$$W^{\tilde{q}}_0 = (\mathbb{1} + \delta w^{\tilde{q}})W^{\tilde{q}}\,, \tag{12.32b}$$

with the quark and squark mixing matrix counterterms $\delta u^{q_{\mathrm{L/R}}}, \delta w^{\tilde{q}}$, respectively. We again use an OS scheme, and obtain for the counterterms the relations (cf. [200, 291]),

$$\delta u^{q_{\mathrm{L/R}}} = \frac{1}{4}\left(\delta Z^{q_{\mathrm{L/R}}} - \delta Z^{q_{\mathrm{L/R}}\dagger}\right), \tag{12.33a}$$

$$\delta w^{\tilde{q}} = \frac{1}{4}\left(\delta Z^{\tilde{q}} - \delta Z^{\tilde{q}\dagger}\right). \tag{12.33b}$$

In Eqs. (12.30) and (12.31) we see that for degenerate squark masses or vanishing quark masses the off-diagonal δZ counterterms are ill-defined and diverge. In order to obtain finite expressions, we have to apply the limits of vanishing quark or degenerate squark masses carefully when we combine the field and the mixing matrix counterterms (which also depend

on the δZ counterterms) that appear in the counterterm amplitudes. We used the limits (cf. [291]),

$$\begin{aligned}\frac{\delta Z_{ij}^{q_{\mathrm{L/R}}\dagger}}{2} + \delta u_{ij}^{q_{\mathrm{L/R}}} \xrightarrow{m_{q_i}\to m_{q_j}} & -\frac{1}{2}\left[\widetilde{\mathrm{Re}}\Sigma_{ij}^{q,\mathrm{L/R}}(m_{q_i}^2)\right] \\ & - \frac{m_{q_i}}{2}\frac{\partial}{\partial p^2}\widetilde{\mathrm{Re}}\Big[m_{q_i}(\Sigma_{ij}^{q,\mathrm{L}}(p^2)+\Sigma_{ij}^{q,\mathrm{R}}(p^2)) + \Sigma_{ij}^{q,\mathrm{Ls}}(p^2) \\ & +\Sigma_{ij}^{q,\mathrm{Rs}}(p^2)\Big]\Big|_{p^2=m_{q_i}^2}\,,\end{aligned} \tag{12.34}$$

$$\begin{aligned}\frac{\delta Z_{ij}^{q_{\mathrm{L/R}}\dagger}}{2} m_{q_j} + \delta u_{ij}^{q_{\mathrm{R/L}}} m_i \xrightarrow{m_{q_i}\to m_{q_j}} & \frac{1}{2}\widetilde{\mathrm{Re}}\left[m_{q_i}\Sigma_{ij}^{q,\mathrm{L/R}}(m_{q_i}^2) + 2\Sigma_{ij}^{q,\mathrm{Rs/Ls}}(m_{q_i}^2)\right] \\ & - \frac{m_{q_i}^2}{2}\frac{\partial}{\partial p^2}\widetilde{\mathrm{Re}}\Big[m_{q_i}(\Sigma_{ij}^{q,\mathrm{L}}(p^2)+\Sigma_{ij}^{q,\mathrm{R}}(p^2)) + \Sigma_{ij}^{q,\mathrm{Ls}}(p^2) \\ & +\Sigma_{ij}^{q,\mathrm{Rs}}(p^2)\Big]\Big|_{p^2=m_{q_i}^2}\,,\end{aligned} \tag{12.35}$$

$$\frac{1}{2}\delta Z_{st}^{\tilde{q}*} + \delta w_{ts}^{\tilde{q}} \xrightarrow{m_{\tilde{q}_s}\to m_{\tilde{q}_t}} -\frac{1}{2}\,\widetilde{\mathrm{Re}}\frac{\partial}{\partial p^2}\Sigma_{st}^{\tilde{q}}(p^2)\Big|_{p^2=m_{\tilde{q}_s}^2}\,, \tag{12.36}$$

$$\begin{aligned}m_{q_i}\delta u_{ij}^{q_{\mathrm{R}}} + m_{q_j}\delta u_{ij}^{q_{\mathrm{L}}\dagger} \xrightarrow{m_{q_i}\to m_{q_j}} & \frac{1}{2}\widetilde{\mathrm{Re}}\Big(m_{q_i}(\Sigma_{ij}^{q,\mathrm{L}}(m_{q_i}^2)+\Sigma_{ij}^{q,\mathrm{R}}(m_{q_i}^2)) \\ & +\Sigma_{ij}^{q,\mathrm{Ls}}(m_{q_i}^2) + \Sigma_{ij}^{q,\mathrm{Rs}}(m_{q_i}^2)\Big)\,.\end{aligned} \tag{12.37}$$

Here we used the relation (cf. [200, 291])

$$\delta Z_{ij}^{\dagger} = \delta Z_{ij}(m_{q_i}^2 \leftrightarrow m_{q_j}^2)\,. \tag{12.38}$$

Thus, in the cases of degenerate squark masses or vanishing quark masses, the overall expressions for the counterterms are still finite and well defined. Be aware that here $\delta Z_{ij}^{\dagger} = (\delta Z^{\dagger})_{ij} = \delta Z_{ji}^{*}$.

12.4.3. Renormalization of the Strong Coupling Constant

We now describe the renormalization of the strong coupling constant g_s. We will only set up the notation and mention the result. For more details, we refer to [293–296]. We split the bare coupling into the renormalized coupling and counterterm as

$$g_s^0 = g_s + \delta g_s\,. \tag{12.39}$$

We use the $\overline{\mathrm{MS}}$ scheme, for which the counterterm is given as

$$\delta g_s^{\overline{\mathrm{MS}}} = -\frac{\alpha_s}{8\pi}\beta_0 g_s \Delta_{\mathrm{UV}}\,, \tag{12.40}$$

with Δ_{UV} defined as

$$\Delta_{\mathrm{UV}} = \frac{1}{\epsilon} - \gamma + \log 4\pi\,, \tag{12.41}$$

and where β_0 can be decomposed into a sum of contributions from light and heavy particles (cf. [295]),

$$\beta_0 = \left[\frac{11}{3}N - \frac{2}{3}n_f\right] + \left[-\frac{2}{3}N - \frac{2}{3} - \frac{1}{3}(n_f+1)\right] \equiv \beta_0^L + \beta_0^H\,, \tag{12.42}$$

with the number of colours N and the number of active flavours n_f. We use the 5-flavour scheme for the running of the coupling in order to be able to use experimental data as input. Thus, we decouple the top quark and all heavy SUSY particles that would otherwise contribute to the running of the strong coupling constant. We thus have the counterterm

$$\delta g_s^{\overline{\text{MS}},5} = \delta g_s^{\overline{\text{MS}}} - \frac{\alpha_s}{8\pi}\left[2\log\frac{m_{\tilde{g}}^2}{\mu_R^2} + \frac{1}{6}\sum_{i=1}^{12}\log\frac{m_{\tilde{q}_i}^2}{\mu_R^2} + \frac{2}{3}\log\frac{m_t^2}{\mu_R^2}\right] g_s\,, \tag{12.43}$$

with the renormalization scale μ_R. The subtraction of the logarithmic terms ensures that only the light quarks contribute to the running of α_s, i.e.

$$\mu_R^2\frac{\mathrm{d}}{\mathrm{d}\mu_R^2}\alpha_s = -\alpha_s\beta_0^L\,. \tag{12.44}$$

12.4.4. SUSY Restoring Counterterms in Dimensional Regularization

In the $\overline{\text{DR}}$ prescription, dimensional reduction is used as a regularization method, where the loop momentum is defined in $D = 4 - 2\epsilon$ dimensions (with a small parameter ϵ), whereas everything else (i.e. the gamma matrices and the other Lorentz structures) remains in 4 dimensions. In the $\overline{\text{MS}}$ scheme, however, dimensional regularization is used, where everything is regularized in D dimension, thereby introducing a mismatch in the degrees of freedom of gauge bosons and their superpartners and thus breaking supersymmetry. Dimensional reduction preserves supersymmetry (at least at one-loop level [297]). In order to restore supersymmetry when calculating loop integrals using dimensional regularization and to obtain the same result as in the $\overline{\text{DR}}$ scheme, additional counterterm shifts have to be included. We follow here [297–299]. We denote the terms in dimensional regularization with DReg and the terms in dimensional reduction with DRed. The transition counterterm contributions will be labelled as δZ^{trans}.

Starting with the gaugino couplings $\hat{g}$ we introduce the shifts

$$\hat{g}_s^{\text{DReg}} = \hat{g}_s^{\text{DRed}}\left(1 + \delta Z_{\hat{g}_s}^{\text{trans}}\right)\,, \qquad \delta Z_{\hat{g}_s}^{\text{trans}} = \frac{g_s^2}{32\pi^2}\frac{5}{3}\,, \tag{12.45a}$$

$$\hat{g}_2^{\text{DReg}} = \hat{g}_2^{\text{DRed}}\left(1 + \delta Z_{\hat{g}_2}^{\text{trans}}\right)\,, \qquad \delta Z_{\hat{g}_2}^{\text{trans}} = -\frac{g_s^2}{32\pi^2}\frac{4}{3}\,, \tag{12.45b}$$

for the couplings g_s and g_2. Here, it is important to note that the gauge couplings g_s, g_2 and the corresponding gaugino couplings indicated with the hat have to be distinguished when using dimensional regularization.

Similarly, we have to shift the Yukawa couplings $\hat{Y}_q$ appearing in the neutralino/chargino couplings to squark-quark pairs. Here, the shift reads

$$\hat{Y}_q^{\text{DReg}} = \hat{Y}_q^{\text{DRed}}\left(1 + \delta Z_{\hat{Y}_q}^{\text{trans}}\right)\,, \qquad \delta Z_{\hat{Y}_q}^{\text{trans}} = -\frac{g_s^2}{32\pi^2}\frac{4}{3}\,. \tag{12.46}$$

Here, also the Yukawa couplings between quarks and a Higgs or the corresponding Yukawa couplings between a quark, squark and Higgsino, indicated with the hat, have to be distinguished in dimensional regularization.

Next, we shift the quark masses and field renormalization constants via

$$m_q^{\text{DReg}} = m_q^{\text{DRed}}\left(1 + \delta Z_{m_q}^{\text{trans}}\right)\,, \qquad \delta Z_{m_q}^{\text{trans}} = \frac{g_s^2}{16\pi^2}\frac{4}{3}\,, \tag{12.47a}$$

$$Z_q^{\text{L/R,DReg}} = Z_q^{\text{L/R,DRed}}\left(1 + \delta Z_q^{\text{trans}}\right)\,, \qquad \delta Z_q^{\text{trans}} = \frac{g_s^2}{16\pi^2}\frac{4}{3}\,. \tag{12.47b}$$

Finally, we also shift the mass and field renormalization constants for the gluino fields,

$$m_{\tilde{g}}^{\text{DReg}} = m_{\tilde{g}}^{\text{DRed}} \left(1 + \delta Z_{m_{\tilde{g}}}^{\text{trans}}\right) , \qquad \delta Z_{m_{\tilde{g}}}^{\text{trans}} = \frac{g_s^2}{16\pi^2} 3 , \tag{12.48a}$$

$$Z_{\tilde{g}}^{\text{L/R,DReg}} = Z_{\tilde{g}}^{\text{L/R,DRed}} \left(1 + \delta Z_{\tilde{g}}^{\text{trans}}\right) , \qquad \delta Z_{\tilde{g}}^{\text{trans}} = \frac{g_s^2}{16\pi^2} 3 . \tag{12.48b}$$

All these counterterms are added to the counterterms described in Sec. 12.4.2 or to the vertex counterterms in the calculation. Here, one has to be careful to not include the shifts twice. When we include the shifts for the mass and field renormalization constants of the gluino and quark fields, we do not need to shift the Yukawa coupling and the gaugino coupling $\hat{g}_2$. For the gluino-squark-quark vertex we then only have to account for the difference in the vertex correction between dimensional reduction and dimensional regularization.

Finally, the strong coupling constant g_s is shifted via

$$g_s^{\text{DReg}} = g_s^{\text{DRed}} \left(1 + \delta Z_{g_s}^{\text{trans}}\right) , \qquad \delta Z_{g_s}^{\text{trans}} = -\frac{3 g_s^2}{96\pi^2} . \tag{12.49}$$

12.4.5. Conversion of $\overline{\text{DR}}$ to OS Parameters

Another aspect we have to consider is that we apply an OS renormalization prescription, but our input parameters are given in the $\overline{\text{DR}}$ scheme. Therefore, we have to convert them properly (cf. [80, 300, 301]).

We start with deriving the necessary counterterms. We move the mixing matrices $W^{\tilde{q}}$ to the left side of Eq. (12.25) and expand the parameters by introducing counterterms. We obtain,

$$\begin{aligned} W^{\tilde{q}\dagger}(\mathbb{1} + \delta w^{\tilde{q}\dagger}) \begin{pmatrix} m_{\tilde{q}_1}^2 + \delta m_{\tilde{q}_1}^2 & 0 \\ 0 & m_{\tilde{q}_2}^2 + \delta m_{\tilde{q}_2}^2 \end{pmatrix} (\mathbb{1} + \delta w^{\tilde{q}}) W^{\tilde{q}} = \\ W^{\tilde{q}\dagger} \begin{pmatrix} m_{\tilde{q}_1}^2 + \delta m_{\tilde{q}_1}^2 & \delta Y_{\tilde{q}} \\ \delta Y_{\tilde{q}}^* & m_{\tilde{q}_2}^2 + \delta m_{\tilde{q}_2}^2 \end{pmatrix} W^{\tilde{q}} , \end{aligned} \tag{12.50}$$

with $\delta Y_{\tilde{q}}$ defined as

$$\delta Y_{\tilde{q}} \equiv \delta w_{12}^{\tilde{q}} (m_{\tilde{q}_1}^2 - m_{\tilde{q}_2}^2) . \tag{12.51}$$

Next, we introduce counterterms in the squark mass matrices of Eq. (12.23) and relate them to the counterterms in Eq. (12.50). Here, we only use the counterterms needed for the one-loop QCD corrections. We have

$$W^{\tilde{u}\dagger} \begin{pmatrix} \delta m_{\tilde{u}_1}^2 & \delta Y_{\tilde{u}} \\ \delta Y_{\tilde{u}}^* & \delta m_{\tilde{u}_2}^2 \end{pmatrix} W^{\tilde{u}} = \tag{12.52a}$$

$$\begin{pmatrix} \delta m_{\tilde{U}}^2 + \delta m_u^2 & \delta m_u \left(A_u^* e^{-i\varphi_u} - \mu_{\text{eff}} \cot\beta\right) + \delta A_u^* m_u e^{-i\varphi_u} \\ \delta m_u \left(A_u e^{i\varphi_u} - \mu_{\text{eff}}^* \cot\beta\right) + \delta A_u m_u e^{i\varphi_u} & \delta m_{\tilde{u}_R}^2 + \delta m_u^2 \end{pmatrix} ,$$

$$W^{\tilde{d}\dagger} \begin{pmatrix} \delta m_{\tilde{d}_1}^2 & \delta Y_{\tilde{d}} \\ \delta Y_{\tilde{d}}^* & \delta m_{\tilde{d}_2}^2 \end{pmatrix} W^{\tilde{d}} = \tag{12.52b}$$

$$\begin{pmatrix} \delta m_{\tilde{D}}^2 + \delta m_d^2 & \delta m_d \left(A_d^* - \mu_{\text{eff}} e^{i\varphi_u} \tan\beta\right) + \delta A_d^* m_d \\ \delta m_d \left(A_d - \mu_{\text{eff}}^* e^{-i\varphi_u} \tan\beta\right) + \delta A_d m_d & \delta m_{\tilde{d}_R}^2 + \delta m_d^2 \end{pmatrix} ,$$

where we considered up-type squarks $\tilde{u}$ and down-type squarks $\tilde{d}$ separately and introduced two counterterms $\delta m_{\tilde{U}}^2$, $\delta m_{\tilde{D}}^2$ for $m_{\tilde{Q}}^2$. In the $\overline{\text{DR}}$ scheme, we only have the input parameter

$m^2_{\tilde{Q}}$ that plays a role in both the up- and down-squark matrices. If we now move to the OS scheme, we can obtain a relation to transform the parameter to an OS parameter from both matrices, and the relations do not coincide. Thus, we have to introduce two parameters $m^{2,\mathrm{OS}}_{\tilde{U}}$ and $m^{2,\mathrm{OS}}_{\tilde{D}}$.

We obtain counterterms for $A_{\tilde{q}}$, $m^2_{\tilde{U}}$, $m^2_{\tilde{D}}$ and $m^2_{\tilde{q}_\mathrm{R}}$ given by

$$\begin{aligned}
\delta A_u = \frac{e^{-i\varphi_u}}{m_u} &\left(W^{\tilde{u}}_{11} W^{\tilde{u}*}_{12} \delta m^2_{\tilde{u}_1} + W^{\tilde{u}*}_{22} W^{\tilde{u}}_{21} \delta m^2_{\tilde{u}_2} + W^{\tilde{u}*}_{12} W^{\tilde{u}}_{21} \delta Y_u + W^{\tilde{u}*}_{22} W^{\tilde{u}}_{11} \delta Y^*_u \right. \\
&\left. - \delta m_u \left(A_u e^{i\varphi_u} - \mu^*_{\mathrm{eff}} \cot\beta\right)\right) , \qquad (12.53a)\\
\delta A_d = \frac{1}{m_d} &\left(W^{\tilde{d}}_{11} W^{\tilde{d}*}_{12} \delta m^2_{\tilde{d}_1} + W^{\tilde{d}*}_{22} W^{\tilde{d}}_{21} \delta m^2_{\tilde{d}_2} + W^{\tilde{d}*}_{12} W^{\tilde{d}}_{21} \delta Y_d + W^{\tilde{d}*}_{22} W^{\tilde{d}}_{11} \delta Y^*_d \right. \\
&\left. - \delta m_d \left(A_d - \mu^*_{\mathrm{eff}} e^{-i\varphi_u} \tan\beta\right)\right) , \qquad (12.53b)\\
\delta m^2_{\tilde{Q}} = |W^{\tilde{q}}_{11}|^2 \delta m^2_{\tilde{q}_1} &+ |W^{\tilde{q}}_{21}|^2 \delta m^2_{\tilde{q}_2} + W^{\tilde{q}*}_{11} W^{\tilde{q}}_{21} \delta Y_{\tilde{q}} + W^{\tilde{q}*}_{21} W^{\tilde{q}}_{11} \delta Y^*_{\tilde{q}} - 2 m_q \delta m_q , \qquad (12.53c)\\
\delta m^2_{\tilde{q}_\mathrm{R}} = |W^{\tilde{q}}_{12}|^2 \delta m^2_{\tilde{q}_1} &+ |W^{\tilde{q}}_{22}|^2 \delta m^2_{\tilde{q}_2} + W^{\tilde{q}*}_{12} W^{\tilde{q}}_{22} \delta Y_{\tilde{q}} + W^{\tilde{q}*}_{22} W^{\tilde{q}}_{12} \delta Y^*_{\tilde{q}} - 2 m_q \delta m_q , \qquad (12.53d)
\end{aligned}$$

where $Q = U, D$ is chosen accordingly to $q = u, d$.

We now relate the $\overline{\mathrm{DR}}$ and OS parameters using that the bare parameters (indicated with 0) have to be independent of the renormalization scheme. Therefore, for a given parameter B we have

$$\begin{aligned}
B^{\overline{\mathrm{DR}}} + \delta B^{\overline{\mathrm{DR}}} = B_0 = B^{\mathrm{OS}} + \delta B^{\mathrm{OS}} \qquad (12.54)\\
\Rightarrow B^{\mathrm{OS}} = B^{\overline{\mathrm{DR}}} - \delta B^{\mathrm{fin}} ,
\end{aligned}$$

where δB^{fin} are the finite terms of the OS counterterm. We thus translate the $\overline{\mathrm{DR}}$ parameters to OS parameters via

$$\begin{aligned}
A^{\mathrm{OS}}_q &= A^{\overline{\mathrm{DR}}}_q - \delta A^{\mathrm{fin}}_q , && (12.55a)\\
m^{2,\mathrm{OS}}_{\tilde{U}} &= m^{2,\overline{\mathrm{DR}}}_{\tilde{Q}} - \delta m^{2,\mathrm{fin}}_{\tilde{U}} , && (12.55b)\\
m^{2,\mathrm{OS}}_{\tilde{D}} &= m^{2,\overline{\mathrm{DR}}}_{\tilde{Q}} - \delta m^{2,\mathrm{fin}}_{\tilde{D}} , && (12.55c)\\
m^{2,\mathrm{OS}}_{\tilde{q}_\mathrm{R}} &= m^{2,\overline{\mathrm{DR}}}_{\tilde{q}_\mathrm{R}} - \delta m^{2,\mathrm{fin}}_{\tilde{q}_\mathrm{R}} . && (12.55d)
\end{aligned}$$

As already mentioned, in the $\overline{\mathrm{DR}}$ scheme the input parameter $m^2_{\tilde{Q}}$ is the same for up and down type squarks, but in the OS scheme we have two quantities $m^{2,\mathrm{OS}}_{\tilde{U}}, m^{2,\mathrm{OS}}_{\tilde{D}}$ that have to be used in the corresponding squark mass matrices.

Similarly, we also shift the gluino mass, which is given by the M_3 parameter at leading order. We obtain

$$m^{\mathrm{OS}}_{\tilde{g}} = |M^{\overline{\mathrm{DR}}}_3| - \delta m^{\mathrm{fin}}_{\tilde{g}} , \qquad (12.56)$$

where we have to include an additional shift to the mass counterterm, as described in Sec. 12.4.4, since we use dimensional regularization in our calculation.[4]

In principle, the self-energies defining the counterterms depend on the OS parameters we want to calculate. Therefore, we use an iterative approach. We use the $\overline{\mathrm{DR}}$ parameters as an initial input, calculate the sfermion and gluino masses and mixing angles and calculate the

[4]The squark masses and their respective counterterms do not obtain an additional shift as the squark self-energies are equal for dimensional reduction and dimensional regularization [298].

counterterms to shift the parameters to approximate OS values. Next, we use the obtained approximate values to again repeat this procedure until the obtained OS values converge. If no convergence is reached after a finite number of steps, we abort the iteration and only use the above transformation to OS parameters once.

Moreover, the bottom and charm quark masses are given in the $\overline{\text{MS}}$ scheme, and we use the routines from `HDECAY` [216, 217] to convert them to OS masses.

CHAPTER 13

Calculation of Two- and Three-Body Decays of Supersymmetric Particles

In this chapter we describe the calculations, which we performed to obtain analytic results for all two-body (Sec. 13.1.1), three-body (Sec. 13.1.2), radiative loop decays (Sec. 13.2) and QCD corrections to two-body decays (Sec. 13.3) of the NMSSM SUSY particles. We specify all the decay channels that we considered, give some technical details on the computation and also mention the absorptive QCD corrections in Sec. 13.3.2. We only present here the calculation, the description of the implementation will be given in Sec. 14.1.

13.1. Leading-Order Decay Widths in the NMSSM

In this section, we describe the LO decay widths. We first discuss the two-body and then the three-body decay channels of the SUSY particle decays. We will suppress generation indices for fermions and sfermions.

13.1.1. Two-Body Decays

We start with the discussion of the two-body decay widths of the SUSY particles in the NMSSM. First, we list all decay channels of all supersymmetric particles into their final states:

- Slepton ($\tilde{l}$) decays: $\tilde{l} \to \tilde{\chi}_i^0 l$, $\tilde{\chi}_k^- \nu$, $H^- \tilde{\nu}$, $W^- \tilde{\nu}$, $\Phi \tilde{l}$, $Z \tilde{l}$
- Sneutrino ($\tilde{\nu}$) decays: $\tilde{\nu} \to \tilde{\chi}_i^0 \nu$, $\tilde{\chi}_k^+ l$, $H^+ \tilde{l}$, $W^+ \tilde{l}$
- Neutralino ($\tilde{\chi}^0$) decays: $\tilde{\chi}_i^0 \to W^\pm \tilde{\chi}_k^\mp$, $H^\pm \tilde{\chi}_k^\mp$, $Z \tilde{\chi}_j^0$, $\Phi \tilde{\chi}_j^0$, $\tilde{f} \bar{f}$, $\tilde{f}^* f$
- Chargino ($\tilde{\chi}^+$) decays: $\tilde{\chi}_k^+ \to W^+ \tilde{\chi}_i^0$, $H^+ \tilde{\chi}_i^0$, $Z \tilde{\chi}_1^+$, $\Phi \tilde{\chi}_1^+$, $\tilde{f} f'$
- Gluino ($\tilde{g}$) decays: $\tilde{g} \to \tilde{q}^* q$, $\tilde{q} \bar{q}$
- Squark ($\tilde{q}$) decays: $\tilde{q} \to \tilde{\chi}_i^0 \tilde{q}'$, $\tilde{\chi}_k^\pm \tilde{q}'$, $\tilde{g} \tilde{q}'$, $H^\pm \tilde{q}'$, $W^\pm \tilde{q}'$, $\Phi \tilde{q}'$, $Z \tilde{q}'$

Here, Φ are the five neutral Higgs scalars, f, f' are generic fermions, and q, q' generic quarks, where the tilde indicates the corresponding superpartners (where we have six sleptons, six up-type and six down-type squarks, respectively), $\tilde{\chi}_i^0$ are the neutralinos ($i = 1, .., 5$, $j = 1, .., 4$), $\tilde{\chi}_k^\pm$ are the charginos ($k = 1, 2$), and we suppressed generation indices for the fermions and sfermions. These are the possible decay channels we considered, but many of them can be kinematically closed.

We already gave a general introduction to two-body decays in Sec. 5.1 and thus use the expression for the LO width given in Eq. (5.1a). We summarize the results needed for the above mentioned decay channels. For this purpose we use a generic notation, where we label both neutralinos and charginos with $\tilde{\chi}$ ($\tilde{\chi} = \tilde{\chi}^0, \tilde{\chi}^\pm$), the vector bosons as V ($V = W, Z$) and generic scalars with S that can be both neutral or charged Higgs scalars ($S = \Phi, H^\pm$). Furthermore, we suppress generation indices and indicate potentially different particles with a prime symbol. The LO widths are then given by

$$\Gamma^{\mathrm{LO}}_{\tilde{\chi}\to\tilde{\chi}'S} = \frac{\lambda(m^2_{\tilde{\chi}}, m^2_{\tilde{\chi}'}, m^2_S)}{16\pi m^3_{\tilde{\chi}}} \frac{N_c}{2} \left((|C^{\mathrm{L}}_{\tilde{\chi}\tilde{\chi}'S}|^2 + |C^{\mathrm{R}}_{\tilde{\chi}\tilde{\chi}'S}|^2)(m^2_{\tilde{\chi}} + m^2_{\tilde{\chi}'} - m^2_S) \right. \tag{13.1a}$$
$$\left. + 4 m_{\tilde{\chi}} m_{\tilde{\chi}'} \mathrm{Re}\left[C^{\mathrm{L}}_{\tilde{\chi}\tilde{\chi}'S} (C^{\mathrm{R}}_{\tilde{\chi}\tilde{\chi}'S})^* \right] \right) ,$$

$$\Gamma^{\mathrm{LO}}_{\tilde{\chi}\to\tilde{\chi}'V} = \frac{\lambda(m^2_{\tilde{\chi}}, m^2_{\tilde{\chi}'}, m^2_V)}{16\pi m^3_{\tilde{\chi}}} \frac{N_c}{2} \left(-12 m_{\tilde{\chi}} m_{\tilde{\chi}'} \mathrm{Re}\left[C^{\mathrm{L}}_{\tilde{\chi}\tilde{\chi}'V} (C^{\mathrm{R}}_{\tilde{\chi}\tilde{\chi}'V})^* \right] \right. \tag{13.1b}$$
$$\left. + (|C^{\mathrm{L}}_{\tilde{\chi}\tilde{\chi}'V}|^2 + |C^{\mathrm{R}}_{\tilde{\chi}\tilde{\chi}'V}|^2) \left(\frac{(m^2_{\tilde{\chi}} - m^2_{\tilde{\chi}'})^2}{m^2_V} + m^2_{\tilde{\chi}} + m^2_{\tilde{\chi}'} - 2m^2_V \right) \right) ,$$

$$\Gamma^{\mathrm{LO}}_{\tilde{\chi}\to f'\tilde{f}} = \frac{\lambda(m^2_{\tilde{\chi}}, m^2_{f'}, m^2_{\tilde{f}})}{16\pi m^3_{\tilde{\chi}}} \frac{N_c}{2} \left((|C^{\mathrm{L}}_{\tilde{\chi}f'\tilde{f}}|^2 + |C^{\mathrm{R}}_{\tilde{\chi}f'\tilde{f}}|^2)(m^2_{\tilde{\chi}} + m^2_{f'} - m^2_{\tilde{f}}) \right. \tag{13.1c}$$
$$\left. + 4 m_{\tilde{\chi}} m_{f'} \mathrm{Re}\left[C^{\mathrm{L}}_{\tilde{\chi}f'\tilde{f}} (C^{\mathrm{R}}_{\tilde{\chi}f'\tilde{f}})^* \right] \right) ,$$

$$\Gamma^{\mathrm{LO}}_{\tilde{f}\to f'\tilde{\chi}} = \frac{\lambda(m^2_{\tilde{f}}, m^2_{f'}, m^2_{\tilde{\chi}})}{16\pi m^3_{\tilde{f}}} N_c \left((|C^{\mathrm{L}}_{\tilde{\chi}f'\tilde{f}}|^2 + |C^{\mathrm{R}}_{\tilde{\chi}f'\tilde{f}}|^2)(m^2_{\tilde{f}} - m^2_{f'} - m^2_{\tilde{\chi}}) \right. \tag{13.1d}$$
$$\left. - 4 m_{f'} m_{\tilde{\chi}} \mathrm{Re}\left[C^{\mathrm{L}}_{\tilde{\chi}f'\tilde{f}} (C^{\mathrm{R}}_{\tilde{\chi}f'\tilde{f}})^* \right] \right) ,$$

$$\Gamma^{\mathrm{LO}}_{\tilde{f}\to\tilde{f}'V} = \frac{\lambda(m^2_{\tilde{f}}, m^2_{\tilde{f}'}, m^2_V)}{16\pi m^3_{\tilde{f}}} N_c |C_{\tilde{f}\tilde{f}'V}|^2 \frac{\lambda(m^2_{\tilde{f}}, m^2_{\tilde{f}'}, m^2_V)^2}{m^2_V} , \tag{13.1e}$$

$$\Gamma^{\mathrm{LO}}_{\tilde{f}\to\tilde{f}'S} = \frac{\lambda(m^2_{\tilde{f}}, m^2_{\tilde{f}'}, m^2_S)}{16\pi m^3_{\tilde{f}}} N_c |C_{\tilde{f}\tilde{f}'S}|^2 . \tag{13.1f}$$

Here $C^{\mathrm{L}}_{\tilde{\chi}\tilde{\chi}'S}$, $C^{\mathrm{R}}_{\tilde{\chi}\tilde{\chi}'S}$, $C^{\mathrm{L}}_{\tilde{\chi}\tilde{\chi}'V}$ and $C^{\mathrm{R}}_{\tilde{\chi}\tilde{\chi}'V}$ are the left- and right-chiral couplings of a pair of neutralinos, charginos (or one neutralino and one chargino) to a scalar S or a vector boson V, respectively. Next, $C^{\mathrm{L}}_{\tilde{\chi}f'\tilde{f}}$ and $C^{\mathrm{R}}_{\tilde{\chi}f'\tilde{f}}$ are the left- and right-chiral couplings of a neutralino or chargino to a fermion f' and sfermion $\tilde{f}$. Then, $C_{\tilde{f}\tilde{f}'V}$ and $C_{\tilde{f}\tilde{f}'S}$ are the couplings of two sfermions, $\tilde{f}$ and $\tilde{f}'$, to a scalar S or a vector boson V, respectively. N_c denotes the colour factor and λ the Källén function from Eq. (5.2). The gluino decay into a squark-quark pair at LO is obtained from Eq. (13.1c), interchanging neutralino/chargino masses and couplings with the gluino masses and couplings and adjusting the colour factor. Similarly, the squark to quark gluino decays can be obtained from Eq. (13.1e). Thus, given the couplings (they can be found e.g. in [63] or [302]) the two-body decays are calculated for all given decay channels.

The colour factor N_c for the slepton and sneutrino decays is 1, the colour factor for neutralino and chargino decays into a squark-quark pair is 3 and otherwise 1. The colour factor for the gluino decays into a squark-quark pair is 1/2. The colour factor of a squark decaying into a quark or squark and an uncoloured particle is 1, and the colour factor of a squark decaying into a quark and a gluino is 4/3.

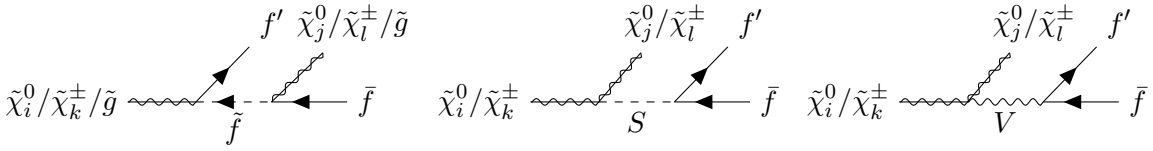

(a) three-body decay topologies to the decays $\tilde{\chi}_i^0/\tilde{\chi}_k^\pm/\tilde{g} \to \overline{f}f\tilde{\chi}_j^0/\tilde{\chi}_l^\pm/\tilde{g}$ $(i,j = 1,..,5,\ k,l = 1,2)$, where in the decays involving gluinos the fermions and sfermions have to be quarks and squarks.

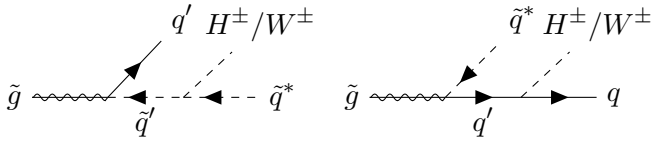

(b) three-body decay topologies to the decays $\tilde{g} \to q\tilde{q}'^* H^+/W^+$.

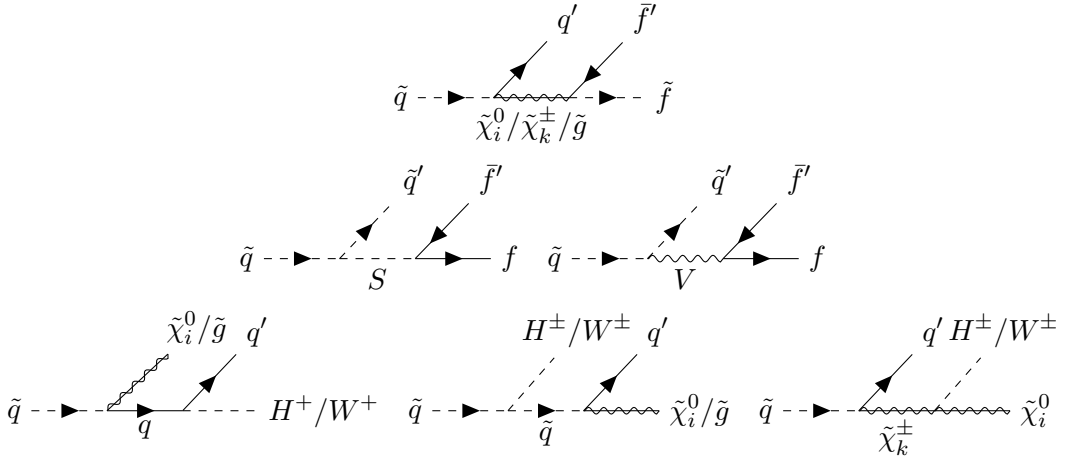

(c) three-body decay topologies to the decays $\tilde{q} \to \tilde{q}' f' \bar{f}$, $\tilde{q} \to q\bar{f}'\tilde{f}$ and $\tilde{q} \to q'\tilde{\chi}_i^0/\tilde{g}\, H^\pm/W^\pm$ $(i = 1,..,5,\ k = 1,2)$.

Figure 13.1.: The different Feynman diagram topologies depicting the three-body decays with generic fermions denoted by f, quarks q, q' and corresponding superpartners. Here, S denotes a generic neutral or charged Higgs scalar.

13.1.2. Three-Body Decays

We now move on to the description of the three-body decays in the NMSSM. They can become important if the two-body decays are kinematically closed, i.e. if the masses of the initial and final state supersymmetric particles are nearly degenerate. We then have to include the three-body decays in order to obtain valid and precise results for the total widths and the branching ratios.

For example, we can consider the second-lightest neutralino $\tilde{\chi}_2^0$ and its decay modes into the lightest neutralino $\tilde{\chi}_1^0$. If their masses are too close to each other, all the two-body decay channels described in Sec. 13.1.1 are kinematically closed. We thus have to consider three-body decays. As can be seen in Fig. 13.1a, we can mediate these three-body processes with a virtual sfermion $\tilde{f}$, e.g. we then have the decay chain $\tilde{\chi}_2^0 \to f\tilde{f}^* \to f\bar{f}\tilde{\chi}_1^0$, where the star here indicates that the sfermion is a virtual particle. If, however, any of the two-body decay channels $\tilde{\chi}_2^0 \to f\tilde{f}$ are already kinematically allowed (considering each possible sfermion-fermion pair), i.e. we can produce the fermion-sfermion pair on-shell, we do not consider the three-body decay $\tilde{\chi}_2^0 \to \tilde{\chi}_1^0 f\bar{f}$. Similarly, we can consider as another example the gluino decays. Regarding the two-body decays, the gluino only decays into a squark-quark pair. If now the squarks are all heavier than the gluino, no two-body decays are possible. Thus, we have to include three-body decays. In this case we can have a virtual squark that then decays

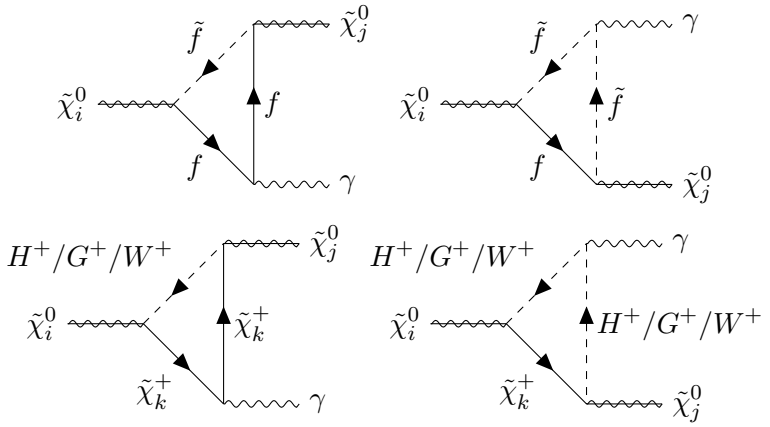

Figure 13.2.: The Feynman diagrams appearing in the radiative neutralino decay [305], $\tilde{\chi}_i^0 \to \gamma\tilde{\chi}_j^0 (i = 2,..,5,\ j = 1,..,4)$ with generic electrically charged fermions f, their superpartners $\tilde{f}$, charginos $\tilde{\chi}_k^+$ $(k = 1,2)$, the charged Higgs boson $H^\pm$, the W boson and the charged Goldstone boson $G^\pm$. The diagrams with inverted arrows also have to be considered.

into e.g. a quark and a neutralino. Thus, we have the three-body decay $\tilde{g} \to q\bar{q}\tilde{\chi}^0$ with a virtual squark. Therefore, in order to check if we need to calculate a given three-body decay, we check if none of the two-body decays that can be seen as a subprocess of the considered three-body decay is allowed. If this is the case, we include the corresponding three-body process. Otherwise, we only include the two-body decays.

The three-body decay channels we included are the following:

- Neutralino ($\tilde{\chi}^0$) decays: $\tilde{\chi}_i^0 \to f\bar{f}\tilde{\chi}_j^0$, $f\bar{f}'\tilde{\chi}_k^\pm$, $q\bar{q}\tilde{g}$
- Chargino ($\tilde{\chi}^+$) decays: $\tilde{\chi}_k^+ \to f\bar{f}\tilde{\chi}_1^+$, $f\bar{f}'\tilde{\chi}_i^0$, $q\bar{q}'\tilde{g}$
- Gluino ($\tilde{g}$) decays: $\tilde{g} \to q\bar{q}\tilde{\chi}_i^0$, $q\bar{q}'\tilde{\chi}_k^\pm$, $q'\tilde{q}H^\pm/W^\pm$
- Squark ($\tilde{q}$) decays: $\tilde{q} \to q'\tilde{\chi}_i^0 W^\pm/H^\pm$, $q'\tilde{g}W^\pm/H^\pm$, $q'\bar{f}'\tilde{f}$, $\tilde{q}'f'\bar{f}$

Here, q, q' denote again generic quarks, f, f' generic fermions, and we suppressed generation indices $(i = 1,..,5,\ j = 1,..,4,\ k = 1,2)$. We did not implement any three-body decays for sleptons and sneutrinos. In App. D, we derive the partial width for three-body decays. Thus, we can use Eq. (D.26) to obtain the results for the three-body decay widths, of the SUSY particles.

Another aspect to consider is the fact that in our theory we have Majorana fermions. In order to calculate Feynman diagrams including them, we use the approach described in [303, 304], as also briefly summarized in App. E.

Due to the large number of decay channels and because the formulas can become quite involved, we refrain from listing them here, but instead refer to our code where they can be found (see Sec. 14.1 for the description of the implementation).

13.2. Radiative Loop Decays

We furthermore include the decays of a heavier neutralino into a lighter neutralino and a photon, $\tilde{\chi}_i^0 \to \gamma\tilde{\chi}_j^0$ $(i = 2,..,5, j = 1,..,4)$. This process may become important if the neutralinos are nearly mass-degenerate and the previously mentioned two-body decays are kinematically closed, whereas this decay channel is always kinematically allowed.

Since neutralinos do not couple to photons directly, this process is not present at tree level but mediated via loops. The contributions at one-loop order can be seen in Fig. 13.2. They are

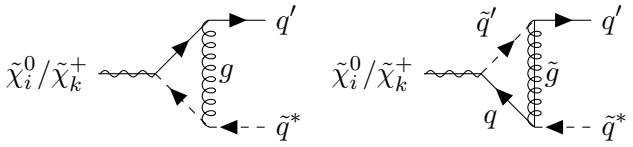

(a) NLO QCD vertex corrections to the decays $\tilde{\chi}_i^0/\tilde{\chi}_k^+ \to q'\tilde{q}^*$ ($i = 1,..,5$, $k = 1,2$).

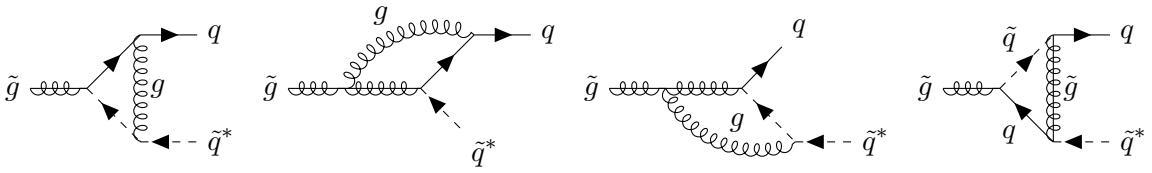

(b) NLO QCD vertex corrections to the decays $\tilde{g} \to q\tilde{q}^*$.

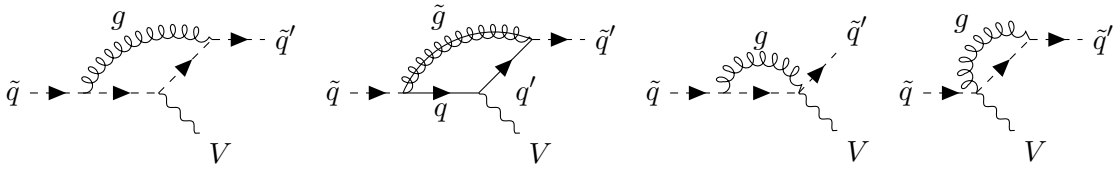

(c) NLO QCD vertex corrections to the decays $\tilde{q} \to \tilde{q}'V$.

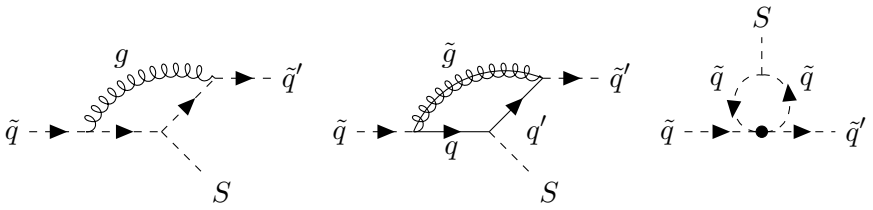

(d) NLO QCD vertex corrections to the decays $\tilde{q} \to \tilde{q}'\Phi$.

Figure 13.3.: Feynman diagrams for the contributions to the QCD vertex corrections of different decay channels. Here, we suppressed indices for the quarks and squarks, S denotes a generic neutral or charged Higgs scalar and V a massive vector boson, $V = W, Z$.

UV finite, since there is no corresponding tree-level coupling and therefore no counterterm. This decay was already calculated in [305] for the MSSM, where also an analytic formula for generic complex couplings was given. We rederived this expression and compared our results analytically. Our calculation is presented in App. G in Sec. G.2.

Additionally, we calculated the loop-induced decay $\tilde{g} \to g\tilde{\chi}_i^0$ ($i = 1,..,5$), i.e. a gluino decaying into a gluon and neutralino, which is obtained from Fig. 13.2 by replacing the initial neutralino by a gluino and using only the quark/squark diagrams with an outgoing gluon and including the corresponding colour factors.

13.3. Next-to-Leading-Order QCD Corrections to Two-Body Decays

We now discuss the QCD corrections to the two-body decays involving quarks, squarks or gluinos. Similarly to Sec. 5.3, the total amplitude $\mathcal{A}^{\text{NLO}}$ consists of virtual vertex corrections $\mathcal{A}^{\text{VC}}$ and the counterterm contributions $\mathcal{A}^{\text{CT}}$ (compare with Fig. 5.1). Since we again renormalize the fields and masses on-shell, the leg contributions and leg counterterms cancel each other (although we have to take into account possible contributions from the imaginary part of the self-energies, as discussed below in Sec. 13.3.2). We also have to include real corrections, see Sec. 13.3.1.

First, we mention all decay channels receiving QCD corrections. This includes all processes involving squarks, quarks or gluinos (i.e. the coloured particles in our theory). Thus, we con-

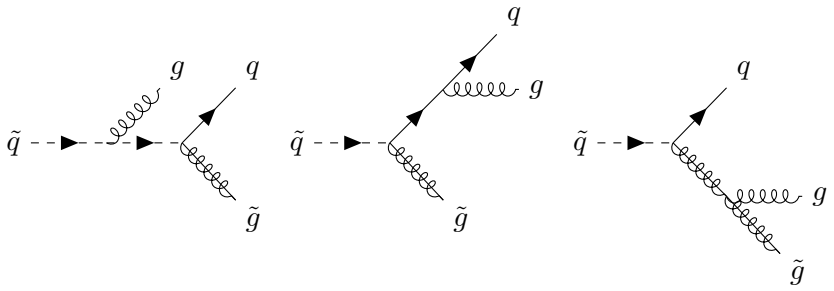

Figure 13.4.: Real corrections to NLO QCD corrections. Here, as an example the squark to quark and gluino decay.

sidered the neutralino/chargino/gluino decays into squark-quark pairs and all squark decays. The Feynman diagrams contributing to the virtual corrections $\mathcal{A}^{\mathrm{VC}}$ for all decay channels can be seen in Fig. 13.3. The counterterm couplings for the amplitude $\mathcal{A}^{\mathrm{CT}}$ are derived in App. F. Finally, all the contributions are combined and we can use Eq. (5.1b) to obtain the NLO-corrected decay widths. We checked numerically that our results are UV finite and gauge-independent, where we used the generic R_ξ gauge and checked if the result is independent of the gauge parameter. Moreover, we compared analytically our result with the literature [291–294, 300, 306–310].

In the model that we considered, the complex NMSSM, we have in general complex couplings potentially leading to CP violation, i.e. particle and antiparticle decays might differ. Therefore, we also calculated all the QCD corrections for the antiparticle decays. We used again the techniques described in [303, 304] to obtain the anti-particle amplitudes, given the results for particles. Thus, the anti-particle amplitudes are obtained from the particle amplitudes by using the complex-conjugated couplings, interchanging the left- and right-chiral couplings and inserting an additional minus sign for fermion-fermion-vector and scalar-scalar-vector vertices. We summarize our approach in App. E.

Another important remark is that we used dimensional regularization to regularize our integrals and thus have to introduce additional shifts to restore supersymmetry [298], as we described in Sec. 12.4.4.

We present the analytic results of the vertex corrections in App. G in Sec. G.1.2. They can also be found in our code (see Sec. 14.1 for the description of the implementation).

13.3.1. IR and Collinear Divergences

For the QCD corrected decay widths, we included diagrams with real gluon emission from coloured in- or outgoing particles, see e.g. Fig. 13.4. The inclusion of these corrections is required to obtain IR finite results, since at 1-loop IR divergences appear due to massless particles (in this case gluons) in the loop. In contrast to our procedure in Sec. 5.3.1, where we introduced an energy cutoff ΔE, we calculated here the full inclusive decay, i.e. we integrated over the full real-emission three-body phase space. The same approach was implemented in `SDECAY` [75, 76] and in [291–294, 300, 306–310]. We re-derived the results and compared them analytically.

To regularize the IR divergences, we introduced a small finite mass λ for the gluon. We checked that numerically our final result does not depend on this parameter. We used the integrals given in [200] that are evaluated for the full phase space. The analytic results can be found in App. G in Sec. G.1.3.

In the case of small quark masses, we also have to regularize collinear divergences. Here, we introduced a small quark mass regulator $m_{q,\mathrm{col}}$ and checked that numerically our final result

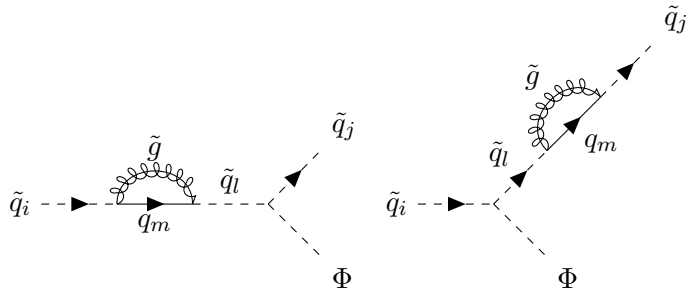

Figure 13.5.: Self-energy contributions to the squark to squark and scalar decay that may not be fully cancelled by our implemented OS scheme due to imaginary branch cuts (similar for other decay channels involving squarks).

does not depend on this parameter. In the combination of the virtual and real corrections, we have to carefully apply the limit of vanishing quark and gluon masses, i.e. we have to consistently apply the limit for all parts of the calculation. Therefore, we first expanded in λ and then in $m_{q,\text{col}}$ and kept only divergent parts in both expansions. At the end, the full result is free of infrared and collinear divergences, but each part of the calculation can separately be divergent. Thus, in order to have a consistent result, for each part the limit has to be performed in the same manner. We compared our results for the real corrections analytically with [307, 310].

13.3.2. Absorptive Corrections

In our definition of the OS scheme, we only absorb the real parts of the loop integrals appearing in the self-energy into the counterterms. These integrals can, however, obtain an imaginary part if the decay into the intermediate particles is kinematically allowed. Thus, self-energy contributions with loop integrals with a non-vanishing imaginary part, where the in- and outgoing states in the self-energy differ,[5] can contribute (compare also with Sec. 5.4 and [311, 312]). Since the gluino does not mix with other particles and the quarks are always lighter than their squark partners, only the squark self-energies with a gluino-quark loop can lead to so-called absorptive corrections. An example of these contributions can be seen in Fig. 13.5. Therefore, for each decay channel involving squarks, the corresponding diagrams have to be included (both for ingoing and outgoing squarks if present), i.e. we included these contributions where we only took into account the imaginary part of the loop integrals.

[5] If the incoming and outgoing particles are identical, this contribution results in the total decay width via the optical theorem [85] and does not lead to an imaginary part that contributes to the decay process considered.

CHAPTER 14

Numerical Evaluation

After the introduction to the NMSSM and the presentation of the setup and the calculation we performed, we can now discuss the implementation of the SUSY particle decays into our code and analyze the results.

In this chapter we first describe how we extended the program `SDECAY` [75, 76] to now calculate the supersymmetric particle decays in the NMSSM and how this code is linked to `NMSSMCALC` [77–82] (Sec. 14.1). We then describe our setup to obtain viable parameter points and the constraints that we applied in Sec. 14.2 and then turn to the numerical evaluation, where we discuss some benchmark point scenarios.

14.1. Implementation

We start with the description of the implementation. As already mentioned, we used the code `SDECAY` as a starting point and extended and adjusted the code to be able to calculate the supersymmetric particle decay widths in the complex NMSSM. The program package `SDECAY` calculates the supersymmetric particle decays in the NMSSM, where the two-body and, if kinematically closed, the three-body decays, as well as the radiative loop decays and NLO QCD corrections to the two-body decays including coloured initial or final states are implemented. It was therefore used as a basis for the development of our implementation of the decays in the NMSSM, as well as to compare analytic and numerical results. We linked our now extended version of `SDECAY` to the program `NMSSMCALC`. This code is a spectrum generator for the CP-conserving and CP-violating NMSSM and calculates the Higgs masses, including one-loop and several two-loop corrections, as well as the Higgs decay widths [77–82]. Furthermore, it computes the loop-corrected effective Higgs self-couplings [158, 161, 313], the muon anomalous magnetic moment, the electric dipole moments, and it can give a W mass prediction [283, 284, 314].

We now mention the computational details needed for our implementation. The couplings required for the calculation where taken from the appendix in [63] as well as [302] and adjusted for the NMSSM and to our notation. The scalar Higgs couplings were already implemented in `NMSSMCALC`. The calculation was performed with the help of `FeynCalc 9.3.1` [225–228]. The implementation of the loop integrals was taken over from `NMSSMCALC` and from `QCDloop` [315]. The integrals needed for the real corrections were taken from [200].

The calculated results were compared analytically with the results in the literature [291–294, 300, 305–310]. Moreover, we used the MSSM-limit of the NMSSM (see Sec. 12.2) and thus generated a parameter point we could use in our implementation and in the code SDECAY to then compare results numerically.

As input, the code uses a spectrum file generated from NMSSMCALC that is also used for the Higgs decay calculation. It is given in SLHA format [316, 317]. The SUSY input parameters are given in the $\overline{\text{DR}}$ scheme, and thus we need to convert them in order to use the OS scheme for the NLO QCD corrections (see also Sec. 12.4.5). Furthermore, in the input file, the Higgs masses and the Higgs rotation matrix are already given with the loop corrections calculated by NMSSMCALC. We thus use them as input when we calculate the Higgs scalar couplings. Moreover, we took over the implementation from HDECAY [216, 217] to convert the $\overline{\text{MS}}$ quark masses of the bottom and charm quark to OS masses. We also took over the running of α_S from HDECAY and we set the masses of the first generation of quarks and the strange quark mass to zero.

In the code, we then implemented all the two-body decays, the necessary three-body decays (if the two-body decays are kinematically not allowed), the radiative decays and the NLO QCD corrections to two-body decays including coloured final or initial states. We furthermore implemented numerical checks to confirm that our results are free of UV, IR and collinear divergences. Similarly, we implemented checks for gauge independence. We also included the anti-particle decays.

The usage of the code is straightforward. As it is an extension of NMSSMCALC it is used in the same manner. Thus, we refer to the manual of NMSSMCALC [318] for details of how to use the code. The results of our program, i.e. the total widths and the branching ratios of the supersymmetric particles into all considered decay channels, are appended to the output file from NMSSMCALC given again in the SLHA format. This can then be used for further analyses.

The code is available at: https://www.itp.kit.edu/~maggie/NMSSMCALC/B_SDECAY/

More information regarding the usage of the code can be found there.

14.2. Parameter Scan and Analysis

Next, we describe the setup to obtain viable parameter points. We used the code BSMArt [271] to perform parameter scans. The program BSMArt uses as default SPheno [319, 320] as a spectrum generator. We adjusted it so that we can use NMSSMCALC with our extended version of SDECAY instead. Next, several other program packages can be linked to BSMArt to apply constraints on the generated parameter points. We used the code HiggsTools [277] to check for the compatibility with current measurements of the detected 125 GeV Higgs boson and searches for additional scalars. For this purpose, NMSSMCALC already gives out effective couplings in the output file that can be used by HiggsTools. Next, we used the program package Smodels [278–282] to check for SUSY searches and collider limits. For the additional input needed for Smodels, a private implementation was used to calculate the production cross sections for all pairs of electroweakinos at LO [314]. Additionally, NMSSMCALC can calculate the EDMs that can then be used to constrain the complex phases that can be present in the model, as described in Sec. 12.3. In our sample scans, we, however, did not apply the EDM limits for illustrative purposes, to see the impact of the complex phases on the decays.

We now mention the additional input parameters that we used. The SM input parameters are given as a block in SLHA format. They were taken over from NMSSMCALC and are given by

```
Block SMINPUTS
         1     1.27955000E+02   # alpha_em^(-1)
         2     1.16637000E-05   # G_F
         3     1.18100000E-01   # alpha_s
         4     9.11876000E+01   # Mz
         5     4.18000000E+00   # m_b^MS(mb)
         6     1.72740000E+02   # m_t
         7     1.77682000E+00   # m_tau
         9     8.03790000E+01   # Mw
        11     5.10998910E-04   # m_e
        13     1.05658367E-01   # m_mu
        21     4.70000000E-03   # m_d
        22     2.20000000E-03   # m_u
        23     0.95000000E-01   # m_s
        24     1.27400000E+00   # m_c
#
```

Here, all quark masses expect for the top quark mass are given as $\overline{\text{MS}}$ values, with the u-,d-,s-quark masses taken at the scale $\mu = 2\,\text{GeV}$, and the c- and b-quark masses at their $\overline{\text{MS}}$ mass. In the code, we then set the up, down, and strange mass to zero. Additionally, the values for the CKM matrix were taken from [321]. Moreover, we used the following input for `NMSSMCALC`:

```
Block MODSEL
  3  1    # NMSSM
  5  2    # 0: CP-conserving; 2: general CP-violation
  6  4    # loop level 1: one 2: two O(alpha_t alpha_s) 3: two O(alpha_t
    alpha_s + alpha_t^2) 4: two O(alpha_t alpha_s + (alpha_t+alpha_lambda+
    alpha_kappa)^2)
  7  3    # for top/stop sector: 1: DRbar scheme no gauge running; 2: DRbar w/
     gauge running 3: OS scheme
  8  0    # 0: MHpm as Input, 1: Alambda as Input
  10 1    # 0: no EDMs calculated (default), 1: EDMs calculated, 2: detailed
    output
  11 0    # 0: no AMMs calculated (default), 1: AMMs calculated, 2: detailed
    output
  12 0    # 0: no effective HHH couplings calculated, 1: effective HHH
    couplings calculated
  13 0    # 0: no loop-corrected W-mass calculated, 1: loop-corrected W-mass
    calculated
#
Block REGFACTOR
  1  1    # regulator factor R to define regulator mass MG^2=R*10^(-3) MUR^2,
    MUR renormaliation scale, used in O((alpha_t+lambda+kappa)^2) correction
#
```

We used our setup to scan the parameter space for viable parameter points. As a first scan, we scanned the input parameters in the following ranges:

$$
\begin{aligned}
&M_1 \in [400, 1000]\text{GeV},\ M_2 \in [400, 1000]\text{GeV},\ M_3 = 2000\,\text{GeV},\\
&A_t \in [-3000, 3000]\text{GeV},\ A_b \in [-2000, 2000]\text{GeV},\ A_\tau \in [-2000, 2000]\text{GeV},\\
&\tan\beta \in [1, 10.0],\ m_{H^\pm} \in [500, 1000]\text{GeV},\ \lambda \in [0.01, 0.5],\ \xi \in [0.01, 1.5],\\
&A_\kappa \in [-2000, 2000]\text{GeV},\ \mu_{\text{eff}} \in [100, 1000]\text{GeV},\ \mathbf{m}_{\tilde{Q},3} \in [400, 3000]\text{GeV},\\
&\mathbf{m}_{\tilde{L}} = \mathbf{m}_{\tilde{l}_\text{R}} = \mathbf{m}_{\tilde{Q},1} = \mathbf{m}_{\tilde{Q},2} = \mathbf{m}_{\tilde{u}_\text{R}} = \mathbf{m}_{\tilde{d}_\text{R}} = 3000\,\text{GeV}.
\end{aligned}
$$

In this first scan, we set all imaginary phases to zero. It should also be noted that in `NMSSMCALC` we have $A_t = A_c = A_u$ and $A_b = A_s = A_d$. With $\mathbf{m}_{\tilde{Q},i}$ $(i = 1, 2, 3)$, the diagonal entries of the matrix $\mathbf{m}_{\tilde{Q}}$ are denoted. For the other mass matrices, we use the same values for all fermion generations. Moreover, we choose μ_{eff} as an input parameter here in accordance with the SLHA input format. It can then be translated into the input parameters v_s and φ_s via

Eq. (12.12). Furthermore, the auxiliary parameter ξ is related to κ via $\kappa = \lambda\xi$. With this setup, we obey the unitarity constraints described in Sec. 12.3. We performed a second scan, where we scanned in addition to the real parameters (in the same ranges as in the first scan) the imaginary parts:

$$\mathrm{Im}(M_1) \in [0, 1.5]\mathrm{GeV},\ \mathrm{Im}(M_2) \in [0, 1.5]\mathrm{GeV},\ \mathrm{Im}(M_3) \in [0, 1.5]\mathrm{GeV},$$
$$\mathrm{Im}(A_t) \in [0, 1.5]\mathrm{GeV},\ \mathrm{Im}(\varphi_u) \in [0, 1.5]$$

The other phases are set to zero.

We now discuss some benchmark point scenarios, which we obtained in our scans to showcase the code and its output. If not specified otherwise, the widths and branching ratios stated are always given including the NLO QCD corrections. We obtained these benchmark points with the above mentioned setup. We start with benchmark point `BP1`. Its input parameters are given by

```
BLOCK EXTPAR #
 1      5.54993515E+02 # M1
 2      6.26336011E+02 # M2
 3      2.00000000E+03 # M3
 11     1.94326772E+03 # At
 12     1.23624370E+03 # Ab
 13    -1.76370552E+03 # Atau
 25     4.45125902E+00 # tanbeta
 27     9.67215098E+02 # H_pm
 61     3.89167627E-01 # lambda
 62     4.91116579E-01 # kappa
 64    -8.10865823E+02 # Akappa
 65     2.14896705E+02 # mu_eff
 32     3.00000000E+03 # mL_2
 33     3.00000000E+03 # mL_3
 35     3.00000000E+03 # mlr_2
 36     3.00000000E+03 # mlr_3
 42     3.00000000E+03 # mQ_2
 43     1.54598767E+03 # mQ_3
 45     3.00000000E+03 # mur_2
 46     3.00000000E+03 # mur_3
 48     3.00000000E+03 # mdr_2
 49     3.00000000E+03 # mdr_3
```

For this benchmark point all imaginary phases are zero. The masses of the supersymmetric particles and the Higgs particles are

- Gluino: $m_{\tilde{g}} = 2175.67\,\mathrm{GeV}$
- Neutralinos: $m_{\tilde{\chi}_i^0} = (196.81\,\mathrm{GeV},\ 221.92\,\mathrm{GeV},\ 549.79\,\mathrm{GeV},\ 558.99\,\mathrm{GeV},\ 640.04\,\mathrm{GeV})$
- Charginos: $m_{\tilde{\chi}_i^\pm} = (206.17\,\mathrm{GeV},\ 639.45\,\mathrm{GeV})$
- Sneutrinos: $m_{\tilde{\nu}} = (2999.37\,\mathrm{GeV},\ 2999.37\,\mathrm{GeV},\ 2999.37\,\mathrm{GeV})$
- Sleptons: $m_{\tilde{l}} = (3000.27\,\mathrm{GeV},\ 3000.35\,\mathrm{GeV},\ 3000.25\,\mathrm{GeV},\ 3000.37\,\mathrm{GeV},\ 2999.51\,\mathrm{GeV},\ 3001.12\,\mathrm{GeV})$
- Up squarks: $m_{\tilde{u}} = (3046.51\,\mathrm{GeV}, 3046.76\,\mathrm{GeV}, 3046.33\,\mathrm{GeV}, 3046.94\,\mathrm{GeV}, 1637.52\,\mathrm{GeV}, 3051.84\,\mathrm{GeV})$
- Down squarks: $m_{\tilde{d}} = (3047.03\,\mathrm{GeV}, 3047.47\,\mathrm{GeV}, 3046.33\,\mathrm{GeV}, 3047.46\,\mathrm{GeV}, 1635.90\,\mathrm{GeV}, 3047.03\,\mathrm{GeV})$
- Neutral Higgs: $m_h = (122.46\,\mathrm{GeV},\ 267.5\,\mathrm{GeV},\ 802.65\,\mathrm{GeV},\ 966.08\,\mathrm{GeV},\ 969.64\,\mathrm{GeV})$

- Charged Higgs: $m_{H^\pm} = 967.215\,\text{GeV}$

Here, we give the squark and slepton masses in the basis $(\tilde{f}_{i,1}, \tilde{f}_{i,2})$, where i is the generation index and $\tilde{f}$ denotes the given sfermion.

In the following, we discuss some features of this benchmark point. Considering the given masses, we already see that the two lightest neutralinos and the lightest chargino have similar masses, and they are the lightest particles in the spectrum. Thus, the only decay channels for the second lightest neutralino and the lightest chargino are three-body decays into the lightest neutralino. The second-lightest neutralino thus decays into a fermion-antifermion pair and the lightest neutralino. The branching ratios for the decays into these channels are in the range of a few percent, with the largest value being 13 % for the process $\tilde{\chi}_2^0 \to d\bar{d}\tilde{\chi}_1^0$ for this benchmark point. The radiative neutralino decay $\tilde{\chi}_2^0 \to \tilde{\chi}_1^0\gamma$ plays no role here, as its branching ratio is only 0.014 %. The total width of the second-lightest neutralino is also small, as only three-body decays and the radiative decay are kinematically allowed. The total width amounts to $1.15 \times 10^{-5}\,\text{GeV}$. The other heavier neutralinos, in contrast, have total widths of the order of a few GeV.

Similarly, the lightest chargino has a total width of only $9.2 \times 10^{-8}\,\text{GeV}$ (compared to e.g. the total width of the heavier chargino given by 6.3 GeV) as also here only three-body decays are kinematically allowed. In this case the most dominant decay process is $\tilde{\chi}_2^\pm \to u\bar{d}\tilde{\chi}_1^0$ with a branching ratio of about 35 %.

The sneutrinos dominantly decay into neutrinos and neutralinos, or charged leptons and charginos. Similarly, the sleptons decay into charged leptons and neutralinos, or neutrinos and charginos. They have a total width of the order of a few tens of GeV.

Next, we discuss the sizes of the NLO QCD corrections. In the following we will investigate the relative NLO correction to the total width of a given particle, which we define by

$$\delta_P^\Gamma \equiv \frac{\Gamma_P^{\text{NLO}} - \Gamma_P^{\text{LO}}}{\Gamma_P^{\text{LO}}}\,, \tag{14.1}$$

where Γ_P^{LO} and Γ_P^{NLO} are the LO and NLO QCD total widths, respectively, for a given particle P. We start with the gluino, which decays predominantly into a squark-quark pair (the radiative decay into a gluon and neutralino is negligible, its branching ratio is below 1 %). The total width of the gluino at LO is given by 24.1 GeV, and at NLO by 24.2 GeV. We thus have a correction $\delta_{\tilde{g}}^\Gamma$ of 0.4 % when we include the NLO corrections to the total width.

The neutralinos and charginos are all lighter than the squarks for this benchmark point. Therefore, they do not have decay channels that receive QCD corrections.

We move on to the squark decays. The up squarks decay predominantly into gluino and up-quark with a branching ratio of 71 % for $\tilde{u}_1$ and 93 % for $\tilde{u}_2$. Since we neglect the up-quark mass, the squark mass matrix in Eq. (12.23a) is already diagonal, and we can identify the mass eigenstates with the left- and right-handed squarks. In this case we have $\tilde{u}_1 = \tilde{u}_\text{L}$ and $\tilde{u}_2 = \tilde{u}_\text{R}$ (the order can in principle also be switched for other benchmark scenarios since the squark mass eigenstates are mass ordered). The left-handed squarks can also decay into charginos with a large wino component, and therefore we have the second largest branching ratio for $\tilde{u}_\text{L}$ being 19 % for the decay into $\tilde{\chi}_2^+$ and a down quark. Moreover, the total width for the left-handed squark is 94.7 GeV at LO and 118.3 GeV at NLO, and have a relative NLO correction $\delta_{\tilde{u}_\text{L}}^\Gamma$ of 24.9 %. For the right-handed squark, we have a total width of 64 GeV at LO and 90 GeV at NLO, i.e. a relative correction $\delta_{\tilde{u}_\text{R}}^\Gamma$ of 40 %. A similar picture can be seen for the other squark superpartners of the lighter quarks, i.e. the $\tilde{d}$, $\tilde{s}$ and $\tilde{c}$ squarks have

similar total widths and the left-handed squark has a larger total width and larger branching ratios of decays into charginos, compared to the right-handed squark.

Next, we turn to the stop decays. The lighter stop is too light to decay into a gluino and a top quark. Thus, it only decays into a neutralino/chargino and a quark with the largest branching ratio of 31 % into $\tilde{\chi}_2^+$ and a bottom quark. The total width is given by 49 GeV at LO and 31.7 GeV at NLO, i.e. we have a relative NLO correction $\delta^{\Gamma}_{\tilde{t}_1}$ of -35 %. Similarly, the lighter sbottom is too light to decay into a gluino and a bottom quark. It also only decays into a neutralino/chargino and a quark with the largest branching ratio of 49 % into $\tilde{\chi}_1^- t$. The total width is given by 48.9 GeV at LO and 31.7 GeV at NLO, with a relative NLO correction $\delta^{\Gamma}_{\tilde{b}_1}$ of -35 %.

The heavier stop can, compared to the lighter stop, additionally decay into a gluino and a top, into a neutral Higgs or Z boson and the lighter stop, or into a charged Higgs or W boson and the lighter sbottom. The largest branching ratio is 48 % for the decay into a gluino and a top quark. The total width at LO is 214.3 GeV and 175.4 GeV at NLO, i.e. we have a relative correction $\delta^{\Gamma}_{\tilde{t}_2}$ of -18 %. We have a similar picture for the heavier sbottom decays. It can also decay into a gluino and a bottom, into a neutral Higgs or Z boson and the lighter sbottom, or into a charged Higgs or W boson and the lighter stop. The heavier sbottom, however, predominantly decays into a gluino and a bottom with a branching ratio of 96 %. The total width at LO is given by 61.3 GeV and at NLO by 86.98 GeV. We therefore have a relative correction $\delta^{\Gamma}_{\tilde{b}_2}$ of 42 %.

We then considered the benchmark point `BP2` with the following input parameters:

```
BLOCK EXTPAR #
 1      4.13344789E+02 # M1
 2      4.70522103E+02 # M2
 3      2.00000000E+03 # M3
 11    -2.88424200E+03 # At
 12     1.20428969E+03 # Ab
 13     1.58373777E+03 # Atau
 25     6.04218125E+00 # tanbeta
 27     9.53319661E+02 # H_pm
 61     3.01781136E-01 # lambda
 62     2.20395222E-01 # abskappa
 64    -1.84002587E+02 # Akappa
 65     2.23336675E+02 # mu_eff
 32     3.00000000E+03 # ml_2
 33     3.00000000E+03 # ml_3
 35     3.00000000E+03 # mer_2
 36     3.00000000E+03 # mer_3
 42     3.00000000E+03 # mq_2
 43     1.88733051E+03 # mq_3
 45     3.00000000E+03 # mur_2
 46     3.00000000E+03 # mur_3
 48     3.00000000E+03 # mdr_2
 49     3.00000000E+03 # mdr_3
BLOCK IMEXTPAR #
 1      7.58497104E-01 # M1
 2      7.79157182E-01 # M2
 3      8.42651944E-01 # M3
 11     1.38029453E+00 # At
 12     0.00000000E+00 # Ab
 13     0.00000000E+00 # Atau
 61     0.00000000E+00 # lambda
 62     0.00000000E+00 # abskappa
 65     0.00000000E+00 # mu_eff
BLOCK CMPLX #
 3     4.36408413E-01 # phiu
```

We here now also have complex phases. It should be noted that this benchmark point results in EDM values that are excluded by the current experimental limits. Nonetheless, we use this point for illustrative purposes to showcase the influence of the complex phases. The masses of the supersymmetric particles and the Higgs particles are

- Gluino: $m_{\tilde{g}} = 2192.63\,\text{GeV}$
- Neutralinos: $m_{\tilde{\chi}_i^0} = (195.65\,\text{GeV},\ 230.57\,\text{GeV},\ 336.2\,\text{GeV},\ 418.27\,\text{GeV},\ 490.88\,\text{GeV})$
- Charginos: $m_{\tilde{\chi}_i^\pm} = (210.76\,\text{GeV},\ 489.66\,\text{GeV})$
- Sneutrinos: $m_{\tilde{\nu}} = (2999.34\,\text{GeV},\ 2999.34\,\text{GeV},\ 2999.34\,\text{GeV})$
- Sleptons: $m_{\tilde{l}} = (3000.29\,\text{GeV},\ 3000.36\,\text{GeV},\ 3000.29\,\text{GeV},\ 3000.36\,\text{GeV},\ 3000.13\,\text{GeV},\ 3000.53\,\text{GeV})$
- Up squarks: $m_{\tilde{u}} = (3051.66\,\text{GeV}, 3051.92\,\text{GeV}, 3051.29\,\text{GeV}, 3052.29\,\text{GeV}, 1970.4\,\text{GeV}, 3061.28\,\text{GeV})$
- Down squarks: $m_{\tilde{d}} = (3052.21\,\text{GeV}, 3052.66\,\text{GeV}, 3052.21\,\text{GeV}, 3052.66\,\text{GeV}, 1975.66\,\text{GeV}, 3052.21\,\text{GeV})$
- Neutral Higgs: $m_h = (122\,\text{GeV}, 275.6\,\text{GeV}, 304.1\,\text{GeV}, 951.18\,\text{GeV}, 952.53\,\text{GeV})$
- Charged Higgs: $m_{H^\pm} = 953.32\,\text{GeV}$

For this benchmark point, we again see that the lightest chargino and the two lightest neutralinos have masses that are close to each other. Thus, the three-body decays are again important here, and the total widths of the lightest chargino and the second-lightest neutralino are small. Furthermore, the branching ratio of the decay channel $\tilde{\chi}_2^0 \to \tilde{\chi}_1^0\gamma$ is 5×10^{-5} and therefore again small.

Since we now have complex couplings and potentially CP violation, the branching ratios of a particle decaying into a specific final state and the anti-particle decay decaying into the anti-particle final state can differ. We thus consider the difference in the branching ratios, defined as

$$\delta^{\text{BR}} \equiv \frac{\text{BR} - \overline{\text{BR}}}{\text{BR}}\,, \tag{14.2}$$

where BR denotes the branching ratio of the considered decay and $\overline{\text{BR}}$ the anti-particle branching ratio, respectively.

Considering the gluino decays, the total width is given by 3.72 GeV at LO and 3.8 GeV at NLO, i.e. we have a relative NLO correction $\delta_{\tilde{g}}^{\Gamma}$ of 2.7 %. Since we now have complex couplings, the decay of the gluino into an antisquark-quark pair can be different from the decay into a squark-antiquark pair. The relative difference δ^{BR} for the decay into a $\tilde{t}_1^* t/\tilde{t}_1 \bar{t}$ pair is -1.8×10^{-6}, and the relative difference for the decay into a $\tilde{b}_1^* b/\tilde{b}_1 \bar{b}$ pair is -6.5×10^{-8}. Thus, the difference in the branching ratios is tiny.

Similarly, we can consider the decay of the up-squark $\tilde{u}_\text{L}$. The total width is given by 94.8 GeV at LO and 117.2 GeV at NLO, i.e. we have a relative correction $\delta_{\tilde{u}_\text{L}}^{\Gamma}$ of 23.6 %. When we consider the decay $\tilde{u}_\text{L} \to \tilde{\chi}_2^+ d$ and the anti particle decay $\tilde{u}_\text{L}^* \to \tilde{\chi}_2^- \bar{d}$, we have a relative difference δ^{BR} between the branching ratios of -1.4×10^{-6}, which is again small. The total widths of the other supersymmetric particles and their relative NLO QCD corrections are in similar ranges as in `BP1`.

This concludes this first investigation of benchmark points obtained by the described program chain.

CHAPTER 15

Conclusion

In this part, we discussed the calculation of supersymmetric particle decays in the NMSSM and the implementation into an extended version of the program `SDECAY`, which was then linked to `NMSSMCALC` in order to obtain benchmark points and perform a numerical analysis. We started with a brief introduction to SUSY and the NMSSM, where we also set up the necessary notation for the calculation and described the constraints that we applied in order to obtain valid benchmark points. Next, we discussed the renormalization of the model needed for the QCD corrections of the two-body decays, where we renormalized the squarks, quarks and gluino fields and masses as well as the mixing matrices of the squarks and quarks. Furthermore, we introduced the counterterm for the strong coupling constant, where we decoupled the top quark and the heavy supersymmetric particles from the running of α_s. Additionally, we mentioned the shifts that we had to introduce in order to restore SUSY, since we used dimensional regularization in our calculation. We also described how to shift the $\overline{\text{DR}}$ input parameters into OS parameters to be consistent with our applied renormalization conditions.

Next, we calculated all the supersymmetric particle decays in the NMSSM. We first discussed the LO two-body decays, where we mentioned all the possible decay channels. In the case of kinematically closed two-body decays, we also have to consider three-body decays, which we subsequently described. Moreover, we included radiative loop decays of neutralinos into photons and lighter neutralinos as well as gluinos into gluons and neutralinos. Finally, we discussed the NLO QCD corrections to the two-body decays involving coloured particles in the final or initial state. We furthermore described the real corrections, collinear divergences and the absorptive corrections, i.e. imaginary self-energy contributions that have to be considered as well.

After the calculation, we presented the implementation of our results into an extension of the program `SDECAY`. We described how our code is linked to `NMSSMCALC` and how it is used. Next, we introduced our setup to obtain viable parameter points. We used the program package `BSMArt` and linked it to `NMSSMCALC` to generate parameter points. Furthermore, we used the tools `HiggsTools` and `SModels` to check that our parameter points fulfil experimental constraints from Higgs searches and measurements as well as from searches and exclusion limits for supersymmetric particles. Finally, we used this setup to create a sample of benchmark points to showcase our code and some results. We saw that we can have scenarios where the

three-body decays become important. Moreover, in the benchmark scenarios we considered, the NLO QCD corrections (where applicable) can change the total widths by up to about 42 %.

CHAPTER 16

Final Conclusion and Outlook

With now over 12 years since the Higgs discovery, the particle physics community continues to perform precision measurements combined with precise theory predictions, both for the SM and BSM theories, to vigorously test the SM and search for new physics. Additionally, the determination of the Higgs self-couplings through Higgs pair production is pursued as it will give key insights on the nature of electroweak symmetry breaking and the Higgs sector in general. Our goal in this thesis was to contribute to these efforts.

In the context of this thesis, we worked on several projects where we discussed BSM theories and performed precision calculations to carry out phenomenological studies. In the first project, we studied the CxSM and calculated the NLO EW corrections to Higgs decays. We renormalized the model, where we introduced several renormalization schemes. We performed an exhaustive parameter scan, including theoretical and experimental constraints. We used the obtained parameter sample to examine the typical sizes of the NLO corrections, which are typically of moderate sizes (up to 25 %) and discussed the origins of potentially large corrections. Furthermore, we investigated the impact of these corrections on the viable parameter space, which does not change the overall shape of the allowed parameter regions so far, but might become important with increasing experimental accuracy. We also discussed the impact of the NLO corrections on di-Higgs production and in the case of vanishing LO widths in the $h_2 \to h_1 h_1$ decay channel, where the NLO corrections can be important.

In the next project, we worked with a composite 2HDM, where we analyzed the impact on di-Higgs production compared to the SM and other 2HDM models. We first introduced the composite 2HDM and then derived from an effective Lagrangian the LO cross section for di-Higgs production. In this context, we also discussed the NLO QCD corrections in the heavy quark limit. We then described our setup to obtain viable parameter points, including theoretical and experimental constraints, particularly constraints from *resonant* and *non-resonant* searches for di-Higgs production. Furthermore, we analyzed the results on inclusive cross sections and differential distributions of Higgs pair production, where we examined the impact of the heavy top partners, the resonant enhancement from the heavy Higgs scalar H and the effective quartic scalar-scalar-fermion-fermion couplings present in our effective Lagrangian approach. In the composite 2HDM, we thus can obtain significant deviations from the SM result for di-Higgs production, but also parameter points with SM-like cross sections, due to interference effects between the various contributions. Moreover, we can

have resonant enhancements similar to elementary 2HDM models. Finally, we compared the composite 2HDM with a type-II 2HDM and a flavour-aligned 2HDM, where in the composite 2HDM we can have larger total widths Γ_H due to larger Yukawa couplings and additional possible decay channels into heavy top partners. These large total widths combined with the additional contributions from heavy top partners and additional effective couplings can lead to interesting interference patterns that can be used to distinguish the composite 2HDM from other 2HDM realizations.

In the final project, we computed the supersymmetric particle decays in the CP-violating NMSSM and implemented the analytic results into an extended version of `SDECAY`, which was then combined with the spectrum generator `NMSSMCALC` to perform phenomenological studies. First, we introduced the NMSSM and set our notation, where we also described the renormalization needed for the QCD corrections of the two-body decays. We then presented the calculation of the supersymmetric particle decays. These comprise the two-body and, if kinematically closed, the three-body decays, as well as radiatively induced two-body decays. Furthermore, the NLO QCD corrections to two-body decays involving coloured particles were considered. We described the implementation of the calculated decay widths into an extended version of the code `SDECAY`, which was then linked to the program `NMSSMCALC` to perform phenomenological studies. We explained our setup to obtain viable parameter points and discussed some benchmark point scenarios. We saw that the three-body decays can become important if the two-body decays are kinematically closed and the QCD corrections can alter the total widths up to 42 % in the benchmark points we considered.

After 12 years of precise investigations of the discovered Higgs boson, there is still room for new physics to be explored, which in turn can be used to explain the shortcomings of the SM. Therefore, the precision calculations for the SM and predictions for the BSM models from the theoretical side, which this thesis is a part of, are further developed. At the same time, the experimental precision for measurements of the SM expectations is increased, and searches for new physics continue. The interplay of both sides has to be advanced in order to unveil the fundamental nature of the scalar sector and the Higgs boson.

APPENDIX A

Form Factors in the Di-Higgs Leading-Order Cross Section

For the form factors in Sec. 9.2.1, we obtain (cf. [74, 101, 153])

$$F_{\triangle}(m_i) = \frac{2m_i}{\hat{s}}[2 + (4m_i^2 - \hat{s})C_{12}]\,, \tag{A.1}$$

$$\begin{aligned} F_{\square}^{hh}(m_i, m_j) = \frac{1}{\hat{s}}\Bigg[& 4 + 8m_i^2 C_{12} + \frac{2}{\hat{s}}[m_h^2 - (m_i + m_j)^2](\hat{u} - m_h^2)(C_{23} + C_{14}) \\ & + \frac{2}{\hat{s}}[m_h^2 - (m_i + m_j)^2](\hat{t} - m_h^2)(C_{13} + C_{24}) \\ & + 2[(m_i + m_j)(2m_i^2(m_i + m_j) - m_i\hat{s}) - m_i^2(\hat{u} + \hat{t})](D_{123} + D_{213} + D_{132}) \\ & - \frac{2}{\hat{s}}[\hat{t}\hat{u} - m_h^4 + s(m_j^2 - m_i^2)][m_h^2 - (m_i + m_j)^2]D_{132}\Bigg]\,, \end{aligned} \tag{A.2}$$

$$\begin{aligned} G_{\square}^{hh}(m_i, m_j) = & \frac{1}{\hat{s}(\hat{u}\hat{t} - m_h^4)} \\ & \big[(\hat{t}^2 + \hat{u}^2 - 4(m_j^2 + m_i m_j)(\hat{t} + \hat{u}) + 4(m_j - m_i)(m_i + m_j)^3 \\ & + 2m_h^4)\hat{s}C_{12} + (m_h^4 + \hat{t}^2 - 2\hat{t}(m_i + m_j)^2)((C_{13} + C_{24})(\hat{t} - m_h^2) - \hat{s}\hat{t}D_{213}) \\ & + (m_h^4 + \hat{u}^2 - 2\hat{u}(m_i + m_j)^2)((C_{23} + C_{14})(\hat{u} - m_h^2) - \hat{s}\hat{u}D_{123}) \\ & - (\hat{t}^2 + \hat{u}^2 - 2m_h^4)(\hat{t} + \hat{u} - 2(m_i + m_j)^2)C_{34} \\ & - (\hat{t} + \hat{u} - 2(m_i + m_j)^2)((\hat{t}\hat{u} - m_h^4)(m_i^2 + m_j^2) + \hat{s}(m_i^2 - m_j^2)^2) \\ & (D_{123} + D_{213} + D_{132}) + 2(m_i^2 - m_j^2)[-(\hat{s} + m_h^2)(m_h^4 + \hat{u}^2 \\ & - 2\hat{u}(m_i + m_j)^2) + (-\hat{s}\hat{u} - \hat{u}^2 - m_h^4)((m_i + m_j)^2 - m_h^2) \\ & + m_h^2(\hat{u} - m_h^2)^2]D_{123} + 2(m_i^2 - m_j^2)[-(\hat{s} + m_h^2)(m_h^4 + \hat{t}^2 - 2\hat{t}(m_i + m_j)^2) \\ & + (-\hat{s}\hat{t} - \hat{t}^2 - m_h^4)((m_i + m_j)^2 - m_h^2) + m_h^2(\hat{t} - m_h^2)^2]D_{213}\big]\,. \end{aligned} \tag{A.3}$$

Next, the form factors $F_{\square,5}^{hh}(m_i, m_j)$ and $G_{\square,5}^{hh}(m_i, m_j)$ can be expressed via

$$F_{\square,5}^{hh}(m_i, m_j) = -F_{\square}^{hh}(m_i, -m_j)\,, \tag{A.4}$$

$$G_{\square,5}^{hh}(m_i, m_j) = -G_{\square}^{hh}(m_i, -m_j)\,. \tag{A.5}$$

The C_{ij} and D_{ijk} integrals are defined as

$$C_{ij}(m_1^2, m_2^2, m_3^2) = \int \frac{d^4q}{i\pi^2} \frac{1}{(q^2 - m_1^2)((q+p_i)^2 - m_2^2)((q+p_i+p_j)^2 - m_3^2)}\,, \tag{A.6}$$

$$D_{ijk}(m_1^2, m_2^2, m_3^2, m_4^2) = \int \frac{d^4q}{i\pi^2} \frac{1}{(q^2 - m_1^2)((q+p_i)^2 - m_2^2)((q+p_i+p_j)^2 - m_3^2)((q+p_i+p_j+p_k)^2 - m_4^2)}\,, \tag{A.7}$$

and we use the abbreviations

$$\begin{aligned}
C_{12} &\equiv C_{12}(m_i^2, m_i^2, m_i^2)\,, \\
C_{13} &\equiv C_{13}(m_i^2, m_i^2, m_j^2)\,, \\
C_{14} &\equiv C_{14}(m_i^2, m_i^2, m_j^2)\,, \\
C_{23} &\equiv C_{23}(m_i^2, m_i^2, m_j^2)\,, \\
C_{24} &\equiv C_{24}(m_i^2, m_i^2, m_j^2)\,, \\
C_{34} &\equiv C_{34}(m_i^2, m_j^2, m_i^2)\,, \\
D_{123} &\equiv D_{123}(m_i^2, m_i^2, m_i^2, m_j^2)\,, \\
D_{213} &\equiv D_{213}(m_i^2, m_i^2, m_i^2, m_j^2)\,, \\
D_{132} &\equiv D_{132}(m_i^2, m_i^2, m_j^2, m_j^2)\,.
\end{aligned} \tag{A.8}$$

For the Mandelstam variables, we used the definition in Eq. (9.12).

APPENDIX B

Benchmark Points in the Composite 2HDM

In Tab. B.1, we give the input values for the benchmark points used in the analysis in Sec. 10.3.2. These points were also used in [74].

Table B.1.: Input parameters of the benchmark points used for the analysis. Taken from [74].

BP	f [GeV]	Δ_L [GeV]	Δ_R [GeV]	Y_1 [GeV]	Y_2 [GeV]	g_ρ
BP1	1139.21	$\begin{pmatrix} 649.392 \\ -1787.9 \end{pmatrix}$	$\begin{pmatrix} -7244.85 \\ 4633.51 \end{pmatrix}$	$\begin{pmatrix} -406.903 & 421.383 \\ -910.863 & -1651.99 \end{pmatrix}$	$\begin{pmatrix} 3996.82 & 2846.41 \\ 2265.86 & 518.944 \end{pmatrix}$	7.02515
BP2	821.74	$\begin{pmatrix} 5172.74 \\ -3835.24 \end{pmatrix}$	$\begin{pmatrix} -2850.8 \\ -759.562 \end{pmatrix}$	$\begin{pmatrix} 3194.11 & 2467.64 \\ 2748.76 & 1489.54 \end{pmatrix}$	$\begin{pmatrix} 457.272 & -1135.19 \\ 5946.7 & -3126.3 \end{pmatrix}$	7.87477
BP3	795.639	$\begin{pmatrix} -168.309 \\ 1137.24 \end{pmatrix}$	$\begin{pmatrix} -2548.98 \\ -2181.22 \end{pmatrix}$	$\begin{pmatrix} -1808.81 & -695.861 \\ 3507.5 & -320.533 \end{pmatrix}$	$\begin{pmatrix} 4348.75 & 399.558 \\ -4182.72 & -1915.42 \end{pmatrix}$	6.7523
BP4	750.293	$\begin{pmatrix} -1007.88 \\ -1351.26 \end{pmatrix}$	$\begin{pmatrix} 1844.02 \\ 1713.76 \end{pmatrix}$	$\begin{pmatrix} 709.119 & -884.948 \\ -5689.43 & 3420.92 \end{pmatrix}$	$\begin{pmatrix} 2833.62 & -2811.59 \\ 5092.76 & 3134.5 \end{pmatrix}$	8.6289

APPENDIX C

Derivation of the Differential p_T Distribution in Di-Higgs Production

In this section, we derive the differential p_T distribution for, in general, different final state scalar particles ϕ, ϕ' (cf. [74]). The two ingoing gluons have momenta p_1 and p_2 and the outgoing scalars have momenta p_3, and p_4, with masses m_3 and m_4 and we have momentum conservation (all momenta are considered as incoming),

$$p_1 + p_2 + p_3 + p_4 = 0\,. \tag{C.1}$$

We also introduce the Källén function λ,

$$\lambda(a,b,c) \equiv \sqrt{a^2 + b^2 + c^2 - 2ab - 2ac - 2bc}\,. \tag{C.2}$$

The formula for the full hadronic cross section into the final state particles ϕ, ϕ' is given by (compare with Eq. (9.22)),

$$\begin{aligned}\sigma_{pp\to\phi\phi'} &= \int_{\tau_0}^1 \mathrm{d}\tau\, \frac{\mathrm{d}\mathcal{L}^{gg}}{\mathrm{d}\tau}\, \hat{\sigma}_{gg\to\phi\phi'}(\hat{s} = \tau s) \\ &= \int_{\tau_0}^1 \mathrm{d}\tau \frac{\mathrm{d}\mathcal{L}^{gg}}{\mathrm{d}\tau} \int_{t_-}^{t_+} \mathrm{d}\hat{t} \left(\frac{\mathrm{d}\hat{\sigma}_{gg\to\phi\phi'}}{\mathrm{d}\hat{t}}\right)_{\hat{s}=\tau s}\,,\end{aligned} \tag{C.3}$$

with

$$\tau_0 = \frac{(m_3 + m_4)^2}{s}\,, \tag{C.4a}$$

$$\hat{t}_\pm = \frac{1}{2}\left(m_3^2 + m_4^2 - \hat{s} \pm \lambda(\hat{s}, m_3^2, m_4^2)\right)\,. \tag{C.4b}$$

The differential distribution is obtained by omitting the τ integration. To obtain the differential cross section with respect to the transverse momentum p_T, we first change the integration variable from $\hat{t}$ to p_T^2 and then switch the τ and the p_T integrations.

We start with the Mandelstam variables from Eq. (9.12) to obtain expressions for the absolute momenta $|\vec{p}_i|$ and the energies E_i $(i = 1, .., 4)$,

$$\begin{aligned}\hat{s} &= (p_1 + p_2)^2 = (E_1 + E_2)^2 \\ &\Rightarrow E_1 = E_2 = \frac{\sqrt{s}}{2} \qquad \text{(C.5a)} \\ \hat{s} &= (p_3 + p_4)^2 = (E_3 + E_4)^2 = (\sqrt{m_3^2 + |\vec{p}|^2} + \sqrt{m_4^2 + |\vec{p}|^2})^2 \\ &\Rightarrow p^2 \equiv |\vec{p}|^2 = \frac{1}{4\hat{s}}\lambda^2(\hat{s}, m_3^2, m_4^2)\,. \qquad \text{(C.5b)}\end{aligned}$$

To obtain the transverse momentum p_T, we project $\vec{p}_3$ to the transverse plane,

$$p_T^2 = \sin^2\theta |\vec{p}_3|^2 = (1 - \cos^2\theta)|\vec{p}_3|^2\,. \qquad \text{(C.6)}$$

Here, θ is the angle between $\vec{p}_1$ and $\vec{p}_3$. We can use the definition of the Mandelstam variable $\hat{t}$ to obtain a relation for $\cos\theta$,

$$\hat{t} = (p_1 + p_3)^2 = m_3^2 - 2E_1E_3 + 2|\vec{p}_1||\vec{p}_3|\cos\theta \qquad \text{(C.7)}$$

$$\Rightarrow \cos\theta = \frac{\hat{t} - m_3^2 + 2E_1E_3}{2|\vec{p}_1||\vec{p}_3|}\,. \qquad \text{(C.8)}$$

Now using $|\vec{p}_1| = E_1$ and $|\vec{p}_3| = p$ we obtain for the transverse momentum,

$$p_T^2 = \frac{(m_4^2 - \hat{s} - \hat{t})\hat{t} + m_3^2(\hat{t} - m_4^2)}{\hat{s}}\,. \qquad \text{(C.9)}$$

This coincides with Eq. (9.13c). Thus, to express $\hat{t}$ in terms of p_T we solve Eq. (C.9) for $\hat{t}$ and obtain two solutions,

$$\hat{t}_{1,2} = \frac{1}{2}\left(m_3^2 + m_4^2 - \hat{s} \pm \sqrt{\lambda^2(\hat{s}, m_3^2, m_4^2) - 4p_T^2\hat{s}}\right)\,. \qquad \text{(C.10)}$$

When solving this quadratic equation, one has to take the square root of $(\hat{t} + (\hat{s} - m_3^2 - m_4^2)/2)^2$. Thus, one has to split up the $\hat{t}$ integration from $\hat{t}_-$ to $\hat{t}_m$ and from $\hat{t}_m$ to $\hat{t}_+$, where $\hat{t}_m$ is the point where $(\hat{t} + (\hat{s} - m_3^2 - m_4^2)/2)^2$ vanishes,

$$\hat{t}_m = \frac{m_3^2 + m_4^2 - \hat{s}}{2}\,. \qquad \text{(C.11)}$$

We now derive the integration boundaries for the p_T^2 integration. We obtain

$$\begin{aligned}p_T^2(\hat{t}_\pm) &= 0\,, \qquad \text{(C.12)} \\ \frac{\mathrm{d}p_T^2}{\mathrm{d}\hat{t}} &= \frac{m_3^2 + m_4^2 - \hat{s} - 2\hat{t}}{\hat{s}} \stackrel{!}{=} 0 \quad \Rightarrow \hat{t}_{\max} = \hat{t}_m\,, \qquad \text{(C.13)} \\ \frac{\mathrm{d}^2p_T^2}{\mathrm{d}\hat{t}^2} &= -\frac{2}{\hat{s}} < 0 \rightarrow \text{Maximum}\,, \qquad \text{(C.14)} \\ p_T^2(\hat{t}_m) &= \frac{\lambda^2(\hat{s}, m_3^2, m_4^2)}{4\hat{s}} \equiv p_{T,\max}^2\,. \qquad \text{(C.15)}\end{aligned}$$

The transverse momentum vanishes at the boundaries of the $\hat{t}$ integration $(\hat{t}_\pm)$ and has its maximum at $\hat{t}_m$, i.e. we integrate p_T^2 from 0 to $p_{T,\max}^2$ but we have to split up the integration. We also need the substitution rule

$$\mathrm{d}\hat{t} = \mathrm{d}p_T^2 \frac{\hat{s}}{m_3^2 + m_4^2 - \hat{s} - 2\hat{t}}\,. \qquad \text{(C.16)}$$

We change the $\hat{t}$ integration to

$$\int_{\hat{t}_-}^{\hat{t}_+} \mathrm{d}\hat{t}\, \frac{\mathrm{d}\hat{\sigma}}{\mathrm{d}\hat{t}} = \int_{\hat{t}_-}^{\hat{t}_m} \mathrm{d}\hat{t}\, \frac{\mathrm{d}\hat{\sigma}}{\mathrm{d}\hat{t}} + \int_{\hat{t}_m}^{\hat{t}_+} \mathrm{d}\hat{t}\, \frac{\mathrm{d}\hat{\sigma}}{\mathrm{d}\hat{t}} \tag{C.17}$$

$$= \int_0^{p_{T,\max}^2} \left(\mathrm{d}p_T^2 \frac{\hat{s}}{m_3^2 + m_4^2 - \hat{s} - 2\hat{t}}\, \frac{\mathrm{d}\hat{\sigma}}{\mathrm{d}\hat{t}} \right)_{\hat{t}=\hat{t}_2} + \int_{p_{T,\max}^2}^0 \left(\mathrm{d}p_T^2 \frac{\hat{s}}{m_3^2 + m_4^2 - \hat{s} - 2\hat{t}}\, \frac{\mathrm{d}\hat{\sigma}}{\mathrm{d}\hat{t}} \right)_{\hat{t}=\hat{t}_1}$$

$$= \int_0^{p_{T,\max}^2} \mathrm{d}p_T^2 \left[\left(\frac{\hat{s}}{m_3^2 + m_4^2 - \hat{s} - 2\hat{t}}\, \frac{\mathrm{d}\hat{\sigma}}{\mathrm{d}\hat{t}} \right)_{\hat{t}=\hat{t}_2(p_T^2)} - \left(\frac{\hat{s}}{m_3^2 + m_4^2 - \hat{s} - 2\hat{t}}\, \frac{\mathrm{d}\hat{\sigma}}{\mathrm{d}\hat{t}} \right)_{\hat{t}=\hat{t}_1(p_T^2)} \right] . \tag{C.18}$$

We now integrate over $p_T^2 \in [0, p_{T,\max}^2]$ and $\tau \in [\tau_0, 1]$ with τ_0 given in Eq. (C.4a). To interchange the integrations we need to solve the inequality,

$$p_T^2 \leq p_{T,\max}^2 = \frac{\lambda^2(\tau s, m_3^2, m_4^2)}{4\tau s}\,, \tag{C.19}$$

for τ. After some simplification, we obtain the relation

$$4(p_T^2 + m_3^2)(p_T^2 + m_4^2) \leq (\tau s - 2p_T^2 - m_3^2 - m_4^2)^2\,, \tag{C.20}$$

where we have to check if the term in brackets on the right hand side is always positive. This is the case, since

$$\tau s - 2p_T^2 - m_3^2 - m_4^2 \geq \tau s - 2p_{T,\max}^2 - m_3^2 - m_4^2 = \frac{\tau^2 s^2 - (m_3^2 + m_4^2)^2}{2\tau s} \tag{C.21}$$

$$\geq \frac{\tau_0^2 s^2 - (m_3^2 + m_4^2)^2}{2\tau s} = \frac{4 m_3 m_4 (m_3^2 + m_4^2)}{\tau s} \geq 0\,. \tag{C.22}$$

Thus, the square root can be taken and we obtain the inequality

$$\tau \geq \frac{1}{s} \left(2\sqrt{(p_T^2 + m_3^2)(p_T^2 + m_4^2)} + 2p_T^2 + m_3^2 + m_4^2 \right) \equiv \tau_{\min}\,. \tag{C.23}$$

The new integration boundaries therefore are given by

$$p_T^2 \in [0, \frac{\lambda^2(s, m_3^2, m_4^2)}{4s}], \quad \tau \in [\tau_{\min}, 1]\,. \tag{C.24}$$

Finally, we obtain the full hadronic cross section

$$\sigma_{pp\to\phi\phi'} = \int_0^{p_{T,\max}^2} \mathrm{d}p_T^2 \left(\frac{\mathrm{d}\hat{\sigma}}{\mathrm{d}p_T^2} \right), \tag{C.25}$$

where

$$\frac{\mathrm{d}\hat{\sigma}}{\mathrm{d}p_T^2} = \int_{\tau_{\min}}^1 d\tau \frac{d\mathcal{L}^{gg}}{d\tau} \times \left[\left(\frac{\hat{s}}{m_3^2 + m_4^2 - \hat{s} - 2\hat{t}}\, \frac{\mathrm{d}\hat{\sigma}}{\mathrm{d}\hat{t}} \right)_{\hat{t}=\hat{t}_2(p_T^2)} - \left(\frac{\hat{s}}{m_3^2 + m_4^2 - \hat{s} - 2\hat{t}}\, \frac{\mathrm{d}\hat{\sigma}}{\mathrm{d}\hat{t}} \right)_{\hat{t}=\hat{t}_1(p_T^2)} \right] . \tag{C.26}$$

APPENDIX D

Generic Formulas for Three-Body Decays

In the following, we derive the kinematics and the formula for the partial width for three-body decays (cf. [322]). First of all, we use the notation

$$P = p_1 + p_2 + p_3\,, \tag{D.1}$$

where $P = (M, \mathbf{0})^{\mathrm{T}}$ is the momentum of the decaying particle in the rest frame of the particle, and p_1, p_2 and p_3 are the momenta of the final state particles with masses m_1, m_2 and m_3. Furthermore, we will work with two different reference frames, the rest frame of the initial state, the centre-of-mass (COM) frame, and the frame where p_2 and p_3 have opposite momenta with the same size (i.e. $\vec{p}_2 = -\vec{p}_3$, in the following labelled S23). Next, we define the following variables,

$$a_i = \frac{2m_i}{M}\,, i = 1, 2, 3\,, \tag{D.2a}$$

$$s_1 = (P - p_1)^2 = (p_2 + p_3)^2\,, \tag{D.2b}$$

$$s_2 = (P - p_2)^2 = (p_1 + p_3)^2\,, \tag{D.2c}$$

$$\lambda(a, b, c) = \sqrt{a^2 + b^2 + c^2 - 2ab - 2ac - 2bc}\,, \tag{D.2d}$$

$$x_i = \frac{2Pp_i}{s}\,. \tag{D.2e}$$

When we go into the COM frame, we see that

$$s_1 = (P - p_1)^2 = M^2 + m_1^2 - 2ME_1 \leq (M - m_1)^2\,, \tag{D.3}$$

where E_1 is the energy of particle 1 in this reference frame, and we used the lower bound $E_1 \geq m_1$. When we go to the frame S23, we can derive a lower bound for s_1,

$$s_1 = (p_2 + p_3)^2 = (E_2 + E_3)^2 \geq (m_2 + m_3)^2\,. \tag{D.4}$$

Next, we want to derive the bounds for s_2. Here we go to the frame S23 and first obtain expressions for $|\vec{p}_1|$ and $|\vec{p}_3|$ (in this frame we have $\vec{P} = \vec{p}_1$),

$$s_1 = (P - p_1)^2 = \left(\sqrt{M^2 + |\vec{p}_1|^2} - \sqrt{m_1^2 + |\vec{p}_1|^2}\right)^2 \tag{D.5}$$

$$\Rightarrow |\vec{p}_1|^2 = \frac{1}{4s_1}\lambda^2(s_1, M^2, m_1^2)\,. \tag{D.6}$$

Similarly we have

$$s_1 = (p_2 + p_3)^2 = \left(\sqrt{m_2^2 + |\vec{p}_3|^2} + \sqrt{m_3^2 + |\vec{p}_3|^2}\right)^2 \tag{D.7}$$

$$\Rightarrow |\vec{p}_3|^2 = \frac{1}{4s_1}\lambda^2(s_1, m_2^2, m_3^2)\,. \tag{D.8}$$

For s_2 we then obtain

$$\begin{aligned} s_2 = (p_1 + p_3)^2 &= m_1^2 + m_3^2 + 2p_1p_3 \\ &= m_1^2 + m_3^2 + \frac{1}{2s_1}\left((M^2 - s_1 - m_1^2)(s_1 + m_3^2 - m_2^2)\right. \\ &\qquad \left. -\lambda(s_1, M^2, m_1^2)\lambda(s_1, m_2^2, m_3^2)\cos\theta\right)\,, \end{aligned} \tag{D.9}$$

where θ is the angle between $\vec{p}_1$ and $\vec{p}_3$. Moreover, we know that

$$s_1 = (P - p_1)^2 = M^2 + m_1^2 - M^2x_1\,, \tag{D.10a}$$

$$s_2 = (P - p_2)^2 = M^2 + m_2^2 - M^2x_2\,. \tag{D.10b}$$

We can solve the above equation for x_2 and we obtain the upper and lower boundaries

$$\begin{aligned} x_{2,\pm} = \left(\left(\frac{1}{8 - 8x_1 + 2a_1^2}\right)\right. &\left((x_1 - 2)(4x_1 - 4 - a_2^2 + a_3^2 - a_1^2)\right. \\ &\left.\left. \pm\sqrt{(a_1^2 - x_1^2)(4a_2^2a_3^2 - (4x_1 - 4 + a_3^2 + a_2^2 - a_1^2)^2)}\right)\right)\,. \end{aligned} \tag{D.11}$$

For x_1 we obtain

$$\frac{2m_1}{M} \le x_1 \le 1 + \frac{m_1^2 - (m_2 + m_3)^2}{M^2}\,. \tag{D.12}$$

Next, we calculate the three-body phase space. We start with

$$\mathrm{d}\Phi_3 = \delta^{(4)}(P - p_1 - p_2 - p_3)\prod_{i=1}^{3}\frac{\mathrm{d}^3p_i}{(2\pi)^3 2E_i}\,. \tag{D.13}$$

Since p_3 is fixed by the momentum conservation, the only angle that is important is β_{12}, which is defined between $\vec{p}_1$ and $\vec{p}_2$, the other three angle integrations, i.e. the integrations over α, ϕ and $\cos\theta$, will be trivial. Thus, we obtain

$$\mathrm{d}\Phi_3 = \delta(M - E_1 - E_2 - E_3)\frac{1}{(2\pi)^9 2^3}\mathrm{d}|\vec{p}_1|\mathrm{d}(\cos\theta)\mathrm{d}\phi\mathrm{d}|\vec{p}_2|\mathrm{d}(\cos\beta_{12})\mathrm{d}\alpha\frac{|\vec{p}_1|^2|\vec{p}_2|^2}{E_1E_2E_3}\,. \tag{D.14}$$

Next we use

$$E = \sqrt{m^2 + p^2} \Rightarrow p\mathrm{d}p = E\mathrm{d}E\,, \tag{D.15}$$

to simplify the phase space to

$$\mathrm{d}\Phi_3 = \delta(M - E_1 - E_2 - E_3)\frac{1}{8(2\pi)^9}\mathrm{d}E_1\mathrm{d}(\cos\theta)\mathrm{d}\phi\mathrm{d}E_2\mathrm{d}(\cos\beta_{12})\mathrm{d}\alpha\frac{|\vec{p}_1||\vec{p}_2|}{E_3}\,. \tag{D.16}$$

We use the COM frame and the relations ($i = 1, 2, 3$)

$$x_i = \frac{2Pp_i}{M^2} = \frac{2E_i}{M} \qquad \Rightarrow \qquad \mathrm{d}E_i = \frac{M}{2}\mathrm{d}x_i\,, \tag{D.17}$$

$$|\vec{p}_i| = \sqrt{E_i^2 - m_i^2} = \frac{M}{2}x_i\beta_i\,, \qquad \beta_i \equiv \sqrt{1 - \frac{4m_i^2}{M^2x_i^2}}\,, \tag{D.18}$$

$$\delta(M - E_1 - E_2 - E_3) = \delta(\frac{M}{2}(2 - x_1 - x_2 - x_3)) = \frac{2}{M}\delta(2 - x_1 - x_2 - x_3)\,, \tag{D.19}$$

to obtain

$$\mathrm{d}\Phi_3 = \delta(2 - x_1 - x_2 - x_3)\frac{1}{8(2\pi)^9}\mathrm{d}x_1\mathrm{d}x_2\mathrm{d}(\cos\theta)\mathrm{d}\phi\mathrm{d}(\cos\beta_{12})\mathrm{d}\alpha\frac{|\vec{p}_1||\vec{p}_2|}{x_3} \tag{D.20}$$

$$= \delta(2 - x_1 - x_2 - x_3)\frac{1}{8(2\pi)^9}\mathrm{d}x_1\mathrm{d}x_2\mathrm{d}(\cos\theta)\mathrm{d}\phi\mathrm{d}(\cos\beta_{12})\mathrm{d}\alpha\frac{M^2}{4}\frac{x_1\beta_1 x_2\beta_2}{x_3}\,. \tag{D.21}$$

Next, we use the relations

$$\begin{aligned} x_3^2 &= \frac{4}{M^2}(m_3^2 + |\vec{p}_1 + \vec{p}_2|^2) \\ &= \frac{4}{M^2}(m_3^2 + \frac{M^2}{4}x1^2 - m_1^2 + \frac{M^2}{4}x_2^2 - m_2^2 + \frac{2M^2}{4}x_1x_2\beta_1\beta_2\cos\beta_{12}) \\ &= \frac{4(m_3^2 - m_1^2 - m_2^2)}{M^2} + x_1^2 + x_2^2 + 2x_1x_2\beta_1\beta_2\cos\beta_{12} \qquad \text{(D.22)} \\ &\Rightarrow 2x_3\mathrm{d}x_3 = 2x_1x_2\beta_1\beta_2 d(\cos\beta_{12}) \\ &\Rightarrow d(\cos\beta_{12}) = \frac{x_3\mathrm{d}x_3}{x_1x_2\beta_1\beta_2}\,. \qquad \text{(D.23)} \end{aligned}$$

Thus, we obtain the differential phase space

$$\begin{aligned} \mathrm{d}\Phi_3 &= \delta(2 - x_1 - x_2 - x_3)\frac{M^2}{32(2\pi)^9}\mathrm{d}x_1\mathrm{d}x_2\mathrm{d}x_3\mathrm{d}(\cos\theta)\mathrm{d}\phi\mathrm{d}\alpha \qquad \text{(D.24)} \\ &= \frac{M^2}{32(2\pi)^9}\mathrm{d}x_1\mathrm{d}x_2\mathrm{d}(\cos\theta)\mathrm{d}\phi\mathrm{d}\alpha\Big|_{x_1+x_2+x_3=2}\,. \end{aligned}$$

In a three-body decay, all angle integrations are trivial, and we obtain

$$\mathrm{d}\Phi_3 = \frac{M^2}{16(2\pi)^7}\mathrm{d}x_1\mathrm{d}x_2\Big|_{x_1+x_2+x_3=2}\,. \tag{D.25}$$

The differential three-body decay width can then be written as

$$\mathrm{d}\Gamma = \frac{(2\pi)^4}{2M}|\overline{\mathcal{A}}|^2\mathrm{d}\Phi_3 = \frac{M}{32(2\pi)^3}|\overline{\mathcal{A}}|^2\mathrm{d}x_1\mathrm{d}x_2\Big|_{x_1+x_2+x_3=2}\,, \tag{D.26}$$

with the integration boundaries for x_1 and x_2 given in Eqs. (D.11) and (D.12). With $\mathcal{A}$ the sum of all amplitudes contributing to the decay width is denoted, and $|\overline{\mathcal{A}}|^2$ symbolizes the square of the amplitude, including the sum and the average of the degrees of freedom of the initial and final state particles.

APPENDIX E

Matrix Element Calculation including Majorana Fermions

We give a brief summary of how Feynman diagrams involving Majorana fermions are calculated and how we used this formalism to calculate decay widths of antiparticles, given the decay amplitudes. We follow here [303, 304].

We start with an interaction Lagrangian $\mathcal{L}_{\text{Int}}$, given by

$$\mathcal{L}_{\text{Int}} = \overline{X}\Gamma X = h^i_{abc}\overline{X}_a\Gamma_i X_b \Phi_c \,, \tag{E.1}$$

with a fermion field X, a vector or scalar field Φ, a coupling constant h^i_{abc} and a Lorentz structure $\Gamma_i = 1, \gamma_5, \gamma_\mu\gamma_5, \sigma_{\mu\nu}$. We can also write the Lagrangian in terms of charge-conjugated fields, $\tilde{X} = C\overline{X}^{\mathrm{T}}$, with the charge conjugation matrix C, i.e. we have

$$\mathcal{L}_{\text{Int}} = \overline{\tilde{X}}\Gamma'\tilde{X} \,, \tag{E.2}$$

with $\Gamma'_i = C\Gamma^{\mathrm{T}}C^\dagger = \eta\Gamma_i$. The coefficients η for each Lorentz structure are given by

$$\eta = \begin{cases} 1 \,, \Gamma_i = 1, \gamma_5, \gamma_\mu\gamma_5 \\ -1 \,, \Gamma_i = \gamma_\mu, \sigma_{\mu\nu} \end{cases} . \tag{E.3}$$

The main idea of the derivation of Feynman rules involving Majorana fermions is now to select a custom chosen fermion flow, that does not have to coincide with the fermion flow indicated by the arrows on fermion propagators. After we selected a flow for each fermion chain, we can then read the amplitude from the Feynman diagrams. Here, we have to closely inspect each vertex including fermions. If our chosen fermion flow coincides with the fermion flow indicated by the Dirac fermions, we use the vertex given by Γ, and if they do not coincide, we use Γ'. If we only have Majorana fermions at the vertex without an arrow, we have $\Gamma = \Gamma'$ and only have one expression.

Similarly, we have to be careful with fermion propagators and spinors for external fermion lines, they also will depend on our chosen fermion flow. The algorithm also works if we have already charge-conjugated fields in the Lagrangian. Finally, the relative sign between different amplitudes can also be determined. See [303, 304] for more information.

Next, we want to calculate the antiparticle amplitudes and decay widths, given the particle amplitudes. First of all, this means that given an amplitude, we have to invert all Dirac fermion and charged scalar arrows, and at each vertex we have to use the hermitian conjugated coupling. We have for scalar-fermion-fermion interactions

$$\overline{X}_a(AP_\mathrm{L} + BP_\mathrm{R})X_b\Phi_c \to \overline{X}_b(B^*P_\mathrm{L} + A^*P_\mathrm{R})X_a\Phi_c\,, \tag{E.4}$$

i.e. we have to use the conjugated couplings and we have to interchange the left- and right-chiral parts (with A, B being generic complex couplings, X fermion and Φ scalar fields, respectively).

For vector-fermion-fermion interactions we have

$$\overline{X}_a\gamma_\mu(AP_\mathrm{L} + BP_\mathrm{R})X_bV^\mu \to \overline{X}_b\gamma_\mu(A^*P_\mathrm{L} + B^*P_\mathrm{R})X_aV^{\mu*}\,, \tag{E.5}$$

i.e. we only use the conjugated couplings and do not have to interchange left- and right-chiral couplings so far (due to the additional γ_μ). Here V^μ denotes a generic vector boson.

If we want to keep our structure of the particle amplitude for the antiparticle amplitude, we also keep our chosen fermion flow and now have to reconsider all vertices appearing in the Feynman diagram since the Dirac arrows were inverted. As can be seen from Eq. (E.3), vertices involving only scalars ($\Gamma_i = 1$), or fermion-fermion-scalar interactions (($\Gamma_i = 1, \gamma_5$) do not receive an additional sign. Fermion-fermion-vector interactions are, however, more subtle as they contain $\Gamma_i = \gamma_\mu, \gamma_\mu\gamma_5$, which transform differently under charge conjugation. As a result, we obtain an overall sign for terms proportional to γ^μ and no sign for terms proportional to $\gamma^\mu\gamma_5$. This leads to a switch of left- and right-chiral couplings for these vertices and an overall minus sign.

If we have scalar-scalar-vector interactions, they do not contain any Dirac matrices, but they contain a factor $(p_i + p_f)^\mu$ where p_i is the ingoing and p_j is the outgoing momentum of the scalars, and by reversing the arrow on the charged scalars we also reverse the momenta. Thus, we obtain an additional minus sign, similar to the fermion-fermion-vector interaction.

Finally, one more interaction that we need to consider is the gluino-gluino-gluon vertex. The gluino is a Majorana fermion, thus one would maybe expect no sign change here when considering the charge-conjugated vertex. But the Feynman rule reads $g_s f^{abc}\gamma_\mu$, with the strong coupling constant g_s, f^{abc} the structure constants of $SU(3)$, with a being the ingoing gluino colour index, c the outgoing gluino colour index and b the colour index of the gluon. Thus, we also have to interchange ingoing and outgoing colour indices and pick up a minus sign again. One could consider more vertices, we here focused only on the Feynman rules that appeared in our calculation.

To give an example, we can consider the NLO corrections to the decay $\tilde{\chi}^0 \to q\tilde{q}^*$ of a neutralino into a quark and an anti-squark, given by Fig. 13.3a. Similarly, we can have the decay $\tilde{\chi}^0 \to \bar{q}\tilde{q}$ into an anti-quark and a squark, where the arrows in Fig. 13.3a would be reversed. Given the decay amplitude for the first process, we can use the same result for the decay into the anti-particles, but now we have to use the complex conjugated couplings and interchange the left- and right-chiral couplings at each neutralino-squark-quark and gluino-squark-quark interaction. Additionally, we obtain a minus sign at the gluon-quark-quark vertex and the gluon-squark-squark vertex. Since we have then two minus signs, they cancel each other.

To conclude and summarize, given a particle amplitude, we can keep our chosen fermion flow and amplitude structure. We then have to interchange left- and right-chiral couplings, use the conjugated coupling at each vertex, and at each scalar-scalar-vector or fermion-fermion-vector vertex we pick up an additional minus sign.

APPENDIX F

Counterterms for the QCD Corrections in the NMSSM

In the following, we derive the counterterms needed for the renormalization of the NLO QCD corrections. The Feynman rules were taken from [63]. If dimensional regularization is used in the calculation, the additional contributions described in Sec. 12.4.4 have to be included as well.

In Fig. F.1, we summarized all the couplings that are required in the NLO QCD calculation. The couplings mentioned in the figure are given by

$$C_{\tilde{q}_t\tilde{q}_s Z} = \frac{g_2}{c_{\mathrm{W}}}\left(\sum_{i=1}^{3} T_{3L}^{\tilde{q}} W_{s,2i-1}^{\tilde{q}} W_{t,2i-1}^{\tilde{q}*} - s_{\mathrm{W}}^2 Q_{\tilde{q}}\delta_{st}\right), \tag{F.1a}$$

$$C_{\tilde{q}_t\tilde{q}'_s W} = \frac{g_2}{\sqrt{2}}\left(\sum_{i=1}^{3} W_{s,2i-1}^{\tilde{q}'} W_{t,2i-1}^{\tilde{q}*}\right), \tag{F.1b}$$

for the couplings of squarks to gauge bosons ($s,t = 1,..,6$),

$$C_{isk}^{\mathrm{L}} = \mathcal{U}_{k2}\sum_{j,n=1}^{3} V_{in}^{\mathrm{CKM}} Y_{d_n} U_{nj}^{d_{\mathrm{R}}} W_{s,2j}^{\tilde{d}*} - g_2\mathcal{U}_{k1}\sum_{j=1}^{3} U_{ij}^{u_{\mathrm{L}}} W_{s,2j-1}^{\tilde{d}*} \equiv c_{isk}^{1,\mathrm{L}} + c_{isk}^{2,\mathrm{L}} \tag{F.2a}$$

$$c_{isknp}^{3,\mathrm{L}} \equiv \mathcal{U}_{k2}\sum_{j=1}^{3} V_{ip}^{\mathrm{CKM}} \frac{\sqrt{2}}{v\cos\beta} U_{nj}^{d_{\mathrm{R}}} W_{s,2j}^{\tilde{d}*} \tag{F.2b}$$

$$D_{isk}^{\mathrm{L}} = \mathcal{V}_{k2}\sum_{j,n=1}^{3} V_{ni}^{\mathrm{CKM}*} Y_{u_n} U_{nj}^{u_{\mathrm{R}}} W_{s,2j}^{\tilde{u}*} - g_2\mathcal{V}_{k1}\sum_{j=1}^{3} U_{ij}^{d_{\mathrm{L}}} W_{s,2j-1}^{\tilde{u}*} \equiv d_{isk}^{1,\mathrm{L}} + d_{isk}^{2,\mathrm{L}} \tag{F.2c}$$

$$d_{isknp}^{3,\mathrm{L}} \equiv \mathcal{V}_{k2}\sum_{j=1}^{3} V_{pi}^{\mathrm{CKM}*} \frac{\sqrt{2}}{v\sin\beta} U_{nj}^{u_{\mathrm{R}}} W_{s,2j}^{\tilde{u}*} \tag{F.2d}$$

$$E_{isk}^{\mathrm{R}} = \mathcal{U}_{k2} Y_{d_i}\sum_{j=1}^{3} U_{ij}^{d_{\mathrm{L}}*} W_{s,2j-1}^{\tilde{u}} \equiv m_{d_i} e_{isk}^{\mathrm{R}}, \tag{F.2e}$$

$$F_{isk}^{\mathrm{R}} = \mathcal{V}_{k2} Y_{u_i}\sum_{j=1}^{3} U_{ij}^{u_{\mathrm{L}}*} W_{s,2j-1}^{\tilde{d}} \equiv m_{u_i} f_{isk}^{\mathrm{R}}, \tag{F.2f}$$

for the squark-quark-chargino couplings ($s = 1,..,6,\ i,n,p = 1,2,3,\ k = 1,2$),

$$G^{u_L}_{isl} = -\sqrt{2}g_2\left(\frac{1}{2}Z^*_{l2} + \frac{1}{6}\tan\theta_W Z^*_{l1}\right)\sum_{j=1}^{3} W^{\tilde{u}}_{s,2j-1}U^{u_L *}_{ij} - Y_{u_i}Z^*_{l4}\sum_{j=1}^{3} W^{\tilde{u}}_{s,2j}U^{u_R *}_{ij} \tag{F.3a}$$
$$\equiv g^{1,u_L}_{isl} + m_{u_i}g^{2,u_L}_{isl}\,,$$
$$G^{u_R}_{isl} = \frac{2\sqrt{2}}{3}g_2\tan\theta_W Z_{l1}\sum_{j=1}^{3} W^{\tilde{u}}_{s,2j}U^{u_R *}_{ij} - Y_{u_i}Z_{l4}\sum_{j=1}^{3} W^{\tilde{u}}_{s,2j-1}U^{u_L *}_{ij}\,, \tag{F.3b}$$
$$\equiv g^{1,u_R}_{isl} + m_{u_i}g^{2,u_R}_{isl}\,,$$
$$G^{d_L}_{isl} = \sqrt{2}g_2\left(\frac{1}{2}Z^*_{l2} - \frac{1}{6}\tan\theta_W Z^*_{l1}\right)\sum_{j=1}^{3} W^{\tilde{d}}_{s,2j-1}U^{d_L *}_{ij} - Y_{d_i}Z^*_{l3}\sum_{j=1}^{3} W^{\tilde{d}}_{s,2j}U^{d_R *}_{ij} \tag{F.3c}$$
$$\equiv g^{1,d_L}_{isl} + m_{d_i}g^{2,d_L}_{isl}\,,$$
$$G^{d_R}_{isl} = -\frac{\sqrt{2}}{3}g_2\tan\theta_W Z_{l1}\sum_{j=1}^{3} W^{\tilde{d}}_{s,2j}U^{d_R *}_{ij} - Y_{d_i}Z_{l3}\sum_{j=1}^{3} W^{\tilde{d}}_{s,2j-1}U^{d_L *}_{ij}\,, \tag{F.3d}$$
$$\equiv g^{1,d_R}_{isl} + m_{d_i}g^{2,d_R}_{isl}\,,$$

for the squark-quark-neutralino couplings ($s = 1,..,6,\ i = 1,2,3,\ l = 1,..,5$) and

$$C^{\tilde{g},q_L}_{si} = \sqrt{2}g_s\sum_{j=1}^{3} U^{q_R}_{ij}W^{\tilde{q}*}_{s,2j}\,,\quad C^{\tilde{g},q_R}_{si} = -\sqrt{2}g_s\sum_{j=1}^{3} U^{q_L}_{ij}W^{\tilde{q}*}_{s,2j-1}\,, \tag{F.4}$$

for the squark-quark-gluino couplings ($s = 1,..,6,\ i = 1,2,3$). We omit the scalar couplings as they are rather involved, they can be extracted from the code `NMSSMCALC` [77–82]. In the couplings we have the gauge couplings g_2, g_s, the sine s_W, cosine c_W and tangent of the weak mixing angle θ_W, the weak isospin $T^{\tilde{q}}_{3L}$ and fractional charge $Q_{\tilde{q}}$ of the squarks, the Kronecker delta δ_{st}, the squark rotation matrices $W^{\tilde{q}}$, the CKM matrix V^{CKM}, the chargino rotation matrices $\mathcal{U},\mathcal{V}$, the quark rotation matrices U^{q_L}, U^{q_R} ($q = u,d$), the neutralino rotation matrix Z and the Yukawa couplings Y_{u_i}, Y_{d_i} ($i = 1,..,3$) defined by

$$Y_{u_i} = \frac{m_{u_i}\sqrt{2}}{v\sin\beta}\,,\quad Y_{d_i} = \frac{m_{d_i}\sqrt{2}}{v\cos\beta}\,, \tag{F.5}$$

with the VEV v, the mixing angle β and the up-type and down-type quark masses m_{u_i}, m_{d_i}, respectively. We also introduced abbreviations for parts of the couplings that we will use in the following. We then insert the counterterms for the rotation matrices, the masses and the field renormalization constants. We obtain for the squark-squark-V vertices ($V = W,Z$)

$$\delta C_{\tilde{q}_t\tilde{q}'_s V} = C_{\tilde{q}_w\tilde{q}'_s V}((\delta w^{\tilde{q}}_{tw})^* + \frac{\delta Z^{\tilde{q}}_{wt}}{2}) + C_{\tilde{q}_t\tilde{q}'_w V}(\delta w^{\tilde{q}'}_{sw} + \frac{(\delta Z^{\tilde{q}'}_{ws})^*}{2})\,, \tag{F.6}$$

where the squarks $\tilde{q},\tilde{q}'$ can be of different flavour if the W boson vertex is considered and we implicitly sum over the index $w = 1,..,6$. Next, the counterterms for the squark-squark-scalar couplings read

$$\begin{aligned}\delta C_{\tilde{q}_t\tilde{q}_s\Phi} =& C_{\tilde{q}_t\tilde{q}_w\Phi}(\delta w^{\tilde{q}}_{sw} + \frac{(\delta Z^{\tilde{q}}_{ws})^*}{2}) + C_{\tilde{q}_w\tilde{q}_s\Phi}((\delta w^{\tilde{q}}_{tw})^* + \frac{\delta Z^{\tilde{q}}_{wt}}{2}) \\ &+ \frac{\partial C_{\tilde{q}_t\tilde{q}_s\Phi}}{\partial m_q}\delta m_q + \frac{\partial C_{\tilde{q}_t\tilde{q}_s\Phi}}{\partial A_q}\delta A_q\end{aligned} \tag{F.7a}$$

$$\begin{aligned}\delta C_{\tilde{q}_t\tilde{q}'_s H^\pm} =& C_{\tilde{q}_t\tilde{q}'_w H^\pm}(\delta w^{\tilde{q}'}_{sw} + \frac{(\delta Z^{\tilde{q}'}_{ws})^*}{2}) + C_{\tilde{q}_w\tilde{q}'_s H^\pm}((\delta w^{\tilde{q}}_{tw})^* + \frac{\delta Z^{\tilde{q}}_{wt}}{2}) \\ &+ \frac{\partial C_{\tilde{q}_t\tilde{q}'_s H^\pm}}{\partial m_q}\delta m_q + \frac{\partial C_{\tilde{q}_t\tilde{q}'_s H^\pm}}{\partial m_{q'}}\delta m_{q'} + \frac{\partial C_{\tilde{q}_t\tilde{q}'_s H^\pm}}{\partial A_q}\delta A_q + \frac{\partial C_{\tilde{q}_t\tilde{q}'_s H^\pm}}{\partial A_{q'}}\delta A_{q'}\,,\end{aligned} \tag{F.7b}$$

where also the quark mass counterterm and the A_q counterterm are inserted, since the coupling can also depend on these input parameters and we again sum over the index w. The labels q, q' here indicate the corresponding quark flavour to the considered squarks and Φ denotes the five neutral scalars.

Next, we have the squark-quark-neutralino counterterms,

$$\begin{aligned}\delta G^{q_\mathrm{L}}_{isl} &= g^{2,q_\mathrm{L}}_{isl}\delta m_{q_i} + G^{q_\mathrm{L}}_{iwl}(\delta w^{\tilde{q}}_{sw} + \frac{(\delta Z^{\tilde{q}}_{ws})^*}{2}) \\ &\quad + g^{1,q_\mathrm{L}}_{msl}((\delta u^{q_\mathrm{L}}_{im})^* + \frac{\delta Z^{q_\mathrm{L}}_{mi}}{2}) + g^{2,q_\mathrm{L}}_{msl}(m_{q_i}(\delta u^{q_\mathrm{R}}_{im})^* + m_{q_m}\frac{\delta Z^{q_\mathrm{L}}_{mi}}{2}) \end{aligned} \tag{F.8a}$$

$$\begin{aligned}\delta G^{q_\mathrm{R}}_{isl} &= g^{2,q_\mathrm{R}}_{isl}\delta m_{q_i} + G^{q_\mathrm{R}}_{iwl}(\delta w^{\tilde{q}}_{sw} + \frac{(\delta Z^{\tilde{q}}_{ws})^*}{2}) \\ &\quad + g^{1,q_\mathrm{R}}_{msl}((\delta u^{q_\mathrm{R}}_{im})^* + \frac{\delta Z^{q_\mathrm{R}}_{mi}}{2}) + g^{2,q_\mathrm{R}}_{msl}(m_{q_i}(\delta u^{q_\mathrm{L}}_{im})^* + m_{q_m}\frac{\delta Z^{q_\mathrm{R}}_{mi}}{2})\,, \end{aligned} \tag{F.8b}$$

and the squark-quark-gluino counterterms,

$$\begin{aligned}\delta C^{\tilde{g},q_\mathrm{L}}_{si} &= C^{\tilde{g},q_\mathrm{L}}_{si}\frac{\delta Z^{\tilde{g}_\mathrm{L}}}{2} + C^{\tilde{g},q_\mathrm{L}}_{wi}((\delta w^{\tilde{q}}_{sw})^* + \frac{\delta Z^{\tilde{q}}_{ws}}{2}) \\ &\quad + C^{\tilde{g},q_\mathrm{L}}_{sm}(\delta u^{q_\mathrm{R}}_{im} + \frac{(\delta Z^{q_\mathrm{R}}_{mi})^*}{2}) + \frac{\delta g_s}{g_s}C^{\tilde{g},q_\mathrm{L}}_{si}\,, \end{aligned} \tag{F.9a}$$

$$\begin{aligned}\delta C^{\tilde{g},q_\mathrm{R}}_{si} &= C^{\tilde{g},q_\mathrm{R}}_{si}\frac{\delta Z^{\tilde{g}_\mathrm{R}}}{2} + C^{\tilde{g},q_\mathrm{R}}_{wi}((\delta w^{\tilde{q}}_{sw})^* + \frac{\delta Z^{\tilde{q}}_{ws}}{2}) \\ &\quad + C^{\tilde{g},q_\mathrm{R}}_{sm}(\delta u^{q_\mathrm{L}}_{im} + \frac{(\delta Z^{q_\mathrm{L}}_{mi})^*}{2}) + \frac{\delta g_s}{g_s}C^{\tilde{g},q_\mathrm{R}}_{si}\,, \end{aligned} \tag{F.9b}$$

where we sum over the indices $m = 1, 2, 3$ and $w = 1, .., 6$. Finally, the squark-quark-chargino counterterms read

$$\delta E^{\mathrm{R}}_{isk} = e^{\mathrm{R}}_{isk}\delta m_{d_i} + E^{\mathrm{R}}_{iwk}((\delta w^{\tilde{u}}_{sw})^* + \frac{\delta Z^{\tilde{u}}_{ws}}{2}) + e^{\mathrm{R}}_{msk}(m_{d_i}(\delta u^{d_\mathrm{L}}_{im})^* + \frac{\delta Z^{d_\mathrm{R}}_{mi}}{2})\,, \tag{F.10a}$$

$$\begin{aligned}\delta D^{\mathrm{L}}_{isk} &= D^{\mathrm{L}}_{iwk}((\delta w^{\tilde{u}}_{sw})^* + \frac{\delta Z^{\tilde{u}}_{ws}}{2}) + d^{3,\mathrm{L}}_{iskmm}\delta m_{u_m} + D^{\mathrm{L}}_{mwk}(\delta u^{d_\mathrm{L}}_{im} + \frac{(\delta Z^{d_\mathrm{L}}_{mi})^*}{2}) \\ &\quad + d^{3,\mathrm{L}}_{iskmp}(m_{u_m}(\delta u^{u_\mathrm{L}}_{mp})^* + m_{u_p}\delta u^{u_\mathrm{R}}_{pm})\,, \end{aligned} \tag{F.10b}$$

$$\delta F^{\mathrm{R}}_{isk} = f^{\mathrm{R}}_{isk}\delta m_{u_i} + F^{\mathrm{R}}_{iwk}((\delta w^{\tilde{d}}_{sw})^* + \frac{\delta Z^{\tilde{d}}_{ws}}{2}) + f^{\mathrm{R}}_{msk}(m_{u_i}(\delta u^{u_\mathrm{L}}_{im})^* + \frac{\delta Z^{u_\mathrm{R}}_{mi}}{2})\,, \tag{F.10c}$$

$$\begin{aligned}\delta C^{\mathrm{L}}_{isk} &= C^{\mathrm{L}}_{iwk}((\delta w^{\tilde{d}}_{sw})^* + \frac{\delta Z^{\tilde{d}}_{ws}}{2}) + c^{3,\mathrm{L}}_{iskmm}\delta m_{d_m} + C^{\mathrm{L}}_{mwk}(\delta u^{u_\mathrm{L}}_{im} + \frac{(\delta Z^{u_\mathrm{L}}_{mi})^*}{2}) \\ &\quad + c^{3,\mathrm{L}}_{iskmp}(m_{d_m}(\delta u^{d_\mathrm{L}}_{mp})^* + m_{d_p}\delta u^{d_\mathrm{R}}_{pm})\,, \end{aligned} \tag{F.10d}$$

where we sum over $m, p = 1, 2, 3$ and $w = 1, .., 6$. In this notation, we can see how we can apply the limits described in Sec. 12.4.2 in the case of vanishing quark masses or degenerate squark masses.

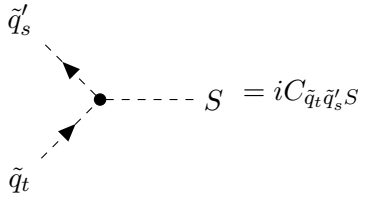

(a) Feynman rule for the squark-squark-scalar interaction with coupling $C_{\tilde{q}_t\tilde{q}'_s S}$ $(t, s = 1, .., 6)$, where S can be a neutral or charged scalar.

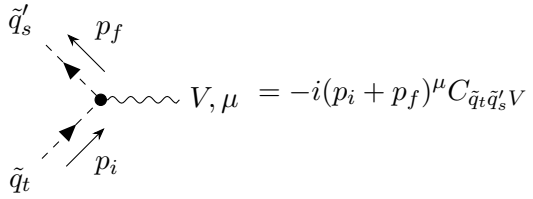

(b) Feynman rule for the squark-squark-boson interaction with coupling $C_{\tilde{q}_t\tilde{q}'_s V}$ $(t, s = 1, .., 6)$ and $V = W, Z$.

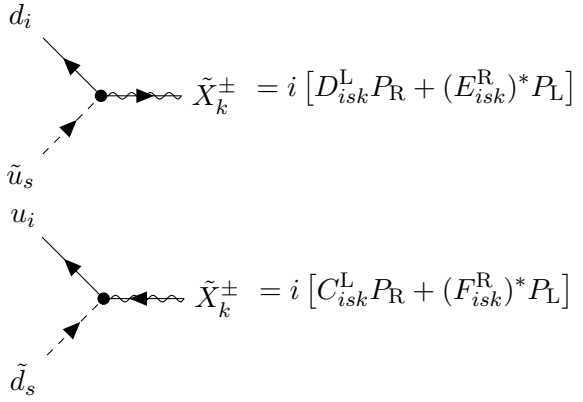

(c) Feynman rule for the squark-quark-chargino interaction with couplings D^{L}_{isk}, E^{R}_{isk}, C^{L}_{isk}, F^{R}_{isk} $(s = 1, .., 6,\ i = 1, 2, 3,\ k = 1, 2)$ and up-type and down-type quarks (squarks) denoted with u $(\tilde{u})$ and d $(\tilde{d})$, respectively. We omit here the charge conjugation matrices and instead use the approach in [304].

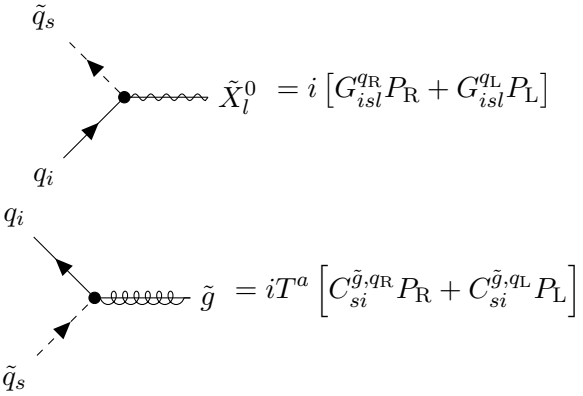

(d) Feynman rules for the quark-squark-neutralino and quark-squark-gluino interaction with couplings $G^{q_{\mathrm{R}}}_{isl}$, $G^{q_{\mathrm{L}}}_{isl}$, $C^{\tilde{g},q_{\mathrm{R}}}_{si}$,$C^{\tilde{g},q_{\mathrm{L}}}_{si}$ $(s = 1, .., 6,\ i = 1, 2, 3,\ l = 1, .., 5)$. The T^a are the generators of the $SU(3)_c$ group.

Figure F.1.: Feynman rules of all couplings that have to be renormalized for the QCD corrections. The definitions of all couplings are given in the Eqs. (F.1), (F.2), (F.3) and (F). Taken from [63].

APPENDIX G

Analytic Expressions for the NLO QCD Corrections and the Radiative Decays in the NMSSM

In the following, we give analytic expressions for the counterterms, the NLO vertex corrections, the real corrections and the radiative two-body decays described in Chapter 13. The expressions were derived using dimensional regularization and can be translated to the expressions obtained in dimensional reduction with the help of the transition counterterms described in Sec. 12.4.4.

G.1. Analytic Expressions for the NLO QCD Corrections

G.1.1. Counterterms

We start with the description of the counterterms. The squark-quark-gluino couplings are denoted as $C^{\tilde{g},q_\mathrm{L}/q_\mathrm{R}}$ for the left- and right-chiral parts (see also Fig. F.1), α_s is the strong coupling constant, λ is the gluon mass introduced to regulate the IR divergences, and ξ_g is the gauge parameter of the gluon in the R_ξ-gauge. The definitions of the counterterms are given in Eqs. (12.30) and (12.31). We also use the Passarino-Veltman decomposition of one-loop integrals [200, 210, 211]. The symbol $\widetilde{\mathrm{Re}}$ indicates that we only take the real part of the loop integrals and not the couplings. All the couplings needed for the calculation were taken from [63] and [302].

We start with the counterterms for the quarks. We will always split up the expression into the several contributions from the self-energy diagrams, indicated with a label in brackets. Thus, the quark mass and wave function renormalization counterterms can be written as

$$\delta m_{q_i} = \delta m_{q_i}^{(g)} + \delta m_{q_i}^{(\tilde{g})}\,, \tag{G.1a}$$

$$\delta Z_{ii}^{q,\mathrm{L/R}} = \delta Z_{ii}^{q,\mathrm{L/R}(g)} + \delta Z_{ii}^{q,\mathrm{L/R}(\tilde{g})}\,, \tag{G.1b}$$

$$\delta Z_{ij}^{q,\mathrm{L/R}} = \delta Z_{ij}^{q,\mathrm{L/R}(g)} + \delta Z_{ij}^{q,\mathrm{L/R}(\tilde{g})}\,(i \neq j)\,, \tag{G.1c}$$

with $i,j = 1,2,3$ and (g) denoting the self-energy diagram with the gluon loop and $\tilde{g}$ the self-energy diagram with the gluino in the loop (compare with Fig. 12.1b).

The contributions to the quark mass counterterm are given by

$$\delta m_{q_i}^{(g)} = \widetilde{\mathrm{Re}}\left[-\frac{\alpha_s}{\pi}\left(\frac{A_0(m_{q_i}^2))}{m_{q_i}} + \frac{m_{q_i}}{3}\right)\right], \tag{G.2a}$$

$$\begin{aligned}\delta m_{q_i}^{(\tilde{g})} = \widetilde{\mathrm{Re}}\Bigg[\sum_{l=1}^{6}\frac{\alpha_s}{12 m_{q_i}\pi}\Big((-A_0(m_{\tilde{g}}^2)+A_0(m_{\tilde{q}_l}^2))(|C_{li}^{\tilde{g},q_\mathrm{L}}|^2+|C_{li}^{\tilde{g},q_\mathrm{R}}|^2)\\ +B_0(m_{q_i}^2,m_{\tilde{g}}^2,m_{\tilde{q}_l}^2)\Big((|C_{li}^{\tilde{g},q_\mathrm{L}}|^2+|C_{li}^{\tilde{g},q_\mathrm{R}}|^2)(m_{q_i}^2-m_{\tilde{q}_l}^2+m_{\tilde{g}}^2)\\ +4m_{\tilde{g}}m_{q_i}\mathrm{Re}\left(C_{li}^{\tilde{g},q_\mathrm{L}}(C_{li}^{\tilde{g},q_\mathrm{R}})^*\right)\Big)\Big)\Bigg],\end{aligned} \tag{G.2b}$$

where we sum over the squarks $\tilde{q}_l$ in the loop. The wave function renormalization counterterms are given by

$$\begin{aligned}\delta Z_{ii}^{q,\mathrm{L}(g)} = \widetilde{\mathrm{Re}}\Bigg[\frac{\alpha_s}{3\pi}\Bigg(-\frac{A_0(m_{q_i}^2)}{m_{q_i}^2}+B_0(0,\lambda^2,\lambda^2)(1-\xi_g)\\ +4m_{q_i}^2 DB_0(m_{q_i}^2,\lambda^2,m_{q_i}^2)+1\Big)\Bigg],\end{aligned} \tag{G.3a}$$

$$\begin{aligned}\delta Z_{ii}^{q,\mathrm{L}(\tilde{g})} = \widetilde{\mathrm{Re}}\Bigg[\sum_{l=1}^{6}\frac{\alpha_s}{6\pi}\Bigg(\frac{-A_0(m_{\tilde{g}}^2)+A_0(m_{\tilde{q}_l}^2)}{m_{q_i}^2}|C_{li}^{\tilde{g},q_\mathrm{L}}|^2\\ -\frac{B_0(m_{q_i}^2,m_{\tilde{g}}^2,m_{\tilde{q}_l}^2)}{m_{q_i}^2}\left((m_{\tilde{q}_l}^2-m_{\tilde{g}}^2)|C_{li}^{\tilde{g},q_\mathrm{L}}|^2+m_{q_i}^2|C_{li}^{\tilde{g},q_\mathrm{R}}|^2\right)\\ -DB_0(m_{q_i}^2,m_{\tilde{g}}^2,m_{\tilde{q}_l}^2)\Big((|C_{li}^{\tilde{g},q_\mathrm{L}}|^2+|C_{li}^{\tilde{g},q_\mathrm{R}}|^2)(m_{q_i}^2-m_{\tilde{q}_l}^2+m_{\tilde{g}}^2)\\ +4m_{\tilde{g}}m_{q_i}\mathrm{Re}\left(C_{li}^{\tilde{g},q_\mathrm{L}}(C_{li}^{\tilde{g},q_\mathrm{R}})^*\right)\Big)\Bigg],\end{aligned} \tag{G.3b}$$

$$\delta Z_{ii}^{q,\mathrm{R}(g)} = \delta Z_{ii}^{q,\mathrm{L}(g)}, \tag{G.3c}$$

$$\delta Z_{ii}^{q,\mathrm{R}(\tilde{g})} = \delta Z_{ii}^{q,\mathrm{L}(\tilde{g})}(C^{\tilde{g},q_\mathrm{L}} \leftrightarrow C^{\tilde{g},q_\mathrm{R}}), \tag{G.3d}$$

for the diagonal part, where we obtain the $\delta Z_{ii}^{q,\mathrm{R}(\tilde{g})}$ by interchanging the left- and right-chiral couplings in $\delta Z_{ii}^{q,\mathrm{L}(\tilde{g})}$. The off-diagonal contributions are given by

$$\delta Z_{ij}^{q,\mathrm{L}(g)} = \delta Z_{ij}^{q,\mathrm{R}(g)} = 0, \tag{G.4a}$$

$$\begin{aligned}\delta Z_{ij}^{q,\mathrm{L}(\tilde{g})} = \widetilde{\mathrm{Re}}\Bigg[\sum_{l=1}^{6}\frac{\alpha_s}{3\pi}\frac{1}{m_{q_i}^2-m_{q_j}^2}\\ \Bigg(\frac{(-A_0(m_{\tilde{g}}^2)+A_0(m_{\tilde{q}_l}^2))(m_{q_i}C_{lj}^{\tilde{g},\mathrm{L}}(C_{li}^{\tilde{g},q_\mathrm{L}})^*+m_{q_j}C_{lj}^{\tilde{g},q_\mathrm{R}}(C_{li}^{\tilde{g},\mathrm{R}})^*)}{m_{q_j}}\\ -\frac{B_0(m_{q_j}^2,m_{\tilde{g}}^2,m_{\tilde{q}_l}^2)}{m_{q_j}}\Big(m_{q_i}C_{lj}^{\tilde{g},q_\mathrm{L}}((C_{li}^{\tilde{g},q_\mathrm{L}})^*(m_{q_j}^2-m_{\tilde{q}_l}^2+m_{\tilde{g}}^2)+2m_{\tilde{g}}m_{q_j}(C_{li}^{\tilde{g},q_\mathrm{R}})^*)\\ +m_{q_j}C_{lj}^{\tilde{g},q_\mathrm{R}}((C_{li}^{\tilde{g},q_\mathrm{R}})^*(m_{q_j}^2-m_{\tilde{q}_l}^2+m_{\tilde{g}}^2)+2m_{\tilde{g}}m_{q_j}(C_{li}^{\tilde{g},q_\mathrm{L}})^*)\Big)\Bigg],\end{aligned} \tag{G.4b}$$

$$\begin{aligned}\delta Z_{ij}^{q,\mathrm{R}(\tilde{g})} = \widetilde{\mathrm{Re}}\Bigg[\sum_{l=1}^{6}\frac{\alpha_s}{3\pi}\frac{1}{m_{q_i}^2-m_{q_j}^2}\\ \Bigg(\frac{(-A_0(m_{\tilde{g}}^2)+A_0(m_{\tilde{q}_l}^2))(m_{q_j}C_{lj}^{\tilde{g},q_\mathrm{L}}(C_{li}^{\tilde{g},q_\mathrm{L}})^*+m_{q_i}C_{lj}^{\tilde{g},q_\mathrm{R}}(C_{li}^{\tilde{g},q_\mathrm{R}})^*)}{m_{q_j}}\\ -\frac{B_0(m_{q_j}^2,m_{\tilde{g}}^2,m_{\tilde{q}_l}^2)}{m_{q_j}}\Big(m_{q_j}(C_{li}^{\tilde{g},q_\mathrm{L}})^*(C_{lj}^{\tilde{g},q_\mathrm{L}}(m_{q_j}^2-m_{\tilde{q}_l}^2+m_{\tilde{g}}^2)+2m_{\tilde{g}}m_{q_i}C_{lj}^{\tilde{g},q_\mathrm{R}})\end{aligned} \tag{G.4c}$$

$$+(C_{li}^{\tilde{g},q_\mathrm{R}})^*(m_{q_i}C_{lj}^{\tilde{g},q_\mathrm{R}}(m_{q_j}^2-m_{\tilde{q}_l}^2+m_{\tilde{g}}^2)+2m_{\tilde{g}}m_{q_j}^2C_{lj}^{\tilde{g},q_\mathrm{L}})\Big)\Big)\Big]\,.$$

Next, we have the gluino counterterms, that can be split up into

$$\delta m_{\tilde{g}} = \delta m_{\tilde{g}}^{(g)} + \delta m_{\tilde{g}}^{(\tilde{q})}\,, \tag{G.5a}$$

$$\delta Z^{\tilde{g},\mathrm{L/R}} = \delta Z^{\tilde{g},\mathrm{L/R}(g)} + \delta Z^{\tilde{g},\mathrm{L/R}(\tilde{q})}\,, \tag{G.5b}$$

where we have the gluon contribution indicated by (g) and the squark-quark loop by $(\tilde{q})$ (compare with Fig. 12.1c). Since the gluino is a Majorana fermion we furthermore have

$$\delta Z^{\tilde{g},\mathrm{L}} = \delta Z^{\tilde{g},\mathrm{R}}\,. \tag{G.6}$$

The individual contributions for the mass counterterm are given by

$$\delta m_{\tilde{g}}^{(g)} = \widetilde{\mathrm{Re}}\left[\frac{\alpha_s}{4\pi}\left(-\frac{9A_0(m_{\tilde{g}}^2)}{m_{\tilde{g}}}-3m_{\tilde{g}}\right)\right]\,, \tag{G.7a}$$

$$\begin{aligned}\delta m_{\tilde{g}}^{(\tilde{q})} = \widetilde{\mathrm{Re}}\Bigg[&\sum_{q=u,d}\sum_{l=1}^{6}\sum_{m=1}^{3}\frac{\alpha_s}{16\pi}\frac{1}{m_{\tilde{g}}}\Big((-A_0(m_{q_m}^2)+A_0(m_{\tilde{q}_l}^2))(|C_{lm}^{\tilde{g},q_\mathrm{L}}|^2+|C_{lm}^{\tilde{g},q_\mathrm{R}}|^2)\\ &+B_0(m_{\tilde{g}}^2,m_{q_m}^2,m_{\tilde{q}_l}^2)\Big((|C_{lm}^{\tilde{g},q_\mathrm{L}}|^2+|C_{lm}^{\tilde{g},q_\mathrm{R}}|^2)(-m_{\tilde{q}_l}^2+m_{q_m}^2+m_{\tilde{g}}^2)\\ &+4m_{\tilde{g}}m_{q_m}\mathrm{Re}\left(C_{lm}^{\tilde{g},q_\mathrm{L}}(C_{lm}^{\tilde{g},q_\mathrm{R}})^*\right)\Big)\Big)\Bigg]\,,\end{aligned} \tag{G.7b}$$

where we sum over the up- and down-type quarks and squarks. The contributions to the wave function renormalization counterterm are given by

$$\begin{aligned}\delta Z^{\tilde{g},\mathrm{L}(g)} = \widetilde{\mathrm{Re}}\Bigg[&\frac{3\alpha_s}{4\pi}\Bigg(-\frac{A_0(m_{\tilde{g}}^2))}{m_{\tilde{g}}^2}+B_0(0,\lambda^2,\lambda^2)(1-\xi_g)\\ &+4m_{\tilde{g}}^2DB0(m_{\tilde{g}}^2,\lambda^2,m_{\tilde{g}}^2)+1\Big)\Bigg]\,,\end{aligned} \tag{G.8a}$$

$$\begin{aligned}\delta Z^{\tilde{g},\mathrm{L}(\tilde{q})} = \widetilde{\mathrm{Re}}\Bigg[&\sum_{q=u,d}\sum_{l=1}^{6}\sum_{m=1}^{3}\frac{\alpha_s}{16\pi}\Bigg(\frac{-A_0(m_{q_m}^2)+A_0(m_{\tilde{q}_l}^2)}{m_{\tilde{g}}^2}(|C_{lm}^{\tilde{g},q_\mathrm{L}}|^2+|C_{lm}^{\tilde{g},q_\mathrm{R}}|^2)\\ &-\frac{B_0(m_{\tilde{g}}^2,m_{q_m}^2,m_{\tilde{q}_l}^2)}{m_{\tilde{g}}^2}(|C_{lm}^{\tilde{g},q_\mathrm{L}}|^2+|C_{lm}^{\tilde{g},q_\mathrm{R}}|^2)(-m_{q_m}^2+m_{\tilde{q}_l}^2+m_{\tilde{g}}^2)\\ &-2DB_0(m_{\tilde{g}}^2,m_{q_m}^2,m_{\tilde{q}_l}^2)\Big((|C_{lm}^{\tilde{g},q_\mathrm{L}}|^2+|C_{lm}^{\tilde{g},q_\mathrm{R}}|^2)(-m_{\tilde{q}_l}^2+m_{q_m}^2+m_{\tilde{g}}^2)\\ &+4m_{\tilde{g}}m_{q_m}\mathrm{Re}\left(C_{lm}^{\tilde{g},q_\mathrm{L}}(C_{lm}^{\tilde{g},q_\mathrm{R}})^*\right)\Big)\Big)\Bigg]\,.\end{aligned} \tag{G.8b}$$

Finally, the squark counterterms can be split up into

$$\delta m_{\tilde{q}_s}^2 = \delta m_{\tilde{q}_s}^{2\,(g)} + \delta m_{\tilde{q}_s}^{2\,(\tilde{g})} + \delta m_{\tilde{q}_s}^{2\,(\tilde{q})}\,, \tag{G.9a}$$

$$\delta Z_{ss}^{\tilde{q}} = \delta Z_{ss}^{\tilde{q}(g)} + \delta Z_{ss}^{\tilde{q}(\tilde{g})} + \delta Z_{ss}^{\tilde{q}(\tilde{q})}\,, \tag{G.9b}$$

$$\delta Z_{st}^{\tilde{q}} = \delta Z_{st}^{\tilde{q}(g)} + \delta Z_{st}^{\tilde{q}(\tilde{g})} + \delta Z_{st}^{\tilde{q}(\tilde{q})}\,(s\neq t)\,, \tag{G.9c}$$

with $s,t=1,..,6$ and we have the gluon (g), the gluino $(\tilde{g})$ and the squark $(\tilde{q})$ contribution (compare with Fig. 12.1a). The contributions to the squark mass counterterm read

$$\delta m_{\tilde{q}_s}^{2\,(g)} = \widetilde{\mathrm{Re}}\left[\frac{\alpha_s}{\pi}\left(-A_0(m_{\tilde{q}_s}^2)-\frac{4m_{\tilde{q}_s}^2}{3}\right)\right]\,, \tag{G.10a}$$

$$\delta m^{2\,(\tilde{g})}_{\tilde{q}_s} = \widetilde{\mathrm{Re}}\left[\sum_{m=1}^{3}\frac{\alpha_s}{3\pi}\left((-A_0(m^2_{\tilde{g}})-A_0(m^2_{q_m}))(|C^{\tilde{g},q_\mathrm{L}}_{sm}|^2+|C^{\tilde{g},q_\mathrm{R}}_{sm}|^2)\right.\right. \tag{G.10b}$$
$$-B_0(m^2_{\tilde{q}_s},m^2_{\tilde{g}},m^2_{q_m})\left((|C^{\tilde{g},q_\mathrm{L}}_{sm}|^2+|C^{\tilde{g},q_\mathrm{R}}_{sm}|^2)(m^2_{q_m}-m^2_{\tilde{q}_s}+m^2_{\tilde{g}})\right.$$
$$\left.\left.\left.+4m_{\tilde{g}}m_{q_m}\mathrm{Re}\left(C^{\tilde{g},q_\mathrm{L}}_{sm}(C^{\tilde{g},q_\mathrm{R}}_{sm})^*\right)\right)\right)\right]\,,$$
$$\delta m^{2\,(\tilde{q})}_{\tilde{q}_s} = \frac{\alpha_s}{4\pi}\sum_{l=1}^{6}A_0(m^2_{\tilde{q}_l})C_{\tilde{q}_s\tilde{q}_l\tilde{q}_s\tilde{q}_l}\,, \tag{G.10c}$$

where we have the quartic squark couplings $C_{\tilde{q}_s\tilde{q}_l\tilde{q}_s\tilde{q}_l}$ that we took from [63]. The contributions to the diagonal wave function renormalization counterterms read

$$\delta Z^{\tilde{q},(g)}_{ss} = \widetilde{\mathrm{Re}}\left[\frac{\alpha_s}{3\pi}\left(\frac{2A_0(m^2_{\tilde{q}_s})}{m^2_{\tilde{q}_s}}+B_0(0,\lambda^2,\lambda^2)(1-\xi_g)\right.\right. \tag{G.11a}$$
$$\left.\left.+4m^2_{\tilde{q}_s}DB_0(m^2_{\tilde{q}_s},\lambda^2,m^2_{\tilde{q}_s})+2\right)\right]\,,$$
$$\delta Z^{\tilde{q},(\tilde{g})}_{ss} = \widetilde{\mathrm{Re}}\left[\sum_{m=1}^{3}\frac{\alpha_s}{3\pi}\left(-B_0(m^2_{\tilde{q}_s},m^2_{\tilde{g}},m^2_{q_m})(|C^{\tilde{g},q_\mathrm{L}}_{sm}|^2+|C^{\tilde{g},q_\mathrm{R}}_{sm}|^2)\right.\right. \tag{G.11b}$$
$$+DB_0(m^2_{\tilde{q}_s},m^2_{\tilde{g}},m^2_{q_m})\left((|C^{\tilde{g},q_\mathrm{L}}_{sm}|^2+|C^{\tilde{g},q_\mathrm{R}}_{sm}|^2)(m^2_{q_m}-m^2_{\tilde{q}_s}+m^2_{\tilde{g}})\right.$$
$$\left.\left.\left.+4m_{\tilde{g}}m_{q_m}\mathrm{Re}\left(C^{\tilde{g},q_\mathrm{L}}_{sm}(C^{\tilde{g},q_\mathrm{R}}_{sm})^*\right)\right)\right)\right]\,,$$
$$\delta Z^{\tilde{q},(\tilde{q})}_{ss} = 0\,. \tag{G.11c}$$

The off-diagonal contributions are given by

$$\delta Z^{\tilde{q},(g)}_{st} = 0\,, \tag{G.12a}$$
$$\delta Z^{\tilde{q},(\tilde{g})}_{st} = \widetilde{\mathrm{Re}}\left[\sum_{m=1}^{3}\frac{2\alpha_s}{3\pi}\frac{1}{m^2_{\tilde{q}_s}-m^2_{\tilde{q}_t}}\right. \tag{G.12b}$$
$$\left(\left(-A_0(m^2_{\tilde{g}})-A_0(m^2_{q_m})\right)\left(C^{\tilde{g},q_\mathrm{L}}_{sm}(C^{\tilde{g},q_\mathrm{L}}_{tm})^*+C^{\tilde{g},q_\mathrm{R}}_{sm}(C^{\tilde{g},q_\mathrm{R}}_{tm})^*\right)\right.$$
$$-B_0(m^2_{\tilde{q}_t},m^2_{\tilde{g}},m^2_{q_m})\left(C^{\tilde{g},q_\mathrm{L}}_{sm}((C^{\tilde{g},q_\mathrm{L}}_{tm})^*(m^2_{q_m}-m^2_{\tilde{q}_t}+m^2_{\tilde{g}})+2m_{\tilde{g}}m_{q_m}(C^{\tilde{g},q_\mathrm{R}}_{tm})^*)\right.$$
$$\left.\left.\left.+C^{\tilde{g},q_\mathrm{R}}_{sm}((C^{\tilde{g},q_\mathrm{R}}_{tm})^*(m^2_{q_m}-m^2_{\tilde{q}_t}+m^2_{\tilde{g}})+2m_{\tilde{g}}m_{q_m}(C^{\tilde{g},q_\mathrm{L}}_{tm})^*)\right)\right)\right]\,,$$
$$\delta Z^{\tilde{q},(\tilde{q})}_{st} = \widetilde{\mathrm{Re}}\left[\frac{\alpha_s}{2\pi}\frac{1}{m^2_{\tilde{q}_s}-m^2_{\tilde{q}_t}}\sum_{l=1}^{6}A_0(m^2_{\tilde{q}_l})C_{\tilde{q}_s\tilde{q}_l\tilde{q}_t\tilde{q}_l}\right]\,. \tag{G.12c}$$

G.1.2. Vertex Corrections

We now give the analytic expressions of the vertex corrections of the NLO QCD corrections to the decay widths. First, we give a brief description of the absorptive corrections presented in Sec. 13.3.2. They consist of the off-diagonal squark self-energy contribution, where we only take the imaginary part of the loop integrals, times the LO amplitude of the process, times the squark propagator, where we then have to be careful with the squark indices (compare with Fig. 13.5). The necessary squark self-energy contribution reads

$$\widetilde{\mathrm{Im}}\Sigma^{\tilde{q}}_{sl}(p^2) = \sum_{m=1}^{3}-\frac{g_s^2}{12\pi^2}\left[\mathrm{Im}\left(B_0(p^2,m^2_{\tilde{g}},m^2_{q_m})\right)\right. \tag{G.13}$$
$$\left(C^{\tilde{g},q_\mathrm{L}}_{sm}((C^{\tilde{g},q_\mathrm{L}}_{lm})^*(m^2_{q_m}+m^2_{\tilde{g}}-p^2)+2m_{\tilde{g}}m_{q_m}(C^{\tilde{g},q_\mathrm{R}}_{lm})^*)\right.$$
$$\left.\left.+C^{\tilde{g},q_\mathrm{R}}_{sm}((C^{\tilde{g},q_\mathrm{R}}_{lm})^*(m^2_{q_m}+m^2_{\tilde{g}}-p^2)+2m_{\tilde{g}}m_{q_m}(C^{\tilde{g},q_\mathrm{L}}_{lm})^*)\right)\right]\,,$$

where we have $s, l = 1, .., 6$, $m = 1, .., 3$ and $s \neq l$ for an ingoing squark s and an outgoing squark l and the momentum p. For a given decay process, we then have to add this contribution for ingoing and outgoing squarks and set the momentum on-shell to the corresponding squark mass, and we have to sum over the intermediate squarks.

We now describe the vertex corrections. We start with the neutralino/chargino vertex corrections, that are depicted in Fig. 13.3a. We use here again the generic notation $\tilde{\chi}$ that can denote a neutralino or chargino ($\tilde{\chi} = \tilde{\chi}^0, \tilde{\chi}^\pm$) and we thus have the generic couplings $C^{\tilde{\chi},q_\mathrm{L}/q_\mathrm{R}}_{nti}$ for the left- and right-chiral couplings between a squark $\tilde{q}'_t$, a quark q_n and a neutralino/chargino $\tilde{\chi}_i$, where $t = 1, .., 6$, $n = 1, 2, 3$ and $i = 1, .., 5$ for neutralinos or $i = 1, 2$ for charginos that we took from [63].

Comparing with Eq. (5.1b), the NLO correction to the decay width can be written as

$$\Delta\Gamma^{\mathrm{NLO}}_{\tilde{\chi}_i \to q'_n \tilde{q}^*_t} = \lambda(m^2_{\tilde{\chi}_i}, m^2_{q'_n}, m^2_{\tilde{q}_t}) \frac{1}{16\pi m^3_{\tilde{\chi}_i}} \frac{1}{2} \sum_{\mathrm{spin,colour}} 2\mathrm{Re}\left[\left(\mathcal{A}^{\mathrm{LO}}_{\tilde{\chi}_i \to q'_n \tilde{q}^*_t}\right)^* \mathcal{A}^{\mathrm{NLO}}_{\tilde{\chi}_i \to q'_n \tilde{q}^*_t}\right], \tag{G.14}$$

where we average and sum over the spin and the colour factor and λ is the Källén function. With $\mathcal{A}^{\mathrm{LO}}$ we denote the LO amplitude and with $\mathcal{A}^{\mathrm{NLO}}$ the sum of all NLO amplitudes. We then define the quantity

$$\mathcal{D}_{\tilde{\chi}_i \to q'_n \tilde{q}^*_t} \equiv \sum_{\mathrm{spin,colour}} \left[\left(\mathcal{A}^{\mathrm{LO}}_{\tilde{\chi}_i \to q'_n \tilde{q}^*_t}\right)^* \mathcal{A}^{\mathrm{NLO}}_{\tilde{\chi}_i \to q'_n \tilde{q}^*_t}\right], \tag{G.15}$$

that we split up into the several contributions,

$$\mathcal{D}_{\tilde{\chi}_i \to q'_n \tilde{q}^*_t} = \mathcal{D}^{(g)}_{\tilde{\chi}_i \to q'_n \tilde{q}^*_t} + \mathcal{D}^{(\tilde{g})}_{\tilde{\chi}_i \to q'_n \tilde{q}^*_t} + \mathcal{D}^{(\mathrm{abs})}_{\tilde{\chi}_i \to q'_n \tilde{q}^*_t}, \tag{G.16}$$

with the gluon contribution (g), the gluino contribution ($\tilde{g}$) and the absorptive corrections (abs) that were already discussed above. The gluon contribution can be written as

$$\begin{aligned}
&\mathcal{D}^{(g)}_{\tilde{\chi}_i \to q'_n \tilde{q}^*_t} = \frac{3g_s^2}{6\pi^2} [\qquad\qquad (\mathrm{G.17})\\
&- m_{\tilde{\chi}_i} B_0(m^2_{\tilde{\chi}_i}, m^2_{q'_n}, m^2_{\tilde{q}_t}) \left(m_{\tilde{\chi}_i} (|C^{\tilde{\chi},q'_\mathrm{L}}_{nti}|^2 + |C^{\tilde{\chi},q'_\mathrm{R}}_{nti}|^2) + 2m_{q_n} \mathrm{Re}\left(C^{\tilde{\chi},q'_\mathrm{L}}_{nti} (C^{\tilde{\chi},q'_\mathrm{R}}_{nti})^* \right) \right)\\
&+ B_0(m^2_{q'_n}, 0, m^2_{q'_n}) \left((m^2_{\tilde{\chi}_i} - m^2_{\tilde{q}_t})(|C^{\tilde{\chi},q'_\mathrm{L}}_{nti}|^2 + |C^{\tilde{\chi},q'_\mathrm{R}}_{nti}|^2) + 2m_{\tilde{\chi}_i} m_{q'_n} \mathrm{Re}\left(C^{\tilde{\chi},q'_\mathrm{L}}_{nti} (C^{\tilde{\chi},q'_\mathrm{R}}_{nti})^* \right) \right)\\
&+ \frac{1}{2} B_0(m^2_{\tilde{q}_t}, 0, m^2_{\tilde{q}_t}) \left((|C^{\tilde{\chi},q'_\mathrm{L}}_{nti}|^2 + |C^{\tilde{\chi},q'_\mathrm{R}}_{nti}|^2)(m^2_{\tilde{\chi}_i} + m^2_{q'_n} + m^2_{\tilde{q}_t}) + 4m_{\tilde{\chi}_i} m_{q'_n} \mathrm{Re}\left(C^{\tilde{\chi},q'_\mathrm{L}}_{nti} (C^{\tilde{\chi},q'_\mathrm{R}}_{nti})^* \right) \right)\\
&+ \frac{1}{2} B_0(0, \lambda^2, \lambda^2)(\xi_g - 1) \left((|C^{\tilde{\chi},q'_\mathrm{L}}_{nti}|^2 + C^{\tilde{\chi},q'_\mathrm{R}}_{nti}|^2)(m^2_{\tilde{\chi}_i} + m^2_{q'_n} - m^2_{\tilde{q}_t}) \right.\\
&\quad \left. + 4m_{\tilde{\chi}_i} m_{q'_n} \mathrm{Re}\left(C^{\tilde{\chi},q'_\mathrm{L}}_{nti} (C^{\tilde{\chi},q'_\mathrm{R}}_{nti})^* \right) \right)\\
&- (m^2_{\tilde{\chi}_i} - m^2_{q'_n} - m^2_{\tilde{q}_t}) C_0(m^2_{q'_n}, m^2_{\tilde{\chi}_i}, m^2_{\tilde{q}_t}, \lambda^2, m^2_{q'_n}, m^2_{\tilde{q}_t}) \left((|C^{\tilde{\chi},q'_\mathrm{L}}_{nti}|^2 + C^{\tilde{\chi},q'_\mathrm{R}}_{nti}|^2)(m^2_{\tilde{\chi}_i} + m^2_{q'_n} - m^2_{\tilde{q}_t}) \right.\\
&\quad \left. + 4m_{\tilde{\chi}_i} m_{q'_n} \mathrm{Re}\left(C^{\tilde{\chi},q'_\mathrm{L}}_{nti} (C^{\tilde{\chi},q'_\mathrm{R}}_{nti})^* \right) \right) \Big] .
\end{aligned}$$

The gluino contribution is given by

$$\begin{aligned}
&\mathcal{D}^{(\tilde{g})}_{\tilde{\chi}_i \to q'_n \tilde{q}^*_t} = \frac{3g_s^2}{12\pi^2} \left[\sum_{l=1}^{6} \sum_{m=1}^{3} \right. \qquad\qquad (\mathrm{G.18})\\
&- B_0(m^2_{\tilde{\chi}_i}, m^2_{q_m}, m^2_{\tilde{q}'_l}) m_{\tilde{\chi}_i} \left(C^{\tilde{g},q'_\mathrm{R}}_{ln} (C^{\tilde{g},q_\mathrm{L}}_{tm} (C^{\tilde{\chi},q'_\mathrm{L}}_{nti})^* (C^{\tilde{\chi},q_\mathrm{L}}_{mli})^* m_{q'_n} + (C^{\tilde{\chi},q'_\mathrm{R}}_{nti})^* (C^{\tilde{g},q_\mathrm{L}}_{tm} (C^{\tilde{\chi},q_\mathrm{L}}_{mli})^* m_{\tilde{\chi}_i} \right.\\
&\quad \left. + (C^{\tilde{\chi},q_\mathrm{R}}_{mli})^* (m_{\tilde{g}} C^{\tilde{g},q_\mathrm{R}}_{tm} + C^{\tilde{g},q_\mathrm{L}}_{tm} m_{q_m}))) + C^{\tilde{g},q'_\mathrm{L}}_{ln} (m_{\tilde{g}} C^{\tilde{g},q_\mathrm{L}}_{tm} (C^{\tilde{\chi},q'_\mathrm{L}}_{nti})^* (C^{\tilde{\chi},q_\mathrm{L}}_{mli})^*
\end{aligned}$$

$$
\begin{aligned}
&+C_{tm}^{\tilde{g},q_R}((C_{nti}^{\tilde{\chi},q'_R})^*(C_{mli}^{\tilde{\chi},q_R})^* m_{q'_n} + (C_{nti}^{\tilde{\chi},q'_L})^*((C_{mli}^{\tilde{\chi},q_R})^* m_{\tilde{\chi}_i} + (C_{mli}^{\tilde{\chi},q_L})^* m_{q_m}))\Big) \\
&- B_0(m_{q'_n}^2, m_{\tilde{g}}^2, m_{\tilde{q}'_l}^2) m_{q'_n} \Big(C_{ln}^{\tilde{g},q'_R}(C_{tm}^{\tilde{g},q_L}(C_{mli}^{\tilde{\chi},q_L})^*(C_{nti}^{\tilde{\chi},q'_R})^* m_{q'_n} + (C_{nti}^{\tilde{\chi},q'_L})^*(C_{tm}^{\tilde{g},q_L}(C_{mli}^{\tilde{\chi},q_L})^* m_{\tilde{\chi}_i} \\
&+(C_{mli}^{\tilde{\chi},q_R})^*(m_{\tilde{g}} C_{tm}^{\tilde{g},q_R} + C_{tm}^{\tilde{g},q_L} m_{q_m}))) + C_{ln}^{\tilde{g},q'_L}(m_{\tilde{g}} C_{tm}^{\tilde{g},q_L}(C_{mli}^{\tilde{\chi},q_L})^*(C_{nti}^{\tilde{\chi},q'_R})^* \\
&+C_{tm}^{\tilde{g},q_R}((C_{nti}^{\tilde{\chi},q'_L})^*(C_{mli}^{\tilde{\chi},q_R})^* m_{q'_n} + (C_{nti}^{\tilde{\chi},q'_R})^*((C_{mli}^{\tilde{\chi},q_R})^* m_{\tilde{\chi}_i} + (C_{mli}^{\tilde{\chi},q_L})^* m_{q_m})))\Big) \\
&+ B_0(m_{\tilde{q}_t}^2, m_{\tilde{g}}^2, m_{q_m}^2) \Big(C_{ln}^{\tilde{g},q'_R}(C_{tm}^{\tilde{g},q_L}(C_{mli}^{\tilde{\chi},q_L})^*(C_{nti}^{\tilde{\chi},q'_R})^* m_{\tilde{q}_t}^2 + (C_{mli}^{\tilde{\chi},q_R})^*((C_{nti}^{\tilde{\chi},q'_R})^* m_{\tilde{\chi}_i} \\
&+(C_{nti}^{\tilde{\chi},q'_L})^* m_{q'_n})(m_{\tilde{g}} C_{tm}^{\tilde{g},q_R} + C_{tm}^{\tilde{g},q_L} m_{q_m})) + C_{ln}^{\tilde{g},q'_L}((C_{nti}^{\tilde{\chi},q'_L})^*(C_{mli}^{\tilde{\chi},q_R})^* C_{tm}^{\tilde{g},q_R} m_{\tilde{q}_t}^2 \\
&+(C_{mli}^{\tilde{\chi},q_L})^*((C_{nti}^{\tilde{\chi},q'_L})^* m_{\tilde{\chi}_i} + (C_{nti}^{\tilde{\chi},q'_R})^* m_{q'_n})(m_{\tilde{g}} C_{tm}^{\tilde{g},q_L} + C_{tm}^{\tilde{g},q_R} m_{q_m}))\Big) \\
&- C_0(m_{\tilde{\chi}_i}^2, m_{q'_n}^2, m_{\tilde{q}_t}^2, m_{q_m}^2, m_{\tilde{q}'_l}^2, m_{\tilde{g}}^2) \Big(C_{ln}^{\tilde{g},q'_R}((C_{nti}^{\tilde{\chi},q'_L})^* m_{q'_n}(m_{\tilde{g}} C_{tm}^{\tilde{g},q_R}(2(C_{mli}^{\tilde{\chi},q_L})^* m_{\tilde{\chi}_i} m_{q_m} \\
&+(C_{mli}^{\tilde{\chi},q_R})^*(m_{\tilde{\chi}_i}^2 + m_{q_m}^2 - m_{\tilde{q}'_l}^2)) + C_{tm}^{\tilde{g},q_L}((C_{mli}^{\tilde{\chi},q_L})^* m_{\tilde{\chi}_i}(m_{\tilde{g}}^2 + m_{q_m}^2 - m_{\tilde{q}_t}^2) \\
&+(C_{mli}^{\tilde{\chi},q_R})^* m_{q_m}(m_{q'_n}^2 + m_{q_m}^2 - m_{\tilde{q}_t}^2 - m_{\tilde{q}'_l}^2))) \\
&+(C_{nti}^{\tilde{\chi},q'_R})^*((C_{mli}^{\tilde{\chi},q_R})^* m_{\tilde{\chi}_i}(C_{tm}^{\tilde{g},q_L} m_{q_m}(m_{\tilde{g}}^2 + m_{q'_n}^2 - m_{\tilde{q}'_l}^2) \\
&+m_{\tilde{g}} C_{tm}^{\tilde{g},q_R}(m_{\tilde{g}}^2 + m_{\tilde{\chi}_i}^2 - m_{\tilde{q}_t}^2 - m_{\tilde{q}'_l}^2)) + (C_{mli}^{\tilde{\chi},q_L})^*(m_{\tilde{g}} C_{tm}^{\tilde{g},q_R} m_{q_m}(m_{\tilde{\chi}_i}^2 + m_{q'_n}^2 - m_{\tilde{q}_t}^2) \\
&+C_{tm}^{\tilde{g},q_L}(m_{\tilde{g}}^2 m_{\tilde{\chi}_i}^2 + m_{q'_n}^2 m_{q_m}^2 - m_{\tilde{q}_t}^2 m_{\tilde{q}'_l}^2)))) + C_{ln}^{\tilde{g},q'_L}(m_{\tilde{g}} C_{tm}^{\tilde{g},q_L}((C_{nti}^{\tilde{\chi},q'_R})^* m_{q'_n}(2(C_{mli}^{\tilde{\chi},q_R})^* m_{\tilde{\chi}_i} m_{q_m} \\
&+(C_{mli}^{\tilde{\chi},q_L})^*(m_{\tilde{\chi}_i}^2 + m_{q_m}^2 - m_{\tilde{q}'_l}^2)) + (C_{nti}^{\tilde{\chi},q'_L})^*((C_{mli}^{\tilde{\chi},q_R})^* m_{q_m}(m_{\tilde{\chi}_i}^2 + m_{q'_n}^2 - m_{\tilde{q}_t}^2) \\
&+(C_{mli}^{\tilde{\chi},q_L})^* m_{\tilde{\chi}_i}(m_{\tilde{g}}^2 + m_{\tilde{\chi}_i}^2 - m_{\tilde{q}_t}^2 - m_{\tilde{q}'_l}^2))) \\
&+C_{tm}^{\tilde{g},q_R}((C_{nti}^{\tilde{\chi},q'_R})^* m_{q'_n}((C_{mli}^{\tilde{\chi},q_R})^* m_{\tilde{\chi}_i}(m_{\tilde{g}}^2 + m_{q_m}^2 - m_{\tilde{q}_t}^2) \\
&+(C_{mli}^{\tilde{\chi},q_L})^* m_{q_m}(m_{q'_n}^2 + m_{q_m}^2 - m_{\tilde{q}_t}^2 - m_{\tilde{q}'_l}^2)) + (C_{nti}^{\tilde{\chi},q'_L})^*((C_{mli}^{\tilde{\chi},q_L})^* m_{\tilde{\chi}_i} m_{q_m}(m_{\tilde{g}}^2 + m_{q'_n}^2 - m_{\tilde{q}'_l}^2) \\
&+(C_{mli}^{\tilde{\chi},q_R})^*(m_{\tilde{g}}^2 m_{\tilde{\chi}_i}^2 + m_{q'_n}^2 m_{q_m}^2 - m_{\tilde{q}_t}^2 m_{\tilde{q}'_l}^2)))))\Big)\Big] \,.
\end{aligned}
$$

Next, we discuss the vertex correction of the gluino to squark-quark decay. The contributing Feynman diagrams are given in Fig. 13.3b. The NLO correction to the decay width can be written as

$$
\Delta\Gamma^{\mathrm{NLO}}_{\tilde{g}\to q_n\tilde{q}_t^*} = \lambda(m_{\tilde{g}}^2, m_{q_n}^2, m_{\tilde{q}_t}^2)\frac{1}{16\pi m_{\tilde{g}}^3}\frac{1}{2}\frac{1}{8}\sum_{\text{spin,colour}} 2\mathrm{Re}\left[\left(\mathcal{A}^{\mathrm{LO}}_{\tilde{g}\to q_n\tilde{q}_t^*}\right)^* \mathcal{A}^{\mathrm{NLO}}_{\tilde{g}\to q_n\tilde{q}_t^*}\right], \tag{G.19}
$$

where we average and sum over the spin and the colour degrees of freedom. We again define the quantity

$$
\mathcal{D}_{\tilde{g}\to q_n\tilde{q}_t^*} \equiv \sum_{\text{spin,colour}} \left[\left(\mathcal{A}^{\mathrm{LO}}_{\tilde{g}\to q_n\tilde{q}_t^*}\right)^* \mathcal{A}^{\mathrm{NLO}}_{\tilde{g}\to q_n\tilde{q}_t^*}\right], \tag{G.20}
$$

that we split up into the several contributions,

$$
\mathcal{D}_{\tilde{g}\to q_n\tilde{q}_t^*} = \mathcal{D}^{(g)}_{\tilde{g}\to q_n\tilde{q}_t^*} + \mathcal{D}^{(\tilde{g})}_{\tilde{g}\to q_n\tilde{q}_t^*} + \mathcal{D}^{(\mathrm{abs})}_{\tilde{g}\to q_n\tilde{q}_t^*} \,. \tag{G.21}
$$

The gluon contribution is given by

$$
\begin{aligned}
&\mathcal{D}^{(g)}_{\tilde{g}\to q_n\tilde{q}_t^*} = \frac{g_s^4}{\pi^2}\,[\\
&-\frac{3}{4}B_0(m_{q_n}^2, m_{\tilde{g}}^2, m_{\tilde{q}_t}^2) m_{q_n}\left(m_{q_n}(|C_{tn}^{\tilde{g},q_L}|^2 + |C_{tn}^{\tilde{g},q_R}|^2) + 2m_{\tilde{g}}\mathrm{Re}\left(C_{tn}^{\tilde{g},q_L}(C_{tn}^{\tilde{g},q_R})^*\right)\right)
\end{aligned} \tag{G.22}
$$

$$
\begin{aligned}
&+\frac{1}{12}m_{\tilde{g}}B_0(m_{\tilde{g}}^2,m_{q_n}^2,m_{\tilde{q}_t}^2)\left(m_{\tilde{g}}(|C_{tn}^{\tilde{g},q_\mathrm{L}}|^2+|C_{tn}^{\tilde{g},q_\mathrm{R}}|^2)+2m_{q_n}\mathrm{Re}\left(C_{tn}^{\tilde{g},q_\mathrm{L}}(C_{tn}^{\tilde{g},q_\mathrm{R}})^*\right)\right)\\
&+\frac{3}{4}B_0(m_{\tilde{q}_t}^2,m_{\tilde{g}}^2,m_{q_n}^2)\left((m_{\tilde{g}}^2+m_{q_n}^2)(|C_{tn}^{\tilde{g},q_\mathrm{L}}|^2+|C_{tn}^{\tilde{g},q_\mathrm{R}}|^2)+4m_{\tilde{g}}m_{q_n}\mathrm{Re}\left(C_{tn}^{\tilde{g},q_\mathrm{L}}(C_{tn}^{\tilde{g},q_\mathrm{R}})^*\right)\right)\\
&+\frac{2}{3}B_0(m_{q_n}^2,0,m_{q_n}^2)\left((m_{\tilde{g}}^2-m_{\tilde{q}_t}^2)(|C_{tn}^{\tilde{g},q_\mathrm{L}}|^2+|C_{tn}^{\tilde{g},q_\mathrm{R}}|^2)+2m_{\tilde{g}}m_{q_n}\mathrm{Re}\left(C_{tn}^{\tilde{g},q_\mathrm{L}}(C_{tn}^{\tilde{g},q_\mathrm{R}})^*\right)\right)\\
&+\frac{3}{2}B_0(m_{\tilde{g}}^2,0,m_{\tilde{g}}^2)\left((m_{q_n}^2-m_{\tilde{q}_t}^2)(|C_{tn}^{\tilde{g},q_\mathrm{L}}|^2+|C_{tn}^{\tilde{g},q_\mathrm{R}}|^2)+2m_{\tilde{g}}m_{q_n}\mathrm{Re}\left(C_{tn}^{\tilde{g},q_\mathrm{L}}(C_{tn}^{\tilde{g},q_\mathrm{R}})^*\right)\right)\\
&-\frac{3}{4}\left((m_{\tilde{g}}^2+m_{q_n}^2-m_{\tilde{q}_t}^2)(|C_{tn}^{\tilde{g},q_\mathrm{L}}|^2+|C_{tn}^{\tilde{g},q_\mathrm{R}}|^2)+4m_{\tilde{g}}m_{q_n}\mathrm{Re}\left(C_{tn}^{\tilde{g},q_\mathrm{L}}(C_{tn}^{\tilde{g},q_\mathrm{R}})^*\right)\right)\\
&+\frac{1}{3}B_0(m_{\tilde{q}_t}^2,0,m_{\tilde{q}_t}^2)\left((m_{\tilde{g}}^2+m_{q_n}^2+m_{\tilde{q}_t}^2)(|C_{tn}^{\tilde{g},q_\mathrm{L}}|^2+|C_{tn}^{\tilde{g},q_\mathrm{R}}|^2)+4m_{\tilde{g}}m_{q_n}\mathrm{Re}\left(C_{tn}^{\tilde{g},q_\mathrm{L}}(C_{tn}^{\tilde{g},q_\mathrm{R}})^*\right)\right)\\
&+\frac{17(\xi_g-1)}{24}B_0(0,\lambda^2,\lambda^2)\left((m_{\tilde{g}}^2+m_{q_n}^2-m_{\tilde{q}_t}^2)(|C_{tn}^{\tilde{g},q_\mathrm{L}}|^2+|C_{tn}^{\tilde{g},q_\mathrm{R}}|^2)+\right.\\
&\left.4m_{\tilde{g}}m_{q_n}\mathrm{Re}\left(C_{tn}^{\tilde{g},q_\mathrm{L}}(C_{tn}^{\tilde{g},q_\mathrm{R}})^*\right)\right)\\
&+\frac{3}{4}(m_{\tilde{g}}^2-m_{q_n}^2+m_{\tilde{q}_t}^2)C_0(m_{\tilde{g}}^2,m_{q_n}^2,m_{\tilde{q}_t}^2,\lambda^2,m_{\tilde{g}}^2,m_{\tilde{q}_t}^2)\left((m_{\tilde{g}}^2+m_{q_n}^2-m_{\tilde{q}_t}^2)(|C_{tn}^{\tilde{g},q_\mathrm{L}}|^2\right.\\
&\left.+|C_{tn}^{\tilde{g},q_\mathrm{R}}|^2)+4m_{\tilde{g}}m_{q_n}\mathrm{Re}\left(C_{tn}^{\tilde{g},q_\mathrm{L}}(C_{tn}^{\tilde{g},q_\mathrm{R}})^*\right)\right)\\
&+\frac{1}{12}(m_{\tilde{g}}^2-m_{q_n}^2-m_{\tilde{q}_t}^2)C_0(m_{q_n}^2,m_{\tilde{g}}^2,m_{\tilde{q}_t}^2,\lambda^2,m_{q_n}^2,m_{\tilde{q}_t}^2)\left((m_{\tilde{g}}^2+m_{q_n}^2-m_{\tilde{q}_t}^2)(|C_{tn}^{\tilde{g},q_\mathrm{L}}|^2\right.\\
&\left.+|C_{tn}^{\tilde{g},q_\mathrm{R}}|^2)+4m_{\tilde{g}}m_{q_n}\mathrm{Re}\left(C_{tn}^{\tilde{g},q_\mathrm{L}}(C_{tn}^{\tilde{g},q_\mathrm{R}})^*\right)\right)\\
&+\frac{3}{4}(m_{\tilde{g}}^2+m_{q_n}^2-m_{\tilde{q}_t}^2)C_0(m_{q_n}^2,m_{\tilde{q}_t}^2,m_{\tilde{g}}^2,\lambda^2,m_{q_n}^2,m_{\tilde{g}}^2)\left((m_{\tilde{g}}^2+m_{q_n}^2-m_{\tilde{q}_t}^2)(|C_{tn}^{\tilde{g},q_\mathrm{L}}|^2\right.\\
&\left.\left.+|C_{tn}^{\tilde{g},q_\mathrm{R}}|^2)+4m_{\tilde{g}}m_{q_n}\mathrm{Re}\left(C_{tn}^{\tilde{g},q_\mathrm{L}}(C_{tn}^{\tilde{g},q_\mathrm{R}})^*\right)\right)\right]\,.
\end{aligned}
$$

The gluino contribution reads

$$
\begin{aligned}
\mathcal{D}^{(\tilde{g})}_{\tilde{g}\to q_n\tilde{q}_t^*}=\frac{g_s^4}{24\pi^2}\Bigg[&\sum_{l=1}^{6}\sum_{m=1}^{3} \qquad\qquad (\mathrm{G.23})\\
&m_{\tilde{g}}B_0(m_{\tilde{g}}^2,m_{q_m}^2,m_{\tilde{q}_l}^2)\left(C_{ln}^{\tilde{g},q_\mathrm{L}}(m_{\tilde{g}}C_{tm}^{\tilde{g},q_\mathrm{L}}(C_{lm}^{\tilde{g},q_\mathrm{L}})^*(C_{tn}^{\tilde{g},q_\mathrm{L}})^*+C_{tm}^{\tilde{g},q_\mathrm{R}}((C_{tn}^{\tilde{g},q_\mathrm{L}})^*(m_{\tilde{g}}(C_{lm}^{\tilde{g},q_\mathrm{R}})^*\right.\\
&\quad+(C_{lm}^{\tilde{g},q_\mathrm{L}})^*m_{q_m})+(C_{lm}^{\tilde{g},q_\mathrm{R}})^*(C_{tn}^{\tilde{g},q_\mathrm{R}})^*m_{q_n}))+C_{ln}^{\tilde{g},q_\mathrm{R}}(m_{\tilde{g}}(C_{lm}^{\tilde{g},q_\mathrm{R}})^*(C_{tn}^{\tilde{g},q_\mathrm{R}})^*C_{tm}^{\tilde{g},q_\mathrm{R}}\\
&\quad\left.+C_{tm}^{\tilde{g},q_\mathrm{L}}((C_{lm}^{\tilde{g},q_\mathrm{R}})^*(C_{tn}^{\tilde{g},q_\mathrm{R}})^*m_{q_m}+(C_{lm}^{\tilde{g},q_\mathrm{L}})^*(m_{\tilde{g}}(C_{tn}^{\tilde{g},q_\mathrm{R}})^*+(C_{tn}^{\tilde{g},q_\mathrm{L}})^*m_{q_n}))\right)\\
&+m_{q_n}B_0(m_{q_n}^2,m_{\tilde{g}}^2,m_{\tilde{q}_l}^2)\left(C_{ln}^{\tilde{g},q_\mathrm{L}}(m_{\tilde{g}}C_{tm}^{\tilde{g},q_\mathrm{L}}(C_{lm}^{\tilde{g},q_\mathrm{L}})^*(C_{tn}^{\tilde{g},q_\mathrm{R}})^*+C_{tm}^{\tilde{g},q_\mathrm{R}}((C_{lm}^{\tilde{g},q_\mathrm{L}})^*(C_{tn}^{\tilde{g},q_\mathrm{R}})^*m_{q_m}\right.\\
&\quad+(C_{lm}^{\tilde{g},q_\mathrm{R}})^*(m_{\tilde{g}}(C_{tn}^{\tilde{g},q_\mathrm{R}})^*+(C_{tn}^{\tilde{g},q_\mathrm{L}})^*m_{q_n})))+C_{ln}^{\tilde{g},q_\mathrm{R}}(m_{\tilde{g}}(C_{tn}^{\tilde{g},q_\mathrm{L}})^*(C_{lm}^{\tilde{g},q_\mathrm{R}})^*C_{tm}^{\tilde{g},q_\mathrm{R}}\\
&\quad\left.+C_{tm}^{\tilde{g},q_\mathrm{L}}((C_{tn}^{\tilde{g},q_\mathrm{L}})^*(C_{lm}^{\tilde{g},q_\mathrm{R}})^*m_{q_m}+(C_{lm}^{\tilde{g},q_\mathrm{L}})^*(m_{\tilde{g}}(C_{tn}^{\tilde{g},q_\mathrm{L}})^*+(C_{tn}^{\tilde{g},q_\mathrm{R}})^*m_{q_n})))\right)\\
&-B_0(m_{\tilde{q}_t}^2,m_{\tilde{g}}^2,m_{q_m}^2)\left(C_{ln}^{\tilde{g},q_\mathrm{R}}(C_{tm}^{\tilde{g},q_\mathrm{L}}(C_{lm}^{\tilde{g},q_\mathrm{L}})^*(C_{tn}^{\tilde{g},q_\mathrm{R}})^*m_{\tilde{q}_t}^2+(C_{lm}^{\tilde{g},q_\mathrm{R}})^*(m_{\tilde{g}}C_{tm}^{\tilde{g},q_\mathrm{R}}\right.\\
&\quad+C_{tm}^{\tilde{g},q_\mathrm{L}}m_{q_m})(m_{\tilde{g}}(C_{tn}^{\tilde{g},q_\mathrm{R}})^*+(C_{tn}^{\tilde{g},q_\mathrm{L}})^*m_{q_n}))+C_{ln}^{\tilde{g},q_\mathrm{L}}((C_{tn}^{\tilde{g},q_\mathrm{L}})^*(C_{lm}^{\tilde{g},q_\mathrm{R}})^*C_{tm}^{\tilde{g},q_\mathrm{R}}m_{\tilde{q}_t}^2\\
&\quad\left.+(C_{lm}^{\tilde{g},q_\mathrm{L}})^*(m_{\tilde{g}}C_{tm}^{\tilde{g},q_\mathrm{L}}+C_{tm}^{\tilde{g},q_\mathrm{R}}m_{q_m})(m_{\tilde{g}}(C_{tn}^{\tilde{g},q_\mathrm{L}})^*+(C_{tn}^{\tilde{g},q_\mathrm{R}})^*m_{q_n}))\right)\\
&+C_0(m_{\tilde{g}}^2,m_{q_n}^2,m_{\tilde{q}_t}^2,m_{q_m}^2,m_{\tilde{q}_l}^2,m_{\tilde{g}}^2)\left(C_{ln}^{\tilde{g},q_\mathrm{L}}(m_{\tilde{g}}C_{tm}^{\tilde{g},q_\mathrm{L}}((C_{lm}^{\tilde{g},q_\mathrm{R}})^*m_{q_m}(2m_{\tilde{g}}(C_{tn}^{\tilde{g},q_\mathrm{R}})^*m_{q_n}\right.\\
&\quad+(C_{tn}^{\tilde{g},q_\mathrm{L}})^*(m_{\tilde{g}}^2+m_{q_n}^2-m_{\tilde{q}_t}^2))+(C_{lm}^{\tilde{g},q_\mathrm{L}})^*((C_{tn}^{\tilde{g},q_\mathrm{R}})^*m_{q_n}(m_{\tilde{g}}^2+m_{q_m}^2-m_{\tilde{q}_l}^2)\\
&\quad+m_{\tilde{g}}(C_{tn}^{\tilde{g},q_\mathrm{L}})^*(2m_{\tilde{g}}^2-m_{\tilde{q}_l}^2-m_{\tilde{q}_t}^2)))+C_{tm}^{\tilde{g},q_\mathrm{R}}((C_{tn}^{\tilde{g},q_\mathrm{R}})^*m_{q_n}(m_{\tilde{g}}(C_{lm}^{\tilde{g},q_\mathrm{R}})^*(m_{\tilde{g}}^2+m_{q_m}^2-m_{\tilde{q}_t}^2)\\
&\quad+(C_{lm}^{\tilde{g},q_\mathrm{L}})^*m_{q_m}(m_{q_m}^2+m_{q_n}^2-m_{\tilde{q}_l}^2-m_{\tilde{q}_t}^2))+(C_{tn}^{\tilde{g},q_\mathrm{L}})^*(m_{\tilde{g}}(C_{lm}^{\tilde{g},q_\mathrm{L}})^*m_{q_m}(m_{\tilde{g}}^2+m_{q_n}^2-m_{\tilde{q}_l}^2)\\
&\quad\left.+(C_{lm}^{\tilde{g},q_\mathrm{R}})^*(m_{\tilde{g}}^4+m_{q_m}^2m_{q_n}^2-m_{\tilde{q}_l}^2m_{\tilde{q}_t}^2))))+C_{ln}^{\tilde{g},q_\mathrm{R}}(m_{\tilde{g}}C_{tm}^{\tilde{g},q_\mathrm{R}}((C_{lm}^{\tilde{g},q_\mathrm{L}})^*m_{q_m}(2m_{\tilde{g}}(C_{tn}^{\tilde{g},q_\mathrm{L}})^*m_{q_n}\right.
\end{aligned}
$$

$$+(C^{\tilde{g},q_R}_{tn})^*(m^2_{\tilde{g}}+m^2_{q_n}-m^2_{\tilde{q}_t}))+(C^{\tilde{g},q_R}_{lm})^*((C^{\tilde{g},q_L}_{tn})^* m_{q_n}(m^2_{\tilde{g}}+m^2_{q_m}-m^2_{\tilde{q}_l})$$
$$+m_{\tilde{g}}(C^{\tilde{g},q_R}_{tn})^*(2m^2_{\tilde{g}}-m^2_{\tilde{q}_l}-m^2_{\tilde{q}_t})))+C^{\tilde{g},q_L}_{tm}((C^{\tilde{g},q_R}_{lm})^* m_{q_m}(m_{\tilde{g}}(C^{\tilde{g},q_R}_{tn})^*(m^2_{\tilde{g}}+m^2_{q_n}-m^2_{\tilde{q}_l})$$
$$+(C^{\tilde{g},q_L}_{tn})^* m_{q_n}(m^2_{q_m}+m^2_{q_n}-m^2_{\tilde{q}_l}-m^2_{\tilde{q}_t}))+(C^{\tilde{g},q_L}_{lm})^*(m_{\tilde{g}}(C^{\tilde{g},q_L}_{tn})^* m_{q_n}(m^2_{\tilde{g}}+m^2_{q_m}-m^2_{\tilde{q}_t})$$
$$+(C^{\tilde{g},q_R}_{tn})^*(m^4_{\tilde{g}}+m^2_{q_m}m^2_{q_n}-m^2_{\tilde{q}_l}m^2_{\tilde{q}_t}))))\Big)\Big]\,.$$

We omit the vertex corrections of the squark to quark and neutralino/chargino/gluino decays. They are obtained from the same diagrams as the above decays, where one has to interchange the kinematics accordingly.

We now give the analytic results for the squark to squark and vector boson decay. Here, we denote vector bosons generically by V, where $V = W, Z$. We thus have the generic squark-squark-V couplings $C_{\tilde{q}_s\tilde{q}'_t V}$ $(s,t = 1,..,6)$ and the left- and right-chiral couplings of the quark-quark-V coupling, $C^{q_L/q_R}_{q_n q'_m V}$ $(m,n = 1,2,3)$. The diagrams contributing to the vertex corrections are given in Fig. 13.3c.

We use the same notation as above, i.e. the NLO correction to the decay width can be written as

$$\Delta\Gamma^{\rm NLO}_{\tilde{q}_s\to\tilde{q}'_t V} = \lambda(m^2_{\tilde{q}_s},m^2_{\tilde{q}'_t},m^2_V)\frac{1}{16\pi m^3_{\tilde{q}_s}}\frac{1}{3}\sum_{\text{polarization,colour}} 2\text{Re}\left[\left(\mathcal{A}^{\rm LO}_{\tilde{q}_s\to\tilde{q}'_t V}\right)^*\mathcal{A}^{\rm NLO}_{\tilde{q}_s\to\tilde{q}'_t V}\right]\,, \quad \text{(G.24)}$$

where we average and sum over the polarization of the vector boson V and the colour of the squarks. We then define the quantity

$$\mathcal{D}_{\tilde{q}_s\to\tilde{q}'_t V} \equiv \sum_{\text{polarization,colour}}\left[\left(\mathcal{A}^{\rm LO}_{\tilde{q}_s\to\tilde{q}'_t V}\right)^*\mathcal{A}^{\rm NLO}_{\tilde{q}_s\to\tilde{q}'_t V}\right]\,, \quad \text{(G.25)}$$

that we split up into the contributions,

$$\mathcal{D}_{\tilde{q}_s\to\tilde{q}'_t V} = \mathcal{D}^{(g)}_{\tilde{q}_s\to\tilde{q}'_t V}+\mathcal{D}^{(\tilde{g})}_{\tilde{q}_s\to\tilde{q}'_t V}+\mathcal{D}^{(\rm abs)}_{\tilde{q}_s\to\tilde{q}'_t V}\,. \quad \text{(G.26)}$$

The gluon contribution is given by

$$\mathcal{D}^{(g)}_{\tilde{q}_s\to\tilde{q}'_t V} = \frac{3g_s^2|C_{\tilde{q}_s\tilde{q}'_t V}|^2}{\pi^2}\,[\quad \text{(G.27)}$$
$$\frac{1}{3}(m^2_{\tilde{q}_s}+m^2_{\tilde{q}'_t}-m^2_V)B_0(m^2_V,m^2_{\tilde{q}_s},m^2_{\tilde{q}'_t})$$
$$+\frac{1}{12m^2_V}B_0(m^2_{\tilde{q}'_t},0,m^2_{\tilde{q}'_t})\left(2m^2_{\tilde{q}'_t}(m^2_{\tilde{q}_s}+m^2_V)+(m^2_V-m^2_{\tilde{q}_s})^2-3m^4_{\tilde{q}'_t}\right)$$
$$+\frac{1}{12m^2_V}B_0(m^2_{\tilde{q}_s},0,m^2_{\tilde{q}_s})\left(2m^2_{\tilde{q}_s}(m^2_{\tilde{q}'_t}+m^2_V)-3m^4_{\tilde{q}_s}+(m^2_V-m^2_{\tilde{q}'_t})^2\right)$$
$$+\frac{1}{12m^2_V}B_0(0,\lambda^2,\lambda^2)(\xi_g-1)\left(-2m^2_{\tilde{q}_s}(m^2_{\tilde{q}'_t}+m^2_V)+m^4_{\tilde{q}_s}+(m^2_V-m^2_{\tilde{q}'_t})^2\right)$$
$$-\frac{1}{6m^2_V}(-m_{\tilde{q}_s}-m_{\tilde{q}'_t}+m_V)(m_{\tilde{q}_s}-m_{\tilde{q}'_t}+m_V)(-m_{\tilde{q}_s}+m_{\tilde{q}'_t}+m_V)$$
$$(m_{\tilde{q}_s}+m_{\tilde{q}'_t}+m_V)(-m^2_{\tilde{q}_s}-m^2_{\tilde{q}'_t}+m^2_V)C_0(m^2_{\tilde{q}_s},m^2_V,m^2_{\tilde{q}'_t},\lambda^2,m^2_{\tilde{q}_s},m^2_{\tilde{q}'_t})\Big]\,.$$

The gluino contribution reads

$$\mathcal{D}^{(\tilde{g})}_{\tilde{q}_s\to\tilde{q}'_t V} = \frac{3g_s^2(C_{\tilde{q}_s\tilde{q}'_t V})^*}{\pi^2}\left[\sum_{m,n=1}^{3}\right. \quad \text{(G.28)}$$

$$
\begin{aligned}
&\frac{1}{12}B_0(m_V^2,m_{q_n}^2,m_{q'_m}^2)\Big(C^{q_\mathrm{R}}_{q_nq'_mV}(2C^{\tilde g,q_\mathrm{R}}_{sn}m_{q_n}(m_{\tilde g}(C^{\tilde g,q'_\mathrm{L}}_{tm})^*+(C^{\tilde g,q'_\mathrm{R}}_{tm})^*m_{q'_m})\\
&\quad+C^{\tilde g,q_\mathrm{L}}_{sn}(2m_{\tilde g}(C^{\tilde g,q'_\mathrm{R}}_{tm})^*m_{q'_m}+(C^{\tilde g,q'_\mathrm{L}}_{tm})^*(2m_{\tilde g}^2+m_V^2-m_{\tilde q_s}^2-m_{\tilde q'_t}^2)))\\
&\quad+C^{q_\mathrm{L}}_{q_nq'_mV}(2(C^{\tilde g,q'_\mathrm{L}}_{tm})^*(m_{\tilde g}C^{\tilde g,q_\mathrm{R}}_{sn}+C^{\tilde g,q_\mathrm{L}}_{sn}m_{q_n})m_{q'_m}\\
&\quad+(C^{\tilde g,q'_\mathrm{R}}_{tm})^*(2m_{\tilde g}C^{\tilde g,q_\mathrm{L}}_{sn}m_{q_n}+C^{\tilde g,q_\mathrm{R}}_{sn}(2m_{\tilde g}^2+m_V^2-m_{\tilde q_s}^2-m_{\tilde q'_t}^2)))\Big)\\
&-\frac{1}{12m_V^2}B_0(m_{\tilde q'_t}^2,m_{\tilde g}^2,m_{q'_m}^2)\Big(C^{q_\mathrm{R}}_{q_nq'_mV}(C^{\tilde g,q_\mathrm{R}}_{sn}m_{q_n}(m_{\tilde g}(C^{\tilde g,q'_\mathrm{L}}_{tm})^*\\
&\quad+(C^{\tilde g,q'_\mathrm{R}}_{tm})^*m_{q'_m})(m_V^2-m_{\tilde q_s}^2+m_{\tilde q'_t}^2)+C^{\tilde g,q_\mathrm{L}}_{sn}(m_{\tilde g}(C^{\tilde g,q'_\mathrm{R}}_{tm})^*m_{q'_m}(m_V^2-m_{\tilde q_s}^2+m_{\tilde q'_t}^2)\\
&\quad+(C^{\tilde g,q'_\mathrm{L}}_{tm})^*(-m_{\tilde q'_t}^4+(m_{\tilde g}^2+m_V^2+m_{\tilde q_s}^2)m_{\tilde q'_t}^2+m_{\tilde g}^2(m_V^2-m_{\tilde q_s}^2))))\\
&\quad+C^{q_\mathrm{L}}_{q_nq'_mV}((C^{\tilde g,q'_\mathrm{L}}_{tm})^*(m_{\tilde g}C^{\tilde g,q_\mathrm{R}}_{sn}+C^{\tilde g,q_\mathrm{L}}_{sn}m_{q_n})m_{q'_m}(m_V^2-m_{\tilde q_s}^2+m_{\tilde q'_t}^2)\\
&\quad+(C^{\tilde g,q'_\mathrm{R}}_{tm})^*(m_{\tilde g}C^{\tilde g,q_\mathrm{L}}_{sn}m_{q_n}(m_V^2-m_{\tilde q_s}^2+m_{\tilde q'_t}^2)\\
&\quad+C^{\tilde g,q_\mathrm{R}}_{sn}(-m_{\tilde q'_t}^4+(m_{\tilde g}^2+m_V^2+m_{\tilde q_s}^2)m_{\tilde q'_t}^2+m_{\tilde g}^2(m_V^2-m_{\tilde q_s}^2))))\Big)\\
&-\frac{1}{12m_V^2}B_0(m_{\tilde q_s}^2,m_{\tilde g}^2,m_{q_n}^2)\Big(C^{q_\mathrm{R}}_{q_nq'_mV}(C^{\tilde g,q_\mathrm{R}}_{sn}m_{q_n}(m_{\tilde g}(C^{\tilde g,q'_\mathrm{L}}_{tm})^*\\
&\quad+(C^{\tilde g,q'_\mathrm{R}}_{tm})^*m_{q'_m})(m_V^2+m_{\tilde q_s}^2-m_{\tilde q'_t}^2)+C^{\tilde g,q_\mathrm{L}}_{sn}(m_{\tilde g}(C^{\tilde g,q'_\mathrm{R}}_{tm})^*m_{q'_m}(m_V^2+m_{\tilde q_s}^2-m_{\tilde q'_t}^2)\\
&\quad+(C^{\tilde g,q'_\mathrm{L}}_{tm})^*(-m_{\tilde q_s}^4+(m_{\tilde g}^2+m_V^2+m_{\tilde q'_t}^2)m_{\tilde q_s}^2+m_{\tilde g}^2(m_V^2-m_{\tilde q'_t}^2))))\\
&\quad+C^{q_\mathrm{L}}_{q_nq'_mV}((C^{\tilde g,q'_\mathrm{L}}_{tm})^*(m_{\tilde g}C^{\tilde g,q_\mathrm{R}}_{sn}+C^{\tilde g,q_\mathrm{L}}_{sn}m_{q_n})m_{q'_m}(m_V^2+m_{\tilde q_s}^2-m_{\tilde q'_t}^2)\\
&\quad+(C^{\tilde g,q'_\mathrm{R}}_{tm})^*(m_{\tilde g}C^{\tilde g,q_\mathrm{L}}_{sn}m_{q_n}(m_V^2+m_{\tilde q_s}^2-m_{\tilde q'_t}^2)\\
&\quad+C^{\tilde g,q_\mathrm{R}}_{sn}(-m_{\tilde q_s}^4+(m_{\tilde g}^2+m_V^2+m_{\tilde q'_t}^2)m_{\tilde q_s}^2+m_{\tilde g}^2(m_V^2-m_{\tilde q'_t}^2))))\Big)\\
&+\frac{1}{12m_V^2}C_0(m_V^2,m_{\tilde q_s}^2,m_{\tilde q'_t}^2,m_{q'_m}^2,m_{q_n}^2,m_{\tilde g}^2)\Big(C^{q_\mathrm{R}}_{q_nq'_mV}(C^{\tilde g,q_\mathrm{L}}_{sn}(m_{\tilde g}(C^{\tilde g,q'_\mathrm{R}}_{tm})^*m_{q'_m}(m_V^4+2m_{\tilde g}^2m_V^2\\
&\quad-(m_{\tilde q_s}^2+m_{\tilde q'_t}^2)m_V^2-m_{q'_m}^2(m_V^2+m_{\tilde q_s}^2-m_{\tilde q'_t}^2)-m_{q_n}^2(m_V^2-m_{\tilde q_s}^2+m_{\tilde q'_t}^2))\\
&\quad+(C^{\tilde g,q'_\mathrm{L}}_{tm})^*(2((m_{\tilde g}^2+m_V^2-m_{\tilde q'_t}^2)m_{\tilde g}^2+m_{\tilde q_s}^2(m_{\tilde q'_t}^2-m_{\tilde g}^2))m_V^2\\
&\quad+m_{q_n}^2(m_{\tilde q'_t}^4-(m_{\tilde g}^2+m_V^2+m_{\tilde q_s}^2)m_{\tilde q'_t}^2+m_{\tilde g}^2(m_{\tilde q_s}^2-m_V^2))\\
&\quad-m_{q'_m}^2(-m_{\tilde q_s}^4+(m_{\tilde g}^2+m_V^2+m_{\tilde q'_t}^2)m_{\tilde q_s}^2+m_{\tilde g}^2(m_V^2-m_{\tilde q'_t}^2))))\\
&\quad-C^{\tilde g,q_\mathrm{R}}_{sn}m_{q_n}((C^{\tilde g,q'_\mathrm{R}}_{tm})^*m_{q'_m}(m_{\tilde q_s}^4-m_V^2m_{\tilde q_s}^2+m_{\tilde q'_t}^4-2m_{\tilde g}^2m_V^2-(m_V^2+2m_{\tilde q_s}^2)m_{\tilde q'_t}^2\\
&\quad+m_{q'_m}^2(m_V^2+m_{\tilde q_s}^2-m_{\tilde q'_t}^2)+m_{q_n}^2(m_V^2-m_{\tilde q_s}^2+m_{\tilde q'_t}^2))\\
&\quad+m_{\tilde g}(C^{\tilde g,q'_\mathrm{L}}_{tm})^*((-2m_{\tilde g}^2-m_V^2+m_{\tilde q_s}^2+m_{\tilde q'_t}^2)m_V^2\\
&\quad+m_{q'_m}^2(m_V^2+m_{\tilde q_s}^2-m_{\tilde q'_t}^2)+m_{q_n}^2(m_V^2-m_{\tilde q_s}^2+m_{\tilde q'_t}^2))))\\
&\quad+C^{q_\mathrm{L}}_{q_nq'_mV}((C^{\tilde g,q'_\mathrm{R}}_{tm})^*(m_{\tilde g}C^{\tilde g,q_\mathrm{L}}_{sn}m_{q_n}(m_V^4+2m_{\tilde g}^2m_V^2-(m_{\tilde q_s}^2+m_{\tilde q'_t}^2)m_V^2\\
&\quad-m_{q'_m}^2(m_V^2+m_{\tilde q_s}^2-m_{\tilde q'_t}^2)-m_{q_n}^2(m_V^2-m_{\tilde q_s}^2+m_{\tilde q'_t}^2))\\
&\quad+C^{\tilde g,q_\mathrm{R}}_{sn}(2((m_{\tilde g}^2+m_V^2-m_{\tilde q'_t}^2)m_{\tilde g}^2+m_{\tilde q_s}^2(m_{\tilde q'_t}^2-m_{\tilde g}^2))m_V^2\\
&\quad+m_{q_n}^2(m_{\tilde q'_t}^4-(m_{\tilde g}^2+m_V^2+m_{\tilde q_s}^2)m_{\tilde q'_t}^2+m_{\tilde g}^2(m_{\tilde q_s}^2-m_V^2))\\
&\quad-m_{q'_m}^2(-m_{\tilde q_s}^4+(m_{\tilde g}^2+m_V^2+m_{\tilde q'_t}^2)m_{\tilde q_s}^2+m_{\tilde g}^2(m_V^2-m_{\tilde q'_t}^2))))\\
&\quad-(C^{\tilde g,q'_\mathrm{L}}_{tm})^*m_{q'_m}(C^{\tilde g,q_\mathrm{L}}_{sn}m_{q_n}(m_{\tilde q_s}^4-m_V^2m_{\tilde q_s}^2+m_{\tilde q'_t}^4-2m_{\tilde g}^2m_V^2-(m_V^2+2m_{\tilde q_s}^2)m_{\tilde q'_t}^2
\end{aligned}
$$

$$+m^2_{q'_m}(m^2_V+m^2_{\tilde{q}_s}-m^2_{\tilde{q}'_t})+m^2_{q_n}(m^2_V-m^2_{\tilde{q}_s}+m^2_{\tilde{q}'_t}))+m_{\tilde{g}}C^{\tilde{g},q_R}_{sn}((-2m^2_{\tilde{g}}-m^2_V+m^2_{\tilde{q}_s}$$
$$+m^2_{\tilde{q}'_t})m^2_V+m^2_{q'_m}(m^2_V+m^2_{\tilde{q}_s}-m^2_{\tilde{q}'_t})+m^2_{q_n}(m^2_V-m^2_{\tilde{q}_s}+m^2_{\tilde{q}'_t}))))\Big)\Big]\,.$$

Finally, we have the squark to squark and scalar decay. Here, we use the generic notation S for either a neutral Higgs scalar Φ or the charged Higgs $H^\pm$. We have the generic squark-squark-scalar couplings $C_{\tilde{q}_s\tilde{q}'_t S}$ and the left- and right-chiral quark-quark-scalar couplings $C^{q_L/q_R}_{qq'S}$. These couplings are already implemented in `NMSSMCALC` and were taken over from there. The diagrams contributing to the vertex corrections are given in Fig. 13.3d.

The NLO correction to the decay width can be written as

$$\Delta\Gamma^{\rm NLO}_{\tilde{q}_s\to\tilde{q}'_t S}=\lambda(m^2_{\tilde{q}_s},m^2_{\tilde{q}'_t},m^2_S)\frac{1}{16\pi m^3_{\tilde{q}_s}}\frac{1}{3}\sum_{\rm colour}2{\rm Re}\left[\left(\mathcal{A}^{\rm LO}_{\tilde{q}_s\to\tilde{q}'_t S}\right)^*\mathcal{A}^{\rm NLO}_{\tilde{q}_s\to\tilde{q}'_t S}\right]\,, \tag{G.29}$$

where we average and sum over the colour of the squarks. We define the quantity

$$\mathcal{D}_{\tilde{q}_s\to\tilde{q}'_t S}\equiv\sum_{\rm colour}\left[\left(\mathcal{A}^{\rm LO}_{\tilde{q}_s\to\tilde{q}'_t S}\right)^*\mathcal{A}^{\rm NLO}_{\tilde{q}_s\to\tilde{q}'_t S}\right]\,, \tag{G.30}$$

that we split up into the contributions,

$$\mathcal{D}_{\tilde{q}_s\to\tilde{q}'_t S}=\mathcal{D}^{(g)}_{\tilde{q}_s\to\tilde{q}'_t S}+\mathcal{D}^{(\tilde{g})}_{\tilde{q}_s\to\tilde{q}'_t S}+\mathcal{D}^{(\tilde{q})}_{\tilde{q}_s\to\tilde{q}'_t S}+\mathcal{D}^{(\rm abs)}_{\tilde{q}_s\to\tilde{q}'_t S}\,, \tag{G.31}$$

where we now also have an additional diagram with the quartic squark coupling. The gluon contribution is given by

$$\mathcal{D}^{(g)}_{\tilde{q}_s\to\tilde{q}'_t S}=-\frac{3g_s^2|C_{\tilde{q}_s\tilde{q}'_t S}|^2}{12\pi^2}\,[\tag{G.32}$$
$$+B_0(m^2_S,m^2_{\tilde{q}_s},m^2_{\tilde{q}'_t})+B_0(m^2_{\tilde{q}_s},0,m^2_{\tilde{q}_s})+B_0(m^2_{\tilde{q}'_t},0,m^2_{\tilde{q}'_t})+B_0(0,\lambda^2,\lambda^2)(\xi_g-1)$$
$$+2(-m^2_S+m^2_{\tilde{q}_s}+m^2_{\tilde{q}'_t})C_0(m^2_{\tilde{q}_s},m^2_S,m^2_{\tilde{q}'_t},\lambda^2,m^2_{\tilde{q}_s},m^2_{\tilde{q}'_t})\Big]\,.$$

The gluino contribution reads

$$\mathcal{D}^{(\tilde{g})}_{\tilde{q}_s\to\tilde{q}'_t S}=\frac{3g_s^2(C_{\tilde{q}_s\tilde{q}'_t S})^*}{12\pi^2}\left[\sum_{m,n=1}^{3}\right. \tag{G.33}$$
$$B_0(m^2_{\tilde{q}_s},m^2_{\tilde{g}},m^2_{q_n})\left((C^{\tilde{g},q'_L}_{tm})^*C^{q_L}_{q_nq'_mS}(m_{q_n}C^{\tilde{g},q_L}_{sn}+m_{\tilde{g}}C^{\tilde{g},q_R}_{sn})\right.$$
$$\left.+(C^{\tilde{g},q'_R}_{tm})^*C^{q_R}_{q_nq'_mS}(m_{\tilde{g}}C^{\tilde{g},q_L}_{sn}+m_{q_n}C^{\tilde{g},q_R}_{sn})\right)$$
$$+B_0(m^2_{\tilde{q}'_t},m^2_{\tilde{g}},m^2_{q'_m})\left(C^{\tilde{g},q_L}_{sn}C^{q_R}_{q_nq'_mS}(m_{q'_m}(C^{\tilde{g},q'_L}_{tm})^*+m_{\tilde{g}}(C^{\tilde{g},q'_R}_{tm})^*)\right.$$
$$\left.+C^{\tilde{g},q_R}_{sn}C^{q_L}_{q_nq'_mS}(m_{\tilde{g}}(C^{\tilde{g},q'_L}_{tm})^*+m_{q'_m}(C^{\tilde{g},q'_R}_{tm})^*)\right)$$
$$+B_0(m^2_S,m^2_{q_n},m^2_{q'_m})\left(C^{\tilde{g},q_L}_{sn}(C^{\tilde{g},q'_L}_{tm})^*(m_{q_n}C^{q_L}_{q_nq'_mS}+m_{q'_m}C^{q_R}_{q_nq'_mS})\right.$$
$$\left.+C^{\tilde{g},q_R}_{sn}(C^{\tilde{g},q'_R}_{tm})^*(m_{q'_m}C^{q_L}_{q_nq'_mS}+m_{q_n}C^{q_R}_{q_nq'_mS})\right)$$
$$+C_0(m^2_S,m^2_{\tilde{q}_s},m^2_{\tilde{q}'_t},m^2_{q'_m},m^2_{q_n},m^2_{\tilde{g}})\left(C^{q_L}_{q_nq'_mS}((C^{\tilde{g},q'_L}_{tm})^*(m_{q_n}C^{\tilde{g},q_L}_{sn}(m^2_{q'_m}+m^2_{\tilde{g}}-m^2_{\tilde{q}'_t})\right.$$
$$+m_{\tilde{g}}C^{\tilde{g},q_R}_{sn}(m^2_{q'_m}-m^2_S+m^2_{q_n}))+m_{q'_m}(C^{\tilde{g},q'_R}_{tm})^*(2m_{\tilde{g}}m_{q_n}C^{\tilde{g},q_L}_{sn}+C^{\tilde{g},q_R}_{sn}(m^2_{\tilde{g}}+m^2_{q_n}-m^2_{\tilde{q}_s})))$$
$$\left.+C^{q_R}_{q_nq'_mS}(C^{\tilde{g},q_L}_{sn}(m_{q'_m}(C^{\tilde{g},q'_L}_{tm})^*(m^2_{\tilde{g}}+m^2_{q_n}-m^2_{\tilde{q}_s})+m_{\tilde{g}}(C^{\tilde{g},q'_R}_{tm})^*(m^2_{q'_m}-m^2_S+m^2_{q_n}))\right.$$

$$+m_{q_n} C_{sn}^{\tilde{g},q_R}(2m_{\tilde{g}} m_{q'_m}(C_{tm}^{\tilde{g},q'_L})^* + (C_{tm}^{\tilde{g},q'_R})^*(m_{q'_m}^2 + m_{\tilde{g}}^2 - m_{\tilde{q}'_t}^2)))\Big)\Big] \,.$$

The contribution including the quartic squark coupling is given by

$$\mathcal{D}_{\tilde{q}_s\to\tilde{q}'_t S}^{(\tilde{g})} = -\frac{3g_s^2 (C_{\tilde{q}_s\tilde{q}'_t S})^*}{16\pi^2}\left[\sum_{l,r=1}^{6} C_{\tilde{q}_l\tilde{q}'_r S} C_{\tilde{q}_s\tilde{q}'_t\tilde{q}'_r\tilde{q}_l} B_0(m_S^2, m_{\tilde{q}_l}^2, m_{\tilde{q}'_r}^2)\right] . \tag{G.34}$$

Here, in the case of a neutral scalar Φ in the final state, only the squark loop with the same flavour in the loop as the initial and final squark contributes. In the case of a charged scalar, $H^\pm$, in the final state, we have different squark flavours in the loop.

G.1.3. Real Corrections

We now present the real corrections to the supersymmetric particle decays, described in Sec. 13.3.1. In Fig. 13.4 we show the real corrections for the squark to quark and gluino decay. Similarly, we have diagrams for the real corrections to the other decay channels. With $\mathcal{A}^{\text{real}}$ we denote the sum of all amplitudes contributing to the real corrections. We will also follow the notation in [200] where the definitions for the integrals I and the overall prefactor were taken from. For the couplings, we use the same notation as in Sec. G.1.2 for the vertex corrections.

We start with the neutralino/chargino decays. The real corrections can be written as

$$\Gamma^{\text{real}}_{\tilde{\chi}_i\to q'_n\tilde{q}_t^*} = \frac{1}{(2\pi)^5}\frac{1}{2m_{\tilde{\chi}_i}}\pi^2\frac{1}{2}\sum_{\text{spin,polarization,colour}} |\mathcal{A}^{\text{real}}_{\tilde{\chi}_i\to q'_n\tilde{q}_t^*}|^2 \,, \tag{G.35}$$

where we average and sum over the spin and colour of the neutralino/chargino, the quark and the squark. Additionally, we sum over the polarization of the emitted gluon. We then obtain

$$\begin{aligned}
\sum_{\text{spin,polarization,colour}} |\mathcal{A}^{\text{real}}_{\tilde{\chi}_i\to q'_n\tilde{q}_t^*}|^2 = -8g_s^2\,[\qquad & \text{(G.36)}\\
&(|C_{nti}^{\tilde{\chi},q'_L}|^2 + |C_{nti}^{\tilde{\chi},q'_R}|^2)\Big(2(m_{\tilde{\chi}_i}^2 + m_{q'_n}^2 - m_{\tilde{q}_t}^2)(m_{\tilde{\chi}_i}^2(I_{01}+I_{02})\\
&-m_{q'_n}^2(I_{01}+I_{02}-I_{11}) - m_{\tilde{q}_t}^2(I_{01}+I_{02}-I_{22}) + I_1 + I_2) + I_1^0\Big)\\
&+8m_{\tilde{\chi}_i}m_{q'_n}\,\text{Re}\left(C_{nti}^{\tilde{\chi},q'_L}(C_{nti}^{\tilde{\chi},q'_R})^*\right)\Big(m_{\tilde{\chi}_i}^2(I_{01}+I_{02}) - m_{q'_n}^2(I_{01}+I_{02}-I_{11})\\
&-m_{\tilde{q}_t}^2(I_{01}+I_{02}-I_{22}) + I_1 + I_2)\Big]\,.
\end{aligned}$$

Next, we have the gluino to squark-quark decay. The real corrections can be written as

$$\Gamma^{\text{real}}_{\tilde{g}\to q'_n\tilde{q}_t^*} = \frac{1}{(2\pi)^5}\frac{1}{2m_{\tilde{g}}}\pi^2\frac{1}{2}\frac{1}{8}\sum_{\text{spin,polarization,colour}} |\mathcal{A}^{\text{real}}_{\tilde{g}\to q'_n\tilde{q}_t^*}|^2 \,, \tag{G.37}$$

where we average and sum over the spin, colour and polarization of the gluino, the quark, the squark and the gluon. The squared amplitude then reads

$$\begin{aligned}
\sum_{\text{spin,polarization,colour}} |\mathcal{A}^{\text{real}}_{\tilde{g}\to q'_n\tilde{q}_t^*}|^2 = -\frac{8}{3}g_s^4\,[\qquad & \text{(G.38)}\\
&(|C_{tn}^{\tilde{g},q_L}|^2 + |C_{tn}^{\tilde{g},q_R}|^2)\,\big(9I + 4I_1^0 + 9I_0^1 + 2m_{q_n}^2(9I_0 + m_{\tilde{g}}^2(9(I_{00}+I_{01}) + 4I_{11})\\
&+ m_{\tilde{q}_t}^2(-9I_{01} + 9I_{02} - 4I_{11} + 4I_{22}) + 4(I_1+I_2)) + 2m_{\tilde{q}_t}^2(-9I_0 + m_{\tilde{g}}^2(-9I_{00} - 8I_{01}\\
&+ I_{02} + 4I_{22}) + m_{\tilde{q}_t}^2(4I_{01} - 5I_{02} - 4I_{22}) - 4(I_1+I_2)) + 2m_{\tilde{g}}^2(9I_0 + m_{\tilde{g}}^2(9I_{00} + 4(I_{01}+I_{02}))
\end{aligned}$$

$$
\begin{aligned}
&+4(I_1+I_2))+2m_{q_n}^4(5I_{01}-4I_{02}+4I_{11})\big)\\
&+8m_{\tilde{g}}m_{q_n}\mathrm{Re}\left(C_{tn}^{\tilde{g},q_\mathrm{L}}(C_{tn}^{\tilde{g},q_\mathrm{R}})^*\right)\big(9I_0+m_{\tilde{g}}^2(9I_{00}+4(I_{01}+I_{02}))+m_{q_n}^2(5I_{01}-4I_{02}+4I_{11})\\
&+m_{\tilde{q}_t}^2(-4I_{01}+5I_{02}+4I_{22})+4(I_1+I_2))\big]\ .
\end{aligned}
$$

In the case of massless quarks in the final state one has to properly perform the limit of vanishing quark masses in the above expressions as we discussed in Sec. 13.3.1. The results can be found in our code or in [307, 310]. We will also again omit the expressions for the squark to quark neutralino/chargino decay and the squark to quark and gluino decay. They can be derived similarly to the above expressions where one has to interchange the kinematics accordingly.

The real corrections for the squark to squark and vector boson decay can be written as

$$
\Gamma^{\mathrm{real}}_{\tilde{q}_s\to\tilde{q}_t'V}=\frac{1}{(2\pi)^5}\frac{1}{2m_{\tilde{q}_s}}\pi^2\frac{1}{3}\sum_{\text{polarization,colour}}|\mathcal{A}^{\mathrm{real}}_{\tilde{q}_s\to\tilde{q}_t'V}|^2\,, \tag{G.39}
$$

where we average and sum over the colour and polarization of the squarks and the emitted gluon. We then have

$$
\begin{aligned}
\sum_{\text{polarization,colour}}|\mathcal{A}^{\mathrm{real}}_{\tilde{q}_s\to\tilde{q}_t'V}|^2&=\frac{16g_s^2}{m_V^2}|C_{\tilde{q}_s\tilde{q}_t'V}|^2\,[\\
&2m_V^2I-m_{\tilde{q}_t'}^4(I_0+m_{\tilde{q}_s}^2(I_{00}-I_{01}-2I_{11})+m_V^2(-(3I_{01}+2I_{11}))+I_1)\\
&+m_{\tilde{q}_t'}^2(2m_{\tilde{q}_s}^2(I_0+m_V^2(I_{00}+I_{01}+I_{11})+I_1)+2m_V^2(I_0+I_1)+m_{\tilde{q}_s}^4(2I_{00}+I_{01}-I_{11})\\
&+m_V^4(-(3I_{01}+I_{11})))+m_V^2m_{\tilde{q}_s}^2(2(I_0+I_1)-m_V^2(I_{00}+3I_{01}))\\
&-m_{\tilde{q}_s}^4(I_0+m_V^2(-(2I_{00}+3I_{01}))+I_1)-m_V^4(I_0+I_1)-(I_{00}+I_{01})m_{\tilde{q}_s}^6\\
&-(I_{01}+I_{11})m_{\tilde{q}_t'}^6+I_{01}m_V^6\big]
\end{aligned} \tag{G.40}
$$

Finally, we have the real correction for the squark to squark and scalar decay. They can be written as

$$
\Gamma^{\mathrm{real}}_{\tilde{q}_s\to\tilde{q}_t'S}=\frac{1}{(2\pi)^5}\frac{1}{2m_{\tilde{q}_s}}\pi^2\frac{1}{3}\sum_{\text{polarization,colour}}|\mathcal{A}^{\mathrm{real}}_{\tilde{q}_s\to\tilde{q}_t'S}|^2\,, \tag{G.41}
$$

where we average and sum over the colour and polarization of the squarks and the emitted gluon. We then have

$$
\begin{aligned}
\sum_{\text{polarization,colour}}|\mathcal{A}^{\mathrm{real}}_{\tilde{q}_s\to\tilde{q}_t'S}|^2&=-16g_s^2|C_{\tilde{q}_s\tilde{q}_t'S}|^2\\
&\left(I_0+(I_{00}+I_{01})m_{\tilde{q}_s}^2+(I_{01}+I_{11})m_{\tilde{q}_t'}^2-I_{01}m_S^2+I_1\right)\ .
\end{aligned} \tag{G.42}
$$

G.2. Analytic Expressions for the Radiative Two-Body Decay

We give the analytic results for the radiative neutralino decay, $\tilde{\chi}_i^0\to\gamma\tilde{\chi}_j^0$ $(i=2,..,5,j=1,..,4)$, discussed in Sec. 13.2. We denote by p_1 the momentum of the ingoing neutralino, $\tilde{\chi}_i^0$, by p_2 the momentum of the outgoing neutralino, $\tilde{\chi}_j^0$, and by p_3 the momentum of the photon, with polarization vector $\epsilon^\mu(p_3)$. Next, we split the amplitude into several parts,

$$
\begin{aligned}
\mathcal{A}_{\tilde{\chi}_i^0\to\gamma\tilde{\chi}_j^0}=\bar{u}(p_2,m_{\tilde{\chi}_j^0})\,(&A\not{\epsilon}(p_3)P_\mathrm{R}+B\not{\epsilon}(p_3)P_\mathrm{L}\\
&+C(p_1\cdot\epsilon(p_3))P_\mathrm{R}+D(p_1\cdot\epsilon(p_3))P_\mathrm{L})\,u(p_1,m_{\tilde{\chi}_i^0})\,,
\end{aligned} \tag{G.43}
$$

with the spinors u, the projection operators $P_{\mathrm{L/R}}$ and the coefficients A, B, C, D. These coefficents obtain contributions from the various Feynman diagrams depicted in Fig. 13.2, where we denote the diagrams with sfermions by $(\tilde{f})$, the diagrams with charginos and W bosons by (W) and the diagrams with charginos and charged Higgs scalars by $(H^\pm)$. We thus have

$$A = A^{(\tilde{f})} + A^{(W)} + A^{(H^\pm)}\,, \tag{G.44}$$

for the coefficient A and similarly for the other coefficients. In the following we need the neutralino-sfermion-fermion couplings, denoted by $G^{f_\mathrm{L}/f_\mathrm{R}}_{mli}$, with an ingoing fermion f_m, sfermion $\tilde{f}_l$ and neutralino $\tilde{\chi}^0_i$ ($m = 1,2,3$, $l = 1,..,6$, $i = 1,..,5$). We also require the neutralino-chargino-$H^\pm$ couplings $C^{\mathrm{L/R}}_{\tilde{\chi}^0_i\tilde{\chi}^\pm_m H^\pm}$ and neutralino-chargino-W couplings $C^{\mathrm{L/R}}_{\tilde{\chi}^0_i\tilde{\chi}^\pm_m W}$ ($i = 1,..,5$, $m = 1,2$) with an ingoing chargino. They were taken from [63].

The contributions from the sfermions read

$$\begin{aligned}
A^{(\tilde{f})} = \sum_{f=U,D,L}\sum_{l=1}^{6}\sum_{m=1}^{3}\frac{eQ_f}{16\pi^2}\,[\; & \qquad\text{(G.45a)}\\
&\frac{m_{\tilde{\chi}^0_i}m_{\tilde{\chi}^0_j}}{(m_{\tilde{\chi}^0_i}-m_{\tilde{\chi}^0_j})(m_{\tilde{\chi}^0_i}+m_{\tilde{\chi}^0_j})}B_0(m^2_{\tilde{\chi}^0_i},m^2_{f_m},m^2_{\tilde{f}_l})\left(G^{f_\mathrm{L}}_{mli}(G^{f_\mathrm{L}}_{mlj})^* - G^{f_\mathrm{R}}_{mlj}(G^{f_\mathrm{R}}_{mli})^*\right)\\
&+\frac{m_{\tilde{\chi}^0_i}m_{\tilde{\chi}^0_j}}{(m_{\tilde{\chi}^0_i}-m_{\tilde{\chi}^0_j})(m_{\tilde{\chi}^0_i}+m_{\tilde{\chi}^0_j})}B_0(m^2_{\tilde{\chi}^0_j},m^2_{f_m},m^2_{\tilde{f}_l})\left(G^{f_\mathrm{R}}_{mlj}(G^{f_\mathrm{R}}_{mli})^* - G^{f_\mathrm{L}}_{mli}(G^{f_\mathrm{L}}_{mlj})^*\right)\\
&+m^2_{\tilde{f}_l}C_0(0,m^2_{\tilde{\chi}^0_i},m^2_{\tilde{\chi}^0_j},m^2_{\tilde{f}_l},m^2_{\tilde{f}_l},m^2_{f_m})\left(G^{f_\mathrm{L}}_{mlj}(G^{f_\mathrm{L}}_{mli})^* - G^{f_\mathrm{R}}_{mli}(G^{f_\mathrm{R}}_{mlj})^*\right)\\
&+m_{f_m}C_0(0,m^2_{\tilde{\chi}^0_i},m^2_{\tilde{\chi}^0_j},m^2_{f_m},m^2_{f_m},m^2_{\tilde{f}_l})\left(G^{f_\mathrm{L}}_{mlj}(m_{f_m}(G^{f_\mathrm{L}}_{mli})^* + m_{\tilde{\chi}^0_i}(G^{f_\mathrm{R}}_{mli})^*\right.\\
&\quad\left.-(G^{f_\mathrm{R}}_{mlj})^*(m_{\tilde{\chi}^0_i}G^{f_\mathrm{L}}_{mli}+m_{f_m}G^{f_\mathrm{R}}_{mli}) - m_{\tilde{\chi}^0_j}G^{f_\mathrm{R}}_{mli}(G^{f_\mathrm{L}}_{mlj})^* + m_{\tilde{\chi}^0_j}G^{f_\mathrm{R}}_{mlj}(G^{f_\mathrm{L}}_{mli})^*\right)\\
&+(G^{f_\mathrm{L}}_{mlj}(G^{f_\mathrm{L}}_{mli})^* - G^{f_\mathrm{R}}_{mli}(G^{f_\mathrm{R}}_{mlj})^*)\Big]\,,
\end{aligned}$$

$$B^{(\tilde{f})} = A^{(\tilde{f})}(G^{f_\mathrm{L}} \leftrightarrow G^{f_\mathrm{R}})\,, \tag{G.45b}$$

$$\begin{aligned}
C^{(\tilde{f})} = \sum_{f=U,D,L}\sum_{l=1}^{6}\sum_{m=1}^{3}\frac{eQ_f}{8\pi^2(m^2_{\tilde{\chi}^0_i}-m^2_{\tilde{\chi}^0_j})}\,[\; & \qquad\text{(G.45c)}\\
&\frac{m_{\tilde{\chi}^0_i}m_{\tilde{\chi}^0_j}}{m^2_{\tilde{\chi}^0_i}-m^2_{\tilde{\chi}^0_j}}B_0(m^2_{\tilde{\chi}^0_i},m^2_{f_m},m^2_{\tilde{f}_l})\left(m_{\tilde{\chi}^0_i}G^{f_\mathrm{L}}_{mlj}(G^{f_\mathrm{L}}_{mli})^* + m_{\tilde{\chi}^0_j}G^{f_\mathrm{L}}_{mli}(G^{f_\mathrm{L}}_{mlj})^*\right.\\
&\quad\left.-m_{\tilde{\chi}^0_i}G^{f_\mathrm{R}}_{mli}(G^{f_\mathrm{R}}_{mlj})^* - m_{\tilde{\chi}^0_j}G^{f_\mathrm{R}}_{mlj}(G^{f_\mathrm{R}}_{mli})^*\right)\\
&+\frac{m_{\tilde{\chi}^0_i}m_{\tilde{\chi}^0_j}}{m^2_{\tilde{\chi}^0_i}-m^2_{\tilde{\chi}^0_j}}B_0(m^2_{\tilde{\chi}^0_j},m^2_{f_m},m^2_{\tilde{f}_l})\left(-m_{\tilde{\chi}^0_i}G^{f_\mathrm{L}}_{mlj}(G^{f_\mathrm{L}}_{mli})^* - m_{\tilde{\chi}^0_j}G^{f_\mathrm{L}}_{mli}(G^{f_\mathrm{L}}_{mlj})^*\right.\\
&\quad\left.+m_{\tilde{\chi}^0_i}G^{f_\mathrm{R}}_{mli}(G^{f_\mathrm{R}}_{mlj})^* + m_{\tilde{\chi}^0_j}G^{f_\mathrm{R}}_{mlj}(G^{f_\mathrm{R}}_{mli})^*\right)\\
&+m^2_{\tilde{f}_l}C_0(0,m^2_{\tilde{\chi}^0_i},m^2_{\tilde{\chi}^0_j},m^2_{\tilde{f}_l},m^2_{\tilde{f}_l},m^2_{f_m})\left(m_{\tilde{\chi}^0_i}G^{f_\mathrm{L}}_{mli}(G^{f_\mathrm{L}}_{mlj})^* + m_{\tilde{\chi}^0_j}G^{f_\mathrm{L}}_{mlj}(G^{f_\mathrm{L}}_{mli})^*\right.\\
&\quad\left.-m_{\tilde{\chi}^0_i}G^{f_\mathrm{R}}_{mlj}(G^{f_\mathrm{R}}_{mli})^* - m_{\tilde{\chi}^0_j}G^{f_\mathrm{R}}_{mli}(G^{f_\mathrm{R}}_{mlj})^*\right)\\
&+m_{f_m}C_0(0,m^2_{\tilde{\chi}^0_i},m^2_{\tilde{\chi}^0_j},m^2_{f_m},m^2_{f_m},m^2_{\tilde{f}_l})\left(m_{f_m}(m_{\tilde{\chi}^0_i}G^{f_\mathrm{L}}_{mli}(G^{f_\mathrm{L}}_{mlj})^* + m_{\tilde{\chi}^0_j}G^{f_\mathrm{L}}_{mlj}(G^{f_\mathrm{L}}_{mli})^*\right.\\
&\quad -m_{\tilde{\chi}^0_i}G^{f_\mathrm{R}}_{mlj}(G^{f_\mathrm{R}}_{mli})^* - m_{\tilde{\chi}^0_j}G^{f_\mathrm{R}}_{mli}(G^{f_\mathrm{R}}_{mlj})^*) + (m_{\tilde{\chi}^0_i}-m_{\tilde{\chi}^0_j})(m_{\tilde{\chi}^0_i}+m_{\tilde{\chi}^0_j})(G^{f_\mathrm{R}}_{mli}(G^{f_\mathrm{L}}_{mlj})^*\\
&\quad\left.-G^{f_\mathrm{R}}_{mlj}(G^{f_\mathrm{L}}_{mli})^*)\right)
\end{aligned}$$

$$+\left(m_{\tilde{\chi}_i^0} G^{f_L}_{mli}(G^{f_L}_{mlj})^* + m_{\tilde{\chi}_j^0} G^{f_L}_{mlj}(G^{f_L}_{mli})^* - m_{\tilde{\chi}_i^0} G^{f_R}_{mlj}(G^{f_R}_{mli})^* - m_{\tilde{\chi}_j^0} G^{f_R}_{mli}(G^{f_R}_{mlj})^*\right)\Big] ,$$

$$D^{(\tilde{f})} = C^{(\tilde{f})}(G^{f_L} \leftrightarrow G^{f_R}) , \tag{G.45d}$$

where we sum over up-type (U) and down-type (D) quarks as well as charged leptons (L) with fractional charges Q_f. The $B^{(\tilde{f})}$ and $D^{(\tilde{f})}$ coefficients are obtained from the $A^{(\tilde{f})}$ and $C^{(\tilde{f})}$ coefficients by interchanging the left- and right-chiral couplings G^{f_L/f_R}.

The contribution involving the charged Higgs, $H^\pm$, can be obtained from the sfermion contributions by using the replacements

$$A^{(H^\pm)} = A^{(\tilde{f})}(m_f \to m_{\tilde{\chi}^\pm},\, m_{\tilde{f}} \to m_{H^\pm},\, G^{f_{L/R}} \to C^{L/R}_{\tilde{\chi}^0 \tilde{\chi}^\pm H^\pm}) , \tag{G.46}$$

i.e. replacing the fermion mass with the chargino mass, the sfermion mass with the charged Higgs mass and the fermion-sfermion-neutralino couplings with the chargino-neutralino-$H^\pm$ couplings. This is true for all coefficients A, B, C and D. Additionally, the sums over the running indices in the loop have to be adjusted accordingly.

The coefficients for the contributions involving charginos and W bosons are given by

$$A^{(W)} = \frac{e}{8\pi^2}\,[\tag{G.47a}$$

$$\frac{m_{\tilde{\chi}_i^0} m_{\tilde{\chi}_j^0}}{(m_{\tilde{\chi}_i^0} - m_{\tilde{\chi}_j^0})^2} B_0(m^2_{\tilde{\chi}_i^0}, m^2_W, m^2_{\tilde{\chi}_m^\pm}) \left(C^R_{\tilde{\chi}_i^0 \tilde{\chi}_m^\pm W}(C^R_{\tilde{\chi}_j^0 \tilde{\chi}_m^\pm W})^* - C^L_{\tilde{\chi}_j^0 \tilde{\chi}_m^\pm W}(C^L_{\tilde{\chi}_i^0 \tilde{\chi}_m^\pm W})^*\right)$$

$$+ \frac{m_{\tilde{\chi}_i^0} m_{\tilde{\chi}_j^0}}{(m_{\tilde{\chi}_i^0} - m_{\tilde{\chi}_j^0})^2} B_0(m^2_{\tilde{\chi}_j^0}, m^2_W, m^2_{\tilde{\chi}_m^\pm}) \left(C^L_{\tilde{\chi}_j^0 \tilde{\chi}_m^\pm W}(C^L_{\tilde{\chi}_i^0 \tilde{\chi}_m^\pm W})^* - C^R_{\tilde{\chi}_i^0 \tilde{\chi}_m^\pm W}(C^R_{\tilde{\chi}_j^0 \tilde{\chi}_m^\pm W})^*\right)$$

$$+ m^2_{\tilde{\chi}_m^\pm} C_0(0, m^2_{\tilde{\chi}_i^0}, m^2_{\tilde{\chi}_j^0}, m^2_{\tilde{\chi}_m^\pm}, m^2_{\tilde{\chi}_m^\pm}, m^2_W) \left(C^R_{\tilde{\chi}_j^0 \tilde{\chi}_m^\pm W}(C^R_{\tilde{\chi}_i^0 \tilde{\chi}_m^\pm W})^* - C^L_{\tilde{\chi}_i^0 \tilde{\chi}_m^\pm W}(C^L_{\tilde{\chi}_j^0 \tilde{\chi}_m^\pm W})^*\right)$$

$$+ C_0(0, m^2_{\tilde{\chi}_i^0}, m^2_{\tilde{\chi}_j^0}, m^2_W, m^2_W, m^2_{\tilde{\chi}_m^\pm}) \Big(C^L_{\tilde{\chi}_i^0 \tilde{\chi}_m^\pm W}((m^2_{\tilde{\chi}_i^0} + m^2_{\tilde{\chi}_j^0} - m^2_W)(C^L_{\tilde{\chi}_j^0 \tilde{\chi}_m^\pm W})^*$$

$$-2m_{\tilde{\chi}_j^0} m_{\tilde{\chi}_m^\pm}(C^R_{\tilde{\chi}_j^0 \tilde{\chi}_m^\pm W})^*) + 2m_{\tilde{\chi}_j^0} C^L_{\tilde{\chi}_j^0 \tilde{\chi}_m^\pm W}(m_{\tilde{\chi}_m^\pm}(C^R_{\tilde{\chi}_i^0 \tilde{\chi}_m^\pm W})^* - m_{\tilde{\chi}_i^0}(C^L_{\tilde{\chi}_i^0 \tilde{\chi}_m^\pm W})^*)$$

$$+2m_{\tilde{\chi}_i^0} m_{\tilde{\chi}_m^\pm}(C^R_{\tilde{\chi}_j^0 \tilde{\chi}_m^\pm W}(C^L_{\tilde{\chi}_i^0 \tilde{\chi}_m^\pm W})^* - C^R_{\tilde{\chi}_i^0 \tilde{\chi}_m^\pm W}(C^L_{\tilde{\chi}_j^0 \tilde{\chi}_m^\pm W})^*)$$

$$-(m^2_{\tilde{\chi}_i^0} + m^2_{\tilde{\chi}_j^0} - m^2_W) C^R_{\tilde{\chi}_j^0 \tilde{\chi}_m^\pm W}(C^R_{\tilde{\chi}_i^0 \tilde{\chi}_m^\pm W})^* + 2m_{\tilde{\chi}_i^0} m_{\tilde{\chi}_j^0} C^R_{\tilde{\chi}_i^0 \tilde{\chi}_m^\pm W}(C^R_{\tilde{\chi}_j^0 \tilde{\chi}_m^\pm W})^*\Big)$$

$$+ \left(C^R_{\tilde{\chi}_j^0 \tilde{\chi}_m^\pm W}(C^R_{\tilde{\chi}_i^0 \tilde{\chi}_m^\pm W})^* - C^L_{\tilde{\chi}_i^0 \tilde{\chi}_m^\pm W}(C^L_{\tilde{\chi}_j^0 \tilde{\chi}_m^\pm W})^*\right)\Big] ,$$

$$B^{(W)} = A^{(W)}(C^L \leftrightarrow C^R) , \tag{G.47b}$$

$$C^{(W)} = \frac{e}{4\pi^2(m^2_{\tilde{\chi}_i^0} - m^2_{\tilde{\chi}_j^0})}\,[\tag{G.47c}$$

$$\frac{m_{\tilde{\chi}_i^0} m_{\tilde{\chi}_j^0}}{m^2_{\tilde{\chi}_i^0} - m^2_{\tilde{\chi}_j^0}} B_0(m^2_{\tilde{\chi}_j^0}, m^2_W, m^2_{\tilde{\chi}_m^\pm}) \Big(m_{\tilde{\chi}_i^0} C^L_{\tilde{\chi}_i^0 \tilde{\chi}_m^\pm W}(C^L_{\tilde{\chi}_j^0 \tilde{\chi}_m^\pm W})^* + m_{\tilde{\chi}_j^0} C^L_{\tilde{\chi}_j^0 \tilde{\chi}_m^\pm W}(C^L_{\tilde{\chi}_i^0 \tilde{\chi}_m^\pm W})^*$$

$$-m_{\tilde{\chi}_i^0} C^R_{\tilde{\chi}_j^0 \tilde{\chi}_m^\pm W}(C^R_{\tilde{\chi}_i^0 \tilde{\chi}_m^\pm W})^* - m_{\tilde{\chi}_j^0} C^R_{\tilde{\chi}_i^0 \tilde{\chi}_m^\pm W}(C^R_{\tilde{\chi}_j^0 \tilde{\chi}_m^\pm W})^*\Big)$$

$$+ \frac{m_{\tilde{\chi}_i^0} m_{\tilde{\chi}_j^0}}{m^2_{\tilde{\chi}_i^0} - m^2_{\tilde{\chi}_j^0}} B_0(m^2_{\tilde{\chi}_i^0}, m^2_W, m^2_{\tilde{\chi}_m^\pm}) \Big(-m_{\tilde{\chi}_i^0} C^L_{\tilde{\chi}_i^0 \tilde{\chi}_m^\pm W}(C^L_{\tilde{\chi}_j^0 \tilde{\chi}_m^\pm W})^*$$

$$-m_{\tilde{\chi}_j^0} C^L_{\tilde{\chi}_j^0 \tilde{\chi}_m^\pm W}(C^L_{\tilde{\chi}_i^0 \tilde{\chi}_m^\pm W})^* + m_{\tilde{\chi}_i^0} C^R_{\tilde{\chi}_j^0 \tilde{\chi}_m^\pm W}(C^R_{\tilde{\chi}_i^0 \tilde{\chi}_m^\pm W})^* + m_{\tilde{\chi}_j^0} C^R_{\tilde{\chi}_i^0 \tilde{\chi}_m^\pm W}(C^R_{\tilde{\chi}_j^0 \tilde{\chi}_m^\pm W})^*\Big)$$

$$
\begin{aligned}
&+ m^2_{\tilde{\chi}^\pm_m} C_0(0, m^2_{\tilde{\chi}^0_i}, m^2_{\tilde{\chi}^0_j}, m^2_{\tilde{\chi}^\pm_m}, m^2_{\tilde{\chi}^\pm_m}, m^2_W) \Big(-m_{\tilde{\chi}^0_i} C^{\mathrm{L}}_{\tilde{\chi}^0_j \tilde{\chi}^\pm_m W} (C^{\mathrm{L}}_{\tilde{\chi}^0_i \tilde{\chi}^\pm_m W})^* \\
&\quad - m_{\tilde{\chi}^0_j} C^{\mathrm{L}}_{\tilde{\chi}^0_i \tilde{\chi}^\pm_m W} (C^{\mathrm{L}}_{\tilde{\chi}^0_j \tilde{\chi}^\pm_m W})^* + m_{\tilde{\chi}^0_i} C^{\mathrm{R}}_{\tilde{\chi}^0_i \tilde{\chi}^\pm_m W} (C^{\mathrm{R}}_{\tilde{\chi}^0_j \tilde{\chi}^\pm_m W})^* + m_{\tilde{\chi}^0_j} C^{\mathrm{R}}_{\tilde{\chi}^0_j \tilde{\chi}^\pm_m W} (C^{\mathrm{R}}_{\tilde{\chi}^0_i \tilde{\chi}^\pm_m W})^* \Big) \\
&+ C_0(0, m^2_{\tilde{\chi}^0_i}, m^2_{\tilde{\chi}^0_j}, m^2_W, m^2_W, m^2_{\tilde{\chi}^\pm_m}) \Big(C^{\mathrm{L}}_{\tilde{\chi}^0_j \tilde{\chi}^\pm_m W} (m_{\tilde{\chi}^0_i} (m^2_{\tilde{\chi}^0_i} - m^2_{\tilde{\chi}^0_j} - m^2_W) (C^{\mathrm{L}}_{\tilde{\chi}^0_i \tilde{\chi}^\pm_m W})^* \\
&\quad + 2 m_{\tilde{\chi}^\pm_m} (m^2_{\tilde{\chi}^0_j} - m^2_{\tilde{\chi}^0_i}) (C^{\mathrm{R}}_{\tilde{\chi}^0_i \tilde{\chi}^\pm_m W})^*) - C^{\mathrm{L}}_{\tilde{\chi}^0_i \tilde{\chi}^\pm_m W} (m_{\tilde{\chi}^0_j} (m^2_{\tilde{\chi}^0_i} - m^2_{\tilde{\chi}^0_j} + m^2_W) (C^{\mathrm{L}}_{\tilde{\chi}^0_j \tilde{\chi}^\pm_m W})^* \\
&\quad + 2 m_{\tilde{\chi}^\pm_m} (m^2_{\tilde{\chi}^0_j} - m^2_{\tilde{\chi}^0_i}) (C^{\mathrm{R}}_{\tilde{\chi}^0_j \tilde{\chi}^\pm_m W})^*) + m_{\tilde{\chi}^0_i} (-m^2_{\tilde{\chi}^0_i} + m^2_{\tilde{\chi}^0_j} + m^2_W) C^{\mathrm{R}}_{\tilde{\chi}^0_i \tilde{\chi}^\pm_m W} (C^{\mathrm{R}}_{\tilde{\chi}^0_j \tilde{\chi}^\pm_m W})^* \\
&\quad + m_{\tilde{\chi}^0_j} (m^2_{\tilde{\chi}^0_i} - m^2_{\tilde{\chi}^0_j} + m^2_W) C^{\mathrm{R}}_{\tilde{\chi}^0_j \tilde{\chi}^\pm_m W} (C^{\mathrm{R}}_{\tilde{\chi}^0_i \tilde{\chi}^\pm_m W})^* \Big) \\
&+ \Big(-m_{\tilde{\chi}^0_i} C^{\mathrm{L}}_{\tilde{\chi}^0_j \tilde{\chi}^\pm_m W} (C^{\mathrm{L}}_{\tilde{\chi}^0_i \tilde{\chi}^\pm_m W})^* - m_{\tilde{\chi}^0_j} C^{\mathrm{L}}_{\tilde{\chi}^0_i \tilde{\chi}^\pm_m W} (C^{\mathrm{L}}_{\tilde{\chi}^0_j \tilde{\chi}^\pm_m W})^* + m_{\tilde{\chi}^0_i} C^{\mathrm{R}}_{\tilde{\chi}^0_i \tilde{\chi}^\pm_m W} (C^{\mathrm{R}}_{\tilde{\chi}^0_j \tilde{\chi}^\pm_m W})^* \\
&\quad + m_{\tilde{\chi}^0_j} C^{\mathrm{R}}_{\tilde{\chi}^0_j \tilde{\chi}^\pm_m W} (C^{\mathrm{R}}_{\tilde{\chi}^0_i \tilde{\chi}^\pm_m W})^* \Big) \Big] \,, \\
D^{(W)} &= C^{(W)} (C^{\mathrm{L}} \leftrightarrow C^{\mathrm{R}}) \,.
\end{aligned}
\tag{G.47d}
$$

The $B^{(W)}$ and $D^{(W)}$ coefficients are obtained from the $A^{(W)}$ and $C^{(W)}$ coefficients by interchanging the left- and right-chiral couplings $C^{\mathrm{L/R}}$. As another remark, one has to be careful with the Goldstone boson ($G^\pm$) contributions. We refer to [305] for more details.

To obtain the decay width, the amplitude in Eq. (G.43) has to be squared and then Eq. (5.1a) to be used.

Acknowledgements (Danksagungen)

In a way is the writing of the acknowledgements the hardest part of a thesis, since you do not know where to start and you are afraid you might forget mentioning someone. Nonetheless, I hope I can do justice to everybody I want to thank and express gratitude for their help.

I start with my supervisor, Prof. Margarate Mühlleitner. It have been amazing 4 years now in her working group and I really enjoyed my time here. I got the opportunity to work on interesting topics, attend international conferences and summer schools and meet a lot of interesting people and I am certainly thankful for this time at the institute. She is an inspiring person and I hope we will continue working together in the future.

Next, I want to thank my second supervisor, Prof. Rui Santos. I really enjoyed working with him, having fruitful discussions in meetings or in person both about physics and other matters. I am grateful to have met him and being under his supervision. I hope we stay in contact and have some collaborations in the future.

Moreover, I want to thank all the people I worked together in projects that constituted this thesis. My special thanks go to João, Kodai, Luigi, Prof. Stefania de Curtis, Prof. Stefano Moretti and Prof. Thi Nhung Dao. Thanks for the interesting meetings and fruitful discussions.

Furthermore, special thanks to all my colleagues at the institute and abroad. I had a great time discussing physics, having coffee together and talking about other topics. My special gratitude goes to Christoph for answering all my SUSY questions and being always there for me when I needed to figure out something, to Karim and Johann for being awesome office mates and most importantly to Lisa, for being my older sister regarding the PhD. You were always there when I had questions on any topic and you helped me countless times with your admin duties and made my live easier in general.

I also want to thank all the people that proofread this thesis, especially Karim, Johann, Christoph, Fran and Sauro. Thanks for your time and input.

Finally, I want to thank my family for always supporting me. Mama, Papa, falls ihr das lest, ihr seid die besten! I want to thank my brother for always being there for me. Moreover, in my 9 years in Karlsruhe I met a lot of amazing people, but there is one group that is unmatched. Simon, Jasmijn, Julia, Janet, Melina, you are the best friends I could have hoped for. Thanks for illuminating my time and being always there for me. Lastly, a special and personal gratitude goes to Julia. At the beginning of this year, I assumed that my life would only continue to be exciting, eventful and fulfilling after I finish my thesis and start my postdoc position in Hamburg at the end of the year. Thanks to you, one of the most stressful times of my life were at the same time one of the best times of my life. Thank you all for being part of this amazing journey.

References

[1] Sheldon L. Glashow. "Partial-symmetries of weak interactions". In: *Nuclear Physics* 22.4 (1961), pp. 579–588. ISSN: 0029-5582. DOI: https://doi.org/10.1016/0029-5582(61)90469-2.

[2] Steven Weinberg. "A Model of Leptons". In: *Phys. Rev. Lett.* 19 (21 Nov. 1967), pp. 1264–1266. DOI: 10.1103/PhysRevLett.19.1264.

[3] Abdus Salam. "Weak and Electromagnetic Interactions". In: *Conf. Proc. C* 680519 (1968), pp. 367–377. DOI: 10.1142/9789812795915_0034.

[4] Peter W. Higgs. "Broken Symmetries and the Masses of Gauge Bosons". In: *Phys. Rev. Lett.* 13 (16 Oct. 1964), pp. 508–509. DOI: 10.1103/PhysRevLett.13.508.

[5] P.W. Higgs. "Broken symmetries, massless particles and gauge fields". In: *Physics Letters* 12.2 (1964), pp. 132–133. ISSN: 0031-9163. DOI: https://doi.org/10.1016/0031-9163(64)91136-9.

[6] F. Englert and R. Brout. "Broken Symmetry and the Mass of Gauge Vector Mesons". In: *Phys. Rev. Lett.* 13 (9 Aug. 1964), pp. 321–323. DOI: 10.1103/PhysRevLett.13.321.

[7] G. S. Guralnik, C. R. Hagen, and T. W. B. Kibble. "Global Conservation Laws and Massless Particles". In: *Phys. Rev. Lett.* 13 (20 Nov. 1964), pp. 585–587. DOI: 10.1103/PhysRevLett.13.585.

[8] T. W. B. Kibble. "Symmetry Breaking in Non-Abelian Gauge Theories". In: *Phys. Rev.* 155 (5 Mar. 1967), pp. 1554–1561. DOI: 10.1103/PhysRev.155.1554.

[9] G. Aad et al. "Observation of a new particle in the search for the Standard Model Higgs boson with the ATLAS detector at the LHC". In: *Physics Letters B* 716.1 (Sept. 2012), pp. 1–29. ISSN: 0370-2693. DOI: 10.1016/j.physletb.2012.08.020.

[10] S. Chatrchyan et al. "Observation of a new boson at a mass of 125 GeV with the CMS experiment at the LHC". In: *Physics Letters B* 716.1 (Sept. 2012), pp. 30–61. ISSN: 0370-2693. DOI: 10.1016/j.physletb.2012.08.021.

[11] N. Aghanim et al. "Planck 2018 results. VI. Cosmological parameters". In: *Astron. Astrophys.* 641 (2020), A6. DOI: 10.1051/0004-6361/201833910. arXiv: 1807.06209 [astro-ph.CO].

[12] C. L. Bennett et al. "Nine-Year Wilkinson Microwave Anisotropy Probe (WMAP) Observations: Final Maps and Results". In: *Astrophys. J. Suppl.* 208 (2013), p. 20. DOI: 10.1088/0067-0049/208/2/20. arXiv: 1212.5225 [astro-ph.CO].

[13] V.A. Kuzmin, V.A. Rubakov, and M.E. Shaposhnikov. "On anomalous electroweak baryon-number non-conservation in the early universe". In: *Physics Letters B* 155.1 (1985), pp. 36–42. ISSN: 0370-2693. DOI: https://doi.org/10.1016/0370-2693(85)91028-7.

[14] Andrew G. Cohen, David B. Kaplan, and Ann E. Nelson. "Baryogenesis at the weal phase transition". In: *Nuclear Physics B* 349.3 (1991), pp. 727–742. ISSN: 0550-3213. DOI: https://doi.org/10.1016/0550-3213(91)90395-E.

[15] Andrew G. Cohen, D. B. Kaplan, and A. E. Nelson. "Progress in electroweak baryogenesis". In: *Ann. Rev. Nucl. Part. Sci.* 43 (1993), pp. 27–70. DOI: 10.1146/annurev.ns.43.120193.000331. arXiv: hep-ph/9302210.

[16] M. Quiros. "Field theory at finite temperature and phase transitions". In: *Helv. Phys. Acta* 67 (1994), pp. 451–583.

[17] Valerii A Rubakov and M E Shaposhnikov. "Electroweak baryon number non-conservation in the early Universe and in high-energy collisions". In: *Physics-Uspekhi* 39.5 (May 1996), pp. 461–502. ISSN: 1468-4780. DOI: 10.1070/pu1996v039n05abeh000145.

[18] K. Funakubo. "CP Violation and Baryogenesis at the Electroweak Phase Transition". In: *Progress of Theoretical Physics* 96.3 (Sept. 1996), pp. 475–519. ISSN: 1347-4081. DOI: 10.1143/ptp.96.475.

[19] Mark Trodden. "Electroweak baryogenesis". In: *Reviews of Modern Physics* 71.5 (Oct. 1999), pp. 1463–1500. ISSN: 1539-0756. DOI: 10.1103/revmodphys.71.1463.

[20] Werner Bernreuther. "CP violation and baryogenesis". In: *Lect. Notes Phys.* 591 (2002), pp. 237–293. arXiv: hep-ph/0205279.

[21] David E. Morrissey and Michael J. Ramsey-Musolf. "Electroweak baryogenesis". In: *New J. Phys.* 14 (2012), p. 125003. DOI: 10.1088/1367-2630/14/12/125003. arXiv: 1206.2942 [hep-ph].

[22] A. D. Sakharov. "Violation of CP Invariance, c Asymmetry, and Baryon Asymmetry of the Universe". In: *Pisma Zh. Eksp. Teor. Fiz.* 5 (1967). [Usp. Fiz. Nauk161,61(1991)], pp. 32–35. DOI: 10.1070/PU1991v034n05ABEH002497.

[23] K. Kajantie et al. "Is There a Hot Electroweak Phase Transition atmH$gtrsim$mW?" In: *Physical Review Letters* 77.14 (Sept. 1996), pp. 2887–2890. ISSN: 1079-7114. DOI: 10.1103/physrevlett.77.2887.

[24] F. Csikor, Z. Fodor, and J. Heitger. "End Point of the Hot Electroweak Phase Transition". In: *Physical Review Letters* 82.1 (Jan. 1999), pp. 21–24. ISSN: 1079-7114. DOI: 10.1103/physrevlett.82.21.

[25] K. Kajantie, K. Rummukainen, and M. Shaposhnikov. "A lattice Monte Carlo study of the hot electroweak phase transition". In: *Nuclear Physics B* 407.2 (Oct. 1993), pp. 356–372. ISSN: 0550-3213. DOI: 10.1016/0550-3213(93)90062-t.

[26] K. Kanaya and S. Kaya. "Critical exponents of a three-dimensional O(4) spin model". In: *Physical Review D* 51.5 (Mar. 1995), pp. 2404–2410. ISSN: 0556-2821. DOI: 10.1103/physrevd.51.2404.

[27] K. Jansen. "Status of the finite temperature electroweak phase transition on the lattice". In: *Nuclear Physics B - Proceedings Supplements* 47.1-3 (Mar. 1996), pp. 196–211. ISSN: 0920-5632. DOI: 10.1016/0920-5632(96)00045-x.

[28] M. B. GAVELA et al. "STANDARD MODEL CP-VIOLATION AND BARYON ASYMMETRY". In: *Modern Physics Letters A* 09.09 (Mar. 1994), pp. 795–809. ISSN: 1793-6632. DOI: 10.1142/s0217732394000629.

[29] David E Morrissey and Michael J Ramsey-Musolf. "Electroweak baryogenesis". In: *New Journal of Physics* 14.12 (Dec. 2012), p. 125003. ISSN: 1367-2630. DOI: 10.1088/1367-2630/14/12/125003.

[30] T Konstandin. "Quantum transport and electroweak baryogenesis". In: *Physics-Uspekhi* 56.8 (Aug. 2013), pp. 747–771. ISSN: 1468-4780. DOI: 10.3367/ufne.0183.201308a.0785.

[31] M. Planck. *Vorlesungen über die Theorie der Wärmestrahlung*. J. A. Barth, 1906.

[32] Vanda Silveira and A. Zee. "SCALAR PHANTOMS". In: *Phys. Lett. B* 161 (1985), pp. 136–140. DOI: 10.1016/0370-2693(85)90624-0.

[33] John McDonald. "Gauge singlet scalars as cold dark matter". In: *Phys. Rev. D* 50 (1994), pp. 3637–3649. DOI: 10.1103/PhysRevD.50.3637. arXiv: hep-ph/0702143.

[34] M. C. Bento et al. "Selfinteracting dark matter and invisibly decaying Higgs". In: *Phys. Rev. D* 62 (2000), p. 041302. DOI: 10.1103/PhysRevD.62.041302. arXiv: astro-ph/0003350.

[35] C. P. Burgess, Maxim Pospelov, and Tonnis ter Veldhuis. "The Minimal model of nonbaryonic dark matter: A Singlet scalar". In: *Nucl. Phys. B* 619 (2001), pp. 709–728. DOI: 10.1016/S0550-3213(01)00513-2. arXiv: hep-ph/0011335.

[36] Hooman Davoudiasl et al. "The New minimal standard model". In: *Phys. Lett. B* 609 (2005), pp. 117–123. DOI: 10.1016/j.physletb.2005.01.026. arXiv: hep-ph/0405097.

[37] Donal O'Connell, Michael J. Ramsey-Musolf, and Mark B. Wise. "Minimal Extension of the Standard Model Scalar Sector". In: *Phys. Rev. D* 75 (2007), p. 037701. DOI: 10.1103/PhysRevD.75.037701. arXiv: hep-ph/0611014.

[38] Omri Bahat-Treidel, Yuval Grossman, and Yoram Rozen. "Hiding the Higgs at the LHC". In: *JHEP* 05 (2007), p. 022. DOI: 10.1088/1126-6708/2007/05/022. arXiv: hep-ph/0611162.

[39] Vernon Barger et al. "LHC Phenomenology of an Extended Standard Model with a Real Scalar Singlet". In: *Phys. Rev. D* 77 (2008), p. 035005. DOI: 10.1103/PhysRevD.77.035005. arXiv: 0706.4311 [hep-ph].

[40] Vernon Barger et al. "Complex Singlet Extension of the Standard Model". In: *Phys. Rev. D* 79 (2009), p. 015018. DOI: 10.1103/PhysRevD.79.015018. arXiv: 0811.0393 [hep-ph].

[41] Matthew Gonderinger et al. "Vacuum Stability, Perturbativity, and Scalar Singlet Dark Matter". In: *JHEP* 01 (2010), p. 053. DOI: 10.1007/JHEP01(2010)053. arXiv: 0910.3167 [hep-ph].

[42] Rita Coimbra, Marco O. P. Sampaio, and Rui Santos. "ScannerS: constraining the phase diagram of a complex scalar singlet at the LHC". In: *The European Physical Journal C* 73.5 (May 2013). ISSN: 1434-6052. DOI: 10.1140/epjc/s10052-013-2428-4.

[43] Raul Costa et al. "Two-loop stability of a complex singlet extended standard model". In: *Physical Review D* 92.2 (July 2015). ISSN: 1550-2368. DOI: 10.1103/physrevd.92.025024.

[44] Raul Costa et al. "Singlet extensions of the standard model at LHC Run 2: benchmarks and comparison with the NMSSM". In: *Journal of High Energy Physics* 2016.6 (June 2016). ISSN: 1029-8479. DOI: 10.1007/jhep06(2016)034.

[45] Savas Dimopoulos and John Preskill. "Massless Composites With Massive Constituents". In: *Nucl. Phys. B* 199 (1982), pp. 206–222. DOI: 10.1016/0550-3213(82)90345-5.

[46] David B. Kaplan, Howard Georgi, and Savas Dimopoulos. "Composite Higgs Scalars". In: *Phys. Lett. B* 136 (1984), pp. 187–190. DOI: 10.1016/0370-2693(84)91178-X.

[47] David B. Kaplan and Howard Georgi. "SU(2) x U(1) Breaking by Vacuum Misalignment". In: *Phys. Lett. B* 136 (1984), pp. 183–186. DOI: 10.1016/0370-2693(84)91177-8.

[48] Tom Banks. "Constraints on SU2ŒU1 breaking by vacuum misalignment". In: *Nucl. Phys. B* 243 (1984), pp. 125–130. DOI: 10.1016/0550-3213(84)90389-4.

[49] Howard Georgi, David B. Kaplan, and Peter Galison. "Calculation of the Composite Higgs Mass". In: *Phys. Lett. B* 143 (1984), pp. 152–154. DOI: 10.1016/0370-2693(84)90823-2.

[50] Howard Georgi and David B. Kaplan. "Composite Higgs and Custodial SU(2)". In: *Phys. Lett. B* 145 (1984), pp. 216–220. DOI: 10.1016/0370-2693(84)90341-1.

[51] Michael J. Dugan, Howard Georgi, and David B. Kaplan. "Anatomy of a Composite Higgs Model". In: *Nucl. Phys. B* 254 (1985), pp. 299–326. DOI: 10.1016/0550-3213(85)90221-4.

[52] Kaustubh Agashe, Roberto Contino, and Alex Pomarol. "The Minimal composite Higgs model". In: *Nucl. Phys. B* 719 (2005), pp. 165–187. DOI: 10.1016/j.nuclphysb.2005.04.035. arXiv: hep-ph/0412089.

[53] Roberto Contino, Leandro Da Rold, and Alex Pomarol. "Light custodians in natural composite Higgs models". In: *Phys. Rev. D* 75 (2007), p. 055014. DOI: 10.1103/PhysRevD.75.055014. arXiv: hep-ph/0612048.

[54] Roberto Contino. "The Higgs as a Composite Nambu-Goldstone Boson". In: *Theoretical Advanced Study Institute in Elementary Particle Physics: Physics of the Large and the Small*. 2011, pp. 235–306. DOI: 10.1142/9789814327183_0005. arXiv: 1005.4269 [hep-ph].

[55] D. V. Volkov and V. P. Akulov. "Is the Neutrino a Goldstone Particle?" In: *Phys. Lett. B* 46 (1973), pp. 109–110. DOI: 10.1016/0370-2693(73)90490-5.

[56] J. Wess and B. Zumino. "Supergauge Transformations in Four-Dimensions". In: *Nucl. Phys. B* 70 (1974). Ed. by A. Salam and E. Sezgin, pp. 39–50. DOI: 10.1016/0550-3213(74)90355-1.

[57] Hans Peter Nilles. "Supersymmetry, Supergravity and Particle Physics". In: *Phys. Rept.* 110 (1984), pp. 1–162. DOI: 10.1016/0370-1573(84)90008-5.

[58] Howard E. Haber and Gordon L. Kane. "The Search for Supersymmetry: Probing Physics Beyond the Standard Model". In: *Phys. Rept.* 117 (1985), pp. 75–263. DOI: 10.1016/0370-1573(85)90051-1.

[59] M. F. Sohnius. "Introducing Supersymmetry". In: *Phys. Rept.* 128 (1985), pp. 39–204. DOI: 10.1016/0370-1573(85)90023-7.

[60] J. F. Gunion and Howard E. Haber. "Higgs Bosons in Supersymmetric Models. 1." In: *Nucl. Phys. B* 272 (1986). [Erratum: Nucl.Phys.B 402, 567–569 (1993)], p. 1. DOI: 10.1016/0550-3213(86)90340-8.

[61] J. F. Gunion and Howard E. Haber. "Higgs Bosons in Supersymmetric Models. 2. Implications for Phenomenology". In: *Nucl. Phys. B* 278 (1986). Ed. by S. C. Loken. [Erratum: Nucl.Phys.B 402, 569–569 (1993)], p. 449. DOI: 10.1016/0550-3213(86)90050-7.

[62] Stephen P. Martin. "A Supersymmetry primer". In: *Adv. Ser. Direct. High Energy Phys.* 18 (1998). Ed. by Gordon L. Kane, pp. 1–98. DOI: 10.1142/9789812839657_0001. arXiv: hep-ph/9709356.

[63] M. Drees, R. Godbole, and P. Roy. *Theory and Phenomenology of Sparticles: An account of four-dimensional N=1 supersymmetry in High Energy Physics*. 2004.

[64] Howard E. Haber and Laurel Stephenson Haskins. "Supersymmetric Theory and Models". In: *Theoretical Advanced Study Institute in Elementary Particle Physics: Anticipating the Next Discoveries in Particle Physics*. WSP, 2018, pp. 355–499. DOI: 10.1142/9789813233348_0006. arXiv: 1712.05926 [hep-ph].

[65] J. Mrazek et al. "The Other Natural Two Higgs Doublet Model". In: *Nucl. Phys. B* 853 (2011), pp. 1–48. DOI: 10.1016/j.nuclphysb.2011.07.008. arXiv: 1105.5403 [hep-ph].

[66] Stefania De Curtis et al. "Perturbative unitarity bounds in composite two-Higgs doublet models". In: *Phys. Rev. D* 94.5 (2016), p. 055017. DOI: 10.1103/PhysRevD.94.055017. arXiv: 1602.06437 [hep-ph].

[67] Stefania De Curtis et al. "LHC Phenomenology of Composite 2-Higgs Doublet Models". In: *Eur. Phys. J. C* 77.8 (2017), p. 513. DOI: 10.1140/epjc/s10052-017-5082-4. arXiv: 1610.02687 [hep-ph].

[68] Stefania De Curtis et al. "Single and double SM-like Higgs boson production at future electron-positron colliders in composite 2HDMs". In: *Phys. Rev. D* 95.9 (2017), p. 095026. DOI: 10.1103/PhysRevD.95.095026. arXiv: 1702.07260 [hep-ph].

[69] Stefania De Curtis et al. "A concrete composite 2-Higgs doublet model". In: *Journal of High Energy Physics* 2018.12 (Dec. 2018). ISSN: 1029-8479. DOI: 10.1007/jhep12(2018)051.

[70] M. Maniatis. "The Next-to-Minimal Supersymmetric extension of the Standard Model reviewed". In: *International Journal of Modern Physics A* 25.18n19 (2010), pp. 3505–3602. DOI: 10.1142/S0217751X10049827. arXiv: 0906.0777 [hep-ph].

[71] Ulrich Ellwanger, Cyril Hugonie, and Ana M. Teixeira. "The Next-to-Minimal Supersymmetric Standard Model". In: *Physics Reports* 496.12 (Nov. 2010), pp. 1–77. ISSN: 0370-1573. DOI: 10.1016/j.physrep.2010.07.001.

[72] Felix Egle et al. "One-loop corrections to the Higgs boson invisible decay in a complex singlet extension of the SM". In: *Phys. Rev. D* 106.9 (2022), p. 095030. DOI: 10.1103/PhysRevD.106.095030. arXiv: 2202.04035 [hep-ph].

[73] Felix Egle et al. "Electroweak corrections to Higgs boson decays in a Complex Singlet extension of the SM and their phenomenological impact". In: *JHEP* 11 (2023), p. 116. DOI: 10.1007/JHEP11(2023)116. arXiv: 2306.04127 [hep-ph].

[74] Stefania De Curtis et al. "Composite 2-Higgs doublet model: strong effects on Higgs pair production". In: *JHEP* 06 (2024), p. 063. DOI: 10.1007/JHEP06(2024)063. arXiv: 2310.10471 [hep-ph].

[75] M. Mühlleitner, A. Djouadi, and Y. Mambrini. "SDECAY: a Fortran code for the decays of the supersymmetric particles in the MSSM". In: *Computer Physics Communications* 168.1 (May 2005), pp. 46–70. ISSN: 0010-4655. DOI: 10.1016/j.cpc.2005.01.012.

[76] A. Djouadi, M. M. Muhlleitner, and M. Spira. "Decays of supersymmetric particles: The Program SUSY-HIT (SUspect-SdecaY-Hdecay-InTerface)". In: *Acta Phys. Polon. B* 38 (2007). Ed. by K. Fialkowski and B. Muryn, pp. 635–644. arXiv: hep-ph/0609292.

[77] K. Ender et al. "Analysis of the NMSSM Higgs boson masses at one-loop level". In: *Physical Review D* 85.7 (Apr. 2012). ISSN: 1550-2368. DOI: 10.1103/physrevd.85.075024.

[78] T. Graf et al. "Higgs boson masses in the complex NMSSM at one-loop level". In: *Journal of High Energy Physics* 2012.10 (Oct. 2012). ISSN: 1029-8479. DOI: 10.1007/jhep10(2012)122.

[79] J. Baglio et al. "NMSSMCALC: A program package for the calculation of loop-corrected Higgs boson masses and decay widths in the (complex) NMSSM". In: *Computer Physics Communications* 185.12 (Dec. 2014), pp. 3372–3391. ISSN: 0010-4655. DOI: 10.1016/j.cpc.2014.08.005.

[80] Margarete Mühlleitner et al. "Two-loop contributions of the order $\mathcal{O}(\alpha_t\alpha_s)$ to the masses of the Higgs bosons in the CP-violating NMSSM". In: *JHEP* 05 (2015), p. 128. DOI: 10.1007/JHEP05(2015)128. arXiv: 1412.0918 [hep-ph].

[81] Thi Nhung Dao et al. "Two-loop $\mathcal{O}(\alpha_t^2)$ corrections to the neutral Higgs boson masses in the CP-violating NMSSM". In: *Journal of High Energy Physics* 2019.8 (Aug. 2019). ISSN: 1029-8479. DOI: 10.1007/jhep08(2019)114.

[82] Thi Nhung Dao et al. "Two-loop $\mathcal{O}((\alpha_t + \alpha_\lambda + \alpha_\kappa)^2)$ corrections to the Higgs boson masses in the CP-violating NMSSM". In: *JHEP* 09 (2021), p. 193. DOI: 10.1007/JHEP09(2021)193. arXiv: 2106.06990 [hep-ph].

[83] Ramona Gröber. "Aspects of Higgs Physics and New Physics at the LHC". German. PhD thesis. 2014. DOI: 10.5445/IR/1000040802.

[84] John F. Gunion et al. *The Higgs Hunter's Guide*. Vol. 80. 2000. ISBN: 978-0-429-49644-8. DOI: 10.1201/9780429496448.

[85] Michael E. Peskin and Daniel V. Schroeder. *An Introduction to quantum field theory*. Advanced book program. Westview Press Reading (Mass.), 1995. ISBN: 9780201503975, 0201503972.

[86] Giuliano Panico and Andrea Wulzer. *The Composite Nambu-Goldstone Higgs*. Vol. 913. Springer, 2016. DOI: 10.1007/978-3-319-22617-0. arXiv: 1506.01961 [hep-ph].

[87] Michael Dine. "Naturalness Under Stress". In: *Ann. Rev. Nucl. Part. Sci.* 65 (2015), pp. 43–62. DOI: 10.1146/annurev-nucl-102014-022053. arXiv: 1501.01035 [hep-ph].

[88] Csaba Csáki, Salvator Lombardo, and Ofri Telem. "TASI Lectures on Non-supersymmetric BSM Models". In: *Proceedings, Theoretical Advanced Study Institute in Elementary Particle Physics : Anticipating the Next Discoveries in Particle Physics (TASI 2016): Boulder, CO, USA, June 6-July 1, 2016*. Ed. by Rouven Essig and Ian Low. WSP, 2018, pp. 501–570. DOI: 10.1142/9789813233348_0007. arXiv: 1811.04279 [hep-ph].

[89] Timothy Cohen. *As Scales Become Separated: Lectures on Effective Field Theory*. 2020. arXiv: 1903.03622 [hep-ph].

[90] Raman Sundrum. "Unfolding Particle Physics Hierarchies with Supersymmetry and Extra Dimensions". In: *PoS* TASI2022 (2024), p. 010. DOI: 10.22323/1.439.0010. arXiv: 2306.07173 [hep-ph].

[91] Nathaniel Craig. "Twenty Ways to Solve the Hierarchy Problem". Talk given at the Aspen 2017 Winter Conference "From the LHC to Dark Matter and Beyond". 2017.

[92] Gerard 't Hooft. "Naturalness, chiral symmetry, and spontaneous chiral symmetry breaking". In: *NATO Sci. Ser. B* 59 (1980). Ed. by Gerard 't Hooft et al., pp. 135–157. DOI: 10.1007/978-1-4684-7571-5_9.

[93] S. Dawson. *The MSSM and Why it Works*. 1997. arXiv: hep-ph/9712464 [hep-ph].

[94] A DJOUADI. "The anatomy of electroweak symmetry breaking Tome II: The Higgs bosons in the Minimal Supersymmetric Model". In: *Physics Reports* 459.16 (Apr. 2008), pp. 1–241. ISSN: 0370-1573. DOI: 10.1016/j.physrep.2007.10.005.

[95] Christopher T. Hill and Elizabeth H. Simmons. "Strong dynamics and electroweak symmetry breaking". In: *Physics Reports* 381.46 (July 2003), pp. 235–402. ISSN: 0370-1573. DOI: 10.1016/s0370-1573(03)00140-6.

[96] Joshua Ellis. "TikZ-Feynman: Feynman diagrams with TikZ". In: *Comput. Phys. Commun.* 210 (2017), pp. 103–123. DOI: 10.1016/j.cpc.2016.08.019. arXiv: 1601.05437 [hep-ph].

[97] Georges Aad et al. "A detailed map of Higgs boson interactions by the ATLAS experiment ten years after the discovery". In: *Nature* 607.7917 (2022). [Erratum: Nature 612, E24 (2022)], pp. 52–59. DOI: 10.1038/s41586-022-04893-w. arXiv: 2207.00092 [hep-ex].

[98] A. Tumasyan et al. "A portrait of the Higgs boson by the CMS experiment ten years after the discovery". In: *Nature* 607.7917 (July 2022), pp. 60–68. ISSN: 1476-4687. DOI: 10.1038/s41586-022-04892-x.

[99] E.W.N. Glover and J.J. van der Bij. "Higgs boson pair production via gluon fusion". In: *Nuclear Physics B* 309.2 (1988), pp. 282–294. ISSN: 0550-3213. DOI: https://doi.org/10.1016/0550-3213(88)90083-1.

[100] Duane A. Dicus, Chung Kao, and Scott S.D. Willenbrock. "Higgs boson pair production from gluon fusion". In: *Physics Letters B* 203.4 (1988), pp. 457–461. ISSN: 0370-2693. DOI: https://doi.org/10.1016/0370-2693(88)90202-X.

[101] T. Plehn, M. Spira, and P. M. Zerwas. "Pair production of neutral Higgs particles in gluon-gluon collisions". In: *Nucl. Phys. B* 479 (1996). [Erratum: Nucl.Phys.B 531, 655–655 (1998)], pp. 46–64. DOI: 10.1016/0550-3213(96)00418-X. arXiv: hep-ph/9603205.

[102] S. Dawson, S. Dittmaier, and M. Spira. "Neutral Higgs-boson pair production at hadron colliders: QCD corrections". In: *Physical Review D* 58.11 (Nov. 1998). ISSN: 1089-4918. DOI: 10.1103/physrevd.58.115012.

[103] Ding Yu Shao et al. "Threshold resummation effects in Higgs boson pair production at the LHC". In: *JHEP* 07 (2013), p. 169. DOI: 10.1007/JHEP07(2013)169. arXiv: 1301.1245 [hep-ph].

[104] Jonathan Grigo et al. "On the Higgs boson pair production at the LHC". In: *Nucl. Phys. B* 875 (2013), pp. 1–17. DOI: 10.1016/j.nuclphysb.2013.06.024. arXiv: 1305.7340 [hep-ph].

[105] Daniel de Florian and Javier Mazzitelli. "Next-to-Next-to-Leading Order QCD Corrections to Higgs Boson Pair Production". In: *PoS* LL2014 (2014). Ed. by Martina Mende, p. 029. DOI: 10.22323/1.211.0029. arXiv: 1405.4704 [hep-ph].

[106] Jonathan Grigo, Kirill Melnikov, and Matthias Steinhauser. "Virtual corrections to Higgs boson pair production in the large top quark mass limit". In: *Nucl. Phys. B* 888 (2014), pp. 17–29. DOI: 10.1016/j.nuclphysb.2014.09.003. arXiv: 1408.2422 [hep-ph].

[107] F. Maltoni, E. Vryonidou, and M. Zaro. "Top-quark mass effects in double and triple Higgs production in gluon-gluon fusion at NLO". In: *JHEP* 11 (2014), p. 079. DOI: 10.1007/JHEP11(2014)079. arXiv: 1408.6542 [hep-ph].

[108] Jonathan Grigo, Jens Hoff, and Matthias Steinhauser. "Higgs boson pair production: top quark mass effects at NLO and NNLO". In: *Nucl. Phys. B* 900 (2015), pp. 412–430. DOI: 10.1016/j.nuclphysb.2015.09.012. arXiv: 1508.00909 [hep-ph].

[109] Daniel de Florian et al. "Differential Higgs Boson Pair Production at Next-to-Next-to-Leading Order in QCD". In: *JHEP* 09 (2016), p. 151. DOI: 10.1007/JHEP09(2016)151. arXiv: 1606.09519 [hep-ph].

[110] S. Borowka et al. "Higgs Boson Pair Production in Gluon Fusion at Next-to-Leading Order with Full Top-Quark Mass Dependence". In: *Phys. Rev. Lett.* 117.1 (2016). [Erratum: Phys.Rev.Lett. 117, 079901 (2016)], p. 012001. DOI: 10.1103/PhysRevLett.117.079901. arXiv: 1604.06447 [hep-ph].

[111] S. Borowka et al. "Full top quark mass dependence in Higgs boson pair production at NLO". In: *JHEP* 10 (2016), p. 107. DOI: 10.1007/JHEP10(2016)107. arXiv: 1608.04798 [hep-ph].

[112] Giancarlo Ferrera and Joao Pires. "Transverse-momentum resummation for Higgs boson pair production at the LHC with top-quark mass effects". In: *JHEP* 02 (2017), p. 139. DOI: 10.1007/JHEP02(2017)139. arXiv: 1609.01691 [hep-ph].

[113] G. Heinrich et al. "NLO predictions for Higgs boson pair production with full top quark mass dependence matched to parton showers". In: *JHEP* 08 (2017), p. 088. DOI: 10.1007/JHEP08(2017)088. arXiv: 1703.09252 [hep-ph].

[114] Stephen Jones and Silvan Kuttimalai. "Parton Shower and NLO-Matching uncertainties in Higgs Boson Pair Production". In: *JHEP* 02 (2018), p. 176. DOI: 10.1007/JHEP02(2018)176. arXiv: 1711.03319 [hep-ph].

[115] Ramona Gröber, Andreas Maier, and Thomas Rauh. "Reconstruction of top-quark mass effects in Higgs pair production and other gluon-fusion processes". In: *JHEP* 03 (2018), p. 020. DOI: 10.1007/JHEP03(2018)020. arXiv: 1709.07799 [hep-ph].

[116] Julien Baglio et al. "Gluon fusion into Higgs pairs at NLO QCD and the top mass scheme". In: *Eur. Phys. J. C* 79.6 (2019), p. 459. DOI: 10.1140/epjc/s10052-019-6973-3. arXiv: 1811.05692 [hep-ph].

[117] M. Grazzini et al. "Higgs boson pair production at NNLO with top quark mass effects". In: *Journal of High Energy Physics* 2018.5 (May 2018). ISSN: 1029-8479. DOI: 10.1007/jhep05(2018)059.

[118] Daniel De Florian and Javier Mazzitelli. "Soft gluon resummation for Higgs boson pair production including finite M_t effects". In: *JHEP* 08 (2018), p. 156. DOI: 10.1007/JHEP08(2018)156. arXiv: 1807.03704 [hep-ph].

[119] Roberto Bonciani et al. "Analytical Method for Next-to-Leading-Order QCD Corrections to Double-Higgs Production". In: *Phys. Rev. Lett.* 121.16 (2018), p. 162003. DOI: 10.1103/PhysRevLett.121.162003. arXiv: 1806.11564 [hep-ph].

[120] Joshua Davies et al. "Double Higgs boson production at NLO in the high-energy limit: complete analytic results". In: *JHEP* 01 (2019), p. 176. DOI: 10.1007/JHEP01(2019)176. arXiv: 1811.05489 [hep-ph].

[121] Joshua Davies et al. "Double Higgs boson production at NLO: combining the exact numerical result and high-energy expansion". In: *JHEP* 11 (2019), p. 024. DOI: 10.1007/JHEP11(2019)024. arXiv: 1907.06408 [hep-ph].

[122] Joshua Davies and Matthias Steinhauser. "Three-loop form factors for Higgs boson pair production in the large top mass limit". In: *JHEP* 10 (2019), p. 166. DOI: 10.1007/JHEP10(2019)166. arXiv: 1909.01361 [hep-ph].

[123] Long-Bin Chen et al. "Higgs boson pair production via gluon fusion at N3LO in QCD". In: *Physics Letters B* 803 (Apr. 2020), p. 135292. ISSN: 0370-2693. DOI: 10.1016/j.physletb.2020.135292.

[124] Long-Bin Chen et al. "The gluon-fusion production of Higgs boson pair: N^3LO QCD corrections and top-quark mass effects". In: *JHEP* 03 (2020), p. 072. DOI: 10.1007/JHEP03(2020)072. arXiv: 1912.13001 [hep-ph].

[125] Joshua Davies et al. "Real-virtual corrections to Higgs boson pair production at NNLO: three closed top quark loops". In: *JHEP* 05 (2019), p. 157. DOI: 10.1007/JHEP05(2019)157. arXiv: 1904.11998 [hep-ph].

[126] J. Baglio et al. "Higgs-Pair Production via Gluon Fusion at Hadron Colliders: NLO QCD Corrections". In: *JHEP* 04 (2020), p. 181. DOI: 10.1007/JHEP04(2020)181. arXiv: 2003.03227 [hep-ph].

[127] J. Baglio et al. "$gg \to HH$: Combined uncertainties". In: *Phys. Rev. D* 103.5 (2021), p. 056002. DOI: 10.1103/PhysRevD.103.056002. arXiv: 2008.11626 [hep-ph].

[128] Joshua Davies et al. "Real corrections to Higgs boson pair production at NNLO in the large top quark mass limit". In: *JHEP* 01 (2022), p. 049. DOI: 10.1007/JHEP01(2022)049. arXiv: 2110.03697 [hep-ph].

[129] Margarete Mühlleitner, Johannes Schlenk, and Michael Spira. "Top-Yukawa-induced corrections to Higgs pair production". In: *JHEP* 10 (2022), p. 185. DOI: 10.1007/JHEP10(2022)185. arXiv: 2207.02524 [hep-ph].

[130] Joshua Davies et al. "Higgs boson contribution to the leading two-loop Yukawa corrections to gg → HH". In: *JHEP* 08 (2022), p. 259. DOI: 10.1007/JHEP08(2022)259. arXiv: 2207.02587 [hep-ph].

[131] Huan-Yu Bi et al. "Electroweak Corrections to Double Higgs Production at the LHC". In: *Phys. Rev. Lett.* 132.23 (2024), p. 231802. DOI: 10.1103/PhysRevLett.132.231802. arXiv: 2311.16963 [hep-ph].

[132] Joshua Davies et al. "Next-to-leading order electroweak corrections to $gg \to HH$ and $gg \to gH$ in the large-m_t limit". In: *JHEP* 10 (2023), p. 033. DOI: 10.1007/JHEP10(2023)033. arXiv: 2308.01355 [hep-ph].

[133] Joshua Davies et al. "Three-loop corrections to Higgs boson pair production: reducible contribution". In: (May 2024). arXiv: 2405.20372 [hep-ph].

[134] Gudrun Heinrich et al. "Electroweak corrections to Higgs boson pair production: The top-Yukawa and self-coupling contributions". In: (July 2024). arXiv: 2407.04653 [hep-ph].

[135] Abdesslam Arhrib et al. "Double Neutral Higgs production in the Two-Higgs doublet model at the LHC". In: *JHEP* 08 (2009), p. 035. DOI: 10.1088/1126-6708/2009/08/035. arXiv: 0906.0387 [hep-ph].

[136] Benoit Hespel, David Lopez-Val, and Eleni Vryonidou. "Higgs pair production via gluon fusion in the Two-Higgs-Doublet Model". In: *JHEP* 09 (2014), p. 124. DOI: 10.1007/JHEP09(2014)124. arXiv: 1407.0281 [hep-ph].

[137] Julien Baglio et al. "Benchmarks for Higgs Pair Production and Heavy Higgs boson Searches in the Two-Higgs-Doublet Model of Type II". In: *Phys. Rev. D* 90.1 (2014), p. 015008. DOI: 10.1103/PhysRevD.90.015008. arXiv: 1403.1264 [hep-ph].

[138] Chien-Yi Chen, S. Dawson, and I. M. Lewis. "Exploring resonant di-Higgs boson production in the Higgs singlet model". In: *Phys. Rev. D* 91.3 (2015), p. 035015. DOI: 10.1103/PhysRevD.91.035015. arXiv: 1410.5488 [hep-ph].

[139] S. Dawson, A. Ismail, and Ian Low. "Whats in the loop? The anatomy of double Higgs production". In: *Phys. Rev. D* 91.11 (2015), p. 115008. DOI: 10.1103/PhysRevD.91.115008. arXiv: 1504.05596 [hep-ph].

[140] S. Dawson and I. M. Lewis. "NLO corrections to double Higgs boson production in the Higgs singlet model". In: *Phys. Rev. D* 92.9 (2015), p. 094023. DOI: 10.1103/PhysRevD.92.094023. arXiv: 1508.05397 [hep-ph].

[141] Ramona Grober et al. "NLO QCD Corrections to Higgs Pair Production including Dimension-6 Operators". In: *JHEP* 09 (2015), p. 092. DOI: 10.1007/JHEP09(2015)092. arXiv: 1504.06577 [hep-ph].

[142] Ligong Bian, Ning Chen, and Yun Jiang. "Higgs pair production in the CP-violating two-Higgs-doublet model". In: *Int. J. Mod. Phys. A* 32.34 (2017), p. 1746002. DOI: 10.1142/S0217751X17460022. arXiv: 1712.01632 [hep-ph].

[143] Philipp Basler, Margarete Mühlleitner, and Jonas Wittbrodt. "The CP-Violating 2HDM in Light of a Strong First Order Electroweak Phase Transition and Implications for Higgs Pair Production". In: *JHEP* 03 (2018), p. 061. DOI: 10.1007/JHEP03(2018)061. arXiv: 1711.04097 [hep-ph].

[144] R. Grober, M. Muhlleitner, and M. Spira. "Higgs Pair Production at NLO QCD for CP-violating Higgs Sectors". In: *Nucl. Phys. B* 925 (2017), pp. 1–27. DOI: 10.1016/j.nuclphysb.2017.10.002. arXiv: 1705.05314 [hep-ph].

[145] S. Dawson and M. Sullivan. "Enhanced di-Higgs boson production in the complex Higgs singlet model". In: *Phys. Rev. D* 97.1 (2018), p. 015022. DOI: 10.1103/PhysRevD.97.015022. arXiv: 1711.06683 [hep-ph].

[146] Philipp Basler et al. "Showcasing HH production: Benchmarks for the LHC and HL-LHC". In: *Phys. Rev. D* 99.5 (2019), p. 055048. DOI: 10.1103/PhysRevD.99.055048. arXiv: 1812.03542 [hep-ph].

[147] Philipp Basler et al. "Di-Higgs boson peaks and top valleys: Interference effects in Higgs sector extensions". In: *Phys. Rev. D* 101.1 (2020), p. 015019. DOI: 10.1103/PhysRevD.101.015019. arXiv: 1909.09987 [hep-ph].

[148] Biswaranjan Das et al. "Quantum interference effects in Higgs boson pair-production beyond the Standard Model". In: *Eur. Phys. J. C* 81.4 (2021), p. 347. DOI: 10.1140/epjc/s10052-021-09023-w. arXiv: 2012.09587 [hep-ph].

[149] F. Arco, S. Heinemeyer, and M. J. Herrero. "Exploring sizable triple Higgs couplings in the 2HDM". In: *Eur. Phys. J. C* 80.9 (2020), p. 884. DOI: 10.1140/epjc/s10052-020-8406-8. arXiv: 2005.10576 [hep-ph].

[150] Hamza Abouabid et al. "Benchmarking di-Higgs production in various extended Higgs sector models". In: *Journal of High Energy Physics* 2022.9 (Sept. 2022). ISSN: 1029-8479. DOI: 10.1007/jhep09(2022)011.

[151] J. Baglio et al. "Full NLO QCD predictions for Higgs-pair production in the 2-Higgs-doublet model". In: *Eur. Phys. J. C* 83.9 (2023), p. 826. DOI: 10.1140/epjc/s10052-023-11957-2. arXiv: 2303.05409 [hep-ph].

[152] R. Grober and M. Muhlleitner. "Composite Higgs Boson Pair Production at the LHC". In: *JHEP* 06 (2011), p. 020. DOI: 10.1007/JHEP06(2011)020. arXiv: 1012.1562 [hep-ph].

[153] M. Gillioz et al. "Higgs Low-Energy Theorem (and its corrections) in Composite Models". In: *JHEP* 10 (2012), p. 004. DOI: 10.1007/JHEP10(2012)004. arXiv: 1206.7120 [hep-ph].

[154] Ramona Grober, Margarete Muhlleitner, and Michael Spira. "Signs of Composite Higgs Pair Production at Next-to-Leading Order". In: *JHEP* 06 (2016), p. 080. DOI: 10.1007/JHEP06(2016)080. arXiv: 1602.05851 [hep-ph].

[155] Shinya Kanemura et al. "Single and double production of the Higgs boson at hadron and lepton colliders in minimal composite Higgs models". In: *Physical Review D* 94.1 (July 2016). ISSN: 2470-0029. DOI: 10.1103/physrevd.94.015028.

[156] Kingman Cheung et al. "Disentangling new physics effects on nonresonant Higgs boson pair production from gluon fusion". In: *Physical Review D* 103.1 (Jan. 2021). DOI: 10.1103/physrevd.103.015019.

[157] Zhaoxia Heng, Liangliang Shang, and Peihua Wan. "Pair production of a 125 GeV Higgs boson in MSSM and NMSSM at the ILC". In: *JHEP* 10 (2013), p. 047. DOI: 10.1007/JHEP10(2013)047. arXiv: 1306.0279 [hep-ph].

[158] Dao Thi Nhung et al. "Higher Order Corrections to the Trilinear Higgs Self-Couplings in the Real NMSSM". In: *JHEP* 11 (2013), p. 181. DOI: 10.1007/JHEP11(2013)181. arXiv: 1306.3926 [hep-ph].

[159] Ulrich Ellwanger. "Higgs pair production in the NMSSM at the LHC". In: *JHEP* 08 (2013), p. 077. DOI: 10.1007/JHEP08(2013)077. arXiv: 1306.5541 [hep-ph].

[160] Junjie Cao et al. "Exploring the Higgs Sector of a Most Natural NMSSM and its Prediction on Higgs Pair Production at the LHC". In: *JHEP* 12 (2014), p. 026. DOI: 10.1007/JHEP12(2014)026. arXiv: 1409.8431 [hep-ph].

[161] M. Mühlleitner, Dao Thi Nhung, and Hanna Ziesche. "The order $\mathcal{O}(\alpha_t\alpha_s)$ corrections to the trilinear Higgs self-couplings in the complex NMSSM". In: *JHEP* 12 (2015), p. 034. DOI: 10.1007/JHEP12(2015)034. arXiv: 1506.03321 [hep-ph].

[162] Stefan Liebler et al. "The hMSSM approach for Higgs self-couplings revisited". In: *Eur. Phys. J. C* 79.1 (2019), p. 65. DOI: 10.1140/epjc/s10052-019-6594-x. arXiv: 1810.10979 [hep-ph].

[163] Peisi Huang and Yu Hang Ng. "Di-Higgs Production in SUSY models at the LHC". In: *Eur. Phys. J. Plus* 135.8 (2020), p. 660. DOI: 10.1140/epjp/s13360-020-00677-1. arXiv: 1910.13968 [hep-ph].

[164] G. Aad et al. "Constraints on the Higgs boson self-coupling from single- and double-Higgs production with the ATLAS detector using pp collisions at $\sqrt{s} = 13\,\text{TeV}$". In: *Physics Letters B* 843 (Aug. 2023), p. 137745. ISSN: 0370-2693. DOI: 10.1016/j.physletb.2023.137745.

[165] M. Aaboud *et al.* ATLAS. "Search for pair production of Higgs bosons in the $b\bar{b}b\bar{b}$ final state using proton-proton collisions at $\sqrt{s} = 13$ TeV with the ATLAS detector". In: *Journal of High Energy Physics* 2019.1 (Jan. 2019). DOI: 10.1007/jhep01(2019)030.

[166] M. Aaboud *et al.* ATLAS. "Search for Resonant and Nonresonant Higgs Boson Pair Production in the $b\bar{b}\tau^+\tau^-$ Decay Channel in pp Collisions at $\sqrt{s} = 13$ TeV with the ATLAS Detector". In: *Physical Review Letters* 121.19 (Nov. 2018). DOI: 10.1103/physrevlett.121.191801.

[167] M. Aaboud *et al.* ATLAS. "Erratum: Search for Resonant and Nonresonant Higgs Boson Pair Production in the $b\bar{b}\tau^+\tau^-$ Decay Channel in pp Collisions at $\sqrt{s} = 13$ TeV with the ATLAS Detector [Phys. Rev. Lett. 121, 191801 (2018)]". In: *Phys. Rev. Lett.* 122 (8 Feb. 2019), p. 089901. DOI: 10.1103/PhysRevLett.122.089901.

[168] G. Aad *et al.* ATLAS. "Reconstruction and identification of boosted di-τ systems in a search for Higgs boson pairs using 13 TeV proton-proton collision data in ATLAS". In: *Journal of High Energy Physics* 2020.11 (Nov. 2020), p. 163. ISSN: 1029-8479. DOI: 10.1007/JHEP11(2020)163.

[169] M. Aaboud *et al.* ATLAS. "Search for Higgs boson pair production in the $\gamma\gamma b\bar{b}$ final state with 13 TeV pp collision data collected by the ATLAS experiment". In: *Journal of High Energy Physics* 2018.11 (Nov. 2018). DOI: 10.1007/jhep11(2018)040.

[170] M. Aaboud *et al.* ATLAS. "Search for Higgs boson pair production in the $b\bar{b}WW^*$ decay mode at $\sqrt{s} = 13$ TeV with the ATLAS detector". In: *Journal of High Energy Physics* 2019.4 (Apr. 2019). DOI: 10.1007/jhep04(2019)092.

[171] A. M. Sirunyan *et al.* CMS. "Search for resonant pair production of Higgs bosons in the $bbZZ$ channel in proton-proton collisions at $\sqrt{s} = 13$ TeV". In: *Physical Review D* 102.3 (Aug. 2020). DOI: 10.1103/physrevd.102.032003.

[172] M. Aaboud *et al.* ATLAS. "Search for Higgs boson pair production in the $\gamma\gamma WW^*$ channel using pp collision data recorded at $\sqrt{s} = 13$ TeV with the ATLAS detector". In: *The European Physical Journal C* 78.12 (Dec. 2018). DOI: 10.1140/epjc/s10052-018-6457-x.

[173] M. Aaboud *et al.* ATLAS. "Search for Higgs boson pair production in the $WW^{(*)}WW^{(*)}$ decay channel using ATLAS data recorded at $\sqrt{s} = 13$ TeV". In: *Journal of High Energy Physics* 2019.5 (May 2019). DOI: 10.1007/jhep05(2019)124.

[174] "Search for resonant Higgs boson pair production in four b quark final state using large-area jets in proton-proton collisions at $\sqrt{s} = 13$ TeV". In: *CMS-PAS-B2G-20-004* (2021).

[175] Georges Aad et al. "Search for Higgs boson pair production in the two bottom quarks plus two photons final state in pp collisions at $\sqrt{s} = 13$ TeV with the ATLAS detector". In: *Phys. Rev. D* 106.5 (2022), p. 052001. DOI: 10.1103/PhysRevD.106.052001. arXiv: 2112.11876 [hep-ex].

[176] Georges Aad et al. "Search for resonant pair production of Higgs bosons in the $b\bar{b}b\bar{b}$ final state using pp collisions at $\sqrt{s} = 13$ TeV with the ATLAS detector". In: *Phys. Rev. D* 105.9 (2022), p. 092002. DOI: 10.1103/PhysRevD.105.092002. arXiv: 2202.07288 [hep-ex].

[177] Georges Aad et al. "Search for resonant and non-resonant Higgs boson pair production in the $b\bar{b}\tau^+\tau^-$ decay channel using 13 TeV pp collision data from the ATLAS detector". In: *JHEP* 07 (2023), p. 040. DOI: 10.1007/JHEP07(2023)040. arXiv: 2209.10910 [hep-ex].

[178] Felix Egle. "Higgs Decay into Dark Matter in the CxSM at Next-to-Leading Order". Online; accessed: 2024-07-16. Master's thesis. Karlsruhe Institute of Technology (KIT), 2021.

[179] Margarete Mühlleitner et al. *ScannerS: Parameter Scans in Extended Scalar Sectors*. 2020. arXiv: 2007.02985 [hep-ph].

[180] Benjamin W. Lee, C. Quigg, and H. B. Thacker. "Weak interactions at very high energies: The role of the Higgs-boson mass". In: *Phys. Rev. D* 16 (5 Sept. 1977), pp. 1519–1531. DOI: 10.1103/PhysRevD.16.1519.

[181] Michael E. Peskin and Tatsu Takeuchi. "Estimation of oblique electroweak corrections". In: *Phys. Rev. D* 46 (1 July 1992), pp. 381–409. DOI: 10.1103/PhysRevD.46.381.

[182] Ivan Maksymyk, C. P. Burgess, and David London. "BeyondS,T, andU". In: *Physical Review D* 50.1 (July 1994), pp. 529–535. ISSN: 0556-2821. DOI: 10.1103/physrevd.50.529.

[183] P. Bechtle et al. "HiggsBounds: Confronting arbitrary Higgs sectors with exclusion bounds from LEP and the Tevatron". In: *Computer Physics Communications* 181.1 (2010), pp. 138–167. ISSN: 0010-4655. DOI: 10.1016/j.cpc.2009.09.003.

[184] P. Bechtle et al. "HiggsBounds 2.0.0: Confronting neutral and charged Higgs sector predictions with exclusion bounds from LEP and the Tevatron". In: *Computer Physics Communications* 182.12 (Dec. 2011), pp. 2605–2631. ISSN: 0010-4655. DOI: 10.1016/j.cpc.2011.07.015.

[185] Philip Bechtle et al. "HiggsBounds-4: improved tests of extended Higgs sectors against exclusion bounds from LEP, the Tevatron and the LHC". In: *The European Physical Journal C* 74.3 (Mar. 2014). ISSN: 1434-6052. DOI: 10.1140/epjc/s10052-013-2693-2.

[186] Philip Bechtle et al. "Applying exclusion likelihoods from LHC searches to extended Higgs sectors". In: *The European Physical Journal C* 75.9 (Sept. 2015). ISSN: 1434-6052. DOI: 10.1140/epjc/s10052-015-3650-z.

[187] Philip Bechtle et al. "HiggsBounds-5: testing Higgs sectors in the LHC 13 TeV Era". In: *The European Physical Journal C* 80.12 (Dec. 2020). ISSN: 1434-6052. DOI: 10.1140/epjc/s10052-020-08557-9.

[188] Philip Bechtle et al. "HiggsSignals: Confronting arbitrary Higgs sectors with measurements at the Tevatron and the LHC". In: *The European Physical Journal C* 74.2 (Feb. 2014). ISSN: 1434-6052. DOI: 10.1140/epjc/s10052-013-2711-4.

[189] Philip Bechtle et al. "HiggsSignals-2: probing new physics with precision Higgs measurements in the LHC 13 TeV era". In: *The European Physical Journal C* 81.2 (Feb. 2021). ISSN: 1434-6052. DOI: 10.1140/epjc/s10052-021-08942-y.

[190] G. Bélanger et al. "micrOMEGAs 2.0: A program to calculate the relic density of dark matter in a generic model". In: *Computer Physics Communications* 176.5 (Mar. 2007), pp. 367–382. ISSN: 0010-4655. DOI: 10.1016/j.cpc.2006.11.008.

[191] G. Bélanger et al. "Indirect search for dark matter with micrOMEGAs 2.4". In: *Computer Physics Communications* 182.3 (Mar. 2011), pp. 842–856. ISSN: 0010-4655. DOI: 10.1016/j.cpc.2010.11.033.

[192] G. Bélanger, A. Mjallal, and A. Pukhov. "Recasting direct detection limits within micrOMEGAs and implication for non-standard dark matter scenarios". In: *The European Physical Journal C* 81.3 (Mar. 2021). ISSN: 1434-6052. DOI: 10.1140/epjc/s10052-021-09012-z.

[193] Christian Gross, Oleg Lebedev, and Takashi Toma. "Cancellation Mechanism for DarkMatterNucleon Interaction". In: *Phys. Rev. Lett.* 119.19 (2017), p. 191801. DOI: 10.1103/PhysRevLett.119.191801. arXiv: 1708.02253 [hep-ph].

[194] Duarte Azevedo et al. "Testing scalar versus vector dark matter". In: *Phys. Rev. D* 99.1 (2019), p. 015017. DOI: 10.1103/PhysRevD.99.015017. arXiv: 1808.01598 [hep-ph].

[195] Duarte Azevedo et al. "One-loop contribution to dark-matter-nucleon scattering in the pseudo-scalar dark matter model". In: *JHEP* 01 (2019), p. 138. DOI: 10.1007/JHEP01(2019)138. arXiv: 1810.06105 [hep-ph].

[196] Seraina Glaus et al. "Electroweak Corrections in a Pseudo-Nambu Goldstone Dark Matter Model Revisited". In: *JHEP* 12 (2020), p. 034. DOI: 10.1007/JHEP12(2020)034. arXiv: 2008.12985 [hep-ph].

[197] E. Aprile et al. "Dark Matter Search Results from a One Ton-Year Exposure of XENON1T". In: *Phys. Rev. Lett.* 121.11 (2018), p. 111302. DOI: 10.1103/PhysRevLett.121.111302. arXiv: 1805.12562 [astro-ph.CO].

[198] Yue Meng et al. "Dark Matter Search Results from the PandaX-4T Commissioning Run". In: *Phys. Rev. Lett.* 127.26 (2021), p. 261802. DOI: 10.1103/PhysRevLett.127.261802. arXiv: 2107.13438 [hep-ex].

[199] J. Aalbers et al. "First Dark Matter Search Results from the LUX-ZEPLIN (LZ) Experiment". In: *Physical Review Letters* 131.4 (July 2023). ISSN: 1079-7114. DOI: 10.1103/physrevlett.131.041002.

[200] Ansgar Denner. "Techniques for calculation of electroweak radiative corrections at the one loop level and results for W physics at LEP-200". In: *Fortsch. Phys.* 41 (1993), pp. 307–420. DOI: 10.1002/prop.2190410402. arXiv: 0709.1075 [hep-ph].

[201] Marcel Krause et al. "Gauge-independent renormalization of the 2-Higgs-doublet model". In: *Journal of High Energy Physics* 2016.9 (Sept. 2016). ISSN: 1029-8479. DOI: 10.1007/jhep09(2016)143.

[202] Marcel Krause et al. "Gauge-independent renormalization of the N2HDM". In: *Journal of High Energy Physics* 2017.12 (Dec. 2017). ISSN: 1029-8479. DOI: 10.1007/jhep12(2017)077.

[203] J. Fleischer and F. Jegerlehner. "Radiative corrections to Higgs-boson decays in the Weinberg-Salam model". In: *Phys. Rev. D* 23 (9 May 1981), pp. 2001–2026. DOI: 10.1103/PhysRevD.23.2001.

[204] Shinya Kanemura et al. "Higgs coupling constants as a probe of new physics". In: *Physical Review D* 70.11 (Dec. 2004). ISSN: 1550-2368. DOI: 10.1103/physrevd.70.115002.

[205] John M. Cornwall and Joannis Papavassiliou. "Gauge Invariant Three Gluon Vertex in QCD". In: *Phys. Rev.* D40 (1989), p. 3474. DOI: 10.1103/PhysRevD.40.3474.

[206] Joannis Papavassiliou. "Gauge Invariant Proper Selfenergies and Vertices in Gauge Theories with Broken Symmetry". In: *Phys. Rev.* D41 (1990), p. 3179. DOI: 10.1103/PhysRevD.41.3179.

[207] Giuseppe Degrassi and Alberto Sirlin. "Gauge-invariant self-energies and vertex parts of the standard model in the pinch technique framework". In: *Phys. Rev. D* 46 (7 Oct. 1992), pp. 3104–3116. DOI: 10.1103/PhysRevD.46.3104.

[208] Joannis Papavassiliou. "Gauge independent transverse and longitudinal self-energies and vertices via the pinch technique". In: *Phys. Rev.* D50 (1994), pp. 5958–5970. DOI: 10.1103/PhysRevD.50.5958. arXiv: hep-ph/9406258 [hep-ph].

[209] Daniele Binosi and Joannis Papavassiliou. "Pinch technique: Theory and applications". In: *Physics Reports* 479.1-6 (Aug. 2009), pp. 1–152. ISSN: 0370-1573. DOI: 10.1016/j.physrep.2009.05.001.

[210] G. 't Hooft and M. Veltman. "Scalar one-loop integrals". In: *Nuclear Physics B* 153 (1979), pp. 365–401. ISSN: 0550-3213. DOI: https://doi.org/10.1016/0550-3213(79)90605-9.

[211] G. Passarino and M. Veltman. "One-loop corrections for e+e- annihilation into $\mu+\mu-$ in the Weinberg model". In: *Nuclear Physics B* 160.1 (1979), pp. 151–207. ISSN: 0550-3213. DOI: https://doi.org/10.1016/0550-3213(79)90234-7.

[212] Duarte Azevedo et al. "One-loop corrections to the Higgs boson invisible decay in the dark doublet phase of the N2HDM". In: *Journal of High Energy Physics* 2021.10 (Oct. 2021). ISSN: 1029-8479. DOI: 10.1007/jhep10(2021)044.

[213] A. Bredenstein et al. "Precise predictions for the Higgs-boson decay $H \to WW/ZZ \to$ 4 leptons". In: *Physical Review D* 74.1 (July 2006). ISSN: 1550-2368. DOI: 10.1103/physrevd.74.013004.

[214] A. Sirlin. "Radiative corrections in the $\mathrm{SU}(2)_L \times \mathrm{U}(1)$ theory: A simple renormalization framework". In: *Phys. Rev. D* 22 (4 Aug. 1980), pp. 971–981. DOI: 10.1103/PhysRevD.22.971.

[215] Marcel Krause, Margarete Mühlleitner, and Michael Spira. "2HDECAY A program for the calculation of electroweak one-loop corrections to Higgs decays in the Two-Higgs-Doublet Model including state-of-the-art QCD corrections". In: *Comput. Phys. Commun.* 246 (2020), p. 106852. DOI: 10.1016/j.cpc.2019.08.003. arXiv: 1810.00768 [hep-ph].

[216] A. Djouadi, J. Kalinowski, and M. Spira. "HDECAY: A Program for Higgs boson decays in the standard model and its supersymmetric extension". In: *Comput. Phys. Commun.* 108 (1998), pp. 56–74. DOI: 10.1016/S0010-4655(97)00123-9. arXiv: hep-ph/9704448.

[217] Abdelhak Djouadi et al. "HDECAY: Twenty$_{++}$ years after". In: *Comput. Phys. Commun.* 238 (2019), pp. 214–231. DOI: 10.1016/j.cpc.2018.12.010. arXiv: 1801.09506 [hep-ph].

[218] Raul Costa et al. "Singlet Extensions of the Standard Model at LHC Run 2: Benchmarks and Comparison with the NMSSM". In: *JHEP* 06 (2016), p. 034. DOI: 10.1007/JHEP06(2016)034. arXiv: 1512.05355 [hep-ph].

[219] Robin Lorenz. "Full One-loop Electroweak Corrections to the Decays $H^+ \to W^+h/H$ in the Two-Higgs-Doublet Model". Online; accessed: 2024-07-21. Master's thesis. Karlsruhe Institute of Technology (KIT), 2015.

[220] Florian Staub. "From superpotential to model files for FeynArts and CalcHep/CompHep". In: *Computer Physics Communications* 181.6 (June 2010), pp. 1077–1086. ISSN: 0010-4655. DOI: 10.1016/j.cpc.2010.01.011.

[221] Florian Staub. "SARAH 3.2: Dirac gauginos, UFO output, and more". In: *Computer Physics Communications* 184.7 (July 2013), pp. 1792–1809. ISSN: 0010-4655. DOI: 10.1016/j.cpc.2013.02.019.

[222] Florian Staub. "SARAH 4: A tool for (not only SUSY) model builders". In: *Computer Physics Communications* 185.6 (June 2014), pp. 1773–1790. ISSN: 0010-4655. DOI: 10.1016/j.cpc.2014.02.018.

[223] Florian Staub. "Exploring New Models in All Detail withSARAH". In: *Advances in High Energy Physics* 2015 (2015), pp. 1–126. ISSN: 1687-7365. DOI: 10.1155/2015/840780.

[224] Thomas Hahn. "Generating Feynman diagrams and amplitudes with FeynArts 3". In: *Computer Physics Communications* 140.3 (2001), pp. 418–431. ISSN: 0010-4655. DOI: https://doi.org/10.1016/S0010-4655(01)00290-9.

[225] R. Mertig, M. Böhm, and A. Denner. "Feyn Calc - Computer-algebraic calculation of Feynman amplitudes". In: *Computer Physics Communications* 64.3 (1991), pp. 345–359. ISSN: 0010-4655. DOI: https://doi.org/10.1016/0010-4655(91)90130-D.

[226] Vladyslav Shtabovenko, Rolf Mertig, and Frederik Orellana. "New developments in FeynCalc 9.0". In: *Computer Physics Communications* 207 (Oct. 2016), pp. 432–444. ISSN: 0010-4655. DOI: 10.1016/j.cpc.2016.06.008.

[227] Vladyslav Shtabovenko, Rolf Mertig, and Frederik Orellana. "FeynCalc 9.3: New features and improvements". In: *Computer Physics Communications* 256 (Nov. 2020), p. 107478. ISSN: 0010-4655. DOI: 10.1016/j.cpc.2020.107478.

[228] Vladyslav Shtabovenko, Rolf Mertig, and Frederik Orellana. *FeynCalc 10: Do multiloop integrals dream of computer codes?* 2023. arXiv: 2312.14089 [hep-ph].

[229] G. J. van Oldenborgh and J. A. M. Vermaseren. "New Algorithms for One Loop Integrals". In: *Z. Phys. C* 46 (1990), pp. 425–438. DOI: 10.1007/BF01621031.

[230] T. Hahn and M. Perez-Victoria. "Automatized one loop calculations in four-dimensions and D-dimensions". In: *Comput. Phys. Commun.* 118 (1999), pp. 153–165. DOI: 10.1016/S0010-4655(98)00173-8. arXiv: hep-ph/9807565.

[231] Philipp Basler and Margarete Mühlleitner. "BSMPT (Beyond the Standard Model Phase Transitions): A tool for the electroweak phase transition in extended Higgs sectors". In: *Comput. Phys. Commun.* 237 (2019), pp. 62–85. DOI: 10.1016/j.cpc.2018.11.006. arXiv: 1803.02846 [hep-ph].

[232] Philipp Basler, Margarete Mühlleitner, and Jonas Müller. "BSMPT v2 a tool for the electroweak phase transition and the baryon asymmetry of the universe in extended Higgs Sectors". In: *Comput. Phys. Commun.* 269 (2021), p. 108124. DOI: 10.1016/j.cpc.2021.108124. arXiv: 2007.01725 [hep-ph].

[233] Philipp Basler et al. *BSMPT v3 A Tool for Phase Transitions and Primordial Gravitational Waves in Extended Higgs Sectors*. 2024. arXiv: 2404.19037 [hep-ph].

[234] Robert V. Harlander, Stefan Liebler, and Hendrik Mantler. "SusHi: A program for the calculation of Higgs production in gluon fusion and bottom-quark annihilation in the Standard Model and the MSSM". In: *Comput. Phys. Commun.* 184 (2013), pp. 1605–1617. DOI: 10.1016/j.cpc.2013.02.006. arXiv: 1212.3249 [hep-ph].

[235] Stefan Liebler. "Neutral Higgs production at proton colliders in the CP-conserving NMSSM". In: *Eur. Phys. J. C* 75.5 (2015), p. 210. DOI: 10.1140/epjc/s10052-015-3432-7. arXiv: 1502.07972 [hep-ph].

[236] Robert V. Harlander, Stefan Liebler, and Hendrik Mantler. "SusHi Bento: Beyond NNLO and the heavy-top limit". In: *Comput. Phys. Commun.* 212 (2017), pp. 239–257. DOI: 10.1016/j.cpc.2016.10.015. arXiv: 1605.03190 [hep-ph].

[237] Steven Weinberg. "Implications of dynamical symmetry breaking". In: *Phys. Rev. D* 13 (4 Feb. 1976), pp. 974–996. DOI: 10.1103/PhysRevD.13.974.

[238] S. Weinberg. "Implications of dynamical symmetry breaking: An addendum". In: *Phys. Rev. D* 19 (4 Feb. 1979), pp. 1277–1280. DOI: 10.1103/PhysRevD.19.1277.

[239] Leonard Susskind. "Dynamics of spontaneous symmetry breaking in the Weinberg-Salam theory". In: *Phys. Rev. D* 20 (10 Nov. 1979), pp. 2619–2625. DOI: 10.1103/PhysRevD.20.2619.

[240] S. Scherer. *Introduction to Chiral Perturbation Theory*. 2002. arXiv: hep-ph/0210398 [hep-ph].

[241] David B. Kaplan. "Flavor at ssc energies: A new mechanism for dynamically generated fermion masses". In: *Nuclear Physics B* 365.2 (1991), pp. 259–278. ISSN: 0550-3213. DOI: https://doi.org/10.1016/S0550-3213(05)80021-5.

[242] Howard Georgi. "Vector realization of chiral symmetry". In: *Nuclear Physics B* 331.2 (1990), pp. 311–330. ISSN: 0550-3213. DOI: https://doi.org/10.1016/0550-3213(90)90210-5.

[243] Nima Arkani-Hamed, Andrew G. Cohen, and Howard Georgi. "Electroweak symmetry breaking from dimensional deconstruction". In: *Physics Letters B* 513.12 (July 2001), pp. 232–240. ISSN: 0370-2693. DOI: 10.1016/s0370-2693(01)00741-9.

[244] Nima Arkani-Hamed et al. "The Littlest Higgs". In: *Journal of High Energy Physics* 2002.07 (July 2002), pp. 034–034. ISSN: 1029-8479. DOI: 10.1088/1126-6708/2002/07/034.

[245] Nima Arkani-Hamed et al. "The Minimal Moose for a Little Higgs". In: *Journal of High Energy Physics* 2002.08 (Aug. 2002), pp. 021–021. ISSN: 1029-8479. DOI: 10.1088/1126-6708/2002/08/021.

[246] Antonio Pich and Paula Tuzón. "Yukawa alignment in the two-Higgs-doublet model". In: *Physical Review D* 80.9 (Nov. 2009). ISSN: 1550-2368. DOI: 10.1103/physrevd.80.091702.

[247] Paula Tuzon and Antonio Pich. "The Aligned two-Higgs Doublet model". In: *Acta Phys. Polon. Supp.* 3 (2010). Ed. by Henryk Czyz, Maria Krawczyk, and Mikolaj Misiak, pp. 215–220. arXiv: 1001.0293 [hep-ph].

[248] T. D. Lee. "A Theory of Spontaneous T Violation". In: *Phys. Rev. D* 8 (4 Aug. 1973), pp. 1226–1239. DOI: 10.1103/PhysRevD.8.1226.

[249] John F. Gunion and Howard E. Haber. "CP-conserving two-Higgs-doublet model: The approach to the decoupling limit". In: *Physical Review D* 67.7 (Apr. 2003). ISSN: 1089-4918. DOI: 10.1103/physrevd.67.075019.

[250] Ilya F. Ginzburg and Maria Krawczyk. "Symmetries of two Higgs doublet model and CP violation". In: *Phys. Rev. D* 72 (2005), p. 115013. DOI: 10.1103/PhysRevD.72.115013. arXiv: hep-ph/0408011.

[251] Sacha Davidson and Howard E. Haber. "Basis-independent methods for the two-Higgs-doublet model". In: *Phys. Rev. D* 72 (2005). [Erratum: Phys.Rev.D 72, 099902 (2005)], p. 035004. DOI: 10.1103/PhysRevD.72.099902. arXiv: hep-ph/0504050.

[252] Howard E. Haber and Deva O'Neil. "Basis-independent methods for the two-Higgs-doublet model. II. The Significance of tanβ". In: *Phys. Rev. D* 74 (2006). [Erratum: Phys.Rev.D 74, 059905 (2006)], p. 015018. DOI: 10.1103/PhysRevD.74.015018. arXiv: hep-ph/0602242.

[253] G.C. Branco et al. "Theory and phenomenology of two-Higgs-doublet models". In: *Physics Reports* 516.12 (July 2012), pp. 1–102. ISSN: 0370-1573. DOI: 10.1016/j.physrep.2012.02.002.

[254] Sheldon L. Glashow and Steven Weinberg. "Natural conservation laws for neutral currents". In: *Phys. Rev. D* 15 (7 Apr. 1977), pp. 1958–1965. DOI: 10.1103/PhysRevD.15.1958.

[255] Rachid Benbrik et al. "Signatures of vector-like top partners decaying into new neutral scalar or pseudoscalar bosons". In: *JHEP* 05 (2020), p. 028. DOI: 10.1007/JHEP05(2020)028. arXiv: 1907.05929 [hep-ph].

[256] G. Aad et al. "Search for pair-produced vector-like top and bottom partners in events with large missing transverse momentum in pp collisions with the ATLAS detector". In: *The European Physical Journal C* 83.8 (Aug. 2023). ISSN: 1434-6052. DOI: 10.1140/epjc/s10052-023-11790-7.

[257] Gian Francesco Giudice et al. "The strongly-interacting light Higgs". In: *Journal of High Energy Physics* 2007.06 (June 2007), pp. 045–045. ISSN: 1029-8479. DOI: 10.1088/1126-6708/2007/06/045.

[258] M. Spira. *HPAIR*. http://tiger.web.psi.ch/proglist.html.

[259] L. A. Harland-Lang et al. "Parton distributions in the LHC era: MMHT 2014 PDFs". In: *The European Physical Journal C* 75.5 (May 2015). DOI: 10.1140/epjc/s10052-015-3397-6.

[260] Stefano Carrazza, R. Keith Ellis, and Giulia Zanderighi. "QCDLoop: a comprehensive framework for one-loop scalar integrals". In: *Comput. Phys. Commun.* 209 (2016), pp. 134–143. DOI: 10.1016/j.cpc.2016.07.033. arXiv: 1605.03181 [hep-ph].

[261] M. Spira et al. "Higgs boson production at the LHC". In: *Nuclear Physics B* 453.1-2 (Oct. 1995), pp. 17–82. DOI: 10.1016/0550-3213(95)00379-7.

[262] M. Spira. *HIGLU: A Program for the Calculation of the Total Higgs Production Cross Section at Hadron Colliders via Gluon Fusion including QCD Corrections*. 1995. arXiv: hep-ph/9510347 [hep-ph].

[263] Georges Aad et al. "Measurement of the properties of Higgs boson production at $\sqrt{s} = 13$ TeV in the $H \to \gamma\gamma$ channel using 139 fb^{-1} of pp collision data with the ATLAS experiment". In: *JHEP* 07 (2023), p. 088. DOI: 10.1007/JHEP07(2023)088. arXiv: 2207.00348 [hep-ex].

[264] Georges Aad et al. "Climbing to the Top of the ATLAS 13 TeV data". In: (Apr. 2024). arXiv: 2404.10674 [hep-ex].

[265] David Eriksson, Johan Rathsman, and Oscar Stål. "2HDMC two-Higgs-doublet model calculator". In: *Computer Physics Communications* 181.1 (Jan. 2010), pp. 189–205. ISSN: 0010-4655. DOI: 10.1016/j.cpc.2009.09.011.

[266] W Grimus et al. "A precision constraint on multi-Higgs-doublet models". In: *Journal of Physics G: Nuclear and Particle Physics* 35.7 (May 2008), p. 075001. ISSN: 1361-6471. DOI: 10.1088/0954-3899/35/7/075001.

[267] M. Misiak et al. "Updated NNLO QCD predictions for the weak radiative B-meson decays". In: *Phys. Rev. Lett.* 114.22 (2015), p. 221801. DOI: 10.1103/PhysRevLett.114.221801. arXiv: 1503.01789 [hep-ph].

[268] Mikolaj Misiak and Matthias Steinhauser. "Weak radiative decays of the B meson and bounds on $M_{H^\pm}$ in the Two-Higgs-Doublet Model". In: *Eur. Phys. J. C* 77.3 (2017), p. 201. DOI: 10.1140/epjc/s10052-017-4776-y. arXiv: 1702.04571 [hep-ph].

[269] J. Haller et al. "Update of the global electroweak fit and constraints on two-Higgs-doublet models". In: *The European Physical Journal C* 78.8 (Aug. 2018). ISSN: 1434-6052. DOI: 10.1140/epjc/s10052-018-6131-3.

[270] M. Misiak, Abdur Rehman, and Matthias Steinhauser. "Towards $\overline{B} \to X_s\gamma$ at the NNLO in QCD without interpolation in m_c". In: *JHEP* 06 (2020), p. 175. DOI: 10.1007/JHEP06(2020)175. arXiv: 2002.01548 [hep-ph].

[271] Mark D. Goodsell and Ari Joury. "BSMArt: Simple and fast parameter space scans". In: *Comput. Phys. Commun.* 297 (2024), p. 109057. DOI: 10.1016/j.cpc.2023.109057. arXiv: 2301.01154 [hep-ph].

[272] Martin Gabelmann. "Two-Loop Corrections to Higgs Boson Masses in the NMSSM". PhD thesis. Karlsruher Institut für Technologie (KIT), 2021. 103 pp. DOI: 10.5445/IR/1000140398.

[273] Sidney Coleman and Jeffrey Mandula. "All Possible Symmetries of the S Matrix". In: *Phys. Rev.* 159 (5 July 1967), pp. 1251–1256. DOI: 10.1103/PhysRev.159.1251.

[274] Rudolf Haag, Jan T. Łopuszański, and Martin Sohnius. "All possible generators of supersymmetries of the S-matrix". In: *Nuclear Physics B* 88.2 (1975), pp. 257–274. ISSN: 0550-3213. DOI: https://doi.org/10.1016/0550-3213(75)90279-5.

[275] T. Fritzsche et al. "Heavy scalar top quark decays in the complex MSSM: A full one-loop analysis". In: *Physical Review D* 86.3 (Aug. 2012). ISSN: 1550-2368. DOI: 10.1103/physrevd.86.035014.

[276] Christoph Borschensky et al. "Higgs Mass Predictions in the CP-Violating High-Scale NMSSM". In: (June 2024). arXiv: 2406.17635 [hep-ph].

[277] Henning Bahl et al. "HiggsTools: BSM scalar phenomenology with new versions of HiggsBounds and HiggsSignals". In: *Computer Physics Communications* 291 (Oct. 2023), p. 108803. ISSN: 0010-4655. DOI: 10.1016/j.cpc.2023.108803.

[278] Sabine Kraml et al. "SModelS: a tool for interpreting simplified-model results from the LHC and its application to supersymmetry". In: *Eur.Phys.J.* C74 (2014), p. 2868. DOI: 10.1140/epjc/s10052-014-2868-5. arXiv: 1312.4175 [hep-ph].

[279] Federico Ambrogi et al. "SModelS v1.1 user manual". In: (2017). arXiv: 1701.06586 [hep-ph].

[280] Federico Ambrogi et al. "SModelS v1.2: long-lived particles, combination of signal regions, and other novelties". In: *Comput. Phys. Commun.* 251 (2020), p. 106848. DOI: 10.1016/j.cpc.2019.07.013. arXiv: 1811.10624 [hep-ph].

[281] Gaël Alguero et al. "Constraining new physics with SModelS version 2". In: *JHEP* 08 (2022), p. 068. DOI: 10.1007/JHEP08(2022)068. arXiv: 2112.00769 [hep-ph].

[282] Mohammad Mahdi Altakach et al. "SModelS v2.3: Enabling global likelihood analyses". In: *SciPost Phys.* 15.5 (2023), p. 185. DOI: 10.21468/SciPostPhys.15.5.185. arXiv: 2306.17676 [hep-ph].

[283] S.F. King et al. "Exploring the CP-violating NMSSM: EDM constraints and phenomenology". In: *Nuclear Physics B* 901 (Dec. 2015), pp. 526–555. ISSN: 0550-3213. DOI: 10.1016/j.nuclphysb.2015.11.003.

[284] Thi Nhung Dao, Duc Ninh Le, and Margarete Mühlleitner. "Leptonic anomalous magnetic and electric dipole moments in the CP-violating NMSSM with and without inverse seesaw mechanism". In: *Eur. Phys. J. C* 82.10 (2022), p. 954. DOI: 10.1140/epjc/s10052-022-10928-3. arXiv: 2207.12618 [hep-ph].

[285] B. C. Regan et al. "New limit on the electron electric dipole moment". In: *Phys. Rev. Lett.* 88 (2002), p. 071805. DOI: 10.1103/PhysRevLett.88.071805.

[286] C. A. Baker et al. "An Improved experimental limit on the electric dipole moment of the neutron". In: *Phys. Rev. Lett.* 97 (2006), p. 131801. DOI: 10.1103/PhysRevLett.97.131801. arXiv: hep-ex/0602020.

[287] W. C. Griffith et al. "Improved Limit on the Permanent Electric Dipole Moment of Hg-199". In: *Phys. Rev. Lett.* 102 (2009), p. 101601. DOI: 10.1103/PhysRevLett.102.101601. arXiv: 0901.2328 [physics.atom-ph].

[288] Jacob Baron et al. "Order of Magnitude Smaller Limit on the Electric Dipole Moment of the Electron". In: *Science* 343 (2014), pp. 269–272. DOI: 10.1126/science.1248213. arXiv: 1310.7534 [physics.atom-ph].

[289] V. Andreev et al. "Improved limit on the electric dipole moment of the electron". In: *Nature* 562.7727 (2018), pp. 355–360. DOI: 10.1038/s41586-018-0599-8.

[290] M. Masip, R. Munoz-Tapia, and A. Pomarol. "Limits on the mass of the lightest Higgs in supersymmetric models". In: *Phys. Rev. D* 57 (1998), R5340. DOI: 10.1103/PhysRevD.57.R5340. arXiv: hep-ph/9801437.

[291] R. Gröber et al. "Light stop decays: implications for LHC searches". In: *The European Physical Journal C* 75.9 (Sept. 2015). ISSN: 1434-6052. DOI: 10.1140/epjc/s10052-015-3626-z.

[292] R. Gavin et al. "Squark production and decay matched with parton showers at NLO". In: *The European Physical Journal C* 75.1 (Jan. 2015). ISSN: 1434-6052. DOI: 10.1140/epjc/s10052-014-3243-2.

[293] W. Beenakker, R. Höpker, and P.M. Zerwas. "SUSY-QCD decays of squarks and gluinos". In: *Physics Letters B* 378.14 (June 1996), pp. 159–166. ISSN: 0370-2693. DOI: 10.1016/0370-2693(96)00379-6.

[294] W. Beenakker et al. “Stop decays in SUSY-QCD”. In: *Zeitschrift für Physik C Particles and Fields* 75.2 (June 1997), pp. 349–356. ISSN: 1431-5858. DOI: 10.1007/s002880050478.

[295] W. Beenakker et al. “Squark and gluino production at hadron colliders”. In: *Nuclear Physics B* 492.12 (May 1997), pp. 51–103. ISSN: 0550-3213. DOI: 10.1016/s0550-3213(97)80027-2.

[296] Julien Baglio, Barbara Jäger, and Matthias Kesenheimer. “Precise predictions for electroweakino-pair production in association with a jet at the LHC”. In: *Journal of High Energy Physics* 2018.7 (July 2018). ISSN: 1029-8479. DOI: 10.1007/jhep07(2018)055.

[297] Dominik Stockinger and Philipp Varso. “FeynArts model file for MSSM transition counterterms from DREG to DRED”. In: *Comput. Phys. Commun.* 183 (2012), pp. 422–430. DOI: 10.1016/j.cpc.2011.10.010. arXiv: 1109.6484 [hep-ph].

[298] Stephen P. Martin and Michael T. Vaughn. “Regularization dependence of running couplings in softly broken supersymmetry”. In: *Physics Letters B* 318.2 (1993), pp. 331–337. ISSN: 0370-2693. DOI: https://doi.org/10.1016/0370-2693(93)90136-6.

[299] Philipp Varo. “Supersymmetrie restaurierende Counterterme in Einschleifenordnung”. Online; accessed: 2024-09-09. Diplomarbeit. Institut für Kern- und Teilchenphysik der Technischen Universität Dresden, 2010.

[300] A. Bartl et al. “QCD corrections to Higgs boson decays into squarks in the minimal supersymmetric standard model”. In: *Physics Letters B* 402.34 (June 1997), pp. 303–313. ISSN: 0370-2693. DOI: 10.1016/s0370-2693(97)00457-7.

[301] S. Heinemeyer et al. “The Higgs sector of the complex MSSM at two-loop order: QCD contributions”. In: *Physics Letters B* 652.56 (Sept. 2007), pp. 300–309. ISSN: 0370-2693. DOI: 10.1016/j.physletb.2007.07.030.

[302] Janusz Rosiek. “Complete Set of Feynman Rules for the Minimal Supersymmetric Extension of the Standard Model”. In: *Phys. Rev. D* 41 (1990), p. 3464. DOI: 10.1103/PhysRevD.41.3464. arXiv: hep-ph/9511250.

[303] A. Denner et al. “Compact Feynman rules for Majorana fermions”. In: *Physics Letters B* 291.3 (1992), pp. 278–280. ISSN: 0370-2693. DOI: https://doi.org/10.1016/0370-2693(92)91045-B.

[304] Ansgar Denner et al. “Feynman rules for fermion number violating interactions”. In: *Nucl. Phys. B* 387 (1992), pp. 467–481. DOI: 10.1016/0550-3213(92)90169-C.

[305] Howard E. Haber and Daniel Wyler. “RADIATIVE NEUTRALINO DECAY”. In: *Nucl. Phys. B* 323 (1989), pp. 267–310. DOI: 10.1016/0550-3213(89)90143-0.

[306] S. Kraml et al. “SUSY-QCD corrections to scalar quark decays into charginos and neutralinos”. In: *Physics Letters B* 386.14 (Oct. 1996), pp. 175–182. ISSN: 0370-2693. DOI: 10.1016/0370-2693(96)00944-6.

[307] A. Djouadi, W. Hollik, and C. Jünger. “QCD corrections to scalar quark decays”. In: *Physical Review D* 55.11 (June 1997), pp. 6975–6985. ISSN: 1089-4918. DOI: 10.1103/physrevd.55.6975.

[308] A. Bartl et al. “SUSY-QCD corrections to stop and sbottom decays into Wś and Z0 bosons”. In: *Physics Letters B* 419.14 (Feb. 1998), pp. 243–252. ISSN: 0370-2693. DOI: 10.1016/s0370-2693(97)01475-5.

[309] A. Arhrib et al. “Supersymmetric Higgs boson decays into scalar quarks: QCD corrections”. In: *Physical Review D* 57.9 (May 1998), pp. 5860–5870. ISSN: 1089-4918. DOI: 10.1103/physrevd.57.5860.

[310] W. Hollik, J. M. Lindert, and D. Pagani. "NLO corrections to squark-squark production and decay at the LHC". In: *Journal of High Energy Physics* 2013.3 (Mar. 2013). ISSN: 1029-8479. DOI: 10.1007/jhep03(2013)139.

[311] A. C. Fowler and G. Weiglein. "Precise predictions for Higgs production in neutralino decays in the complex MSSM". In: *Journal of High Energy Physics* 2010.1 (Jan. 2010). ISSN: 1029-8479. DOI: 10.1007/jhep01(2010)108.

[312] Aoife Bharucha et al. "Consistent on shell renormalisation of electroweakinos in the complex MSSM: LHC and LC predictions". In: *Journal of High Energy Physics* 2013.5 (May 2013). ISSN: 1029-8479. DOI: 10.1007/jhep05(2013)053.

[313] Christoph Borschensky et al. "The trilinear Higgs self-couplings at $\mathcal{O}(\alpha_t^2)$ in the CP-violating NMSSM". In: *Eur. Phys. J. C* 83.2 (2023), p. 118. DOI: 10.1140/epjc/s10052-023-11215-5. arXiv: 2210.02104 [hep-ph].

[314] Thi Nhung Dao, Martin Gabelmann, and Margarete Mühlleitner. "The $\mathcal{O}(\alpha_t+\alpha_\lambda+\alpha_\kappa)^2$ correction to the ρ parameter and its effect on the W boson mass calculation in the complex NMSSM". In: *Eur. Phys. J. C* 83.11 (2023), p. 1079. DOI: 10.1140/epjc/s10052-023-12236-w. arXiv: 2308.04059 [hep-ph].

[315] R. Keith Ellis and Giulia Zanderighi. "Scalar one-loop integrals for QCD". In: *Journal of High Energy Physics* 2008.02 (Feb. 2008), pp. 002–002. ISSN: 1029-8479. DOI: 10.1088/1126-6708/2008/02/002.

[316] P Skands et al. "SUSY Les Houches Accord: Interfacing SUSY Spectrum Calculators, Decay Packages, and Event Generators". In: *Journal of High Energy Physics* 2004.07 (July 2004), pp. 036–036. ISSN: 1029-8479. DOI: 10.1088/1126-6708/2004/07/036.

[317] B.C. Allanach et al. "SUSY Les Houches Accord 2". In: *Computer Physics Communications* 180.1 (Jan. 2009), pp. 8–25. ISSN: 0010-4655. DOI: 10.1016/j.cpc.2008.08.004.

[318] J. Baglio et al. *NMSSMCALC*. https://www.itp.kit.edu/~maggie/NMSSMCALC/.

[319] W. Porod. "SPheno, a program for calculating supersymmetric spectra, SUSY particle decays and SUSY particle production at e+e- colliders". In: *Computer Physics Communications* 153.2 (June 2003), pp. 275–315. ISSN: 0010-4655. DOI: 10.1016/s0010-4655(03)00222-4.

[320] W. Porod and F. Staub. "SPheno 3.1: extensions including flavour, CP-phases and models beyond the MSSM". In: *Computer Physics Communications* 183.11 (Nov. 2012), pp. 2458–2469. ISSN: 0010-4655. DOI: 10.1016/j.cpc.2012.05.021.

[321] S. Navas et al. "Review of particle physics". In: *Phys. Rev. D* 110.3 (2024), p. 030001. DOI: 10.1103/PhysRevD.110.030001.

[322] Eero Byckling and K. Kajantie. *Particle Kinematics: (Chapters I-VI, X)*. Jyvaskyla, Finland: University of Jyvaskyla, 1971.